8-2012

Biophysical and bioanalytical studies of hyaluronan and lipids.

Kristen Ann Magness 1981-
University of Louisville

BIOPHYSICAL AND BIOANALYTICAL STUDIES OF HYALURONAN AND LIPIDS

By

Kristen Ann Magness
B.A., University of Louisville, 2006
M.S., University of Louisville, 2010

A Dissertation
Submitted to the Faculty of the
College of Arts and Sciences of the University of Louisville
In Part Fulfillment of the Requirements
For the Degree of

Doctor of Philosophy

Department of Chemistry
University of Louisville
Louisville, Kentucky

August 2012

BIOPHYSICAL AND BIOANALYTICAL STUDIES
OF HYALURONAN AND LIPIDS

By

Kristen Ann Magness
B.A., University of Louisville, 2006
M.S., University of Louisville, 2010

A Dissertation Approved on

July 11, 2012

By the following Dissertation Committee:

M. Cecilia Yappert, Dissertation Director

Muriel Maurer

Aleeta Powe

Christine Rich

Douglas Borchman

ACKNOWLEDGMENTS

I owe my deepest gratitude to my mentor, Dr. M. Cecilia Yappert for her encouragement, guidance, and support. Her passion for research has been inspiring to me and I sincerely appreciate her dedication. I would also like to acknowledge and express my gratitude to my committee members, Dr. Douglas Borchman, Dr. Muriel Maurer, Dr. Aleeta Powe and Dr. Christine Rich for their guidance and direction of my research. Special thanks to lab mate, Sarah Milliner, for her friendship and many insightful conversations. I owe many thanks to Dr. Neal Stolowich for his training and support of the NMR instrumentation and to Dr. Donald DuPré for his contribution to the theoretical calculations of this work which aided in the experimental analysis

I would like to thank my high school chemistry teacher, Ava Prebys, who provided me with a strong background which has enabled me to pursue this higher degree. I will be forever grateful for the strong interest in chemistry for which she instilled in me. Also, a special thanks to Dr. Christine Rich who has acted as my mentor since my undergraduate years. Her guidance has been very helpful to me in my pursuit of this degree. She also provided me with wonderful teaching experiences through the GEMS program. I would like to thank Dr. Mark Noble for the teaching experiences which he provided me with. I truly admire his ability as a teacher and his dedication to his students.

I express my deepest gratitude to the University of Louisville Chemistry Department for their financial support and oversight throughout my graduate studies. I thank NSF for their funding of my fellowships through the GEMS grant, and to the School of Interdisciplinary and Graduate Studies for their support.

Most importantly I would like to extend my deepest appreciation for the support of my family and friends who without them none of this would be possible. A very special thanks to my mother, Susan Magness, for her continued encouragement and unconditional love. I will never be able to thank her enough for all the support she has provided me over the years. Thanks to Darin Fox for his companionship and support

through this journey. I express my sincerest gratitude to my dearest friend, Lisa Schultz for her patience and understanding during this process. The ability of these people to make me smile and always remind me of what is important in life has truly been a blessing. Finally I would like to thank all my other family members and friends who have helped make this possible.

ABSTRACT

BIOPHYSICAL AND BIOANALYTICAL STUDIES
OF HYALURONAN AND LIPIDS

Kristen Ann Magness

July 11, 2012

Hyaluronan (HA) is a major structural component of the ocular vitreous humor (VH) and lipids are essential building blocks of cell membranes. However, little is known about their possible interactions. The VH is known to undergo liquefaction throughout the lifetime that may result in complications such as posterior vitreous detachment. The possible roles of lipids in the age-dependent liquefaction of the VH are unknown.

As a first step in this new area of research in our group, model studies of the repeating unit of polymeric HA were performed. This unit contains glucuronate (GlcU) linked to N-acetylglucosamine (GlcNAc) via a 1-3 linkage. The sample contained both α and β anomers leading to significant NMR (nuclear magnetic resonance) spectral complexity. Through the powerful combination of inverse heteronuclear 2D experiments, the resolution and assignment of all resonances for both anomers were achieved. Temperature-dependent changes in the NH resonances revealed the formation of weak or water-mediated intramolecular H-bonds.

The polymeric form of HA was then investigated in D_2O and its interactions with various lipids were probed. The analysis of chemical shifts and bandwidths of ^1H

NMRresonances revealed the strongest interactions to be between HA and unsaturated oleic acid and lyso-oleoyl-phosphatidylcholine.

Because matrix-assisted laser desorption/ionization mass spectrometry (MALDI-MS) will be used to analyze the components of the VH *in situ*, we evaluated changes in relative ionization efficiencies (RIE) when the repeating unit of HA and lipids were present in the model samples. Smaller lipid metabolites caused the greatest reduction of the RIE of HA but phosphatidic acid had no effect. On the other hand, HA decreased the ionization of all lipid species, almost equally, by ~50%. These findings suggest that the interactions of these species in the gas phase lead to partial blockage of the ionization sites. Preliminary results have been obtained for the VH by both NMR and MALDI-MS and do show the presence of lipids within the VH. In addition, oxidation of the VH leads to the presence of oxidized compounds and liquefaction. Future studies will focus on the isolation and characterization of these products of oxidation.

TABLE OF CONTENTS

LIST OF FIGURES

FIGURE PAGE

LIST OF TABLES

TABLE PAGE

CHAPTER 1

INTRODUCTION AND BACKGROUND

This chapter provides background information on the ocular vitreous humor (VH) or gel and surrounding tissues (i.e. lens and retina). Special attention is given to one of VH's most critical components, hyaluronan (HA). In addition, a summary of lipids, their presence in the VH, and what is known about their interactions with HA is presented. It is important to highlight that this is a new area of research in our group. For that reason, most of the results reported in this dissertation are based on model studies and only Chapter 4 presents our initial studies of human VH mass spectral (MS) approaches. In Chapter 5, preliminary nuclear magnetic resonance (NMR) data are shown and the directions for future research in this new field are delineated.

OCULAR VITREOUS HUMOR

Despite comprising over four-fifths of the eye's volume,[1] the VH is one of the least understood regions of the eye.[2] The VH is the transparent, gel-like substance which fills the center of the eye, posterior to the lens and anterior to the retina (Fig. 1-1). It is highly hydrated, yet quite viscous (two to four times more viscous than water),[3] elastic, but interestingly, somewhat rigid. These unique physical properties derive from a biomatrix composed of collagen fibrils and HA in relatively small amounts. Collagen can be considered to act as the scaffold while HA fills the spaces in between (Fig. 1-2).[2,4]

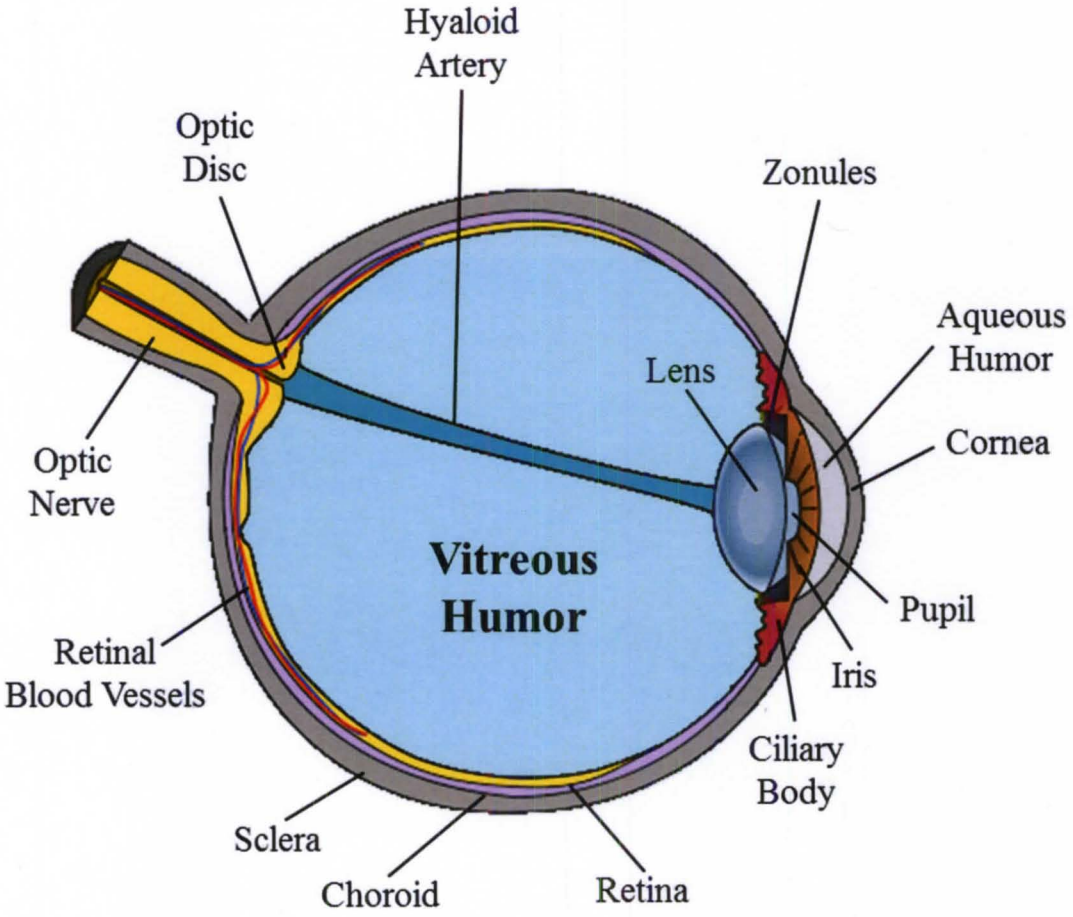

Figure 1-1. Diagram of the eye.
(Source: Adapted from http://en.wikipedia.org/wiki/Vitreous_humour)

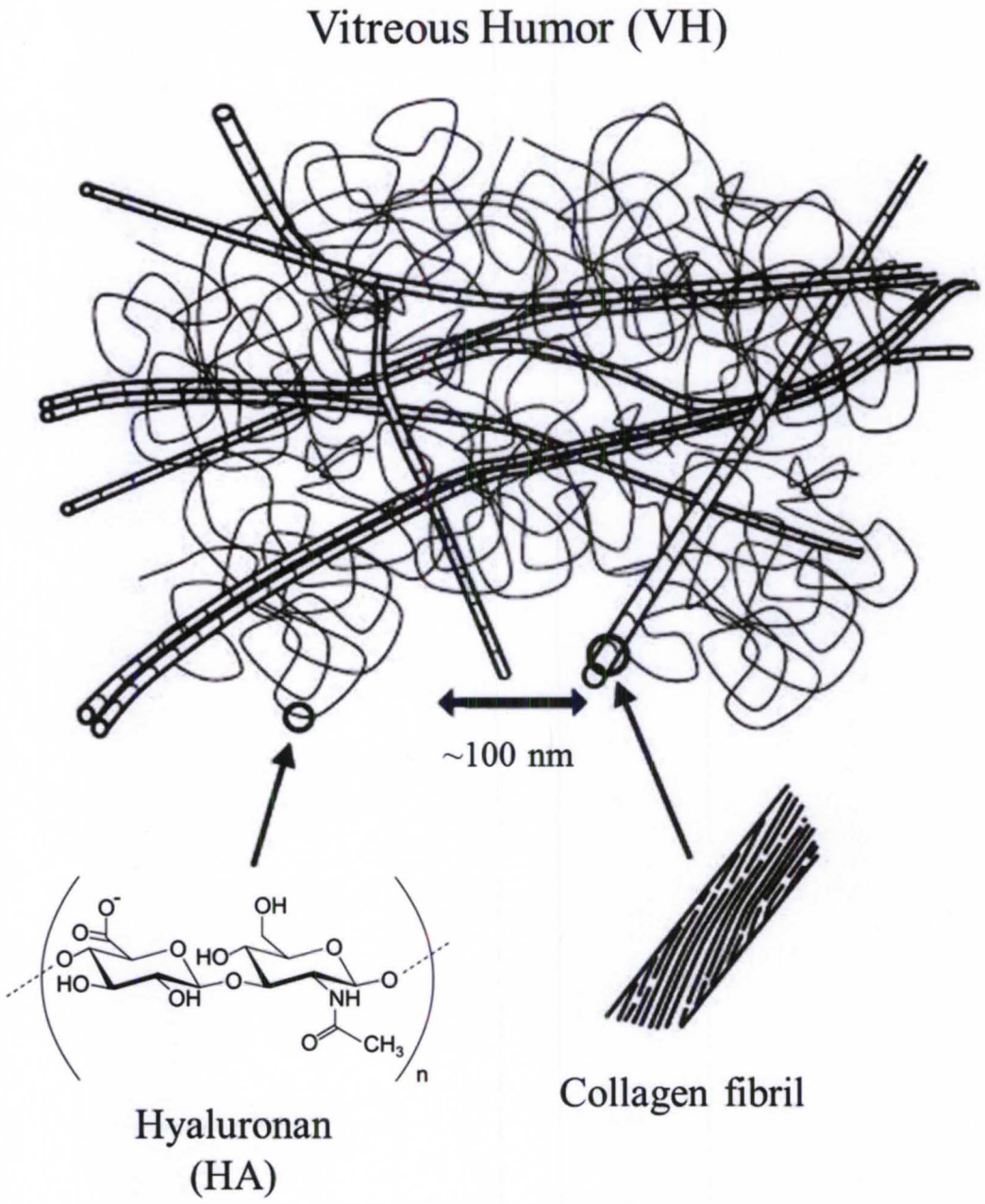

Figure 1-2. Molecular composition and organization of the VH. (Source: Adapted from Kornfield, J. A., *et al. Journal of Biomechanics* 2008, *41*, 1840–1846.[5])

Functions

Although once considered an "inert space filler",[6] recent studies have shown that the VH plays an important role in both the structure and function of the eye. These primary functions can be summarized as follows 1) developmental – mediating proper growth of the eye, 2) optical – maintaining a clear path to the retina and allowing accommodation of the lens, and 3) mechanical – providing support to the various ocular tissues.[7] Additionally, and of relevance to this project, it has been suggested that it serves as a metabolic repository for the surrounding ocular tissues.[7,8]

Anatomy

In the normal adult human eye, the VH is approximately 16.5 mm in length (along the optical axis)[9] and occupies a volume of about 4.5 mL.[1] It is nearly spherical, except for an anterior depression (*patellar fossa*) corresponding to the location of the lens (Fig. 1-3).[1] The *central vitreous* comprises the bulk of the VH and contains the hyaloid canal, a remnant of the embryological hyaloid artery.[4,10] The *vitreous cortex* is a thin outer layer (100-300 μm thick) that surrounds the central vitreous and is distinguished by a higher density of collagen.[1] It attaches to the lens anteriorly and to the retina posteriorly.[11] The *anterior vitreous cortex* runs from the *pars plana* of the ciliary bodies and covers the posterior lens surface.[4] The portion that runs between the *pars plana* and the lens (and adjacent to the zonules) is in direct contact with the aqueous humor, allowing for the exchange of molecules.[4] The *posterior vitreous cortex* is located parallel to the anterior retina, although it is thinned over the macula and absent at the optic nerve.[12,13] The greatest concentration of collagen fibrils is in the *vitreous base*, the annular zone that straddles the *ora serrata* (the jagged junction between the retina and the ciliary body).[1] It extends approximately 1.5-2 mm anteriorly and 3-4 mm posteriorly to the *ora serrata*[4]

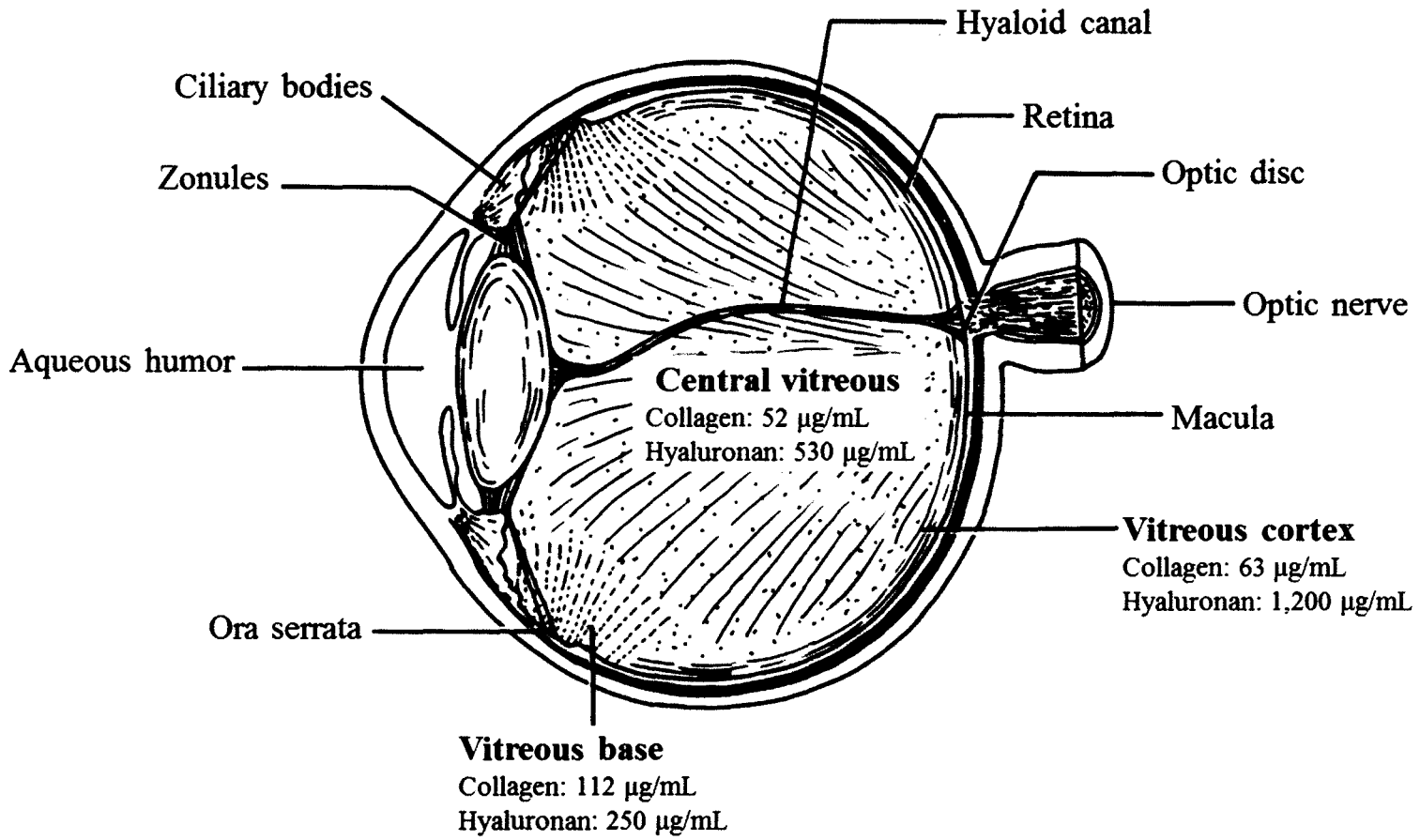

Figure 1-3. Detailed anatomy of the VH and organization of collagen fibrils. (Source: Adapted from Bishop, P. N. *Progress in Retinal and Eye Research* **2000**, *19*, 323–344.[4])

and several millimeters into the VH.[12,14] The vitreous base also represents the region of strongest attachment and is firmly adhered to both the ciliary body and the retina.[11] Vitreous attachments to surrounding ocular tissues (lens, ciliary bodies, and retina) occur through the condensation[3] and insertion[15,16] of vitreous collagen fibrils into the basal *laminae* of the adjacent cells.[12]

No blood vessels penetrate the VH, thus making it avascular.[17] In addition, the VH is nearly acellular.[4] A very small number of cells is present in the vitreous cortex and these cells concentrate in the vitreous base.[2,18] The cell population is predominantly (> 90%) hyalocytes.[2] These cells are metabolically active and synthesize extracellular matrix (ECM) components, including HA and collagen.[19–21] In addition, they have phagocytic and antigen-presenting properties that modulate inflammation and immune response. Other cells resembling macrophages and fibroblasts have also been found, but represent less than ten percent of the total cell population.[4]

Molecular Composition

The VH is highly hydrated being composed almost entirely of water (> 98% by weight).[4,22] Although present in relatively small amounts (~ 0.1% by weight),[22,23] collagen and HA are the major structural components of the VH and are responsible for its physical properties, including its gel-like nature. As stated previously, collagen can be considered to act as the scaffold while HA fills the spaces in between (Fig. 1-2).[2,4] As a first step to understanding this network, we have focused on HA and the possibility of hydrophobic interactions with lipids. The VH exists in two states: liquid (containing non-bound water) and gel (containing bound water).[24] The gel portion contains water that is trapped within the macromolecular network of the VH. On the other hand, the liquid portion includes 'free water' only.[25] The ratio of the two states has been determined by

measuring the freezable (free) and non-freezable (bound) water content.[26,27] This ratio varies significantly with age.[28]

Normal aging processes lead to the liquefaction and contraction of the VH. The liquefaction process does not occur uniformly and begins in the central VH where pockets of liquid form and eventually enlarge and coalesce (Fig. 1-4).[25,28–30] Studies have shown that in humans, liquid vitreous is initially present as early as four years of age.[28] By the time the eye reaches adult size (14 to 18 years), around 20% of the total VH volume consists of liquid VH.[2] After 40 years of age, there is a steady increase in VH liquid and a corresponding decrease in VH gel.[2] By the 8th and 9th decades of life, more than 50% of the VH is liquefied.[31]

The gradual and progressive aggregation of collagen fibrils leads to formation of liquid pockets which are void of collagen fibrils.[32–34] Additionally, depolymerization and conformational changes in HA may also play a role in liquefaction.[35–37] Conformational differences have been detected by circular dichroism (CD) for gel and liquid VH which suggest a conformational change for the carboxylic group.[38] Free radicals, generated by metabolic processes or by photosensitized reactions, have been shown to induce depolymerization and conformational changes in HA.[31,39,40] This is plausible because the cumulative effects of a lifetime of daily exposure to light could indeed influence the structures and interactions of VH collagen and HA.

Liquefaction and thinning of the VH weakens the adhesion between the posterior VH cortex and the inner limiting membrane of the retina and can ultimately lead to posterior vitreous detachment (PVD). PVD occurs when the vitreous separates from the retina (Fig 1-4).[41–44] The most common symptom of PVD is the perception of 'floaters' in the visual field. Floaters result from cells and other organic debris that float freely into

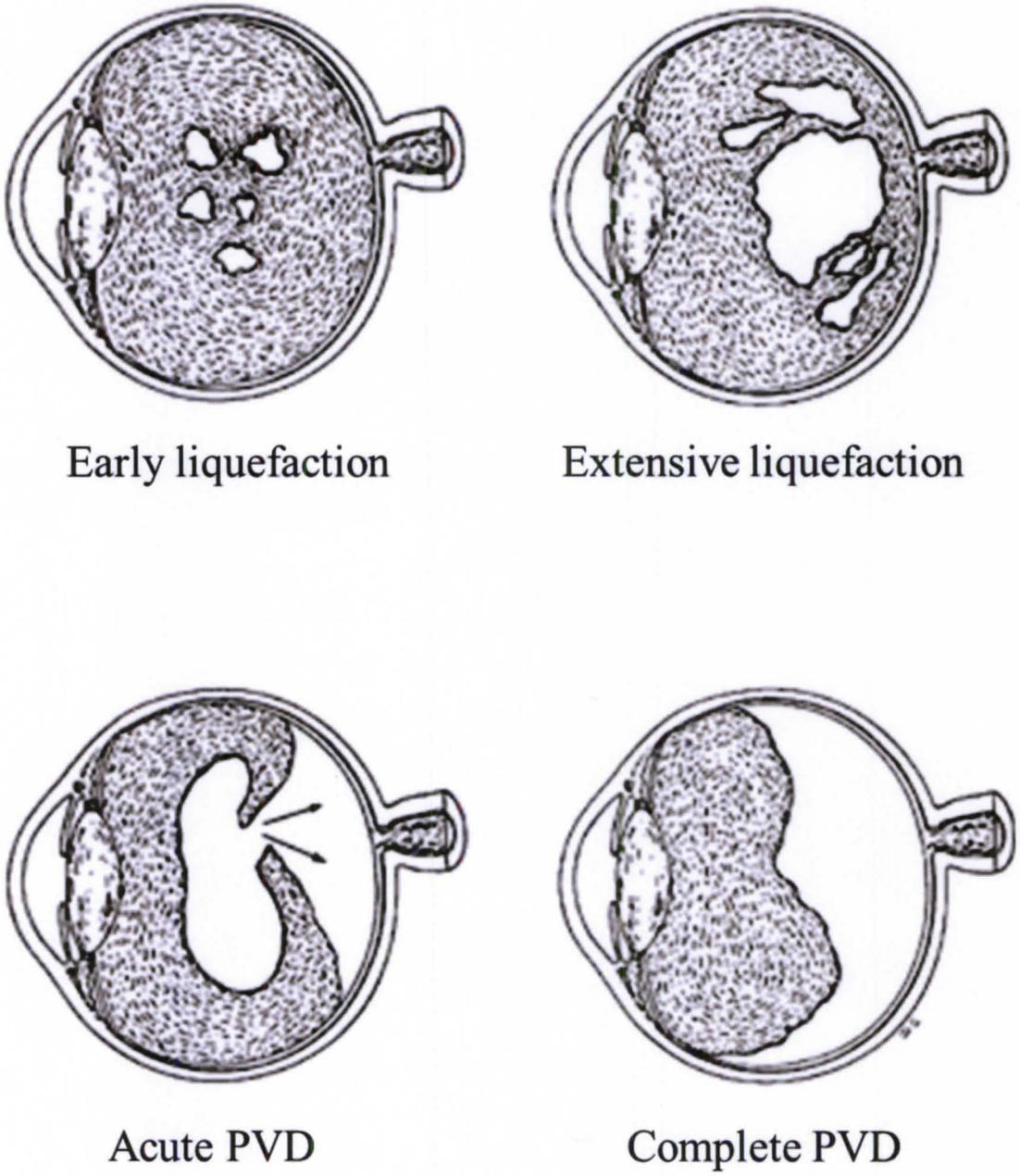

Figure 1-4. Liquefaction and posterior vitreous detachment (PVD) from the retina. (Source: Adapted from Bishop, P. N. *Progress in Retinal and Eye Research* 2000, *19*, 323–344.[4])

the VH.[45] They are perceived visually as spots or strands and because the VH is stagnant, they will remain there unless surgically removed.

It is interesting to note that degradation of the VH by collagenase leads to collapse of the gel network, but leaves a viscous solution of HA. By contrast, the degradation by hyaluronidase (HAase) has led to shrinkage of the VH but not entire gel collapse.[7] On this basis, collagen fibrils provide mechanical strength and the swollen HA macromolecules fill the space in between to prevent collagen aggregation.[46] However, this study only looked at the short-term effects of HA removal. In the long term, it is likely that both collagen and HA are important to the stability of the gel.

Hyaluronan and Other Glycosaminoglycans

Hyaluronan (HA) belongs to a group of compounds known as glycosaminoglycans (GAGs) which are defined as large unbranched polysaccharide chains, made up of repeating disaccharide units (specifically a hexose or hexuronic acid, linked to a hexosamine).[47,48] Besides HA, other GAGs such as chondroitin sulfate (CS) and heparan sulfate (HS) are worth noting. These differ from HA in that they have their own characteristic repeating disaccharide unit and they are sulfated. Interestingly, HA is synthesized in the plasma membrane while all other GAGs are synthesized within the endoplasmic reticulum and Golgi bodies.[49] Hyaluronan is synthesized by transmembrane glycosyltransferase enzymes (HA synthases).[50,51] Monosaccharides are added on the cytoplasmic side of the cell membrane and the growing chain is extruded into the extracellular matrix (ECM) (Fig. 1-5).[51]

Hyaluronan is a polymer composed of repeating disaccharide units of glucuronic (GlcU) and N-acetyl-glucosamine (GlcNAc).[47] The monosaccharide units are linked together through alternating β(1,3) and β(1,4) glycosidic bonds (Fig. 1-6a).[52] HA exists as

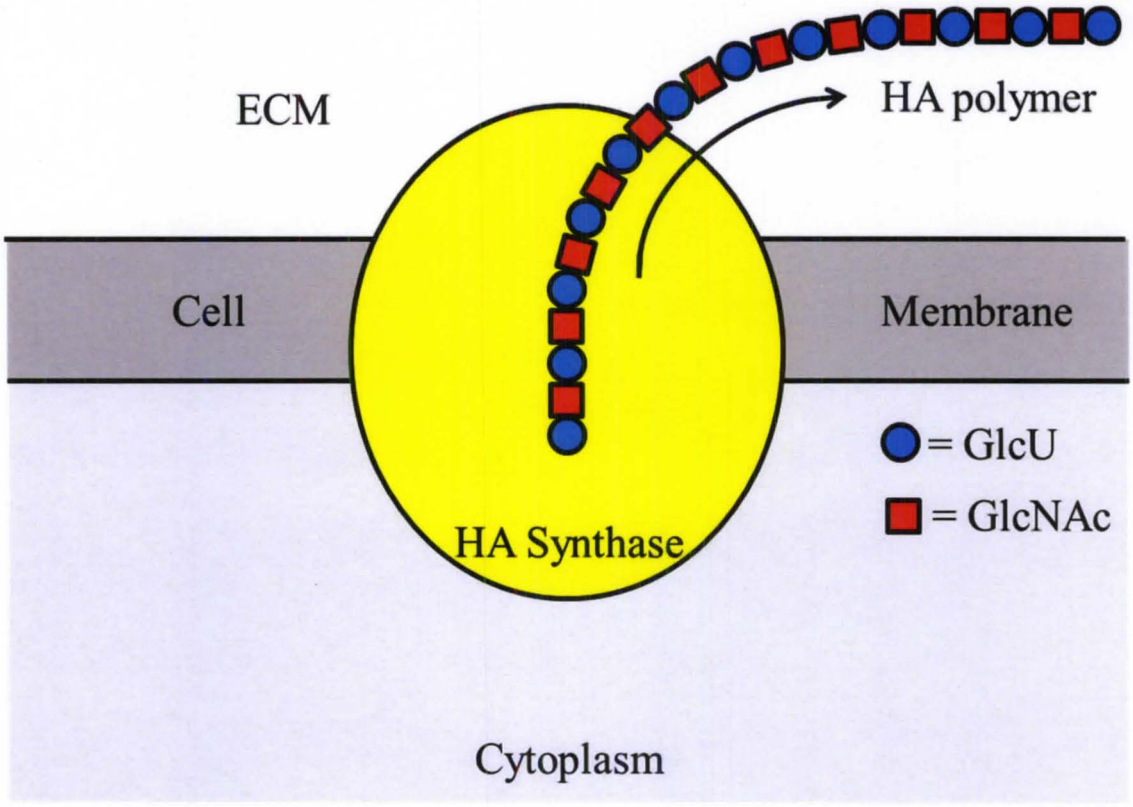

Figure 1-5. Synthesis of HA, by transmembrane protein HA synthase, and extrusion into the extracellular matrix (ECM). (Source: Adapted from http://glycoforum.gr.jp/science /hyaluronan/HA06/HA06E.html)

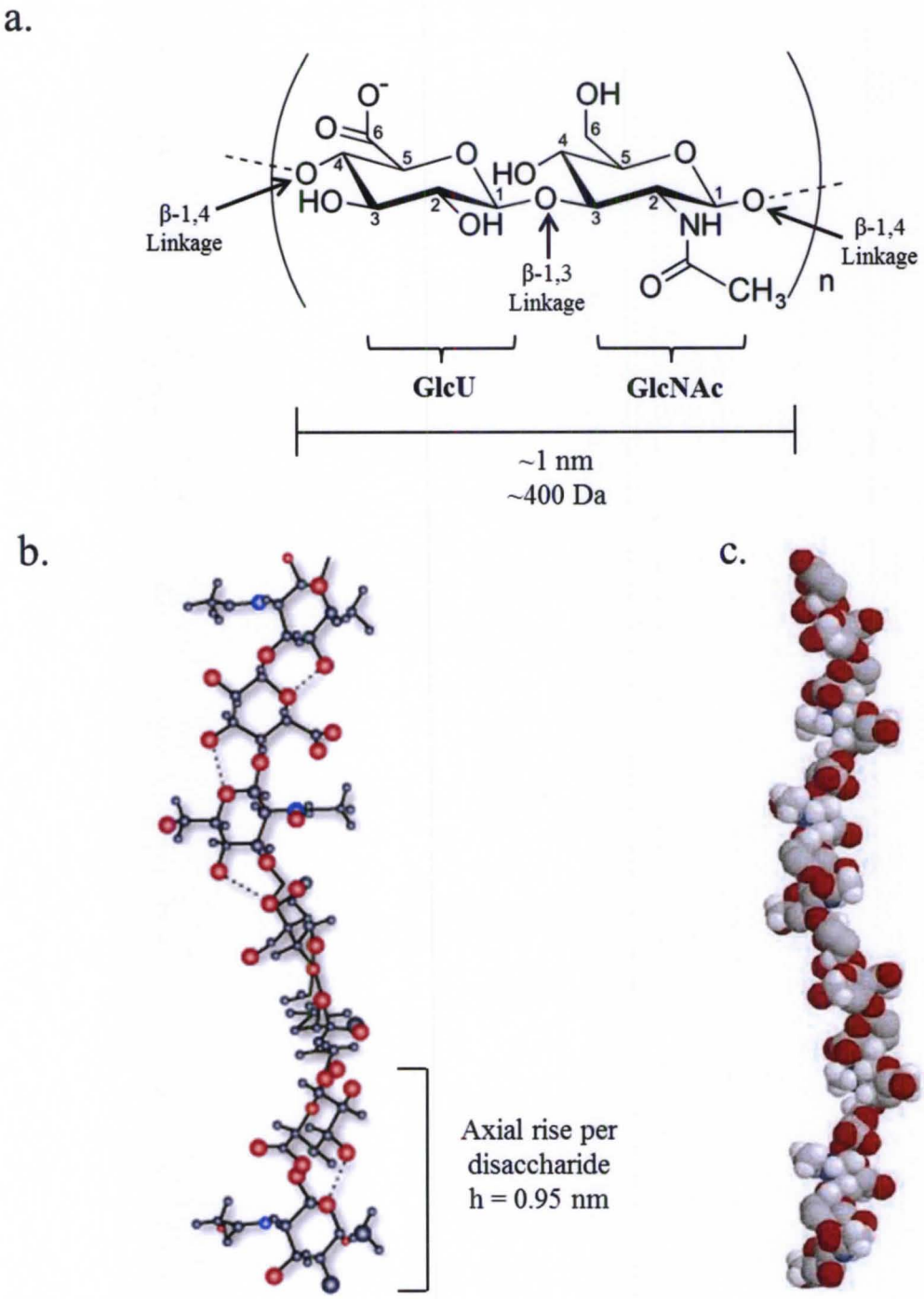

Figure 1-6. Chemical structure of the repeating disaccharide unit of HA (a) and the 3D structure of polymeric HA, in a four-fold helical conformation, represented by ball and stick (b) and space-filling (c) models. (Sources: Adapted from: a) http://glycoforum.gr.jp/science/hyaluronan/HA21E/HA21E.html b) Sheehan, J. K., *et al. Journal of Molecular Biology* **1983**, *169*, 813-827.[53] c) Sheehan, J. K ., *et al. Journal of Molecular Biology* **1998**, *284*, 1425-1437.[54])

a polyanion under physiological conditions as a result of deprotonation of the carboxylic groups (pKa ~ 3)[55] on GlcU residues.[56] The terms hyaluronic acid and hyaluronate have been designated to refer to the acid and the ionized form, respectively.[57] The term hyaluronan is used generally to refer to either form.[57]

The chemical structure of HA is highly conserved throughout nature although it is quite polydisperse in terms of size.[58,59] In human VH, the HA chains have molar masses between 3,000 and 4,500 kDa[60] and chains composed of 7,500 and up to 11,300 disaccharide units. This corresponds with lengths of approximately 10 μm.[52] Branching does not occur in the HA polymer and thus no side chains exist in the polymer, as determined by electron microscopy.[61]

The dynamic nature and conformational versatility of HA has been examined by a number of techniques (i.e. X-ray diffraction, computer simulations, and NMR). X-ray diffraction studies have found left-handed, two-, three-, and four-fold helical conformations under different experimental conditions (i.e. counterion, pH, temperature, humidity).[62,63] A four-fold double helical structure was even observed under more exotic conditions (i.e. Rb^+ or Cs^+ ions).[64] Computer simulations have shown that HA can adopt a range of extended (~1.0 nm axial rise per disaccharide) and condensed (~0.8 nm axial rise per disaccharide) conformations.[54] Under physiological conditions, HA is best characterized as a four-fold helix with 2.8-4.5 disaccharides per turn (Fig. 1-6b and c).[62,63]

In solution, HA can be described as an expanded random coil[58,65–67] occupying a large molecular domain.[49] Due to this configuration, HA chains entangle with each other even at low concentrations.[52] Intramolecular H-bonding[68–70] and water-mediated[71] H bonds help to stiffen the backbone of the HA chain (Fig. 1-7).[52] In addition to stiffening

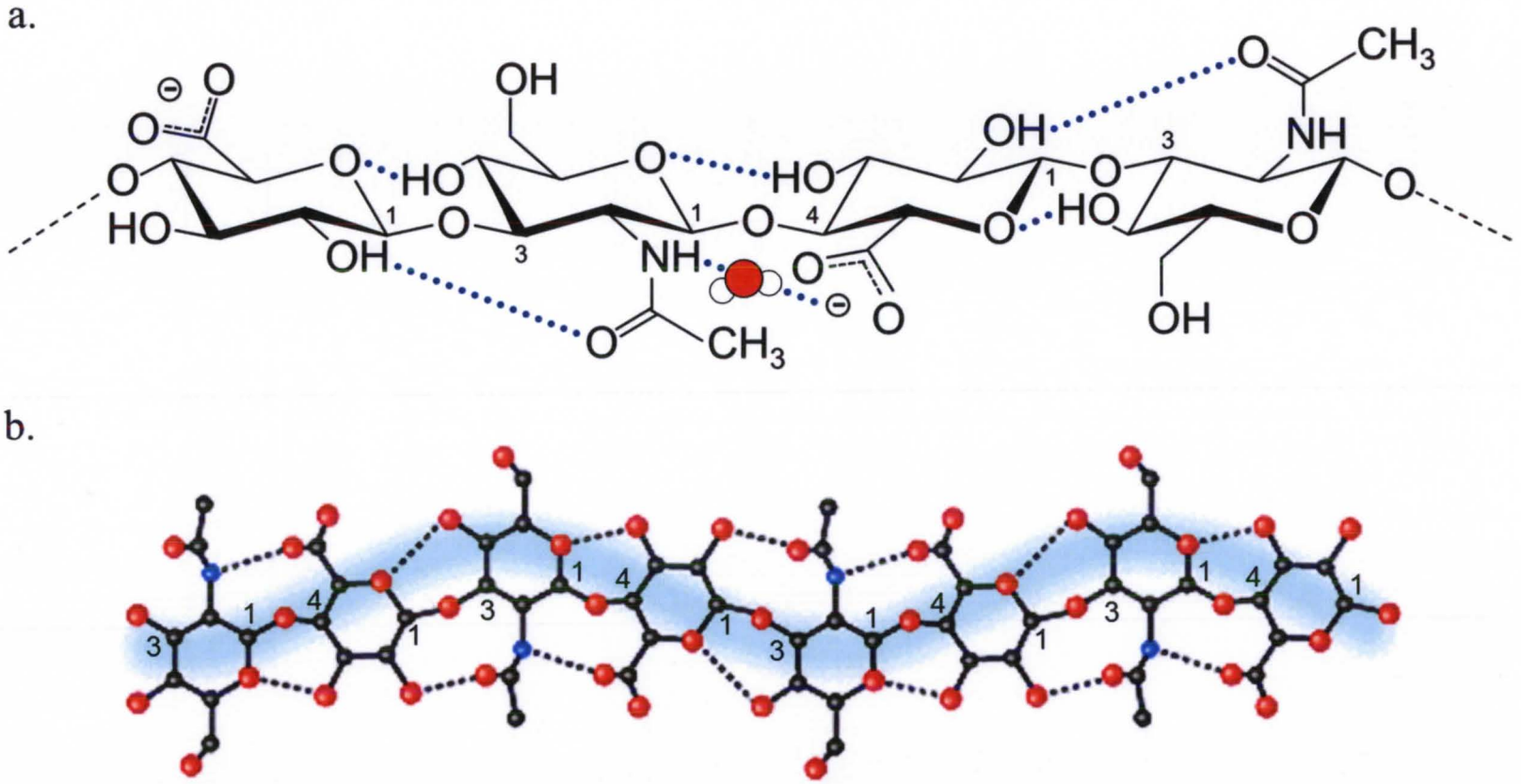

Figure 1-7. Possible intramolecular/intrachain H-bonds of HA, shown in a tetrasaccharide-size repeating unit of HA, based on computer simulations. H-bonds are indicated by the dotted lines. a) Linear depiction featuring a .water bridged H-bond b) Conformation induced due to alternating linkages and H-bonding. (Source: b. Adapted from http://glycoforum.gr.jp/science/hyaluronan/HA02/HA02E.html and Atkins, E. D. T., *et al. International Journal of Biological*

the chain, H-bonding along the chain also generates hydrophobic patches,[72] resulting from the axial hydrogens forming a non-polar, relatively hydrophobic, face while the equatorial side chains form a more polar, hydrophilic face (Fig. 1-8).[52] This creates a 'twisting ribbon-like' structure for HA with alternating hydrophilic and hydrophobic faces (Fig. 1-8b).[52] Rotary shadowing electron microscopy of human and bovine VH detected lateral aggregates of HA in a three-dimensional network.[72] Chain-chain interactions are believed to result from intermolecular H-bonding and/or the association of hydrophobic patches between HA molecules. Intermolecular H-bonding is also responsible for the high viscosity associated with HA.

An important property of HA is steric exclusion, which results from the large molecular domain and entanglement of HA chains.[7] Steric exclusion allows the passage of some molecules, but not others, based on size and shape. Smaller species (i.e. ions) are able to diffuse freely through the VH while the flow of larger molecules (i.e. proteins) is hindered or completely restricted. Additionally, HA solutions are markedly non-ideal in terms of osmotic pressure.[73] Indeed, whereas in an ideal macromolecular solution the osmotic pressure increases linearly with concentration, the pressure of HA rises more rapidly with increasing concentrations (1-10 mg/mL). For this reason, HA acts as an osmotic buffer so that a small decrease in the concentration of HA, due to water influx into the matrix, leads to a marked drop in osmotic pressure and causes water to leave the matrix.[74,75]

Within the VH, HA forms a three-dimensional network interspersed among collagen fibrils, and the network can vary depending on whether the helix is in a compressed or extended configuration.[76] The degree of hydration has a significant influence on the size and configuration of the HA molecular network. Remarkably, the

a.

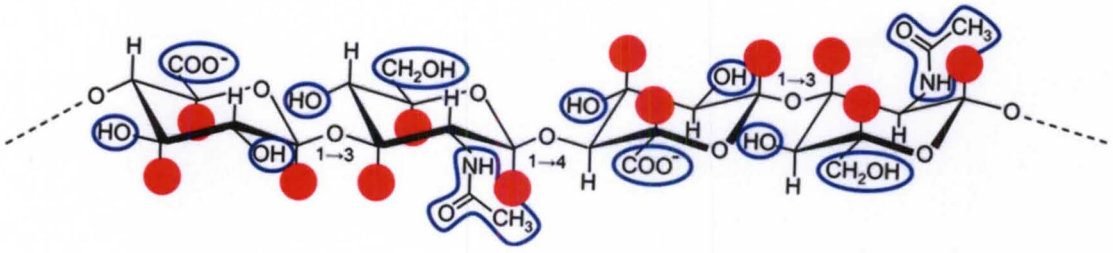

b.

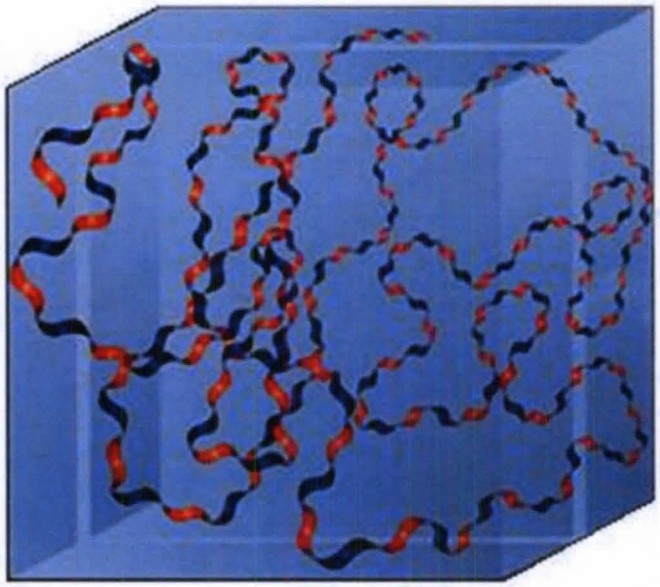

Figure 1-8. Hydrophilic (blue) and hydrophobic (red) patches of the HA polymer at the molecular level (a) and in solution in a 3D domain (b). (Source: b. Adapted from http://glycoforum.gr.jp/science/hyaluronan/HA01/HA01E.html)

volume of the unhydrated HA molecule is about 0.66 cm^3/g whereas the hydrated specific volume is 2,000 to 3,000 cm^3/g (more than three orders of magnitude increase)[76] Hyaluronan also interacts with the surrounding mobile ions and can undergo changes in its conformation.[46] A decrease in the surrounding ionic strength can cause the anionic charges on the polysaccharide backbone to repel one another, resulting in an extended configuration of HA.[2] An increase in ionic strength allows closer association of HA molecules causing a compressed configuration that can lead to contraction of the entire VH body. As a result of HA's entanglement and immobilization within the VH collagen fibril matrix, this mechanical force can be transmitted by collagen fibrils to the surrounding ocular structures (i.e. retina, optic disc) and may be important in certain pathological conditions that feature fluctuations in ionic balance and hydration (i.e. diabetes).[2]

The VH gel is heterogeneous in nature and concentration gradients of several molecular components exist within the various regions.[7] The highest concentration of HA is found in the posterior VH and its concentration decreases anteriorly, with the lowest concentration found in the retrolental area.[22] Throughout the life span leading to the adult stage, changes in HA concentration occur. There is a four-fold increase in HA concentration during the first two decades of life, and then it remains steady (~ 0.2 mg/mL) past the age of twenty until around 70 years of age when it again increases (> 0.3 mg/mL).[25] The large increase of HA concentration early on in life parallels the period of eye growth but the synthesis of HA far exceeds the rate of eye enlargement. As HA synthesis stabilizes, concentrations remain constant due to escape of HA into the anterior segment of the eye and possible re-uptake by hyalocytes.[2] With age, liquefaction occurs

and the volume of the liquid VH increases. The relative increase later on in life represents the accumulation of HA in the liquid portion of VH.[2]

Other Glycosaminoglycans. A small portion of the collagen in the VH is in the form of a proteoglycan where it contains a covalently bound chondroitin sulfate (CS) side chain. These CS side chains can act to bridge neighboring collagen fibrils as illustrated in Figure 1-9.[7] Most of the CS in the VH is in the form of the versican proteoglycan which is believed to form complexes with HA as well as with microfibrillar proteins such as fibulin-1 and fibulin-2.[4] Another GAG, heparan sulfate was detected in bovine VH and in chick VH. However, it is not clear whether it is a true component of the VH or a contaminant from adjacent basement membranes, such as those in the internal limiting lamina of the retina.[4]

Collagen, Other Proteins, and Amino Acids

Collagen is the major structural protein of the VH. Within the VH, these collagen fibrils are orientated in specific directions (Fig. 1-3). Individual collagen molecules assemble to form major collagen fibrils which can be visualized by electron microscopy (Fig. 1-10).[77,78] These fibrils are rope-like in nature, with a diameter of 10-20 nm, and are characterized by high tensile strength.[79] They are heterotypic in that they contain molecules of different types of collagen. Collagen fibrils in the VH are characterized by protruding N-propeptide regions extending outward from the collagen fibril. These extensions result from the incomplete processing of procollagen by collagenase and may mediate interactions with other ECM components of the VH. As mentioned previously, one of the outer collagen types is a proteoglycan containing covalently bound CS side chains which often bridges neighboring collagen fibrils.[80] In this way, adjacent collagen fibrils appear to form a ladder-like configuration (Fig. 1-9).[2]

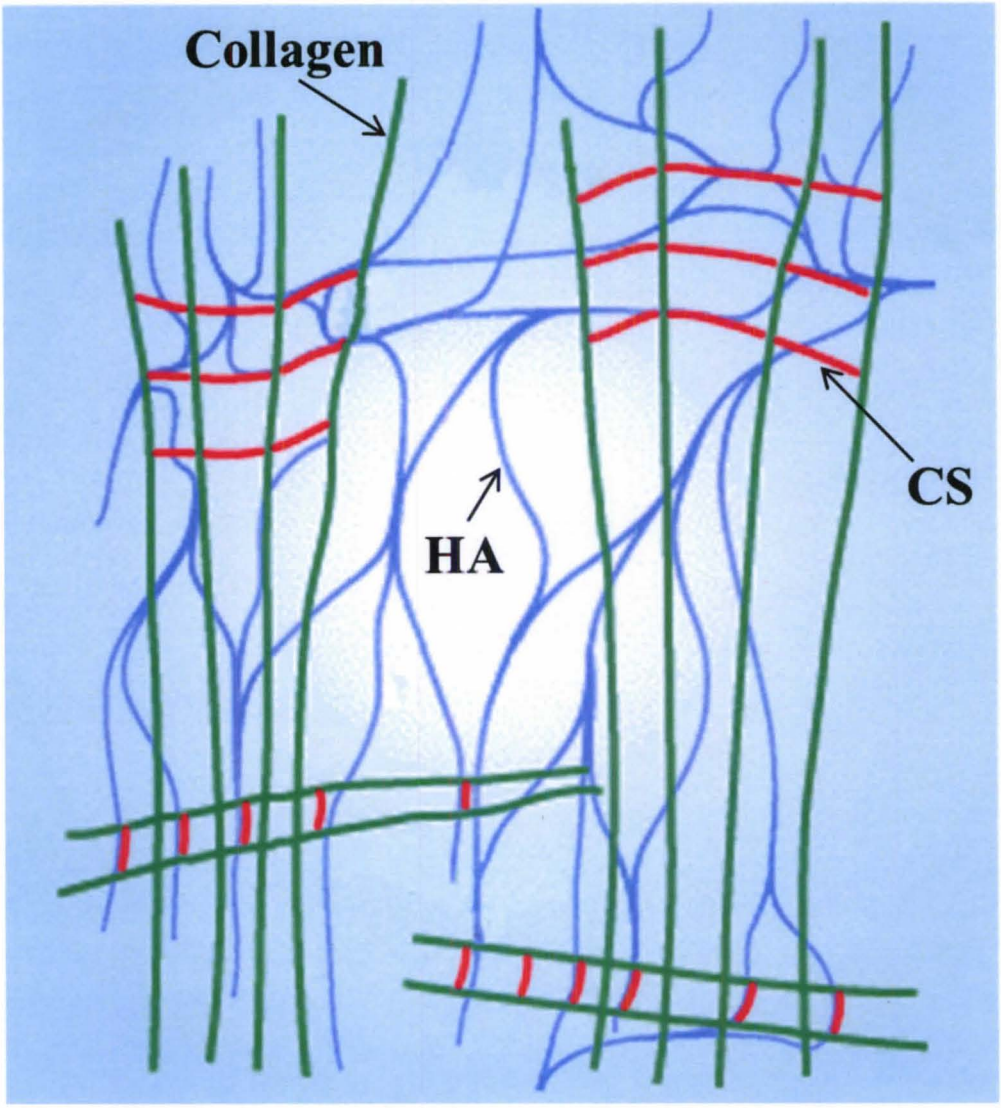

Figure 1-9. Molecular organization of hyaluronan, HA (blue), collagen (green), and chondroitin sulfate, CS (red) in the VH. (Source: Adapted from http://www.glycoforum.gr.jp/science/hyaluronan/HA02/HA02E.html and Scott, J. E. *Eye* **1992**, *6*, 553–555.[80])

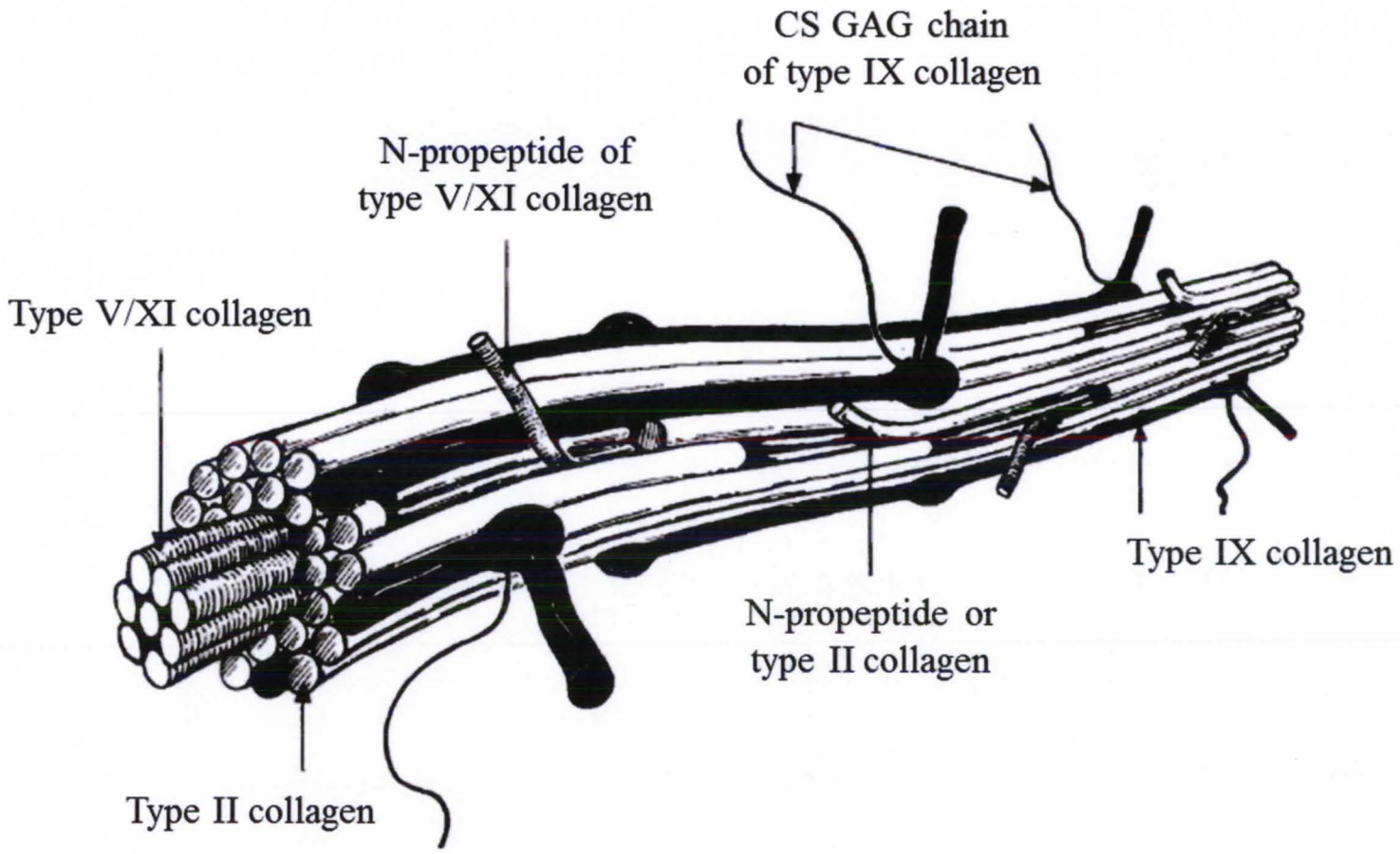

Figure 1-10. Major heterotypic collagen fibril in the VH (not to scale). (Source: Adapted from Bishop, P. *Eye* **1996**, *10*, 664–670.[81])

Collagen is synthesized by both hyalocytes and by retinal cells.[82] The highest concentration of collagen is found in the VH base, followed by the VH cortex.[2] The lowest concentration of collagen is seen within the central VH. Balazs and Denlinger originally determined that collagen concentration decreases during the first decade of life as a result of no net synthesis of collagen as the eye grows.[25] The discovery of procollagen,[83] the presence of immature cross-links,[84] and morphological evidence of vitreous collagen synthesis by the peripheral retina in the adult eye[43] suggest some (albeit at a very low-level) postnatal synthesis of collagen.[85] From 20 to 40 years of age, there are no significant changes in collagen content which is consistent with the long life span of the molecule and its lack of significant turnover.[25] However, collagen concentration begins to increase past the age of 40 as significant liquefaction begins to occur and the portion of gel VH decreases.

Other Proteins. In addition to collagen, non-collagenous structural proteins are found in the VH. These include fibrillin-containing microfibrils (which are more abundant than type VI collagen microfibril), opticin, and VIT1.[4] Opticin is found bound to the surface of collagen fibrils and is believed to be important in collagen fibril assembly and in preventing aggregation of adjacent collagen fibrils into bundles.

Soluble proteins also exist and have been found to resemble serum proteins. This finding led investigators to conclude that the soluble proteins of VH derive from plasma and are constantly renewed. According to Balazs, the glycoprotein content in the VH is high, as these constitute 20% to the total non-collagenous protein content. Sialic acid-containing glycoproteins are more numerous in the VH than in the serum, and more abundant among non-collagenous VH proteins. Cartilage oligomeric protein (COMP) is an acidic glycoprotein present in the VH but its function is currently not known.

Amino acids. Amino acids are present at concentrations one-fifth of those found in plasma.[86] The highest concentrations are found anteriorly.[2] This may be due to uptake and utilization of amino acids by the retina and led Reddy to propose that the VH acts as a metabolic repository for retinal protein metabolism.[87]

Other Compounds

Other molecules exist in the VH, albeit at very low concentrations. Concentration gradients are typically found with higher concentrations in the anterior region. Various ions are present; sodium, chloride, and bicarbonate ions are the most abundant. Low-molecular weight (MW) compounds (i.e. amino acids, glucose, lactic and ascorbic acids) have also been detected within the VH. Interestingly, ascorbic acid is found at concentrations ten times greater than those found in serum.[2,88] It is thought to be actively secreted by the ciliary body epithelium.[89,90] The purpose of such high concentration may relate to its ability to absorb UV light and to serve as a free-radical scavenger that may protect the VH, retina, and lens from the negative effects of metabolic and light-induced generation of radical oxygen species.[39,91,92] Lipids have been detected in the VH. Because of the relevance of the presence of lipids in the VH in this project, this topic is discussed in the next section.

LIPIDS

Our group has been studying lipids for over two decades and has successfully detected and analyzed them in mammalian lens and other biological tissues.[93–97] However, our group has yet to study lipids in the VH. Of special interest to this project are glycero-, and sphingo- phospholipids (PLs and SLs), glycolipids (GLs), and their metabolites (Fig. 1-11).

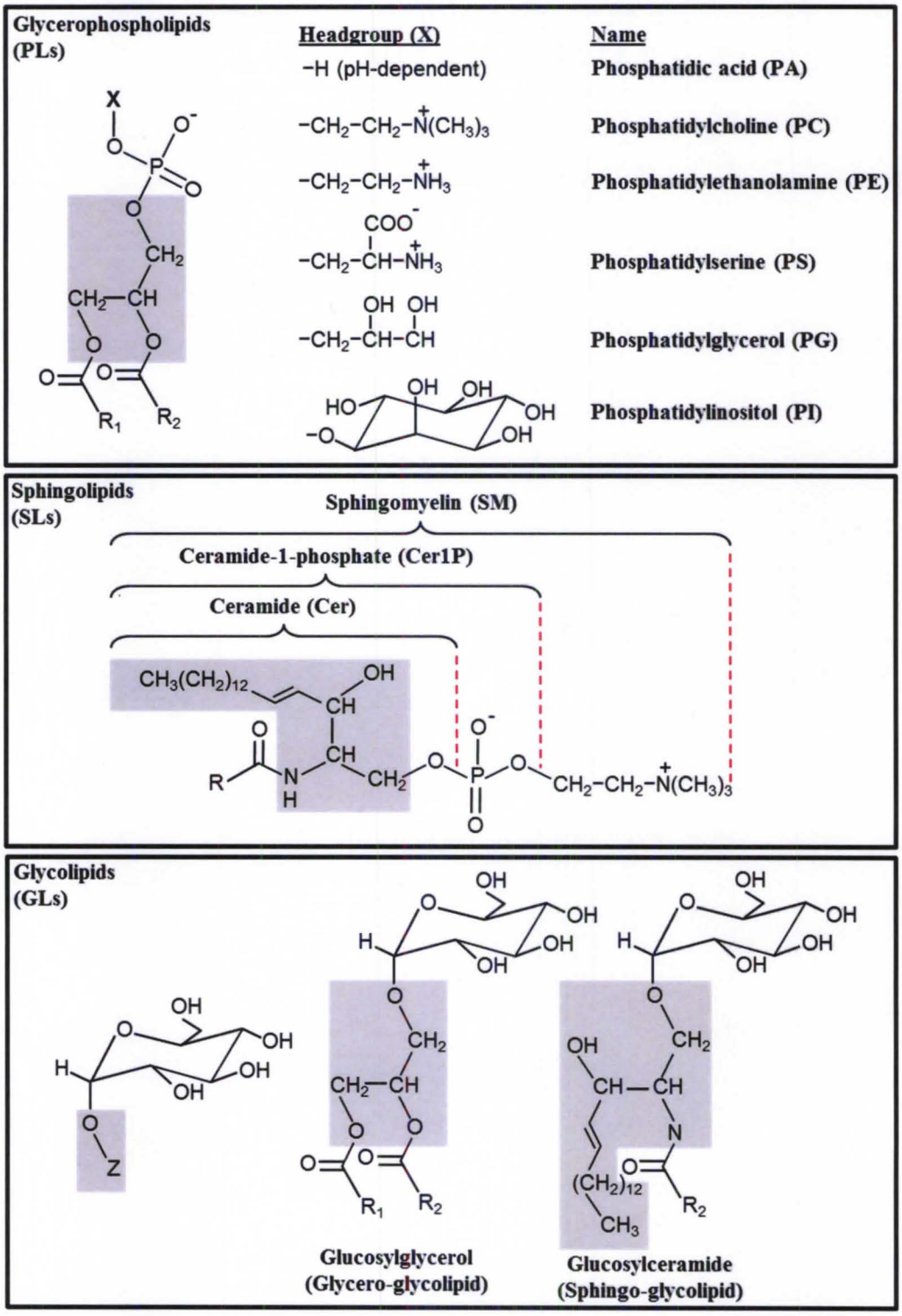

Figure 1-11. Lipid structures and classifications: glycerophospholipids (PLs), sphingolipids (SLs), and glycolipids (GLs). R_1 and R_2 designate fatty acid acyl chains. Glycerol and sphingosine backbones are shown in gray.

Lipids in the VH

In the 1960s, Renshaw and coworkers analyzed the fatty acid composition of lipids in saponified tissues of different parts of the ox eye.[98] Fatty acids were subsequently extracted, methylated, and analyzed by gas chromatography (GC). In the VH, fatty acids were determined to be present at a concentration of 5.3 mg/g dry weight. Of all the fatty acids present, palmitic (16:0) acid was the most abundant (21%), followed by 20% linoleic (18:2), 17% oleic (18:1), and 12% stearic (18:0) acids. Interestingly, linoleic acid was reported to be present in amounts almost three times greater than those found in the aqueous humor, and oleic acid was found in quantities twice as high as those in the aqueous humor. On the other hand, larger fatty acids, containing chain lengths of twenty or more carbons, were present in significantly less amounts in the vitreous body compared to the aqueous humor. Broekhuyse found the total lipid content to be high in the retina and relatively low elsewhere in the eye (i.e. lens and VH).[99] He extracted PLs from calf eyes using chloroform-methanol mixtures, labeled them with ^{32}P, and quantitatively analyzed them through 2D thin layer chromatography (TLC). He found the most abundant PLs in the VH to be phosphatidylcholine, PC, (36.0%); sphingomyelin, SM, (30.5%); and phosphatidylethanolamine, PE, (15.3%). Lyso-phosphatidylcholine (LPC) was shown to make up only 0.5% of total lipid content in the VH.

In 1975, Swann *et al.* found significant quantities of fatty acids in rabbit VH, particularly palmitic (16:0) and stearic acids (18:0).[100] With the use of gas chromatography (GC), they analyzed an insoluble protein fraction (85% collagen) that was obtained after melting and separation by centrifugation. Because they had to derivatize the lipids to allow for GC analysis, the actual entity of the lipids containing these fatty acids could not be determined.

In 1976, Kim and Cotlier, studied the PL distribution and fatty acid composition in the aqueous humor, lens, and VH of rabbit using TLC and GC analysis.[101] They determined the major PLs in the VH to be phosphatidylcholine (PC) and phosphatidylethanolamine (PE) and the major fatty acids from PC to be palmitic acid (16:0) and myristic acid (14:0).[101] They determined the composition of PLs in lens and VH to be remarkably similar and suggested that PE may derive from lens or retinal tissue.[101] In addition, they found the levels of PLs in all these tissues to be dramatically lower than those in serum.[101]

In 1986, the fatty acid compositions of VH from canine and human eyes were studied.[102] It was determined that the fatty acid composition of VH is similar in both species. They found that 55% of the acyl chains were saturated with the major components being palmitic and stearic acid. Among unsaturated fatty acids, linoleic (18:2) and arachidonic (20:4) acids were the most abundant.[103] Interestingly, the total content and composition of fatty acids in human VH did not change significantly between the ages of 37 and 82 years.

Glycolipids in the VH

Gaucher disease is a lipid-storage disease caused by the deficiency of glucocerebrosidase and leads to high levels of glucosylceramide.[104–107] This disease has been shown to affect the VH. Indeed, VH opacities were found to be present in approximately 3% of a series of 80 patients with type 1 Gaucher disease.[108] Only those who had undergone a spleenectomy showed a tendency to form VH aggregates. Grabowski *et al.* suggested that this is probably due to the presence of higher levels of circulating glucosylceramide in these patients, thus resulting in manifestations in unusual systemic locations, such as the eye.[108] The pathophysiological mechanism of

glucosylceramide deposition in the VH cavity is unclear. Tketomi *et al.* analyzed the SLs in the VH of patients with Gaucher disease using matrix-assisted laser desorption ionization mass spectrometry (MALDI-MS).[109] They found ions with *m/z* values corresponding to different ceramide monohexoside (CMH) species. In addition, they detected several species of sphingomyelin (SM).[109] Both CMH and SM were found to have oleoyl (18:1) acyl chains, but with differences in the location of the site of unsaturation. The results were as follows: a) the *m/z* values of the ions found in the mass spectra for the control and the Gaucher-disease patient corresponded to different SM species, and b) the mass spectrum of the VH from the Gaucher-disease patient showed additional ions with *m/z* values corresponding to different CMH species. The researchers indicated that the accumulation of CMH in VH bodies from Gaucher disease patients could be easily detected with the MALDI-MS.

HA-LIPID INTERACTIONS

To date, very few reports have explored HA in combination with hydrophobic molecules, such as lipids. Some investigators have reported that HA can interact with the hydrophobic regions of molecules such as lecithin[110] and the hydrophobic surface of graphite.[111] It is likely that these interactions occur through the hydrophobic patches on HA. However, no studies have been undertaken to examine the exact nature of the interactions at the atomic level.

Biological interactions between HA and lipids have come to light in recent studies. Lipoproteins and HA have been isolated from human aorta fibrous plaque lesions digested by elastase and fractionated by gel-filtration chromatography (GFC).[112] Fractions were analyzed by molecular sieve chromatography and ultracentrifugation and found HA associated with lipoproteins. The complete absence of other GAGs associated

with the lipoproteins suggests that the HA-lipid interaction may play a role in the aggregation and entrapment of macromolecules in arterial connective tissue. Ionov and coworkers studied the interactions of lipid monolayers with HA to gain insight into HA's interactions with the cell membrane by thermodynamic and x-ray diffraction analysis.[113] They found that HA was capable of modifying the membrane structure. The presence of charges induces a specific organization of HA at the water/membrane interface. This effect may in turn influence the membrane transport processes.

Antioxidative properties of HA have also been studied in biological systems. Modified HA (HyPE), HA polymer covalently linked to PE, was found to interact with low-density lipoproteins (LDL) as indicated by photon correlation spectroscopy, and broadened ^{1}H NMR signals of the LDL's PLs.[114] The interaction was shown to inhibit copper-induced oxidation of the LDL polyunsaturated fatty acids. The small amount of HyPE (just a tenth of the concentration of PLs in LDLs) required to inhibit all LDL oxidation indicates the antioxidative behavior of HyPE cannot be attributed to competitive binding of Cu to HA. Instead, formation of a sugar network around the LDL has been proposed. The antioxidative effect was large for low-MW HA and only slight for high-MW HA. This information may be useful in the prevention of atherosclerosis which involves the oxidation of LDL's. Unmodified HA polymer and fragments were also shown to exhibit antioxidant properties in lipid model systems (stratum corneum intercellular lipid matrix) exposed to ultraviolet (UV) radiation by reacting with radicals and reducing the amount lipid peroxidation secondary products formed.[115] Mass spectrometric studies showed that HA was degraded after acting as an antioxidant, and electron paramagnetic resonance (EPR) studies suggested an iron chelation to HA as the mechanism responsible for its antioxidant behavior.

Modified liposomes containing covalently bound HA have been investigated for their application in drug delivery. These modified liposomes offered advantages of long circulation and high affinity to overexpressed recognition sites in tumors. It has also been shown that HA acts as a cryoprotectant for lyophilized liposomes, preventing the fusion of unilamellar liposomes into multilamellar liposomes.[116] It was suggested that the mechanism involves retention of structure-stabilizing H-bonds at the liposomal surface upon lyophilization. PL-HA microparticles have been used to encapsulate dexamethasone, an anti-inflammatory drug used in the treatment of acute and chronic posterious segment eye diseases (i.e. uveitis) and in cases of neovascularization (i.e. proliferative vitreoretinopathy and subretinal neovascularization).[117] In the absence of HA, dexamethasone led to strong particle aggregation, whereas in the presence of HA, aggregation was practically suppressed. Hyaluronan also did not affect the release kinetics of dexamethasone. Another study looked at the interaction and adsorption of HA onto the surface of a hydrophilic corticosteroid drug.[118] The extent of adsorption was influenced by the conformation of the HA molecules in the solution from which adsorption occurred. Significant adsorption occurred in HA solutions of low concentrations (0.1% w/v) due to hydrophobic interactions with patches along the HA chains. At higher concentrations, adsorption was reduced due to the formation of a tertiary network in which the hydrophobic patches are used for intermolecular interactions.

The interactions between high-MW HA with di-palmitoyl-phosphatidylcholine (DPPC) liposomes in aqueous buffer were studied using electron microscopy and rheometric analysis.[119] The supramolecular structure resulting from incubation of HA with DPPC liposomes was visualized by rotary shadowing electron microscopy and

revealed "large, holey, and somewhat overlapping membranes interconnected or locked by HA threads". In the presence of DPPC, HA experienced a decrease in viscosity making it more labile to degradative enzymes.

The only models for the interactions between HA and lipids have been proposed by Ghosh and coworkers. In 1994, they studied the chain flexibility of HA in the presence and absence of PLs using ^{1}H NMR spin-spin relaxation measurements of the acetamido-methyl protons (based on the methods of Darke and Finer[120]; discussed in Chapter 2).[121] Sonication of high- and low-MW HA polymer with DPPC for periods of up to 60 minutes, markedly increased chain flexibility. The interactions were independent of HA concentration (up to 0.5 mg/mL) or MW but were dependent on the sonication times. They suggested a possible ionic interaction between HA's negatively-charged carboxylate and DPPC's positively-charged choline moiety. Moreover, they proposed that DPPC molecules compete for hydrophobic patches along the HA chain which are normally responsible for intra- and interchain interactions which confer stiffness to the HA molecules (Fig. 1-12a). Multi-angle laser light scattering (MALLS) provided evidence for the increase in MW of HA after sonication with DPPC. This is of biological relevance in synovial fluid where inflamed joints show substantially elevated PL content. In 1997, they applied negative stain and rotary shadowing electron microscopy to study HA of different MWs in PL suspensions (DPPC or egg lecithin) that were in the form of either unilamellar or multilamellar vesicles.[110] Both unilamellar and multilamellar vesicles, in the presence of high-MW HA, gave rise to largely perforated membrane-like structures and 12 nm thick cylinders ('rollers') with a tendency to aggregate and form sheets. Low-MW HA appeared to induce fragmentation of liposomes and the formation of a few short rollers. They proposed a model for the roller structure where HA molecules

a.

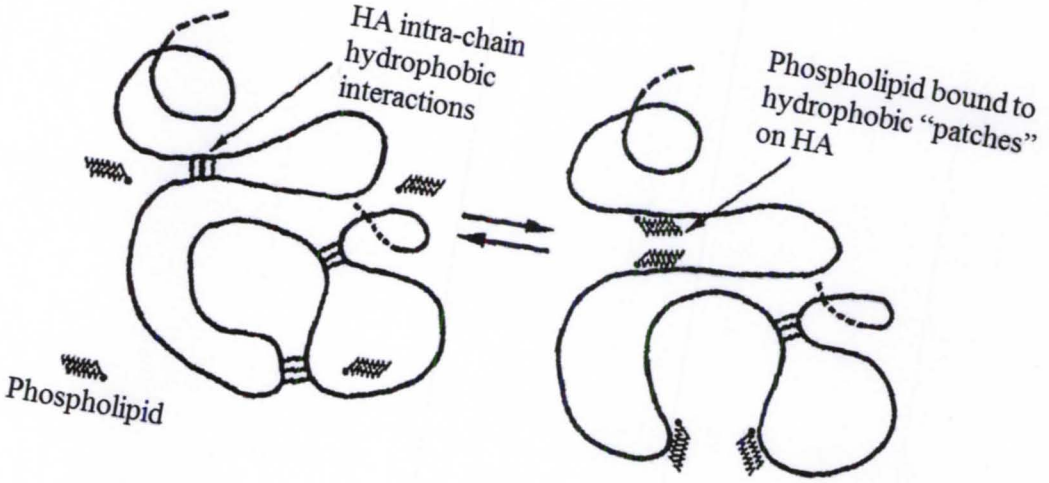

b.

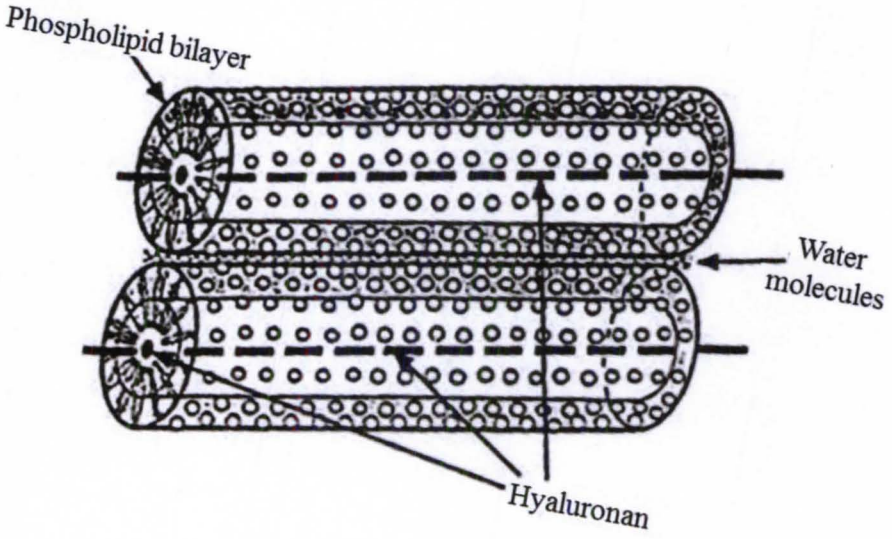

Figure 1-12. Previously proposed models for the interaction of HA and PLs inferred from a) ^{1}H NMR peak widths and b) electron microscopy. (Source: Adapted from a) Ghosh, P. *et al. Heterocycles* 1994, *38*, 1757–1774.[122] b) Ghosh, P., *et al. Journal of Structural Biology* 1997, *120*, 1–10.[110])

form a central filament surrounded by a PL bilayer radiating outward from the HA central core (Fig. 1-12b). The charged ends, corresponding to the PL headgroup, allow for the formation of a thin layer of water between adjacent cylinders. These studies, however, only skim the surface of possible interactions between HA and DPPC and do not address the changes that may occur at the atomic/molecular level.

REASONS FOR THIS PROJECT

The liquefaction of the VH, which is associated with aging, begins as early as the second decade of life and almost 50% of the VH is liquefied by the 8^{th} and 9^{th} decades of life. Additionally, diabetic patients develop VH degeneration earlier in life. Liquefaction is the result of the collapse or contraction of the collagen/HA network, the major component of the VH. However, the age-related changes that cause this liquefaction are not known at the molecular level. Previous work from our group has shown significant age-related changes in the composition of human lens lipids. Whereas fetal lens epithelial cells contain significant amounts of lipids with high degree of unsaturation, adult human lens fibers are largely void of unsaturated hydrophobic tails. This is a consequence of the preferential loss of unsaturated species by enzymatic degradation and/or chemical oxidation to create unsaturated and oxidized fatty acid degradation products.[12] The fate of these lipid metabolites, as well as the fate of retinal lipid metabolites, is not known. The possible effects that they may have on the VH remain to be explored. It is possible that they may find their way to the VH where they could undergo further oxidation and disrupt the biomatrix network by causing local increases in the acidity and/or by intercalation with the matrix. As a result, the forces that hold the water/collagen/HA network together may be compromised leading to liquefaction of the VH. Although much

is known about the structure and properties of HA, very little is known about its possible interactions with lipids.

Chapters 2 and 3 focus on NMR model studies of the HA disaccharide and polymer, respectively. Changes in chemical shifts and line widths are followed with changes in temperature and the presence of lipids. Because we wish to analyze lipids *in situ* by MALDI-MS in human VH, Chapter 4 explores first *in vitro*, the potential effects of HA and lipids on their relative ionization efficiencies (RIE's) in model studies. Then the initial mass spectral studies of human VH are reported. Finally, Chapter 5 highlights the main findings of this project and possible directions of future studies.

CHAPTER 2

NMR MODEL STUDIES OF HYALURONAN DISACCHARIDE

INTRODUCTION

This chapter focuses on the NMR analysis performed on a mixture of the α and β anomers of the unsaturated form of the repeating unit of hyaluronan (HA). This disaccharide (ΔDiHA) contains an N-acetylglucosamine (GlcNAc) and a glucuronic (ΔGlcU) acid unit which features a double bond between C4 and C5 of GlcU (ΔGlcU-(1→3)-GlcNAc). The power of 'inverse' two-dimensional NMR experiments is highlighted. This section provides information on previous NMR studies performed on HA oligosaccharides and discusses the basic principles of NMR spectral methods (both 1D and 2D).

NMR Spectroscopy Background

1D-NMR: Basic Principles and Chemical Information Obtained

Basic Principles. Nuclear magnetic resonance (NMR) spectroscopy is a powerful technique for determination of molecular structure and conformation. It rivals only X-ray crystallography in the precise structural information it can provide.[123] However, NMR can be applied to molecules in aqueous solutions that mimic physiological conditions, so that the effects of concentration, temperature, pH and interactions with other biomolecules can be studied.[124–126] This technique is based on absorption of radiofrequency (rf) radiation by nuclei with a non-zero quantum spin number ($I \neq 0$).[125]

In the studies presented in this dissertation, one- and two-dimensional experiments were carried out for the proton (^{1}H), carbon (^{13}C), and phosphorus (^{31}P) nuclei within the sample. These nuclei all have a spin quantum number I = 1/2 which leads to two possible orientations for the spins.[125] In the presence of a large magnetic field, the energy levels corresponding to these orientations are split. The lower energy state (α) has a (slight) excess of nuclei that when irradiated with radiation whose energy matches the difference between the two levels (resonance condition), absorb this energy and the spins are flipped into the higher energy state (β).[125] The relaxation processes allow the excited spins to return to their equilibrium state (excess of α spins), as described below. The free induction decay (FID) signal is recorded as a function of time and converted to the frequency domain by Fourier transform (FT).

Chemical Information Obtained. The specific energies that are absorbed depend on the electromagnetic environment (nearby electrons and nuclei) of specific nuclei in a molecule.[126] From the analysis of chemical shifts (δ), coupling constants (J-values), and integrations of the various resonances, molecular identification is possible and conformational details can be inferred.

Relaxation processes allow nuclei to return to the lower energy state and reflect molecular motion.[125] Spin-lattice and spin-spin relaxation with time constants T_1 and T_2, respectively, govern how fast relaxation can take place. Spin-lattice (longitudinal) relaxation occurs through the re-establishment of the Boltzmann distribution of spin states whereas spin-spin (transverse) relaxation occurs through the loss of phase coherence among nuclei. Both T_1 and T_2 depend on the tumbling or correlation time (τ_c), the time it takes for a spin to rotate one radian (Fig. 2-1).[127] Larger molecules tumble more slowly (longer τ_c) and have fast spin-spin relaxation (small T_2). Spin-spin relaxation

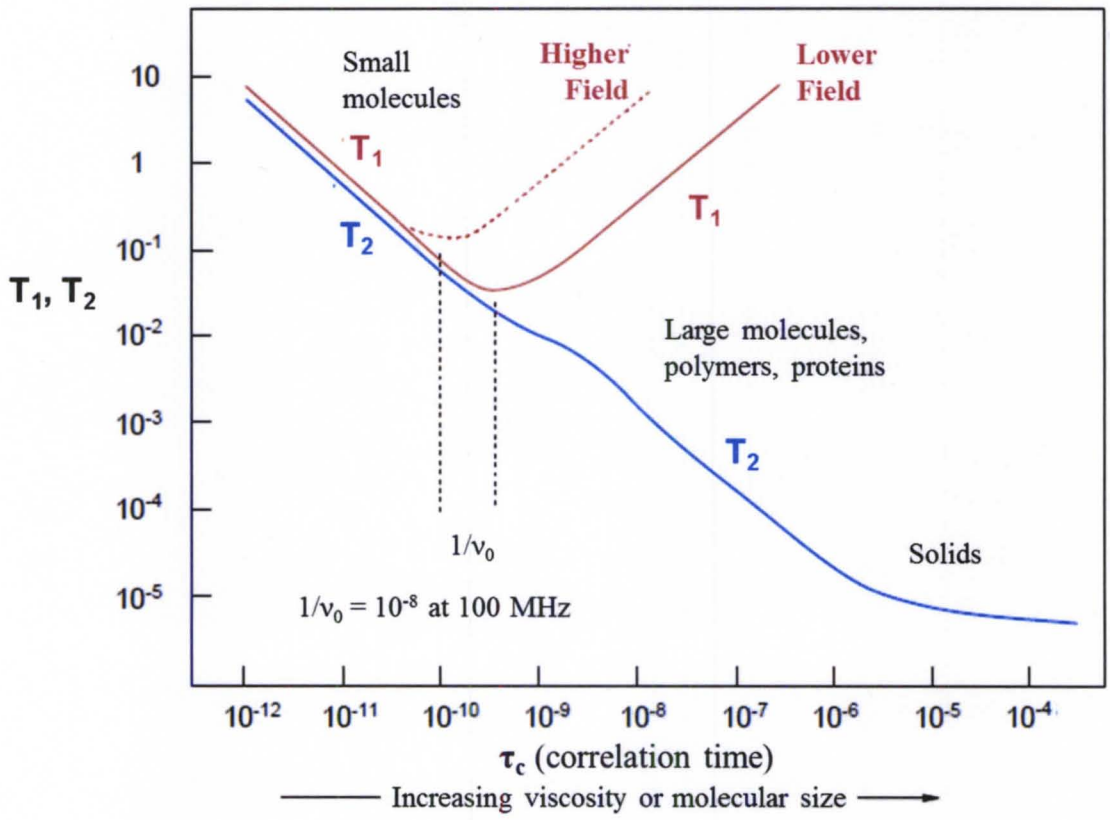

Figure 2-1. Relationship between correlation (tumbling) times (τ_c) and relaxation times (T_1 and T_2). (Source: Adapted from http://www.chem.wisc.edu/areas/reich/nmr/08-tech-01-relax.htm)

time (T_2), and hence motion, can be inferred from the resonance linewidths at half-height ($\Delta\nu_{1/2}$) according to:

$$\Delta\nu_{1/2} = \frac{1}{\pi T_2}$$

Variations in T_2 reflect changes in relative molecular motions (i.e. flexible vs. rigid) and are observed spectrally as the narrowing (flexible, long T_2) and broadening (more rigid, short T_2) of the resonances.[127] Aggregates and larger molecules have longer correlation times (τ_c) and small T_2 as they lose their phase coherence faster and therefore give rise to broad peaks.[127]

Besides the information obtained on chemical environment and motions of spins within a molecule, the strength of H-bonds can be inferred from temperature studies in which changes in chemical shift for N-**H** and O-**H** resonances are measured as a function of temperature.[128–134] The rate of change ($\Delta\delta/\Delta T$) is referred to as temperature coefficient and can be used to assess the contribution of intra- and intermolecular H-bonds to molecular structure.[129,133] Decrease in chemical shifts (upfield shifts) are expected upon increasing the temperature due to weakening of H-bonds with solvent molecules (or in the case of bigger molecules, a moiety farther away in the same molecule). As the H-bond weakens, the degree of deshielding of the donor proton diminishes quickly if the H-bond is of intermolecular nature. Therefore, large (and negative) temperature coefficients suggest the involvement of the monitored proton in inter-molecular H-bonds (with either the solvent or another molecule of itself) while small coefficients reflect intra-molecular H-bonds in the molecule.[133]

2D-NMR: Basic Principles and Chemical Information Obtained

Basic Principles. Two-dimensional NMR spectroscopy is used to study interactions of various types between two nuclei. The phase coherence is allowed to evolve in one spin and then magnetization is transferred, after rf (radiofrequency) pulses, to a second spin during a mixing time.[127] The 2D spectra contain two chemical shift axes and from the observed off-diagonal (cross) peaks, correlations between nuclei can be made. Interactions (magnetization transfers) can occur either through bond or through space.

Chemical Information Obtained. Through-bond 2D conventional experiments include ^{1}H-^{1}H COrrelation SpectroscopY (COSY), ^{1}H-^{1}H TOtal Correlation SpectroscopY (TOCSY), and HETeronuclear CORrelation Spectroscopy (HETCOR). COSY and TOCSY both provide information on correlations (connectivities) between different protons in the same molecule. COSY provides vicinal ^{1}H-^{1}H couplings while TOCSY provides long-range (up to three-four bonds) ^{1}H-^{1}H couplings.[127] HETCOR provides information on the connectivity between protons and a heteroatom, often ^{13}C or ^{15}N. In HETCOR, the ^{13}C magnetization is directly detected. Because of the low abundance of ^{13}C and the smaller value of its magnetogyric ratio γ ($\gamma_{13C} \sim 0.25\ \gamma_{1H}$), the sensitivity of this approach is not very high.[127] However, new techniques for heteronuclear 2D experiments have improved sensitivity significantly, as presented in the next section.

Through-space interactions (< 5 Å) can be detected through Nuclear Overhauser Effect SpectroscopY (NOESY) and Rotating frame Overhauser Effect SpectroscopY (ROESY).[127] Spatial relationships among protons (homonuclear NOESY) and other

heteroatoms (hetero-nuclear NOESY) can be analyzed to obtain structural/conformational details on a molecule or a molecular ensemble.

Inverse Heteronuclear 2D NMR. Inverse 2D NMR experiments offer enhanced sensitivity relative to more traditional heteronuclear experiments such as HETCOR. This is a result of direct detection of ^{1}H nuclei and indirect detection of heteroatoms such as ^{13}C or ^{15}N.[127] The observed signal intensity increases proportionally with γ^2 of the detected nuclei.[126] The large γ for ^{1}H (four times that of ^{13}C) results in increased signal strength by a factor of sixteen. However, the noise in the signal increases with the square root of the detected frequency. Therefore, since the precession frequency of ^{1}H nuclei is four times greater than that for ^{13}C, the noise increases by a factor of two. Overall then, the signal-to-noise ratio (S/N) is eight times greater in an inverse ^{1}H-^{13}C experiment.[126]

As mentioned above, inverse techniques take advantage of this difference in γ by directly detecting protons. The high isotopic abundance of ^{1}H is irrelevant here because detection is dependent on the number of ^{1}H-^{13}C pairs in the sample, which is limited by the natural abundance of ^{13}C. Another advantage is that a proton can only be attached to one ^{13}C so that complexities of refocusing ^{13}C antiphase coherence (caused by different optimal times for CH, CH_2, and CH_3) are avoided.[126] A proton coupled to ^{13}C is always a doublet and never a triplet or quartet. The disadvantage to inverse 2D experiments is the appearance of undesirable ^{12}C artifacts that result when ^{1}H nuclei are observed directly, because both the 1.1% of protons attached to ^{13}C and the 98.9% attached to ^{12}C nuclei produce a signal.[126] The large signal corresponding to protons attached to ^{12}C will have a much smaller J-value than that of the signal corresponding to protons attached to ^{13}C (~150 Hz).

Heteronuclear single quantum correlation (HSQC) experiments examine one-bond correlations between different nuclei (i.e. ^{13}C and ^{1}H) through the evolution and transfer of phase coherence. [127] In a two spin-paired system, single quantum coherence refers to the simple magnetization of one spin changing its state ($\alpha \rightarrow \beta$ or $\beta \rightarrow \alpha$). In heteronuclear multiple quantum correlation (HMQC) experiments, zero quantum ($\alpha\beta \rightarrow \beta\alpha$ and $\beta\alpha \rightarrow \alpha\beta$) and double quantum ($\alpha\alpha \rightarrow \beta\beta$ or $\beta\beta \rightarrow \alpha\alpha$) coherences are allowed to evolve and converted back to the single quantum coherence that is detectable.[126]

Additionally, inverse experiments have the ability to see long-range interactions between ^{1}H and heteroatoms over distances of two and three bonds. Heteronuclear multiple bond correlation (HMBC) experiments allow long-range interactions over distances of two- and three-bonds to be observed.[126] HMBC uses multiple quantum transitions similar to HMQC but much smaller J-values are selected for coherence transfer (10 Hz for HMBC vs. 150 Hz for HMQC) so that two- and three-bond correlations ($^{2,3}J_{CH} \sim 10$ Hz) are observed and the $^{1}J_{CH} \sim 150$ Hz is rejected.[127] These experiments provide a means for determining connectivities between atoms, and carbon skeletons of organic molecules can be traced out.[126]

Previous NMR Studies of HA Oligosaccharides

Polymeric HA faces several challenges for NMR analysis including poor chemical shift dispersion and spectral overlap. Additionally, its inherently large size and viscous nature gives rise to slow correlation times and thus small T_2 values.[125] This results in the broadening of resonances reducing spectral resolution. Due to the challenges facing NMR analysis of polymeric HA, researchers have turned to oligosaccharides ($n \leq 10$) as models for structural studies of the polysaccharide (n

>10).[135] Oligosaccharides can also be prepared at higher concentration than the polymer without causing excess viscosity and line broadening.

Unfortunately, oligosaccharides are much more sensitive to 'end-effects' than polymeric HA.[135] End-effects result from differences in chemical structure and environment for terminal rings, relative to more interior rings, because they lack one glycosidic bond each. These effects result in unique chemical shifts for equivalent nuclei at different positions (terminal, penultimate, or interior) within the chain, and sequence-specific assignments are therefore necessary.[136–138] Chemical shifts are also affected by which monosaccharide (GlcU or GlcNAc) appears at the reducing end.[135] Mutorotation of the anomeric carbon generates the α and β anomer causing anomeric-specific resonances in the terminal and penultimate rings at the reducing end (Fig. 2-2a; Table 2-1).[139,136,140] Interior saccharides provide the best approximation to the polymer and end-effects diminish with increasing chain length.[135,141]

The vast majority of past NMR work, presented in the sections below, has focused on the fully saturated form of HA oligosaccharides. However, an unsaturated form (Fig. 2-2b), ΔDiHA, featuring a double bond between C4 and C5 of GlcU is also possible. The double bond appears at the non-reducing terminus and is formed under certain enzymatic conditions.[142–145] Specifically, the use of certain enzymes such as chondroitinase or HA lyase derived from bacterial sources is required. This chapter will investigate the unsaturated form of the HA disaccharide in both anomeric forms.

HA Chemical Shift Assignments

Oligosaccharides of HA have been extensively studied by NMR in a variety of conditions and solvents, to approximate the polymer conformation. Assignments for di- and tetrasaccharides have been reported, but with some disagreement.[138,146,147] Most recently

a.

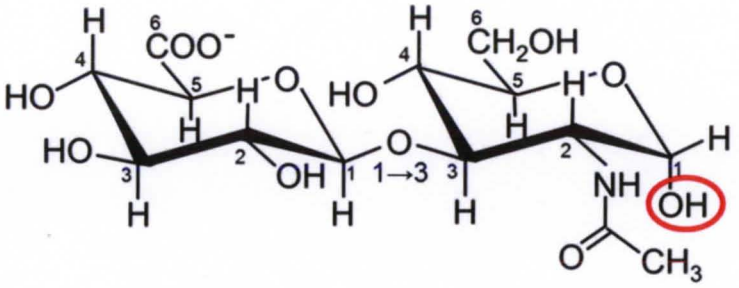

HA
α anomer

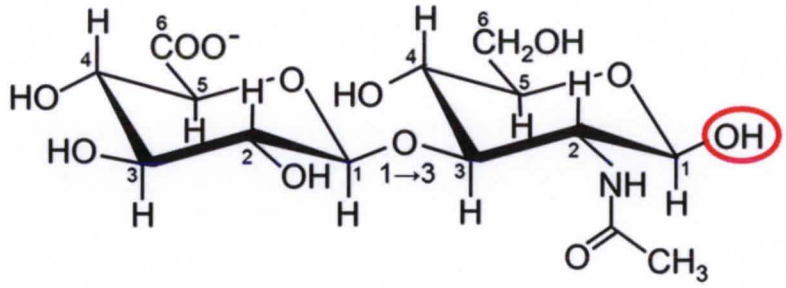

HA
β anomer

b.

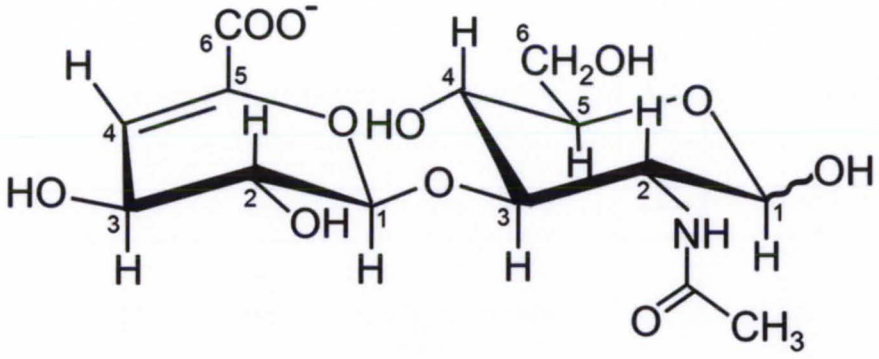

ΔDiHA

Figure 2-2. a) Anomeric forms of HA disaccharide: α and β b) Unsaturated form of HA disaccharide (ΔDiHA). (b). b) Unsaturated HA disaccharide (

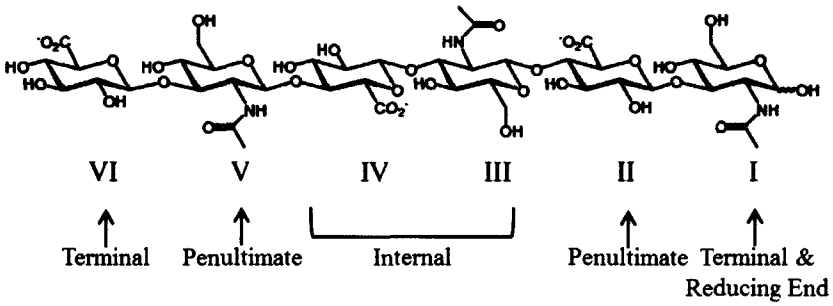

	Nucleus	α		β
I-GlcNAc	H-1	5.155		4.711
	H-3	3.889		3.714
	H-5	3.867		3.468
II-GlcU	H-1	4.506		4.463
	H-3	3.582		3.578
	H-5	3.708		3.699
III-GlcNAc	H-1		4.548	
	H-3		3.707	
	H-5		3.476	
IV-GlcU	H-1		4.457	
	H-3		3.577	
	H-5		3.704	
V-GlcNAc	H-1		4.554	
	H-3		3.705	
	H-5		3.477	
VI-GlcU	H-1		4.455	
	H-3		3.495	
	H-5		3.722	

Table 2-1. Selected ^{1}H NMR chemical shifts for terminal, penultimate, and residues of HA hexasaccharide. Chemical shifts were measured in 5-10% (v/v) D_2O at pH 6.0, 24.4°C and referenced relative to $\delta_{DSS}(^{1}H)$. Source: Adapted from Almond, A., *et al. Carbohydrate Research* **2006**, *341*, 2803–2815.[135])

Blundell and Almond reported the ^{1}H, ^{13}C, and ^{15}N resonance assignments and J-values ($^{1}J_{C,H}$ and $^{3}J_{H,H}$) for HA oligosaccharides up to hexasaccharide-size in D_2O (Table 2-1).[135] This group achieved excellent resolution with the use of a 900 MHz NMR spectrometer. Two-dimensional experiments, TOCSY, COSY, NOESY and ^{1}H-^{13}C and ^{1}H-^{15}N HSQC were also performed on some oligosaccharides.

To date, ^{1}H and ^{13}C chemical shift assignments of unsaturated HA oligosaccharides have been limited to only the tetrasaccharide size in D_2O/H_2O for the assignment of ring and amide (N**H**) protons.[135] Rapid exchange of hydroxyl (O**H**) protons with the solvent prevented the assignments for these resonances being made. Amide and hydroxyl proton resonances of unsaturated HA oligosaccharides (di- to decasaccharide size) have been assigned in acetone-d_6/H_2O mixtures at sub-zero temperatures.[148]

Spectral overlap can be reduced through the use of isotopic enrichment and multidimensional NMR experiments. Two-dimensional NMR experiments use the greater chemical shift dispersion of a heteronucleus (C or N) to resolve coincident ^{1}H resonances. The use of isotopically (^{13}C or ^{15}N) labeled oligosaccharides enhances the sensitivity of these experiments because of increased concentrations of NMR-active nuclei. In HA analysis, ^{15}N enrichment allows the measurement of properties at sequence-specific positions within the HA molecules via ^{1}H-^{15}N HSQC.[149–151] However, new carbon-carbon and long-range scalar couplings can complicate the spectral analysis. These new couplings cause broadening and decrease the resolution. Blundell and Almond have exploited these couplings in ^{1}H-^{13}C HSQC and designed a pulse sequence that produces filtered spectra with fewer resonances, and degenerate ^{1}H resonances can be potentially

resolved.[152] The sensitivity of ^{15}N nuclei to end-effects has been shown to allow resolution and assignment of central amide groups up to decasaccharide-size.

Intramolecular Hydrogen Bonds and the Role of Solvent

The exchangeable amide (N**H**) and hydroxyl (O**H**) protons of HA oligosaccharides have been extensively investigated to gain insight into H-bonding interactions. The role of the solvent is crucial in these investigations. Early NMR work of HA oligosaccharides was performed in deuterated dimethyl sulfoxide (DMSO-d_6) to avoid exchange of N**H** and O**H** protons with solvent (i.e. deuterium (^2H) from the D_2O) and thus allowing the detection of all exchangeable resonances. However, DMSO does not provide an ideal model for biological systems which are composed primarily of water. In comparison to water, DMSO is incapable of being a H-bond donor.

DMSO Studies. Scott and Heatley were among the first researchers to examine the N**H** and O**H** protons on HA. Using DMSO as the solvent, they found ^1H NMR evidence that supported four strong intramolecular H-bonds inferred from computer simulations (Fig. 1-7).[69,70,136,139,153] Of particular interest was a H-bond involving the amide group that can act as a H-bond donor (N**H**) and/or a H-bond acceptor (C=**O**). Two N**H** resonances (δ 7.8 and 9.3 ppm) were observed in HA tetra-, hexa-, and octasaccharides.[136] Interestingly, only the downfield peak (9.3 ppm) was observed for polymeric HA and only the upfield resonance (7.8 ppm) was observed in the GlcNAc monosaccharide and HA disaccharide.[136] Based on changes in relative intensities upon increasing chain length (1:1, 2:1, and 3:1 from tetra- to hexa- to octasaccharide) the downfield resonances was attributed to N**H** protons on internal residues and the upfield resonance assigned N**H** of a terminal GlcNAc. As the polymer size increased, the upfield resonance became too small to be detected. On the basis of the downfield change in

chemical shift ($\Delta\delta$ = 1.5 ppm) as well as the lower rate of disappearance upon deuteration, the downfield resonance (9.3 ppm) was attributed to intramolecular H-bonding of N**H** on interior rings to the neighboring carboxylate oxygen across the β1-4 glycosidic bond. Coupling constants (6-8 Hz) were found to be consistent with a *trans* orientation of N**H** relative to the ring proton at *N*-H2.[70] Furthermore, they found the coupling constant of internal N**H** proton resonances to be significantly lower (6.2 Hz) compared to terminal resonances (~ 7-8 Hz) indicating a greater deviation (35-40°) from the *trans* orientation and a conformation where internal NH groups are ~ 90° to *U*-H2 (Fig. 2-3a and b). This deviation from the *trans* orientation and also planarity was consistent with rotation required to form a H-bond between N**H** and the carboxylate **O** of ΔGlcU. Similar arguments, as well as temperature and concentration dependent studies, were used to propose the other three intramolecular H-bonds shown in Figure 1-7.[70,139,153]

D_2O/H_2O Studies. Cowman and her group questioned whether any intramolecular H-bond would persist in aqueous solutions and reexamined the exchangeable proton resonances of HA in aqueous 4:1 H_2O:D_2O solution at pH 2.5 and 5.5 (due to broadening at neutral pH).[137] Only the N**H** resonance was observed but not O**H** resonances due to rapid exchange of O**H** protons with water protons. They found N**H** resonances corresponding to internal and external GlcNAc residues, in agreement with Scott.[136] However, her group did not observe the large downfield shift of the internal residue resonance or the reduction of the coupling constant. They determined the coupling constant to be ~ 9 Hz representing a nearly pure *trans* relationship where the acetamido group is perpendicular with respect to the ring (Fig. 2-3a).[137] The coupling constant was found to be essentially dependent on chain length, residue position, and pH. This finding suggested a constant NH orientation and was incompatible with the 35-40° deviation

from the purely *trans* orientation as required for the formation of the stable H-bonding proposed by Scott and Heatley (Fig. 2-3b). Cowman's group was unable to find evidence supporting the existence of a stable amide intramolecular H-bond and their coupling constant data was incompatible with the orientation proposed in DMSO.

D_2O/DMSO Studies. In light of this evidence, Scott and Heatley reexamined their previous model. Through stepwise addition of water to DMSO (although only going up to 12% D_2O in DMSO), they found the N**H** chemical shifts gradually shifted upfield toward the values found in water, and saturation-transfer experiments suggested a slow exchange of the N**H** protons in the internal residues.[71] The slow rate of exchange and hindrance of exchange for internal N**H** resonances was consistent with the formation of a "firm water bridge". They proposed the replacement of the direct H-bond between N**H** and CO**O**$^-$ with that of an indirect, water-mediated H-bond (Fig. 2-3c). The analysis of the equilibrium between free and water-bound N**H** forms indicated that only one water molecule takes part in a water-mediated intramolecular H-bond. This water-bridged arrangement allowed the N**H** bond to be in the completely *trans* arrangement (relative to the *U*-H2 bond) as required by the coupling constant determined by Cowman (Fig. 2-3c).[137]

Theoretical Approach. Almond and Blundell have used computer simulations and molecular modeling to gain insight into the H-bonding patterns of the amide proton in HA oligosaccharide using parameters that replicate biological conditions. Molecular dynamic simulations, combined with NMR data, indicated that in solution, the amide proton (N**H**) is *trans* with respect to *N*-H2 and can librate symmetrically around that orientation without making a persistent and stable intramolecular H-bond to the CO**O** group. Instead, weak and transient H-bonds with short lifetimes (ns) are observed and are

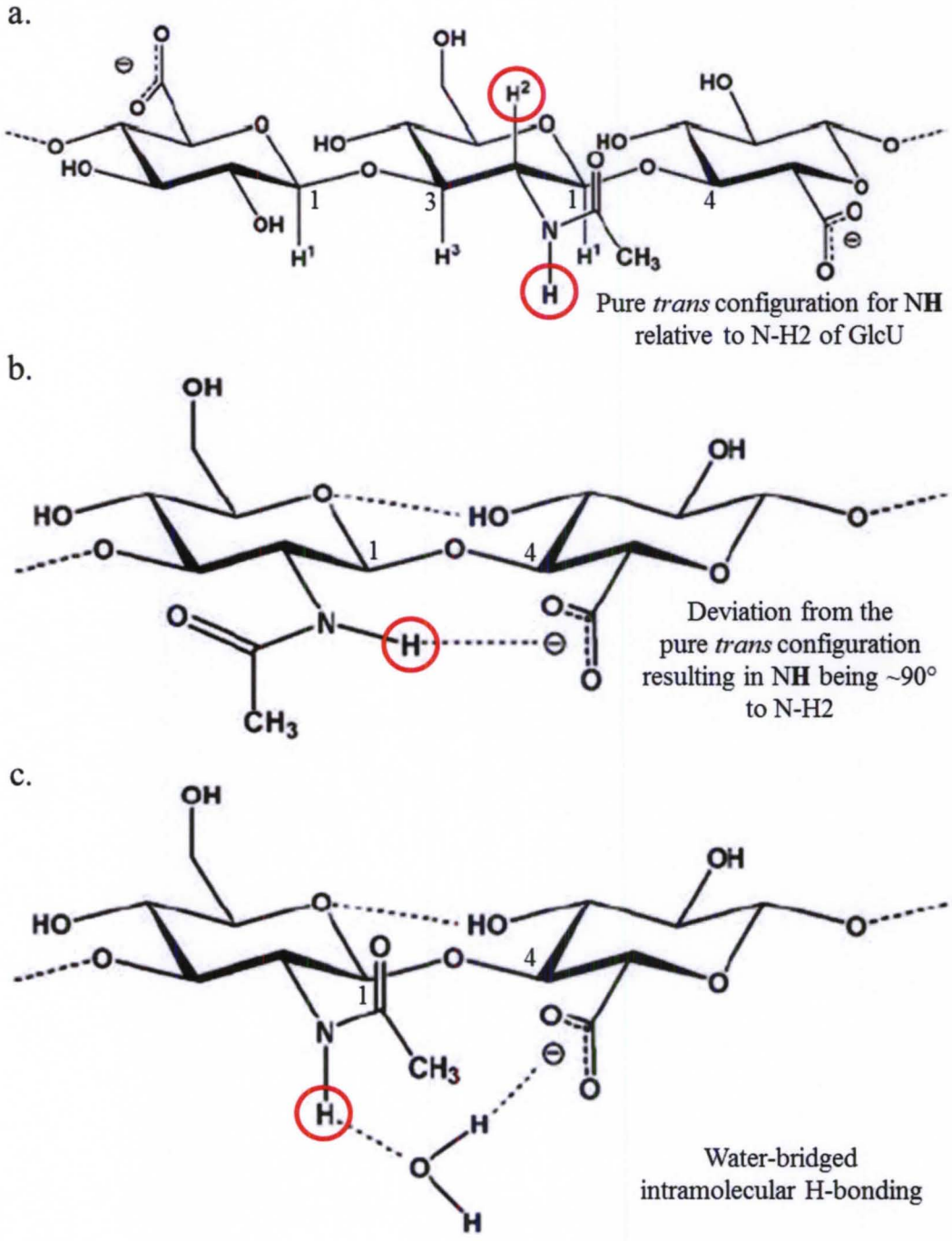

Figure 2-3. Conformational arrangements of N**H** with respect to *N*-H2. H-bonds are indicated by the dotted line. Model predicted from a) computer simulations and b) ^{1}H NMR experiments in DMSO. c) Model featuring a bridged water molecule. (Source: Adapted from Almond, A., *et al. Biochem. J.* 2006, *396*, 487.[154])

proposed to be interchanging with solvent molecules across glycosidic linkages. This may explain some stabilization to the solution structure while permitting local dynamics. NMR results, X-ray diffraction data, molecular dynamic simulations as well as studies of an aqueous solution of ^{15}N labeled-HA have provided insight into intramolecular H-bonds involving the amide proton.[154] Almond and Blundell concluded that weak intramolecular H-bonding is likely to exist in HA oligosaccharides, but these H-bonds do not persist for an extended amount of time due to constant exchange with the solvent.

Role of the Solvent

Cowman's group has analyzed the effects of various solution conditions (including solvent, pH, and ionic strength) on the conformational and dynamic polysaccharide for HA oligosaccharides up to low-MW polymer size.[141,155] Previous studies on the role of the solvent are discussed in this chapter, while reports on the role of pH and ionic strength are summarized in the following chapter. Additionally, her group looked at the position-dependent and polymer lengths effects on chemical shifts.

Conformational Analysis. Differences in chemical shifts were reported in ^{13}C spectra of HA acquired in DMSO and H_2O.[155] All but one of the resonances moved downfield in DMSO, with the most common shift being approximately 1-2 ppm. Solvent-sensitive carbons fall into the following groups: 1) linkage carbons (especially those of the β-1,3 linkage), 2) acetamido-carbonyl carbons, and 3) carboxylate group-associated carbons. The largest differences in chemical shifts occurred for carbons of the β-1,3 linkage and the amide and carboxylate groups. Smaller changes were observed for carbons at the β-1,4 linkage. They concluded that HA conformation differs in aqueous solutions by having an altered amide orientation that place N**H** *trans* with respect to *N*-H2 and a probable alteration in the β-1,3 glycosidic linkage conformation. They proposed

that these substantial changes in environments reflect differences in solvation, conformation, and H-bonding between DMSO and D_2O.

Dynamic Analysis. Dynamics of molecular flexibility and segmental motion in HA can be probed by analysis of NMR relaxation parameters. Relaxation parameters can be investigated either indirectly by linewidths ($\Delta\nu_{1/2} = (\pi T_2)^{-1}$) or directly by measuring longitudinal and transverse relaxations time (T_1 and T_2) and NOEs of carbons. T_1 values depend predominantly on dipolar interaction between the carbon and attached hydrogen. They are strongly related to the fraction of local motions on the nanosecond time scale. In oligosaccharides, this corresponds to segmental motions of a few sugars in the chain and by other hindered motions.[155] T_1 is an intrinsic measure of local stiffness such as what may be conferred by H-bonding.

In addition to solvent-dependent changes in chemical shifts, Cowman's group also looked at the effect of the solvent (DMSO vs. H_2O/D_2O) on measured T_1 values of ^{13}C nuclei in HA tetrasaccharide.[155] In general, for short HA chains, the nonreducing and reducing terminal residues show much greater mobility than penultimate residues, which are in turn more mobile than interior residues. In DMSO, the variation in T_1 across the chain is small. In H_2O, the variation in T_1 is more marked across the chain and thus a greater difference in T_1 values between the terminal and more interior residues exists. This suggests a greater uniformity in dynamics at various positions along the chain in the HA tetrasaccharide in DMSO. They also found that T_1 values were less in DMSO compared to values obtained in water which was attributed at least in part due to the greater viscosity of DMSO relative to H_2O. Their findings suggest the more dynamic nature of conformation-stabilized H-bonds for HA chains in aqueous solutions. They

propose the possibility that DMSO may alter the distribution of correlation times and lead to a more efficient relaxation process.

Temperature Coefficients in Aqueous Solution

Temperature studies of HA oligosaccharide have focused around the amide and hydroxyl protons in order to evaluate their involvement in H-bonding. Temperature coefficients of protons involved in H-bonds are expected to be smaller (less negative) than those freely exchanging with water ($\Delta\delta/\Delta T$ = -11 ppb/K or ppb/°C).[154] For O**H** protons of oligosaccharides in DMSO, strong H-bonds give temperature coefficients > -3 ppb/K.[156] Interior N**H** protons in HA oligomers in DMSO report temperature coefficients of -4.3 ppb/K indicating a medium-strength H-bond to the CO**O**$^-$ group.[70]

Almond and Blundell have analyzed the temperature coefficients of N**H** protons and nitrogen nuclei, for HA oligosaccharides up to small polymer size (n = 22) in H_2O/D_2O mixtures, using ^1H and ^{15}N-enriched NMR, respectively.[154,151] A summary of N**H** temperature coefficients for some of the species analyzed are provided in Table 2-2. Differences in N**H** temperature coefficients between interior residues and α- and β-reducing terminal rings suggest that N**H**, as well as ^{15}N temperature coefficients may be reflections of subtleties in local geometry, intramolecular H-bonds, and water structure. All interior amide protons report a temperature coefficient of ~ -6.7 ppb/K at pH 6.0, but increased to -8.1 ppb/K at pH 1.4.[154] Protonation of GlcU carboxylate groups, by decreasing the pH, was shown to perturb the amide proton environment, consistent with data from molecular dynamics simulations that a transient and sparsely populated H-bond may exist between these groups. Since the reported temperature coefficients for N**H** protons of HA are significantly more negative than the cutoff described above (-4.3 ppb/K), it was proposed that the interior N**H** groups do not make stable, long-lived H-

	NH Temperature Coefficients (ppb/K)		
Saccharide	**α**	**β**	**ψ**
(pH 6.0)			
GlcNAc	-9.0	-7.8	-----
ΔHA_4	-9.0	-7.6	-6.9
HA_p	-----	-----	-6.7
(pH 1.4)			
GlcNAc	-8.8	-7.7	-----
ΔHA_4	-9.0	-7.5	-8.1
HA_p	-----	-----	-8.1

Table 2-2. Previously reported N**H** temperature coefficients ($\Delta\delta/\Delta T$) for the GlcNAc monosaccharide, the unsaturated HA tetrasaccharide (ΔHA_4), and the low-MW HA polymer (2,500-8,000 Da). α and β designate the anomeric conformation at C1 of the reducing terminus. ψ represents the internal NH groups. Temperature studies were conducted in 10% D_2O/H_2O at pH 6.0 and 1.4. (Source: Adapted from Almond, A., *et al. Biochem. J.* 2006, *396*, 487.[154])

bonds with the CO**O**$^-$ group in either its protonated or charged state, or through a stable water-bridge.

Mixtures of H_2O and acetone-d_6 have been used to study hydroxyl protons at sub-zero temperatures in order to reduce the exchange rate with water. Using this method, temperature coefficients have been analyzed for both N**H** and O**H** protons of the methyl glycoside of HA[157] and of unsaturated di-, tetra-, hexa-, and octa-saccharides of HA.[148] Analysis of ΔDiHA showed N**H** resonances at 8.51 ($\Delta\delta/\Delta T$ = -8.6 ppb/K) and 8.66 ppm ($\Delta\delta/\Delta T$ = -7.4 ppb/K) corresponding to the α and β anomers respectively. Temperature coefficients of the O**H** resonances on GlcNAc varied from -6.3 ppb/K (*N*-OH1α) to -11.7 ppb/K (*N*-OH6). Temperature coefficients of the O**H** protons on ΔGlcU (*U*-OH2 and *U*-OH3) were slightly larger (more negative) than those of GlcNAc suggesting slightly weaker H-bonding for ΔGlcU. The *U*-OH3 resonance was most affected by temperature as reflected by its large temperature coefficient of -13.3 ppb/K. To date, no studies have analyzed the temperature coefficients of exchangeable protons of HA oligosaccharides in purely aqueous solutions.

The aim of the studies presented in this chapter is to provide initial model studies for a HA oligosaccharide so that future results related to the polymer can be understood. The unsaturated form of HA disaccharide, ΔDiHA, which features a double bond between C4 and C5 of GlcU (ΔGlcU-(1→3)-GlcNAc), was chosen for this purpose since, to date, only a few studies have examined the unsaturated form of HA oligosaccharides. Additionally, spectral assignments are also complicated by the presence of both α and β anomers in small oligosaccharides. Chemical shift assignments were necessarily made on ΔDiHA through careful analysis of ^1H and inverse 2D NMR spectra. Temperature studies were also carried out in both D_2O and H_2O solvents in order to gain insight into H-

bonding. Our analysis represents the first time that exchangeable resonances of ΔDiHA were examined in a purely aqueous environment, using water suppression techniques.

EXPERIMENTAL

Chemicals

Analyte. Hyaluronic acid disaccharide sodium salt or alpha-4-deoxy-L-*threo*-hex-4-enopyranosyluronic acid-[1→3] (α-ΔGlcU-(1→3)-GlcNAc or ΔDiHA) was purchased from Sigma-Aldrich (St. Louis, MO).

Solvents. D_2O was purchased from Sigma-Aldrich (St. Louis, MO). In studies, requiring water as solvent, Barnstead Nanopure water (17.8 MΩ, • cm) was used.

Sample Preparation

ΔDiHA was prepared in either D_2O or water at a concentration of 1.67 mg/mL (4.18 μM). Water was used as solvent in temperature-dependent studies where exchangeable protons were examined. In all other cases, D_2O was used as solvent.

NMR Analysis

One-Dimensional NMR. NMR spectra were obtained on either a 500 or a 700 MHz NMR spectrometer. The Varian INOVA 500 MHz NMR instrument is equipped with a 5 mm $^{1}H\{^{13}C/^{15}N\}$ triple resonance pulsed field gradient (PFG) probe (Palo Alto, CA). The Varian VNMRS 700 MHz NMR spectrometer is equipped with a 5 mm $^{1}H\{^{13}C/^{15}N\}$ ^{13}C enhanced PFG cold probe (Palo Alto, CA). All 1D ^{1}H spectra were acquired with a minimum of 250 scans, 45° pulse width, and a relaxation delay of 1.000 second. All spectra were obtained at 25 °C unless stated otherwise. Spectra were processed using either MestReC, version 4.7.0, or the newer MestReNova, version 7.1.2, software (Santiago de Compostela, Spain).

A coaxial insert containing 1.0 mM 4,4-dimethyl-4-silapentane-1-sulfonic acid (DSS) dissolved in D_2O was added to the NMR tube for referencing and locking in ΔDiHA solutions where H_2O was required as solvent. Chemical shifts were referenced to DSS in the temperature studies for exchangeable protons and to the acetamido-methyl protons of ΔDiHA (2.06 ppm @ 25 to 45°C or 2.05 ppm @ 50°C and above) in all other studies. The acetamido-methyl proton chemical shift was determined with the use of the insert and referencing to DSS at 25 °C. At higher temperatures, DSS was referenced according to the chemical shift calculated based on its temperature coefficient (-0.5 ppb/K), as recommended by IUPAC guidelines.

Two-Dimensional NMR. Gradient heteronuclear single quantum correlation (gHSQC) and gradient heteronuclear multiple bond correlation (gHMBC) spectra were obtained on the Varian VNMRS 700 MHz NMR spectrometer equipped with a 5 mm $^{1}H\{^{13}C/^{15}N\}$ ^{13}C enhanced PFG cold probe (Palo Alto, CA). HSQC was performed using 512 increments with 16 scan per increment, and relaxation delay of 1.000 second. HMBC was performed using 250 scans, relaxation delay of 1.000 second, mixing time of 0.080 second, and a one-bond coupling constant of 140 Hz. All spectra were obtained at 25 °C unless stated otherwise. ^{1}H Chemical shifts were referenced to the acetamido-methyl protons as described above. In the ^{13}C dimension, the acetamido-methyl carbon was used as reference (23.30 ppm @ 25 °C and 23.50 ppm @ 55°C).

Labeling of NMR Assignments. The non-exchangeable ring protons of ΔDiHA have been designated as either *U* or *N* for ΔGlcU and GlcNAc, respectively. Assignments take the format of *X*-Yn (or *X*-Ynz when necessary) where *X* refers to monosaccharide residue (*U* or *N*), Y refers to either proton or carbon (H or C), n refers to the ring position of the atom of interest, and z indicates the anomeric conformation (α or β). For example,

U-C1α refers to the carbon at position one of ΔGlcU corresponding to the α anomer of ΔDiHA, and *U*-H1α refers to the proton attached to carbon one of ΔGlcU, of the α anomer of ΔDiHA. The methylene protons of C6 of N-acetyl glucosamine are designated as 6 and 6'. The methyl group of GlcNAc is designated *N*-CH_3 for both ^{1}H and ^{13}C NMR. The exchangeable amide and hydroxyl protons are designated N**H** and *X*-O**H**n, respectively.

RESULTS AND DISCUSSION

No previous studies have examined the ΔDiHA disaccharide that contains a double bond between C4 and C5 of GlcU (ΔGlcU-(1→3)-GlcNAc). The presence of a double bond in ΔGlcU is the result of enzymatic cleavage using chondroitinase or HAases from bacterial sources. However, this site of unsaturation is expected to lead to conformational changes that, in addition to the absence of a hydroxyl group at C4, would affect the H-bonding interactions relative to the fully saturated form. Additionally, the spectra of the disaccharide is further complicated by the presence of GlcNAc in both the α and β anomeric forms. It is interesting to note that this disaccharide was purchased as the α anomer. However, in an amphoteric solvent such as H_2O, the β anomer is generated through mutorotation. This effect also leads to conversion of the α and β anomers in other carbohydrates with anomeric centers. This causes two unique resonances, often with different chemical shifts, depending on the anomeric form (Fig. 2-2). Two-dimensional NMR was required to complete and confirm the resonance assignments discussed in this section. Additionally, temperature studies were carried out. Temperature-dependent changes in chemical shifts may be used as an indicator of conformation rearrangements and changes in H-bonding arrangements.

Chemical Shift Assignments

One-Dimensional NMR of ΔDiHA

^{1}H and ^{13}C NMR spectra were collected for ΔDiHA, however ^{13}C NMR spectra were of poor S/N and therefore are not included. ^{1}H NMR studies were performed on 400, 500, and 700 MHz NMR spectrometers. However, the 700 MHz spectrometer was necessary to resolve all ring proton resonances of both anomers. The region between 3.4 and 4.2 ppm is shown for comparison in Figure 2-4 to illustrate the enhanced spectral resolution capabilities of the 700 MHz NMR spectrometer compared to the 500 MHz. Additionally, the 700 MHz NMR offers enhanced sensitivity with the use of a cryogenic 'cold' probe that reduces thermal noise in the detection system.

Studies carried out on the 700 MHz NMR were performed using D_2O as solvent, as water suppression on this instrument needs further optimization. All non-exchangeable protons were resolved (see the full ^{1}H spectrum in Appendix B, Fig. B-1). The methyl protons of GlcNAc were observed at 2.06 ppm and used as a reference based on its chemical shift relative to DSS. Ring proton resonances were observed in the region between 3.4 and 6.0 ppm and could be divided into two sets on either side of the solvent (HOD) peak at 4.80 ppm. The doublet seen for *N*-H1β at 4.76 ppm overlapped partially with the HOD peak but could still be resolved.

Preliminary assignments of for ΔDiHA were based on previous reports of the fully saturated form of HA disaccharide[147] and the unsaturated form of the HA tetrasaccharide (ΔHA_4).[135] Chemical shifts and assignments were in good agreement with those published for the GlcNAc residue of the fully saturated HA disaccharide. However, assignments for the ΔGlcU unit differed, as expected, from literature values corresponding to the actual GlcU. Chemical shifts and assignments were in better

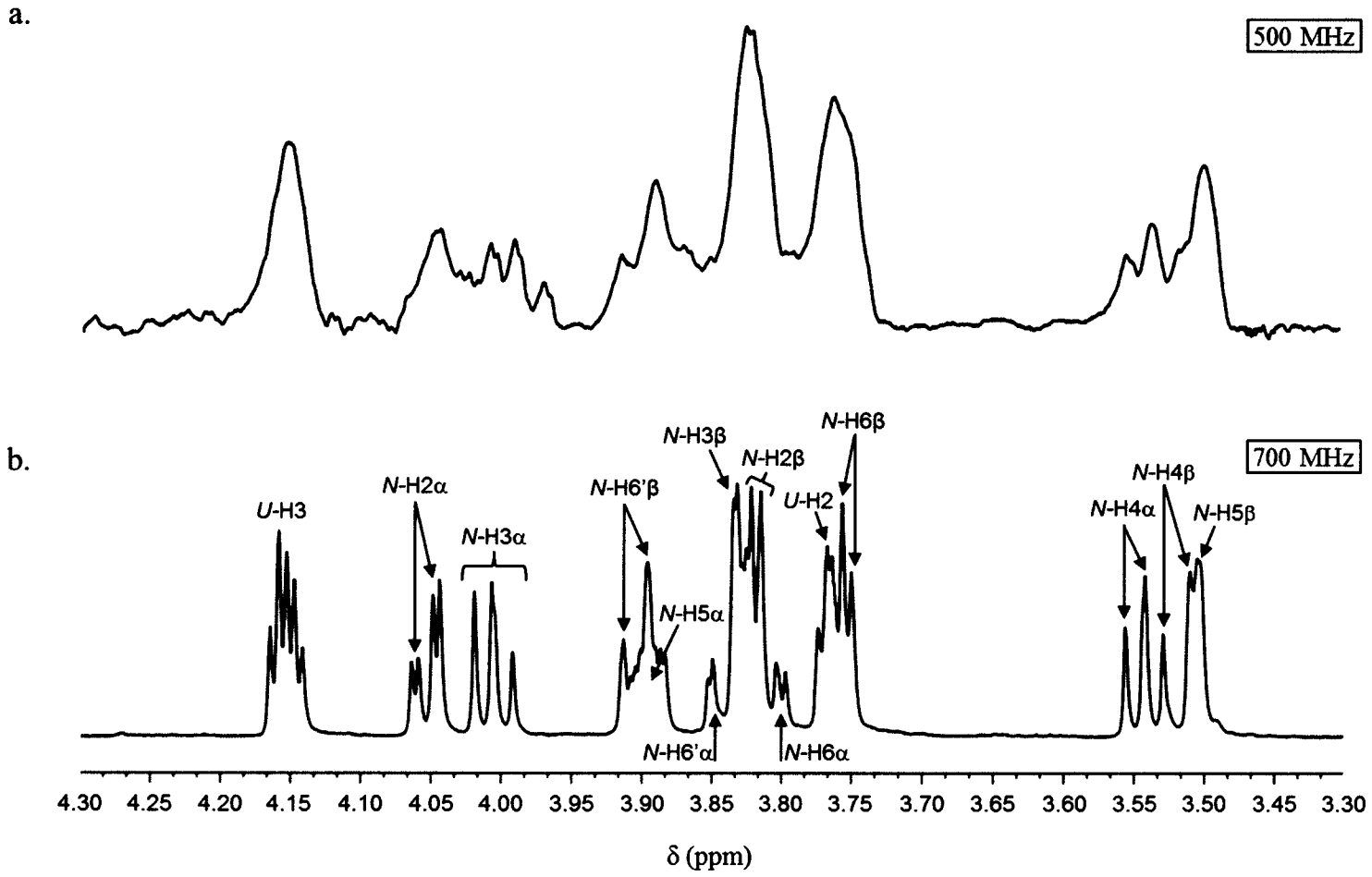

Figure 2-4. ^{1}H NMR spectra of the ring region of ΔDiHA obtained at a) 500 MHz and b) 700 MHz spectral frequencies. Sample was prepared at 1.67 mg/mL in H_2O (a) and D_2O (b).

agreement with those published for the terminal residues of ΔHA_4 Tables 2-3 and 2-4 provide the ^1H and ^{13}C chemical shifts and assignments for non-exchangeable protons of ΔDiHA in D_2O alongside literature assignments for ΔHA_4. Heteronuclear two-dimensional NMR experiments were required to complete and confirm the assignments of ΔDiHA.

In order to visualize the exchangeable amide and hydroxyl protons, studies were necessarily performed in H_2O to avoid exchange with D_2O. Water suppression was therefore necessary and these experiments were carried out on the 500 MHz NMR spectrometer in which water suppression was achieved satisfactorily. Although ΔDiHA contains multiple hydroxyl groups, only one peak (6.09 ppm) was observed suggesting that other resonances are not seen due to the OH groups exchanging with solvent (H_2O). On the other hand, the disaccharide contains only one amide proton but two peaks were observed (8.27 and 8.41 ppm). These two resonances correspond to the α and β anomers, respectively, of ΔDiHA.

Two-Dimensional NMR of ΔDiHA

HSQC results provided correlations between carbons and attached protons and allowed most assignments for ΔGlcU to be made and confirmed ^1H resonance assignments in the GlcNAc residue (Figs. 2-5 and 2-6). Using previously reported ^{13}C assignments for the GlcNAc residue, HSQC data was particularly useful in confirming assignments in the crowded region of the spectrum between 3.75 and 3.95 ppm. This region alone contains resonances from eight different protons of ΔDiHA. Four of those resonances come from the methylene protons attached to C6 of GlcNAc. These $\mathbf{CH_2}$ resonances can be easily distinguished from those corresponding to the **CH** and $\mathbf{CH_3}$ because their sign is negative (blue). This type of information is comparable to that

Select HA Oligosaccharides		Experimental ΔDiHA		Literature ΔHA_4		Difference Exp-Lit	
Residue	**Atom**	**α**	**β**	**α**	**β**	**α**	**β**
I-GlcNAc	**H1**	5.16	4.76	5.15	4.71	0.00	0.04
	H2	4.05	3.82	4.04	3.81	0.01	0.01
	H3	4.01	3.83	3.89	3.72	0.12	0.11
	H4	3.54	3.51	3.55	3.52	-0.01	-0.01
	H5	3.89	3.51	3.87	3.47	0.02	0.04
	H6	3.81	3.75	3.79	3.75	0.02	0.00
	H6'	3.85	3.90	3.83	3.89	0.01	0.01
	H-CH_3	2.06		2.01	2.01	0.05	0.05
	NH	8.27	8.40	8.19	8.27	0.08	0.13
II-GlcU	**H1**	NA		4.51	4.47	----------	
	H2	NA		3.37	3.37	----------	
	H3	NA		3.58	3.58	----------	
	H4	NA		3.75	3.74	----------	
	H5	NA		3.72	3.71	----------	
III-GlcNAc	**H1**	NA		4.58		----------	
	H2	NA		3.85		----------	
	H3	NA		3.81		----------	
	H4	NA		3.51		----------	
	H5	NA		3.50		----------	
	H6'	NA		3.77		----------	
	H6	NA		3.92		----------	
	H–CH_3	NA		2.06		----------	
	NH	NA		8.14		----------	
IV-GlcU	**H1**	5.19	5.17	5.15		0.04	0.02
	H2	3.76		3.74		0.01	
	H3	4.15		4.14		0.02	
	H4	5.86		5.85		0.01	
	H5	NA		NA		----------	

Table 2-3. ^1H chemical shift assignments for the α and β anomers of ΔDiHA obtained at 25 °C in D_2O . These values are compared to previously reported values for the unsaturated HA tetrasaccharide (ΔHA_4) at 25 °C in 5-10% D_2O/H_2O. The acetamido-methyl chemical shift, used as reference, is shaded in gray.

HA Polymer		Experimental ΔDiHA		Literature ΔHA_4		Difference Exp-Lit	
Residue	**Atom**	**α**	**β**	**α**	**β**	**α**	**β**
I-GlcNAc	**C1**	92.24	95.72	93.88	97.59	-1.64	-1.87
	C2	54.57	57.23	55.81	58.45	-1.24	-1.22
	C3	80.96	83.19	82.77	85.17	-1.82	-1.98
	C4	69.77	69.76	71.40	71.36	-1.63	-1.60
	C5	72.75	76.93	74.08	78.26	-1.33	-1.34
	C6	61.99	62.01	63.40	63.57	-1.41	-1.55
	CH_3	23.30		24.82	25.07	-1.52	-1.77
II-GlcU	**C1**	NA		105.66	105.81	----------	
	C2	NA		75.33	75.29	----------	
	C3	NA		76.52		----------	
	C4	NA		82.82		----------	
	C5	NA		79.06		----------	
	COO^-	NA		---------		---------	
III-GlcNAc	**C1**	NA		103.16		----------	
	C2	NA		57.47		----------	
	C3	NA		85.04		----------	
	C4	NA		71.20		----------	
	C5	NA		78.35		----------	
	C6	NA		63.42		----------	
	CH_3	NA		25.28		----------	
IV-GlcU	**C1**	101.86		103.50		-1.64	
	C2	71.19		72.68		-1.49	
	C3	67.51		68.95		-1.45	
	C4	108.48		110.07		-1.59	
	C5	145.55		---------		----------	
	COO^-	176.30		---------		----------	

Table 2-4. ^{13}C chemical shift assignments for the α and β anomers of ΔDiHA obtained at 25 °C in D_2O . These values are compared to previously reported values for the unsaturated HA tetrasaccharide (ΔHA_4) at 25 °C in 5-10% D_2O/H_2O. The acetamido-methyl chemical shift, used as reference, is shaded in gray.

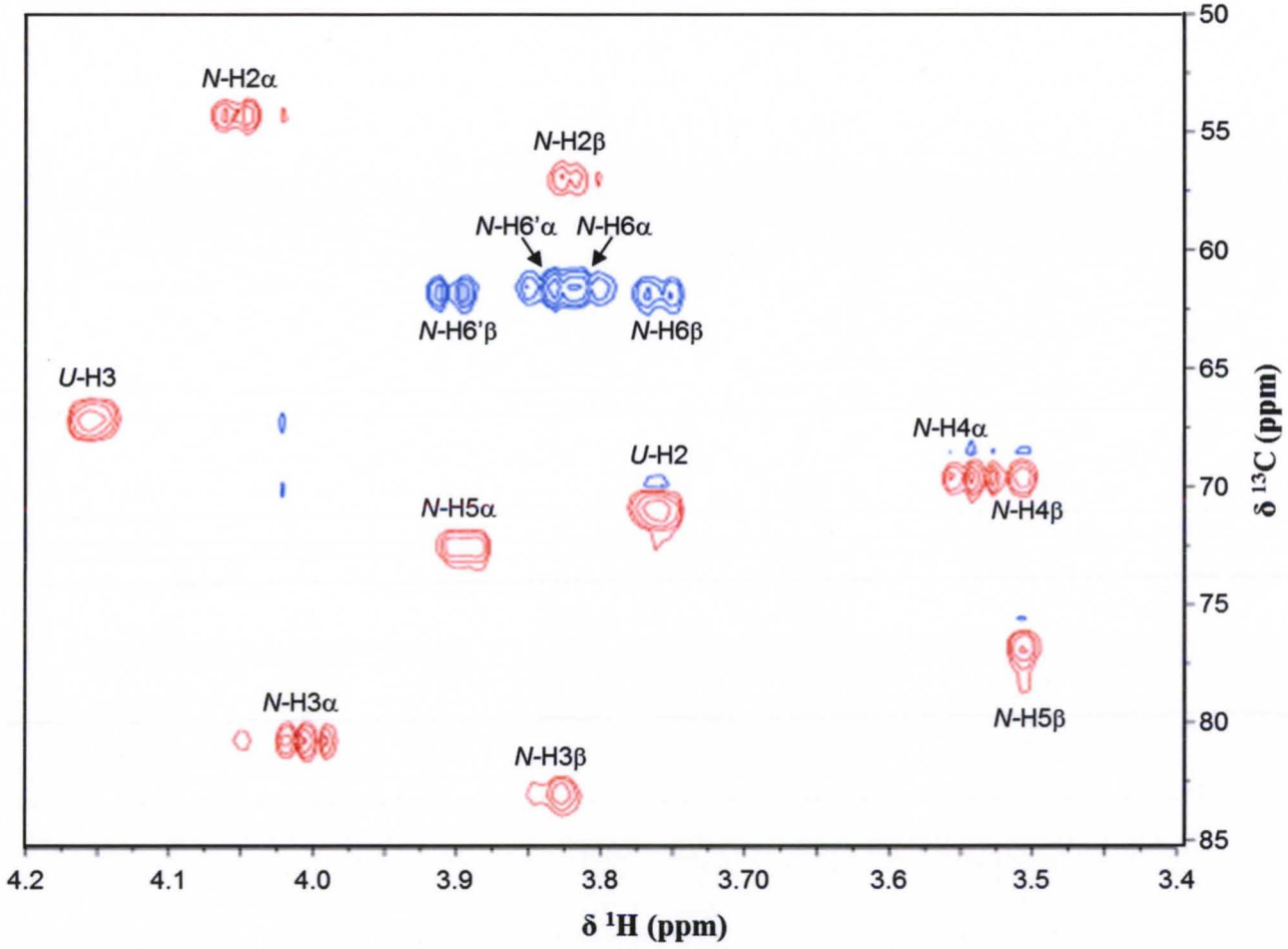

Figure 2-5. HSQC spectrum of the ring region of ΔDiHA (^{1}H range: 3.4 - 4.2 ppm; ^{13}C range: 50 - 85 ppm). Correlations are labeled inside the spectrum. Red cross-peaks correspond to the methine (C**H**) groups and blue cross-peaks correspond to the methylene (C**H$_2$**) group. Sample was prepared at 1.67 mg/mL in D_2O.

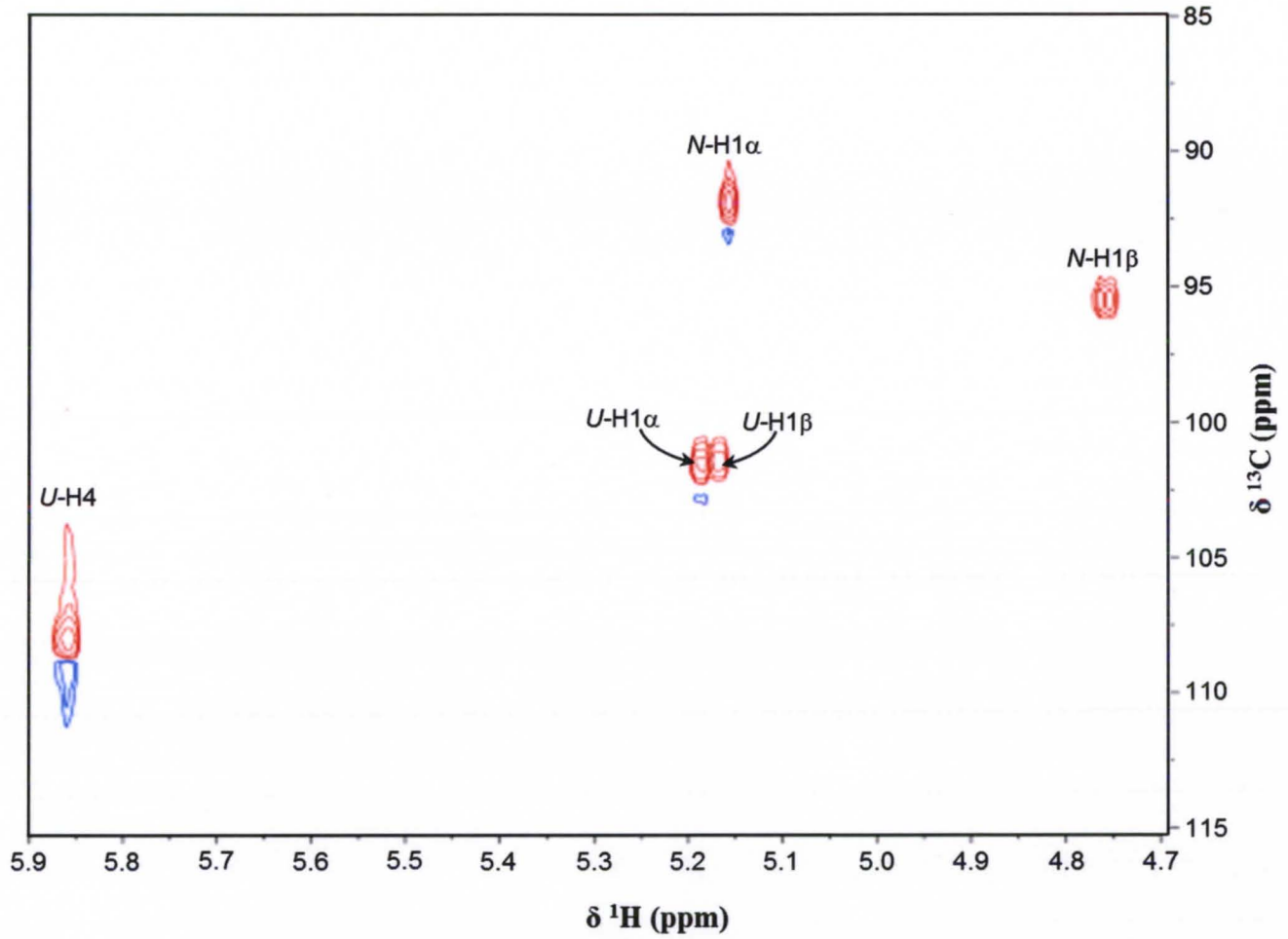

Figure 2-6. HSQC spectrum of the ring region of ΔDiHA (^{1}H range: 4.7 - 5.9 ppm; ^{13}C range: 85 - 115 ppm). Correlations are labeled inside the spectrum. Red cross-peaks correspond to the methine (C**H**) groups and blue cross-peaks correspond to the methylene (C**H$_2$**) group. Sample was prepared at 1.67 mg/mL in D_2O.

obtained from the older, distortionless enhancement by polarization (DEPT) experiment. Because the sample contained both the α and β anomers, two possibilities exist for each of the methylene protons H6 and H6'. The α and β anomers could be distinguished on the basis of the ^{13}C chemical shifts that are slightly different for each anomer. Hence each set of H6 and H6' protons correlate with the same carbon of a particular anomeric conformation. Once assigned to a particular anomer, differences in the ^{1}H chemical shifts allowed the H6 and H6' resonances to be determined.

From HSQC data it was still unclear how to assign the peaks to the left of the solvent peak at higher chemical shifts (4.7-5.2 ppm) that featured the protons attached to C1 in both monosaccharide subunits. For this reason, HMBC was carried out to examine longer-range, multiple bond correlations between protons and carbons up to three bonds away (Figs. 2-7 and 2-8). Using the assignments that were confirmed through HSQC, *N*-H1 could be discerned from *U*-H1 based on its correlations with *N*-H2. Conversely, *U*-H1 could be distinguished on the basis of its connections to *U*-H3. Resonances corresponding to each of the α and β anomers were observed for GlcNAc ring protons. However, this difference in chemical shifts between the two anomers was lost for all ΔGlcU protons except for *U*-H1. The reduction of this effect was reasoned to be as the result of increased distance from the anomeric center. The *U*-H1 proton is adjacent to the glycosidic linkage and represents the closest position on ΔGlcU to the anomeric center of GlcNAc. Blundell and coworkers reported a similar loss of anomer-related differences in chemical shifts for other HA oligosaccharides.[135] Using the 900 MHz NMR they were able to resolve anomeric differences in chemical shifts out to the *U*-H2 proton in disaccharide.

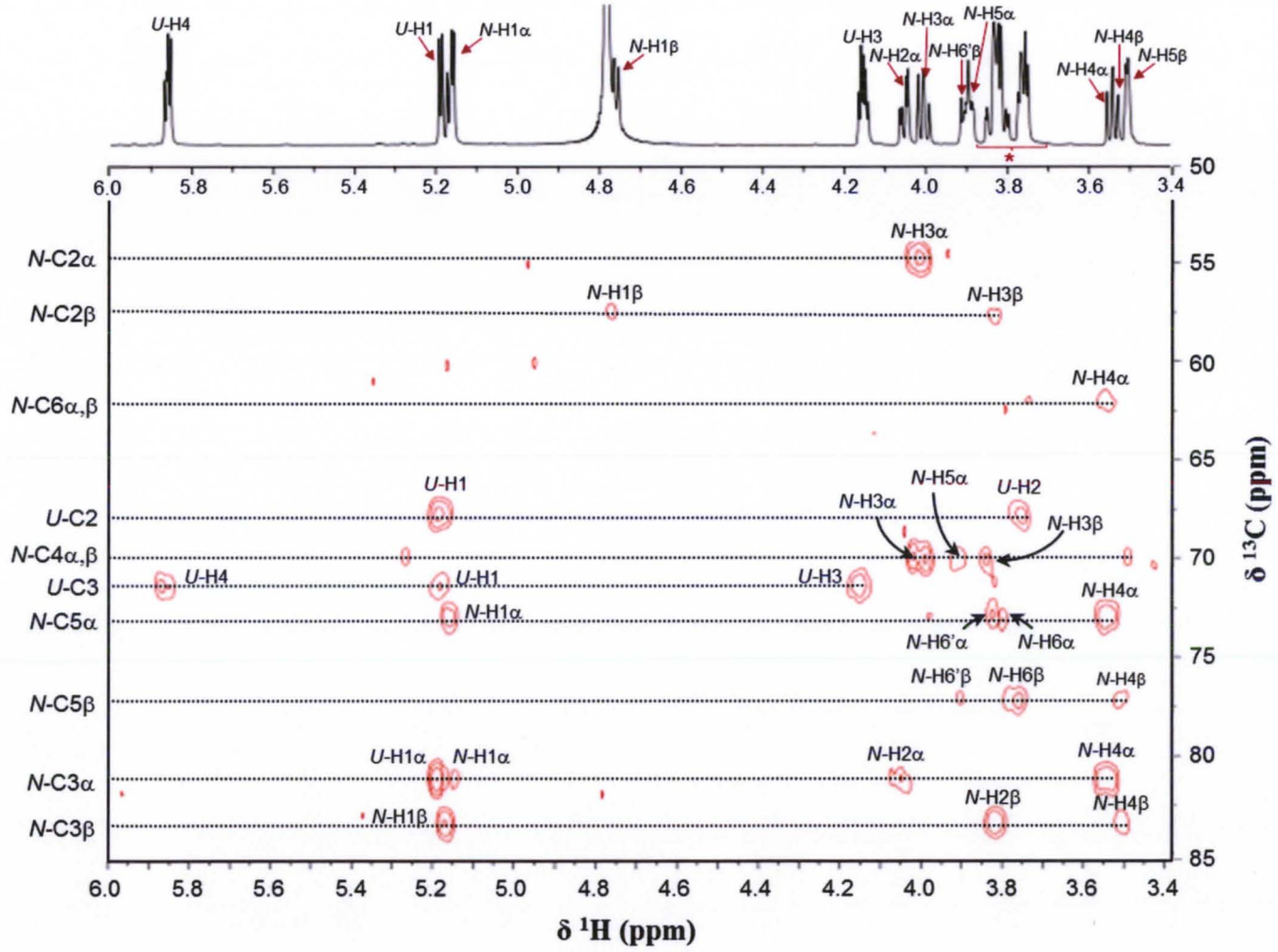

Figure 2-7. HMBC spectrum of the ring region of ΔDiHA (^{1}H range: 3.4 - 6.0 ppm; ^{13}C range: 50 - 85 ppm). Correlations are labeled inside the spectrum. Sample was prepared at 1.67 mg/mL in D_2O. * Crowded region of the 1D ^{1}H spectrum (top).

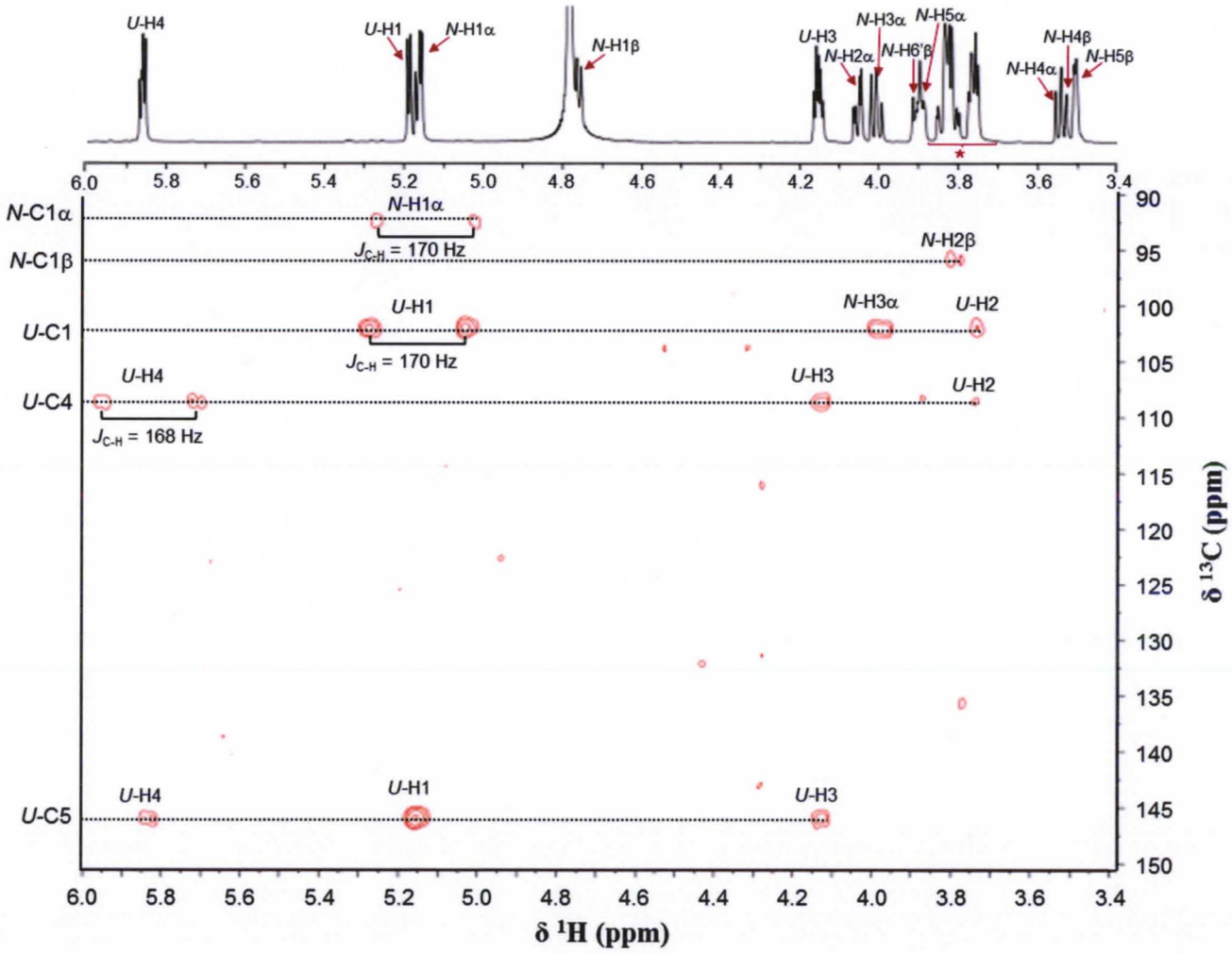

Figure 2-8. HMBC spectrum of the ring region of ΔDiHA (^{1}H range: 3.4 - 6.0 ppm; ^{13}C range: 90 - 150 ppm). Correlations are labeled inside the spectrum. Sample was prepared at 1.67 mg/mL in D_2O. * Crowded region of the 1D ^{1}H spectrum (top).

Anomeric Differences

Correlations were observed over distances of several bonds, with two bonds being most common. Correlations across the glycosidic linkage could also be observed between *N*-C3 and *U*-H1 and vice versa. As seen in Figure 2-8, the resonances for *U*-H1 and *U*-H4 protons are split by $^{1}J_{CH}$. These splittings are considered artifacts and are the result of the threshold set in the pulse sequence. In our experiment, this threshold was set to 140 Hz. Therefore, only those resonances corresponding to protons with a strong coupling constant $^{1}J_{CH}$ (> 140 Hz) were split.

The ^{1}H resonances for ring protons of the α anomer are at a slightly higher chemical shift relative to ring protons of the β anomer. On the other hand, ^{13}C chemical shifts for ring protons are lower in the α anomer compared to the β anomer. This suggest the rearrangement of electron density around the ring protons that results in the deshielding of protons in the α anomer.

Temperature-Dependent Studies of the ΔDiHA by ^{1}H NMR

Resonances for Ring Protons

Temperature studies were performed and both 1D ^{1}H NMR and 2D HSQC spectra were acquired at temperatures up to 55 °C. The overlaid HSQC spectra at 25 °C and 55 °C are shown in Figures 2-9 and 2-10. Increasing the temperature has little effect on most ΔDiHA ring protons. In general, if changes were observed they are in the shielded direction and relatively minute. This can be attributed to weakening of intermolecular H-bonds with the solvent (D_2O) and therefore less hydrophilic interactions. *N*-H2β revealed a slightly higher temperature coefficient than the other ring protons but its value was less than -1 ppb/°C, much lower than those corresponding to the N**H** and O**H** resonances. The slightly greater change in the *N*-H2β may be caused from changes in the H-bonding of

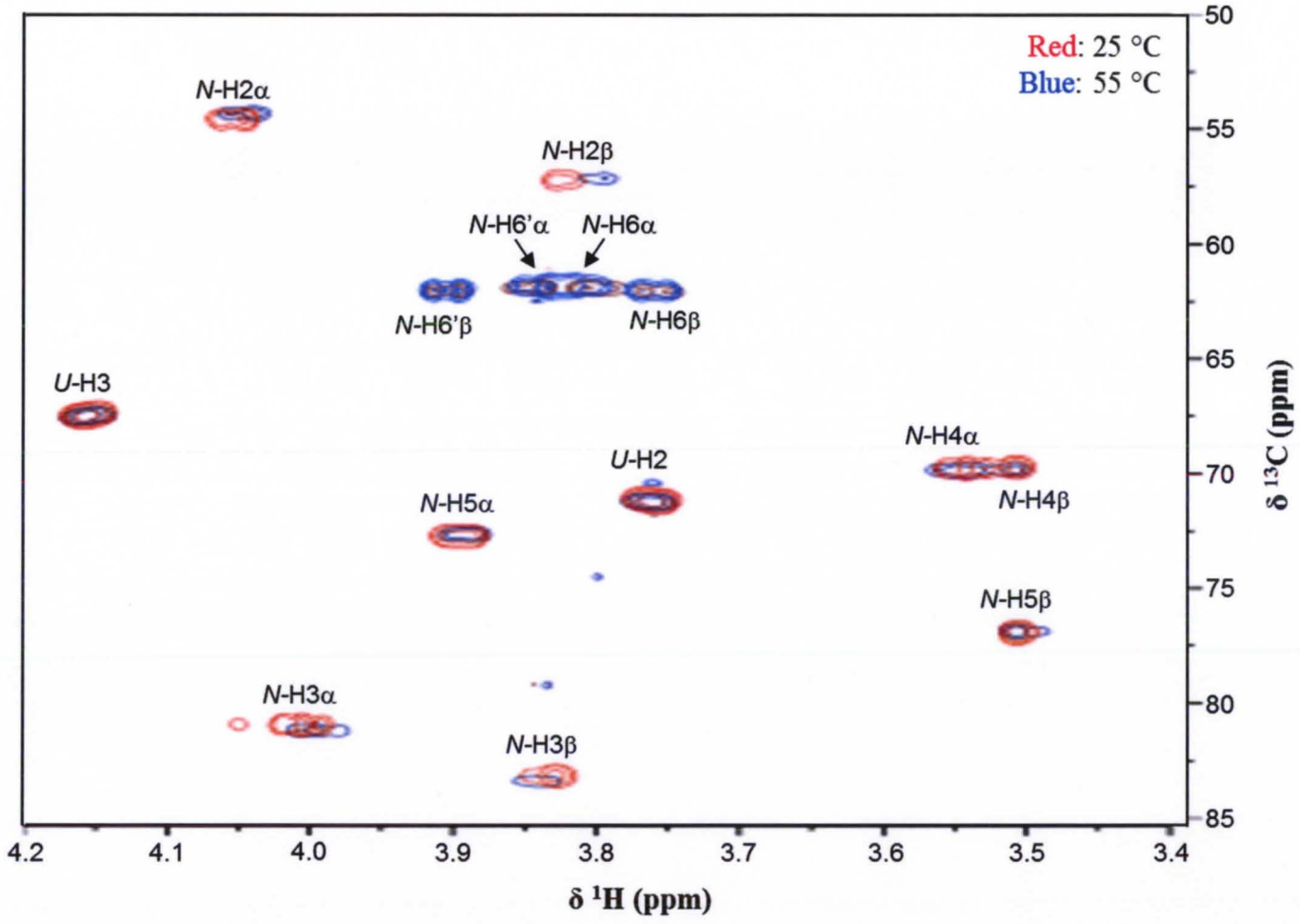

Figure 2-9. HSQC spectra of the ring region of ΔDiHA at 25 °C (red) and 55 °C (blue); (^{1}H range: 3.4 - 4.2 ppm; ^{13}C range: 50 - 85 ppm). Sample was prepared at 1.67 mg/mL in D_2O.

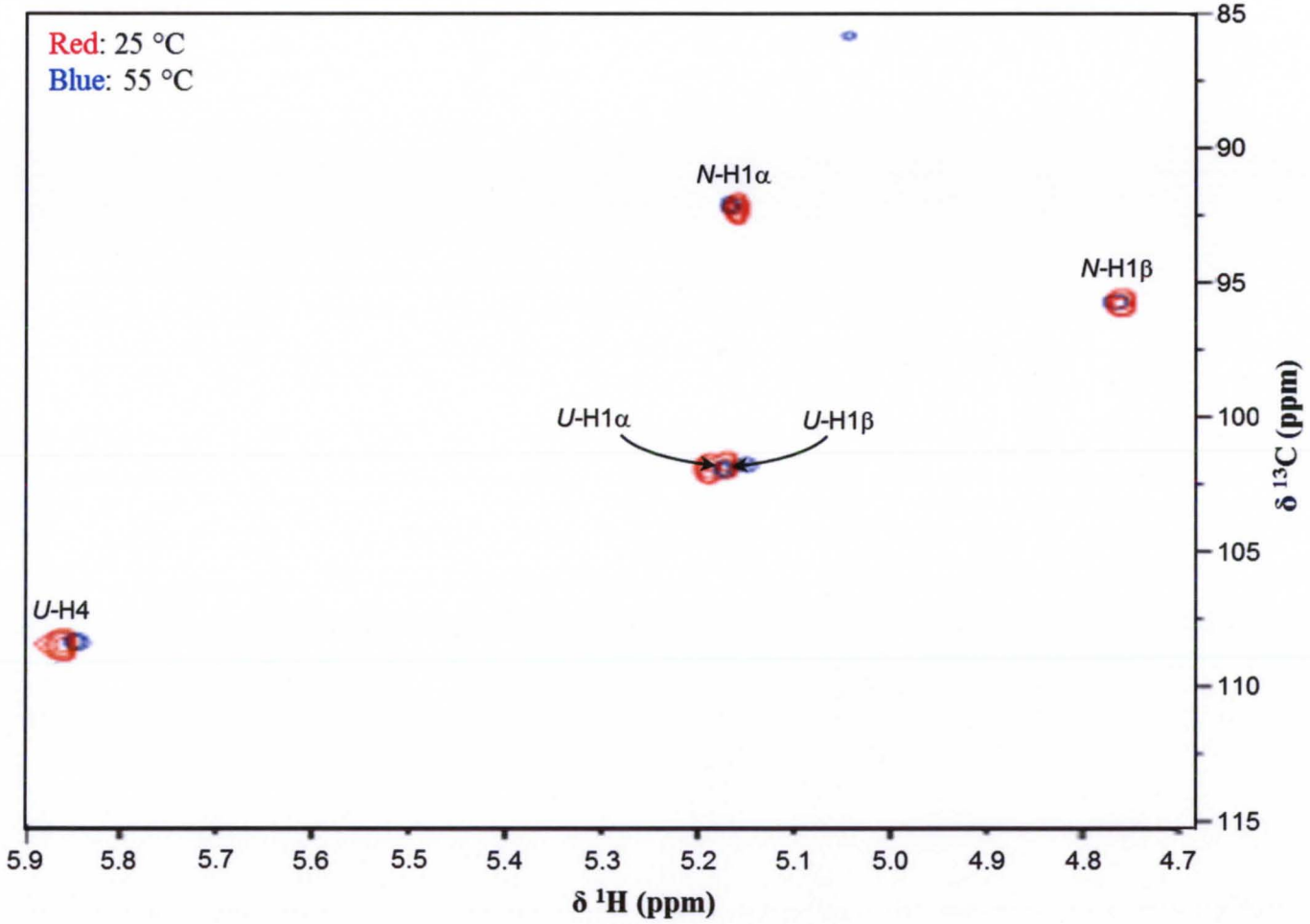

Figure 2-10. HSQC spectra of the ring region of ΔDiHA at 25 °C (red) and 55 °C (blue); (^{1}H range: 4.7 - 5.9 ppm; ^{13}C range: 85 - 115 ppm). Sample was prepared at 1.67 mg/mL in D_2O.

the acetamido group (attached to C2 of GlcNAc) that results in *N*-H2β becoming shielded. A conformational change of the acetamido group that placed the methyl protons closer to *N*-H2 could explain the shielding of *N*-H2β resonance.

Resonances for the Amide Proton

As previously mentioned, two resonances were observed for the amide proton corresponding to the α and β anomers (Fig. 2-11a). Based on previous literature,[154] the resonance with the higher chemical shift (δ = 8.40 ppm at 25 °C) was assigned to the β anomer and that at the lower chemical shift (δ = 8.27 ppm at 25 °C) to the α anomer. These assignments are also in agreement with a lower integration value seen for the β anomer (0.28 at 25 °C, relative to three methyl protons) compared to the integrated area of the resonance for the α anomer (0.51 at 25 °C). This total integration of less than one, suggests that a fraction of the amide protons undergo exchange, most likely with the solvent. The peak widths at half height were similar 17.4 and 16.5 Hz (at 25 °C) for the β and α anomers, respectively. The exchange rate increased at high temperatures (Fig. 2-11a) as reflected by a lowering of the integration values at higher temperatures. At 25 °C, the α anomer resonance was more defined and split into a doublet by *N*-H2. The N**H** proton of the α anomer shows vicinal coupling with *N*-H2. The coupling constant of 9.2 Hz is indicative of a *trans* orientation between N**H** and *N*-H2 as reported in prior works using H_2O/D_2O as solvent.[137,154]

Temperature coefficients were determined to be -4.7 x 10^{-3} ppm/°C (or -4.7 ppb/K) for the β anomer and -5.4 x 10^{-3} ppm/°C (or -5.4 ppb/K) for the α anomer (Fig. 2-11b). Both the negative sign and the absolute value indicate that these amide protons are involved in either weak intramolecular H-bonds or water-mediated intramolecular H-bonding. Although quite similar, the slightly less negative $\Delta\delta/\Delta T$ for the α anomer

a.

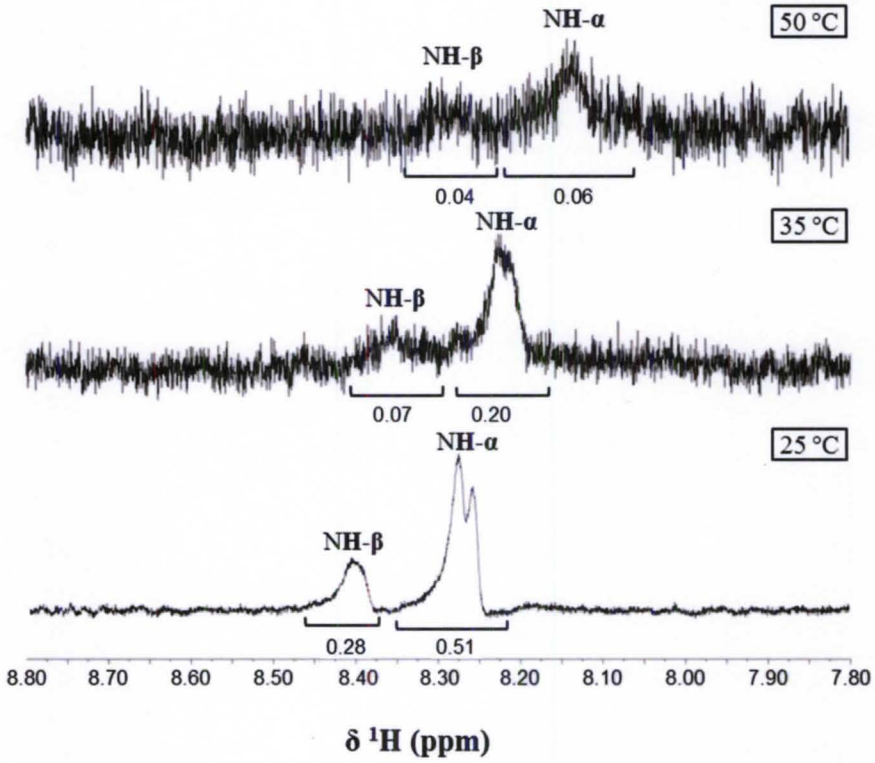

b.

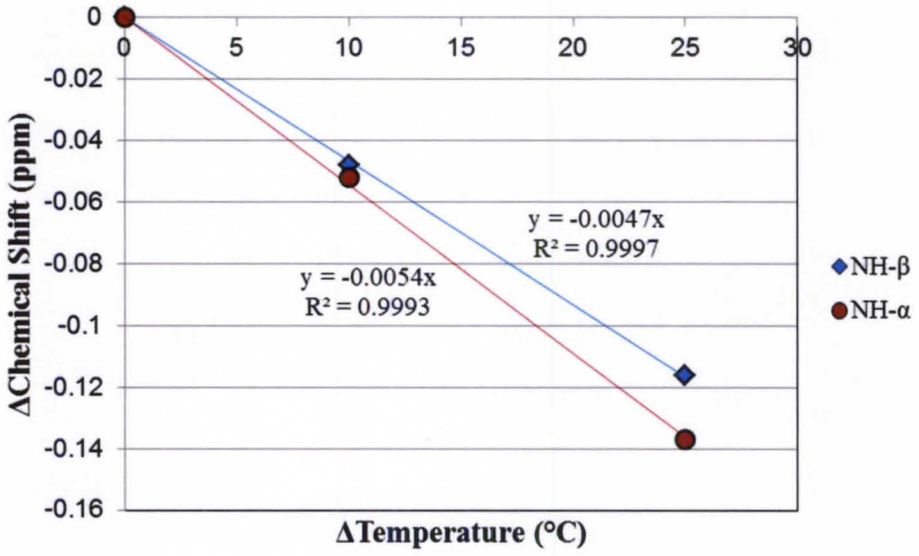

Figure 2-11. Temperature dependence of the amide (N**H**) proton of ΔDiHA a) ^{1}H NMR spectra of the N**H** resonances at 25 °C, 35 °C, and 50 °C. b) Changes in chemical shifts as a function of temperature. Sample was prepared at 1.67 mg/mL in H_2O.

indicates a slightly stronger intramolecular H-bond. Our temperature coefficients areslightly lower than those reported by Almond and Blundell for the ΔHA tetrasaccharide in D_2O/H_2O (-9.0 and -7.6 ppb/K for the α and β anomers, respectively),[154] but they still follow the same trend with the coefficient for the α anomer being more negative than that for the β form. The higher values reported for the tetrasaccharide are possibly due to its larger size and the possibility for intrachain H-bonding which would be weaker than intramolecular or water-mediated intramolecular H-bonding that is found in the disaccharide. Our values are also lower than values previously reported for ΔDiHA ($\Delta\delta/\Delta T$ = -8.6 ppb/K for α and -7.4 ppb/K for β).[148] However, those studies were conducted in acetone-d_6/H_2O mixtures, and the presence of acetone may reduce the cooperativity of H-bonds in water thus weakening the strength of H-bonds with ΔDiHA. This effect would lead to larger (and negative) coefficients relative to those that we observed in water.

To interpret this trend, different H-bonding arrangements for each anomer have been proposed upon rotation of the glycosidic bond. Prior computational studies have reported torsional angles around the β-1,3 glycosidic linkage of 30° and 60°. Where N**H** is in a *trans* orientation with respect to *N*-H2, a rotation of 30° places N**H** in the proximity of *U*-OH2 while a 60° rotation places N**H** near *U*-OH3. Intramolecular H-bonding or water-mediated H-bonding may exist between N**H** and either hydroxyl group, but not both. In the β anomer, these represent the only two possibilities for H-bonding of the amide proton across the β-1,3 glycosidic linkage. Similarly, the α anomer can also H-bond with either of these groups upon rotation. However, in the α anomer, *N*-OH1 is in the axial position and capable of H-bonding with N**H** at either torsional angle, 30° or 60°. Libration of the acetamido group allows for a dynamic H-bonding environment where

N**H** can flip-flop between H-bonding with *N*-OH1 and H-bonding with either *U*-OH2 or *U*-OH3. These dynamic H-bond exchanges in the α anomer cause a reduction in H-bonding strength as reflected by a more negative temperature coefficient compared to that of the β anomer. Hydrogen bonding with *N*-OH1 is not possible in the β configuration, where *N*-OH1 is equatorial to the ring. Librations of the acetamido group do not place N**H** in any position that would allow for H-bonding with any other moiety. This leads to a stronger intramolecular H-bonding in the β anomer as reflected by a less negative temperature coefficient.

Hydroxyl Proton Resonance

Temperature studies of the hydroxyl and amide protons were necessarily conducted in H_2O to allow their observation. Temperatures were increased up to 80 °C but excessive broadening of these resonances limited the temperature range investigated. Spectra for the O**H** resonances are shown up to 60 °C in Figure 2-12a. As previously mentioned, there are several hydroxyl groups on the molecule; however only one was observed suggesting the other hydroxyl group protons are exchanging too rapidly to be detected. Although we have not assigned the detected O**H** resonance, the hydroxyl proton shifted to lower chemical shifts at higher temperatures with a temperature coefficient ($\Delta\delta/\Delta T$) of -7.9 x 10^{-3} ppm/°C (Fig. 2-12b). The relatively large and negative coefficient is indicative of the participation of this proton's in intermolecular H-bonds. This value falls within the range (-6.3 - -13.3 ppb/K) of previously reported O**H** temperature coefficients in acetone-d_6/H_2O mixtures. The use of water as solvent in our studies results in greater exchange rates and more broadening thus leading to the detection of only one O**H** resonance.

a.

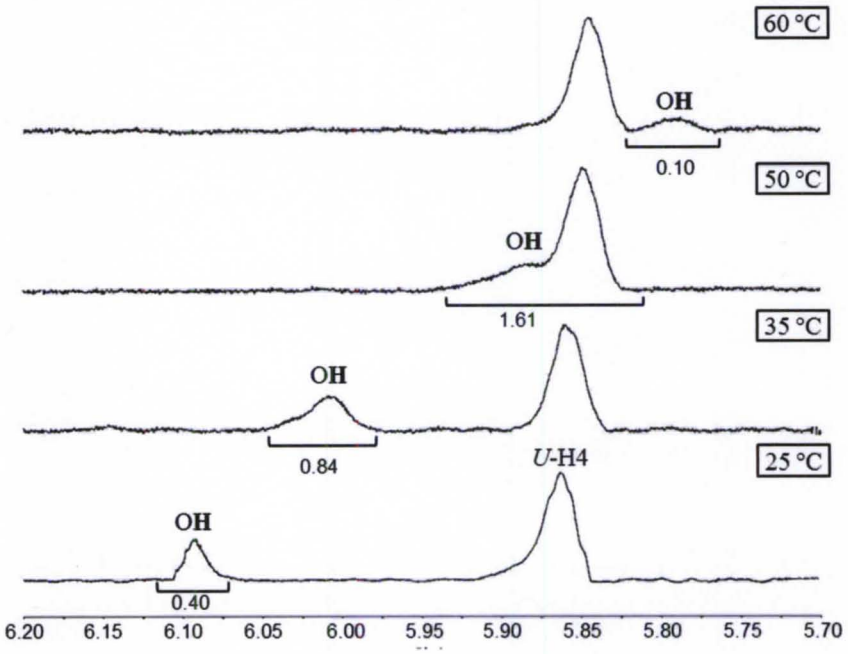

b.

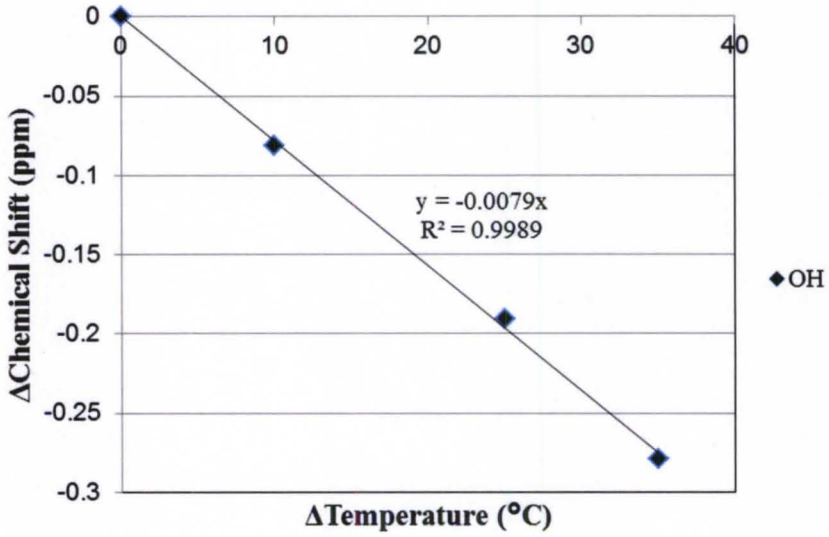

Figure 2-12. Temperature dependence of the hydroxyl (O**H**) proton(s) of ΔDiHA a) ^{1}H NMR spectra of the O**H** resonances at 25 °C, 35 °C, 50 °C, and 60 °C. b) Changes in chemical shifts as a function of temperature. Sample was prepared at 1.67 mg/mL in H_2O.

CONCLUSIONS

Prior to probing possible molecular interactions between HA and lipids, model studies were performed on ΔDiHA. This molecule features a double bond in the GlcU residue that has not been a major focus of past literature. The presence of both the α and β anomers led to significant spectral complexity. The use of powerful inverse 2D NMR techniques enabled resolution and assignment of each and every resonance of both anomers. Differences in chemical shifts between the two anomers were observed for all ring proton resonances of GlcNAc up through *U*-C1 of ΔGlcU. The resonances corresponding to the hydroxyl and amide protons were also detected when water (rather than D_2O) was used as solvent.

Temperature studies were carried out to evaluate intramolecular H-bonding of ΔDiHA and intermolecular H-bonding with the solvent. Ring protons were associated with a very small shielding trend which was attributed to weakening of intermolecular H-bonds with the solvent and less hydrophilic interactions. For the amide proton, the temperature coefficient was similar for the two resonances corresponding to the α and β anomers. The temperature coefficient values for N**H** indicate that they form weak intramolecular or water-mediated intramolecular H-bonds. Due to broadening caused by exchange with the solvent, only one hydroxyl proton resonance is observed. Its temperature coefficient is more negative than those found for N**H** indicating the participation in intermolecular H-bonding with the solvent. This is also evidenced by the broadening of the resonance. No prior analysis of ΔDiHA has been performed in exclusively aqueous solutions, which best mimic the biological environment.

CHAPTER 3

NMR STUDIES OF HA POLYMER/LIPID INTERACTIONS

INTRODUCTION

In biological systems, hyaluronan (HA) exists as a polymer. In this chapter, the polymeric form of HA has been analyzed by ^{1}H and ^{13}C nuclear magnetic resonance (NMR) spectroscopy. Interactions between HA and lipids were also probed by ^{1}H and ^{31}P NMR experiments to provide models that may explain the interactions between HA and lipids. These results can then be used as a foundation for future studies on the causes of the age-related liquefaction of the vitreous humor (VH). This introduction presents an overview of previous conformational and dynamic studies involving polymeric HA.

NMR Challenges

As mentioned in Chapter 2, spectral overlap and poor chemical shift dispersion for resonances of the HA polymer makes analysis difficult. Broadening results from HA's inherently large size and thus large correlation (tumbling) times. Additionally, HA's viscoelastic nature makes sample handling difficult. These challenges are discussed further in the results and discussion section.

Chemical Shift Assignments

Chemical shift assignments for ^{13}C resonances have been made for both native, high-MW (>10^6 Da), and enzymatically digested, low-MW (10^4 Da), polymers.[141,158] These assignments were made in D_2O and H_2O:D_2O (4:1) and required over 100,000

scans. The most recent ^{13}C assignments for the high-MW HA[141] are in good agreement with assignments made for the internal residues of the hexasaccharide (Table. 2-1).[135] ^{1}H chemical shift assignments, however, have only been made for the low-MW polymer in D_2O.[159] Darke and coworkers obtained a ^{1}H spectrum for the high-MW HA polymer in D_2O, but it was so poorly resolved that only two peaks (instead of the expected 12) could be observed (Fig. 3-1).[120] A heteronuclear correlation (HETCOR) spectrum obtained for the low molecular weight polymer at pH of 2.6 in D_2O has also been used to make ^{1}H and ^{13}C assignments.[160]

Intra- and Intermolecular Hydrogen Bonding

Hydrodynamic measurements have described HA as a wormlike coil, stiffened by intramolecular H-bonds. Intramolecular H-bonds have been deduced from X-ray diffraction, NMR, and computer simulation data. Intermolecular H-bonds have been suggested to stabilize tertiary structures. Scott and coworkers have analyzed digested and undigested HA in D_2O by ^{13}C NMR spectroscopy.[161] They observed significant broadening of the acetamido-carbonyl resonance suggesting decreased mobility and restricted rotation of this group. As part of a rigid C(=O)-NH unit, rotation of NH was also similarly restricted. These restrictions in motions were proposed to be due to intermolecular H-bonding between the N**H** and carboxylate groups of neighboring HA molecules. The H-bond was confirmed by comparing esterified HA with unmodified HA. Methyl esterification of carboxylates resulted in sharpening of the carbonyl resonance consistent with increased mobility indicating it was not participating in sterically-restrictive tertiary structures. They have proposed antiparallel arrangements of HA chains which overlap and form meshworks that are stabilized by H-bonding and hydrophobic forces. This highly cooperative structure, similar to the β-sheets seen in proteins, is only

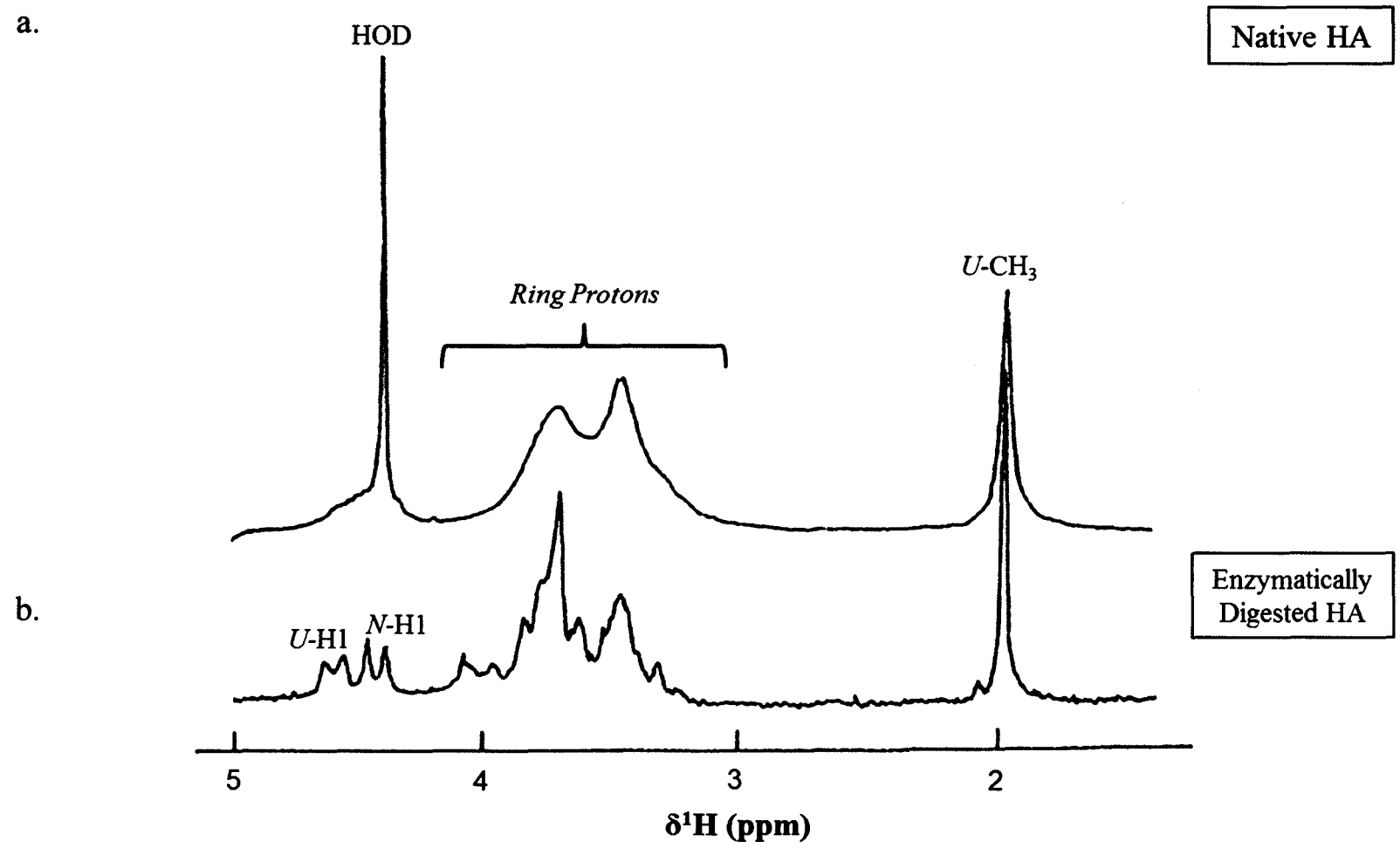

Figure 3-1. ^{1}H NMR spectra at 100 MHz of a) the native HA polysaccharide at 60 °C in D_2O and b) the native polysaccharide following enzymatic digestion at 92 °C by testicular HAase and water suppression. (Source: Adapted from Darke, A., *et al. Journal of Molecular Biology* 1975, *99*, 477–486.[120])

stable in high-MW HA solutions. A β-sheet tertiary structure has therefore been proposed for HA in solution. Sheet and tubular structures may explain its viscoelastic properties in solutions. These results are in agreement with electron microscopy data that reveal the presence of sheets and tube-like tertiary structures in solution.[162] Three kinds of lateral contact have been proposed: 1) antiparallel chains stacked by hydrophobic patches, 2) parallel chains joined by both stacking interactions and H-bonds and 3) crossing chains joined by H-bonds and stacking interactions.

Conformation Studies-Perturbations in Chemical Environment

Effects of pH. Hyaluronan experiences pH-dependent spectral changes in both acidic and alkaline conditions. Alkaline conditions (0.4 M NaOH) were shown to reversibly sharpen considerably both the ^{1}H and ^{13}C resonances in low-MW HA spectra.[158,159] This suggested that segmental motion is enhanced by disruption of some intrachain H-bonds upon ionization of hydroxyl groups (pKa 12-14). In addition, changes in chemical shifts, both upfield and downfield, were observed between neutral and alkaline solutions. In ^{1}H NMR, the greatest changes (~0.1 ppm) were observed for *U*-H2, *N*-H2, and *N*-H4 protons which are attached to groups (OH or NH) capable of mutual intramolecular H-bonding interactions across the β-1,3 glycosidic linkage in neutral solutions.[159] In ^{13}C NMR, most changes in chemical shifts, upon addition of NaOH, were generally small and in the downfield direction.[158] However *N*-C4 moves more downfield (~2 ppm) than any other resonance and three signals, *U*-C1, *U*-C2, and *N*-C3, did not follow the general downfield trend and were instead shifted in the upfield direction. These four ^{13}C signals which behave atypically are also associated with the β-1,3 linkage, either by direct attachment to the glycosidic oxygen or through H-bonding of attached groups (OH or NH) across the linkage. These changes upon alkalinization were attributed

to conformational changes about the β-1,3 linkage, presumably by changes in torsional angles. It was proposed that, under alkaline conditions, repulsive interactions between the ionized hydroxyl groups may be the responsible for conformational changes about the β-1,3 linkage.

Cowman *et al.* analyzed changes in ^{13}C resonances for HA oligosaccharides and polymeric HA under acidic conditions (pH 1.7).[141] Her group found the greatest chemical shift changes to occur for *U*-C5 and *U*-C6 (the carboxylate carbon) of GlcU which were shifted upfield by almost 3 ppm relative to their chemical shifts at pH 7. This large shift corresponded with the protonation of the carboxylic acid group at pH 1.7. In GlcNAc, the largest change in chemical shift, upon acidification, was observed for *N*-C1, which shifted downfield by approximately 0.5 ppm. Cowman's group stated that it was not clear whether this change reflected conformational change or just simply its proximity to the carboxylic acid group.

Almond and Blundell also analyzed pH-dependent changes for HA oligosaccharide up to small polymer sizes. Using NMR-monitored pH titrations ranging from pH 1.4 to 6.0, they analyzed chemical shift changes by ^{1}H NMR of amide proton resonances.[154] It was observed that all N**H** resonances had pH-dependent variations in chemical shift. As a threshold, a downfield shift resonance of ~ 250 ppb/K is associated with a H-bond that is populated ~20% of the time and larger values represent greater occupancies. If a water molecule were tightly bound in a long-lived water-bridge, such an interaction would also be expected to decrease the pKa of the COO^- group below its intrinsic value (pKa ~3). These researchers reported that the N**H** groups in the polymer were not forming significantly populated intramolecular H-bonds to CO**O**$^-$ groups or trapping water molecules in stable bridges.

Ionic Strength. The chemical shifts of carbons in HA have been shown to be little affected by moderate changes in ionic strength, except for carbons of the β-1,3 linkage. [141,163] These carbons show a small upfield shift consistent with chain expansion at low ionic strength.[141] The downfield shift was seen in both aqueous solution containing either 0.15 M NaCl or 0.15 M. KCl. Divalent cations (i.e. Ca^{2+}) caused a slightly more pronounced effect than the monovalent cations for the carbons of the β-1,3 linkage. These differences between divalent and monovalent cations suggested a modest conformation change resulting from the more effective screening of charges along the HA chain in $CaCl_2$ solutions. In addition, a significant upfield shift was observed for the carboxylate carbon of GlcU in the presence of Ca^{2+}. Cowman *et al.* proposed that the change in the carboxylate resonance reflects binding of Ca^{2+} to HA, whereas the linear charge density of single-stranded HA is too low to induce condensation of monovalent counterions.[141] This was observed for both the HA oligosaccharide and polymer without significant differences.

Dynamic Studies

In one of the earliest NMR studies of HA (1975), Darke and coworkers examined the conformational mobility of NaHA dissolved in D_2O by ^1H NMR.[120] Spin-spin relaxations times (T_2) for the acetamido-methyl group protons were measured either directly or from linewidths of the acetamido-methyl resonance. From a bimodal distribution of T_2 values, they identified two types of domains corresponding to different mobilities, specifically stiff and flexible domains. It followed that rapid motions lead to narrow spectral lines, while slow motion led to broadened resonances. However, the calculation that was used to relate line widths to the ratio of stiff to flexible domains was not well described and the origin of some variables involved in the calculation is

unknown.[164] The stiff parts accounted for 55-70% of the HA structure. The proportion of stiff to flexible domains was not altered by changes in ionic strength (0.1-3.0% NaCl), temperature, addition of denaturant (i.e. urea), or moderate changes in pH. The authors concluded that the stiff domains were prevented from equilibrating with the flexible domains by some unknown covalent features. Improvements to instrumentation and methods of interpretation have now shown, however, that the distribution of T_2 values does not resolve so clearly into separate components as seemed apparent in the earlier work.[159] The modern interpretation is that all segments are in continuous equilibrium between stiff and flexible states through the continuous making and breaking of H-bonds.

In 1983, Hoffman *et al.* performed relaxation experiments and measured T_1, T_2, and NOE values over wide ranges of pHs (2.6 to 13.5) and temperatures (20 °C to 95 °C).[160] A strong pH-dependent T_1 variation was detected at the acetamido-carbonyl carbon. This was attributed to reduced segmental mobility likely due to changes in H-bonding of the acetamido group. Additionally, changes in ionic strength did not affect the relaxational behavior or NOE-enhancement of HA. Cowman's group also found that T_1 relaxation times for carbon resonances were largely unaffected by changes in ionic strength (0.5-0.15 mM) and counterion type (NaCl, KCl, $CaCl_2$).[155]

The NMR analysis of polymeric HA in this chapter represents the first time the high-MW polymer has been reported with spectral resolution that yields more than just two broad resonances.[120] Temperature studies were carried out in D_2O for non-exchangeable resonances. Additionally, *ab initio* theoretical predictions of chemical shifts have been used to aid in the interpretation of observed NMR trends. Finally, lipid interactions with the HA polymer were investigated in model studies to gain insight into

the possible disruption of the HA interactions caused by the intercalation of lipids. Contributions from hydrophilic and hydrophobic forces are discussed.

The lipids chosen for the investigation of their possible interactions with HA included fatty acids (FAs), lyso-phosphatidylcholines (LPCs), diacylglycerol (DAG), and phosphatidylcholine (PC). The FAs, stearic acid (SA, 18:0) and oleic acid (OA, 18:1) were selected to assess if the presence of one site of unsaturation in OA affects its interaction with HA. Then, to evaluate if the addition of a polar, positively-charged headgroup (HG) impacts the interactions with HA two LPCs were selected: LPC-OA in which the sole oleoyl chain contains one site of unsaturation and LPC-SA, whose stearoyl chain is saturated. Additionally, the impact of one tail (in FAs and LPCs) versus two tails (in DAG and PC) was evaluated. These lipids enable the study of the nature of hydrophobic (acyl tails) and hydrophilic/electrostatic (polar, charged HG) interactions with HA.

EXPERIMENTAL

Chemicals

Analytes. Polymeric hyaluronic acid (HA) sodium salt from *Streptococcus equi* [poly(β-GlcU-[1→3]-β-GlcNAc-[1→4])] (MW = 1,500 to 1,800 kDa), 1-oleoyl-2-hydroxy-*sn*-glycero-3-phosphocholine (LPC-OA), 1,2-dipalmitoyl-*sn*-glycerol (DAG), stearic acid (SA) and oleic acid (OA) were purchased from Sigma-Aldrich (St. Louis, MO). L-α-Phosphatidylcholine (PC) frog egg yolk (predominantly 34:1) and 1-stearoyl-2-hydroxy-*sn*-glycero-3-phosphocholine (LPC-SA) were obtained from Avanti Polar Lipids, Inc. (Alabaster, AL).

Solvents. D_2O was purchased from Sigma-Aldrich (St. Louis, MO). In studies requiring water as solvent, Barnstead Nanopure water (17.8 MΩ, • cm) was used.

Sample Preparation

HA was prepared in D_2O at a concentration of 5.0 mg/mL (2.0-3.3 μM) for chemical shift assignments and temperature studies. In lipid mixture studies, HA was prepared at a concentration of 10.0 mg/mL in D_2O. Lipid samples were prepared in D_2O at concentrations of 1.0 mg/mL for OA, SA, LPC-OA, and LPC-SA and 2.0 mg/mL for DAG and PC. Lipid samples were ultrasonicated for 20-25 pulses to disrupt multilamellar and form unilamellar vesicles. Equal volumes of HA and lipid were combined so that the final concentration of HA in the mixture was 5 mg/mL. Final concentrations for the lipids in each mixture were 0.5 mg/mL for OA (1.8 mM), SA (1.8 mM), LPC-OA (0.96 mM), and LPC-SA (0.96 mM) and 1.0 mg/mL for DAG (1.8 mM) and PC (1.3 mM). Mixtures were vortexed for approximately 10 seconds to ensure equal distribution of each component. Individual HA and lipid solutions were then diluted by half so that the resulting concentration matched the concentration in the mixture.

NMR Analysis

^1H NMR spectra were obtained on a Varian VNMRS 700 MHz NMR spectrometer equipped with a 5 mm $^1H\{^{13}C/^{15}N\}$ ^{13}C enhanced pulsed field gradient (PFG) cold probe (Palo Alto, CA). All ^1H spectra were acquired with a minimum of 250 scans, 45° pulse width, and a relaxation delay of 1.000 second. All spectra were obtained at 25 °C unless stated otherwise. ^{31}P NMR data were obtained on a Varian-MR 400 MHz equipped with a 5-mm AutoX Dual Broadband PFG probe. Spectra were processed using either MestReC, version 4.7.0, or the newer MestReNova, version 7.1.2, software (Santiago de Compostela, Spain).

A coaxial insert containing 1.0 mM 4,4-dimethyl-4-silapentane-1-sulfonic acid (DSS) for ^{1}H NMR and inorganic phosphate (KH_2PO_4) for ^{31}P NMR dissolved in D_2O was added to the NMR tube for referencing and locking. Chemical shifts in ^{1}H NMR were referenced to DSS in the HA/lipid mixture studies and to the acetamido-methyl protons of HA (2.02 ppm) in all other studies. The acetamido-methyl proton chemical shift was determined with use of the insert and referencing to DSS at 25 °C. Chemical shifts in ^{31}P NMR were referenced to KH_2PO_4. For the HA/lipid for mixture studies, an insert containing 10.0 mM DSS was used and the intensities of reference peaks at 1.74 ppm and 3.10 were used to normalize the control spectra (HA alone and lipid alone) before performing their mathematical summation (with MestReC) for comparison with the spectra obtained for the actual mixtures.

Theoretical Calculations

In collaboration with Professor DuPré, theoretical *ab initio* calculations were performed using the polarizable continuum model (PCM) to aid in the interpretation of experimental results.[165] Theoretical calculations were used to predict the chemical shifts of the disaccharide protons while the polarity of the solvent increased. The absolute values of calculated chemical shifts are of less relevance than the trends that emerge. The predicted trends for the disaccharide were used as the basis for understanding the chemical shifts changes observed experimentally for the polymer. The electronically unperturbed molecule and three solvent dielectric media corresponding to water, methanol and chloroform with dielectric constants (ε) of 78.39, 32.63 and 4.9, respectively, were considered. It is expected that chemical shifts will become more deshielded upon increasing solvent polarity.

The isotropic shielding tensor (σ_{iso}), which is composed of diamagnetic (σ_{diamag}) and paramagnetic components ($\sigma_{paramag}$), determines the degree of shielding for the proton according to:

$$\nu = \gamma B_0(1 - \sigma_{iso})/2\pi$$

$$\sigma_{iso} = \sigma_{paramag} + \sigma_{diamag}$$

Both shielding tensor components are the result of a local induced magnetic field of circulating electrons. The diamagnetic component (usually positive) opposes the local magnetic field. The paramagnetic component (usually negative), on the other hand, aligns itself with it and therefore enhances the magnetic field sensed by the nuclei. Increasing either component results in a shielding effect for the given proton.

The atomic coordinates of HA were obtained from x-ray crystallography data in the protein data bank (PDB: 2BVK). The single point wave function for this model was calculated at the HF/6-31+G(d,p) level of theory using Gaussian 03, version C.02 (Wallingford, CT). NMR shielding tensors and chemical shifts were then obtained with the gauge including atomic orbital (GIAO) method at the same level of theory.[166,167] Chemical shifts were calculated with reference to tetramethylsilane (TMS) using isotropic values of σ (^{1}H; TMS) = 31.65 ppm

RESULTS AND DISCUSSION

NMR Analysis of Polymeric HA

^{1}H and ^{13}C NMR spectral traces were obtained on a 700 MHz cryogenic probe NMR spectrometer to achieve the high resolution and high sensitivity required for polymeric HA. The ^{1}H spectra of high-MW HA (Fig. 3-2a) reveals considerable broadening with respect to the resonances seen for the HA disaccharide (Fig. 3-2b). The

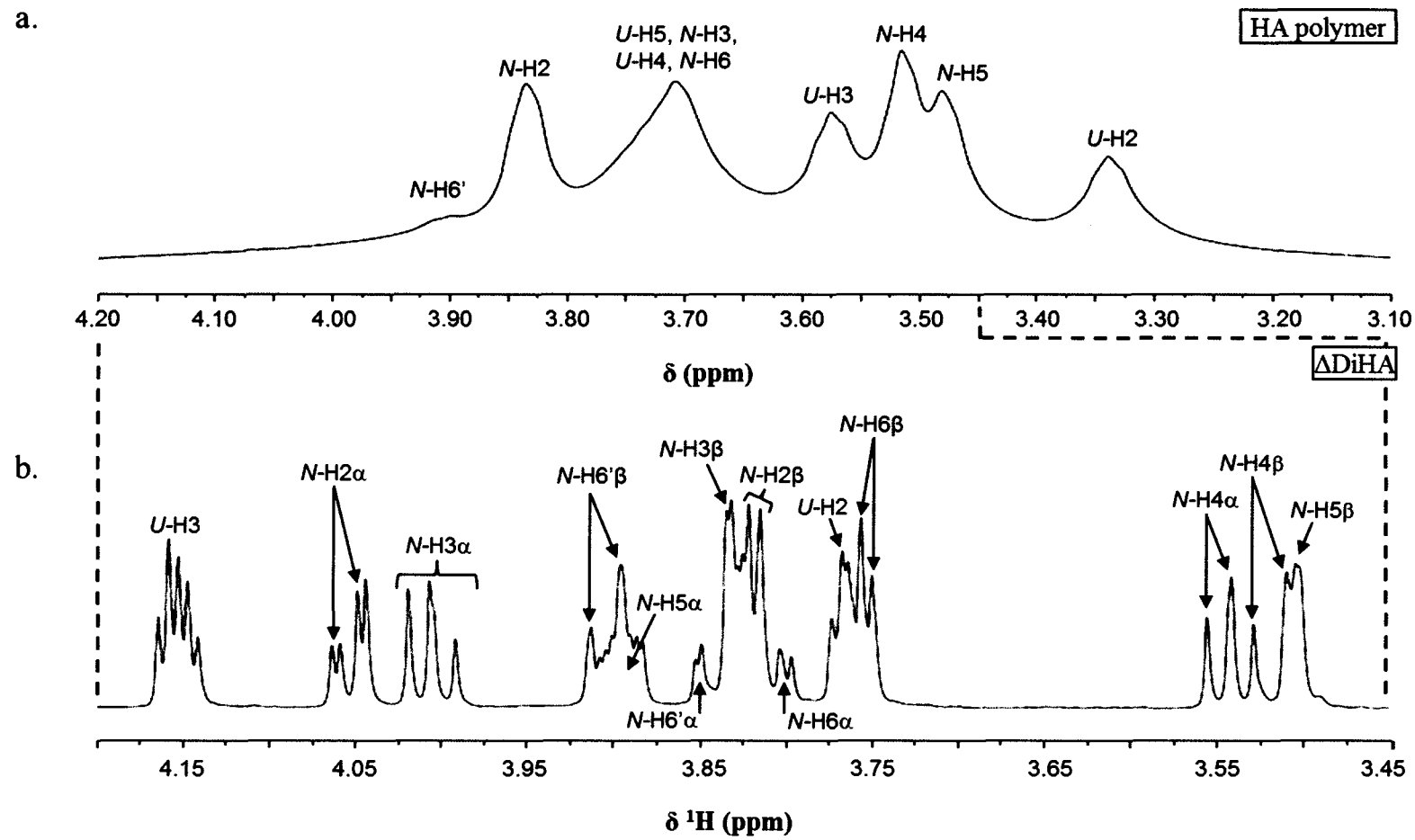

Figure 3-2. Comparison of ^{1}H NMR spectra of a) polymeric HA (3.10 - 4.20 ppm) with b) ΔDiHA (3.45 - 4.20 ppm). Polymeric HA was prepared at 5 mg/mL in D_2O and ΔDiHA was prepared at 1.67 mg/mL in D_2O.

large size and high viscosity of the polymer limits the spectral resolution (see the full ^{1}H spectrum in Appendix B, Fig. B-2).. Inherently long tumbling times and quick loss of phase coherence (small T_2) give rise to broad peaks and limits the achievable spectral resolution and sensitivity (Fig. 2-1). Increasing the concentration from 1 to 10 mg/mL gave rise to even broader peaks.

At HA solution concentrations of 5 mg/mL in D_2O, reasonable sensitivity and resolution were obtained in ^{1}H NMR spectra. All non-exchangeable resonances were detected, although some overlap occurred in the region between 3.65 and 3.80 ppm (Fig. 3-2a). Tentative assignments were made by comparison with ΔDiHA and by comparison with previously reported chemical shifts for interior residues of the HA hexasaccharide[135] which does not show anomeric differences and has been found to be a good approximation to the polymer. Chemical shift assignments are compared, and in good agreement, to literature values reported for the low-MW HA polymer (10^4 Da) in 1979 (Table 3-1). ^{13}C NMR spectra exhibited poor S/N and broadening; however, the observed chemical shifts did correlate well to those reported in the literature. Two-dimensional NMR spectral traces yielded such low S/N that no meaningful data could be obtained.

Temperature-Dependent Studies of the HA Polymer by ^{1}H NMR

Temperature studies of the HA polymer were carried out at 25, 35, 45, 55, and 65 °C (Fig. 3-3). Slight narrowing is observed when increasing the temperature suggesting a more flexible arrangement at higher temperatures. For most polymeric ring protons, increases in temperature caused small ($\leq$ 0.01 ppm) downfield changes in chemical shifts. This suggests an opening up of the polymer, at higher temperatures, causing it to be more exposed to water. The largest downfield shift (~0.01 ppm) was observed for *U*-H2 Interestingly, *N*-H2 and *N*-H4 are shifted slightly upfield at higher temperatures. In order.

HA Polymer		Experimental	Literature	Literature	Difference	Difference
Residue	Atom	High-MW Polymer	Low-MW Polymer	Int. Residues of HA_6	Exp-Lit (Polymer)	Exp-Lit (HA_6)
GlcNAc	H1	4.55	4.55	4.55	0.00	0.00
	H2	3.83	3.83	3.84	0.00	-0.01
	H3	*(3.71)	3.73	3.71	*	*
	H4	3.51	3.51	3.52	0.00	-0.01
	H5	3.48	3.47	3.48	0.01	0.00
	H6	3.9	3.91	3.91	-0.01	-0.01
	H6'	*(3.71)	3.71	3.76	*	*
	H-CH_3	2.02	2.01	2.02	0.01	0.00
GlcU	H1	4.45	4.46	4.46	-0.01	-0.01
	H2	3.33	3.34	3.34	-0.01	-0.01
	H3	3.58	3.58	3.58	0.00	0.00
	H4	*(3.71)	3.74	3.74	*	*
	H5	*(3.71)	3.72	3.70	*	*

Table 3-1. ^1H chemical shift assignments for the high-MW HA polymer. These values are compared to previously reported values for the low-MW HA polymer (in D_2O at 30 °C)[159] and internal residues of the HA hexasaccharide (HA_6) (in 5-10% D_2O/H_2O at 24 °C).[135] * Unresolved peaks.

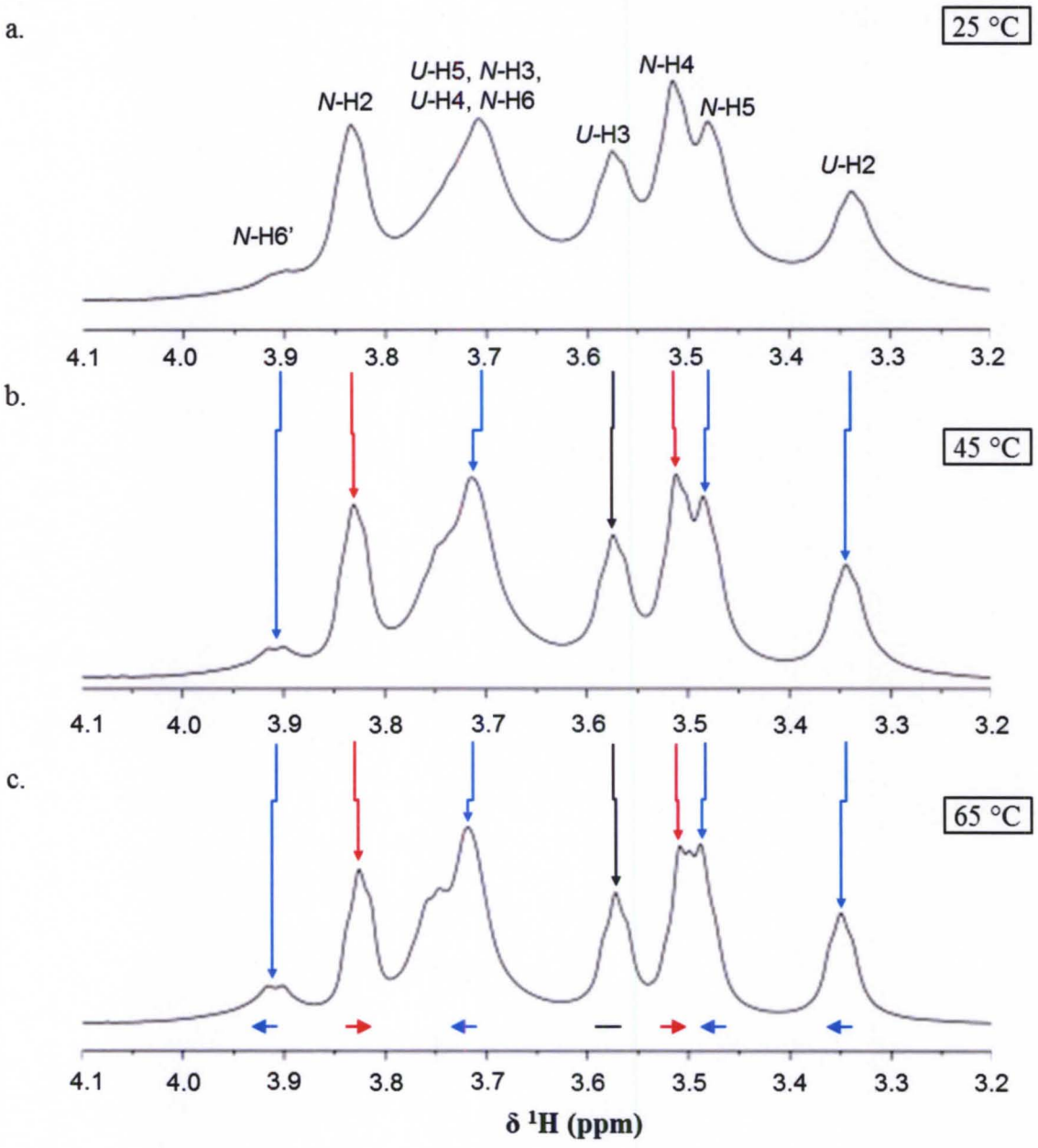

Figure 3-3. ^{1}H NMR spectra of the ring region of polymeric HA a) 25 °C, b) 45 °C, and c) 65 °C. Sample was prepared at 5 mg/mL in D_2O. Shielding trends, upon increasing temperature, are indicated by horizontal and vertical red arrows. Deshielding trends are indicated by blue arrows. Black arrows indicate a reversal in the trends as the temperature was increased.

to understand these experimental anomalies, theoretical *ab initio* calculations were performed using the polarizable continuum model (PCM).

Theoretical Calculations

Predicted chemical shift values for the HA disaccharide in solvents of various polarities ($CHCl_3$, methanol, and water) are provided in Appendix B (Table B-1). However, it is the trends that are of relevance and allow the interpretation of experimental observations of the HA polymer. In agreement with experimental data, a deshielding trend is observed for most ring protons with increasing polarity, relative to the molecule in a cavity with no solvent (Fig. 3-4). However, *N*-H2, *N*-H4, *U*-H2 and *U*-H4, do not follow this trend and become more shielded with increasing polarity of the solvent. A very small shielding trend is also observed for *N*-H6, however there is no statistically significant difference between the solvents. Therefore, these are not included in the interpretation of the observed trends.

Interpretation of Temperature-Dependent Trends

Theoretical trends have been used to predict whether specific protons enter a more or less polar environment upon increasing the temperature. Both experimental and theoretical data show a deshielding trend for most ring protons. Upon increasing the temperature, a small deshielding trend is observed for most ring protons. From theoretical calculations, this can be attributed to the molecule entering a more polar environment. This is expected as deshielding results from greater interaction with water, a polar solvent, (and less interaction with itself) when the temperature is increased. Polar solvents would be expected to attract electrons surrounding the protons in HA thus reducing electron density and leading to deshielding effects and increases in chemical shifts. This is also supported by the observed narrowing at higher temperatures

a.

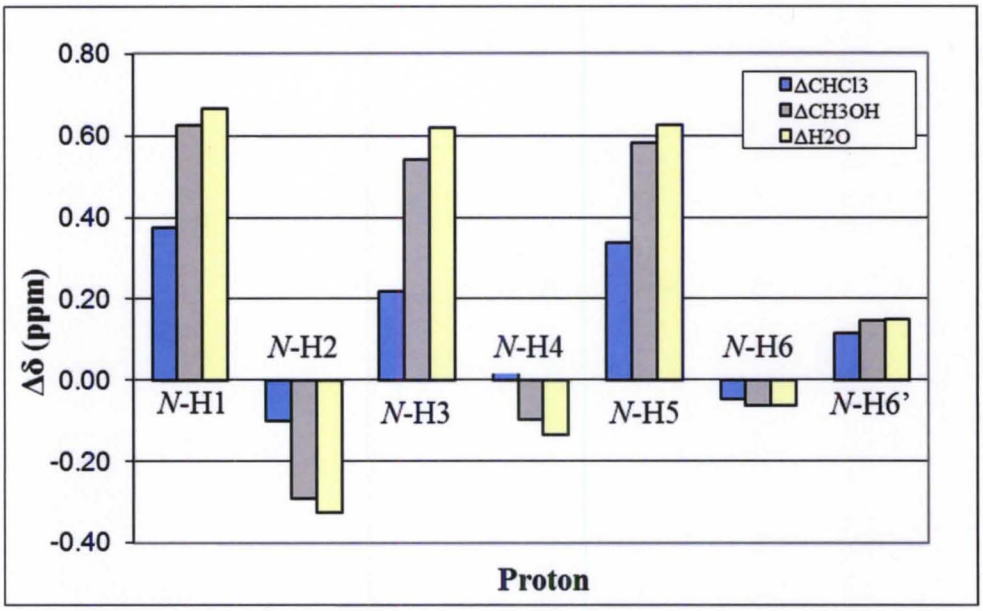

b.

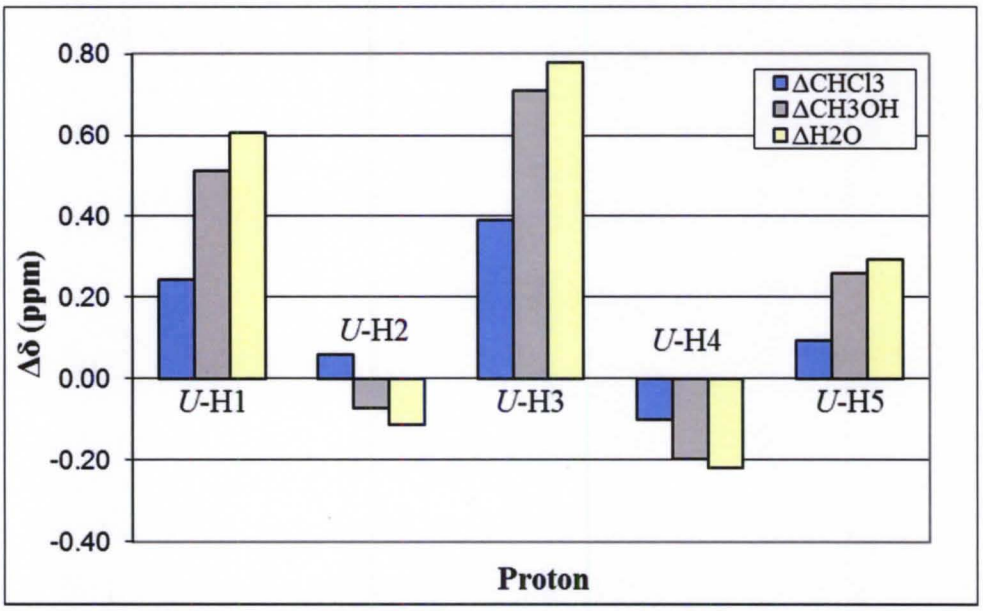

Figure 3-4. Theoretically predicted trends for the HA disaccharide in solvents of different polarities. Changes in chemical shift ($\Delta\delta$), relative to HA in no solvent, are shown for ring protons attached to a) GlcNAc and b) GlcU.

suggesting a more flexible arrangement where HA likely has more contact with the solvent. Thus the downfield trend of the polymer upon increasing the temperature can be attributed to less intra- and interchain interactions and more exposure to H_2O. This trend is opposite to that observed for the ring protons of ΔDiHA in Chapter 2 where weakened H-bonding with the solvent contributed to a general shielding trend at higher temperatures.

Shielding of chemical shifts is observed experimentally for *N*-H2 and *N*-H4 upon increasing the temperature. Theoretical calculations also show shielding upon increasing solvent polarity. This indicates that these protons are entering a more polar environment upon increasing the temperature. This would suggest a greater interaction with water at higher temperatures.

Interestingly, *U*-H2 and *U*-H4 have opposite experimental and theoretical trends. These protons become more deshielded with increasing temperature while theoretically being deshielded in a less polar solvent. Unfortunately, *U*-H4 cannot be resolved experimentally so theoretical trends for this proton cannot be explored further. As stated above, *U*-H2 shows the greatest deshielding trend upon increasing the temperature. According to theoretical trends, this is indicative of a less polar environment. Because the only thing in solution more polar than water is the negatively-charged carboxylate groups of GlcU along the HA chain, this suggests a conformational rearrangement that places *U*-H2 further from a carboxylate moiety upon increasing the temperature.

HA-Lipid Interactions

To understand ^{1}H NMR spectral changes occurring in mixtures, the spectra have been divided into a 'hydrophobic' region (low ppm) and a 'hydrophilic' region (high ppm). The hydrophobic region contains the resonances corresponding to the methyl (-

CH_3) and methylene ($-CH_2$) groups of the lipids as well the amide methyl protons of HA. The hydrophilic region contains the resonances for the ring protons of HA, the choline HG protons of LPCs and PC, and the glycerol backbone protons in DAG, LPCs, and PC. In all HA/lipid mixtures, some degree of broadening of the HA ring protons was observed indicating interactions between the two biomolecules.

DAG and SA

The ^{1}H NMR spectral traces for HA alone, DAG alone, calculated mixture, and the experimental mixture are provided in Figure 3-5. The resonances for DAG and SA were likely undetectable due to the strong hydrophobic forces that occur among molecules in a micellar arrangement. These micelles have increased tumbling times that cause extensive broadening and make the resonances undetectable. In aqueous solutions, micelles are arranged with their polar HG exposed to the solvent and their nonpolar acyl tails in the interior, shielded from the solvent.[168] Micelles are held together primarily by hydrophobic forces involving the acyl tails. If these forces are strong enough, HA is not able to disrupt/break the micelles and no lipid-related signals are detected. Despite not being detected themselves, the effects of DAG and SA on HA were still monitored in order to propose models that take into account the role of the HG and sites of unsaturation, and the impact of one versus two tails.

In aqueous solution, the nonpolar acyl tails of DAG are packed in the interior of the micelle, with the polar glycerol backbone on the exterior exposed to the solvent. The spectrum of HA, after mixing with DAG, reveals broadening of the ring region and also narrowing of the *U*-H2 peak of GlcU. Broadening suggests a closer, more compact arrangement after mixing and leads to the faster loss of spin coherence (small T_2). It isplausible that, in this closer arrangement, the water-exposed glycerol backbones on the

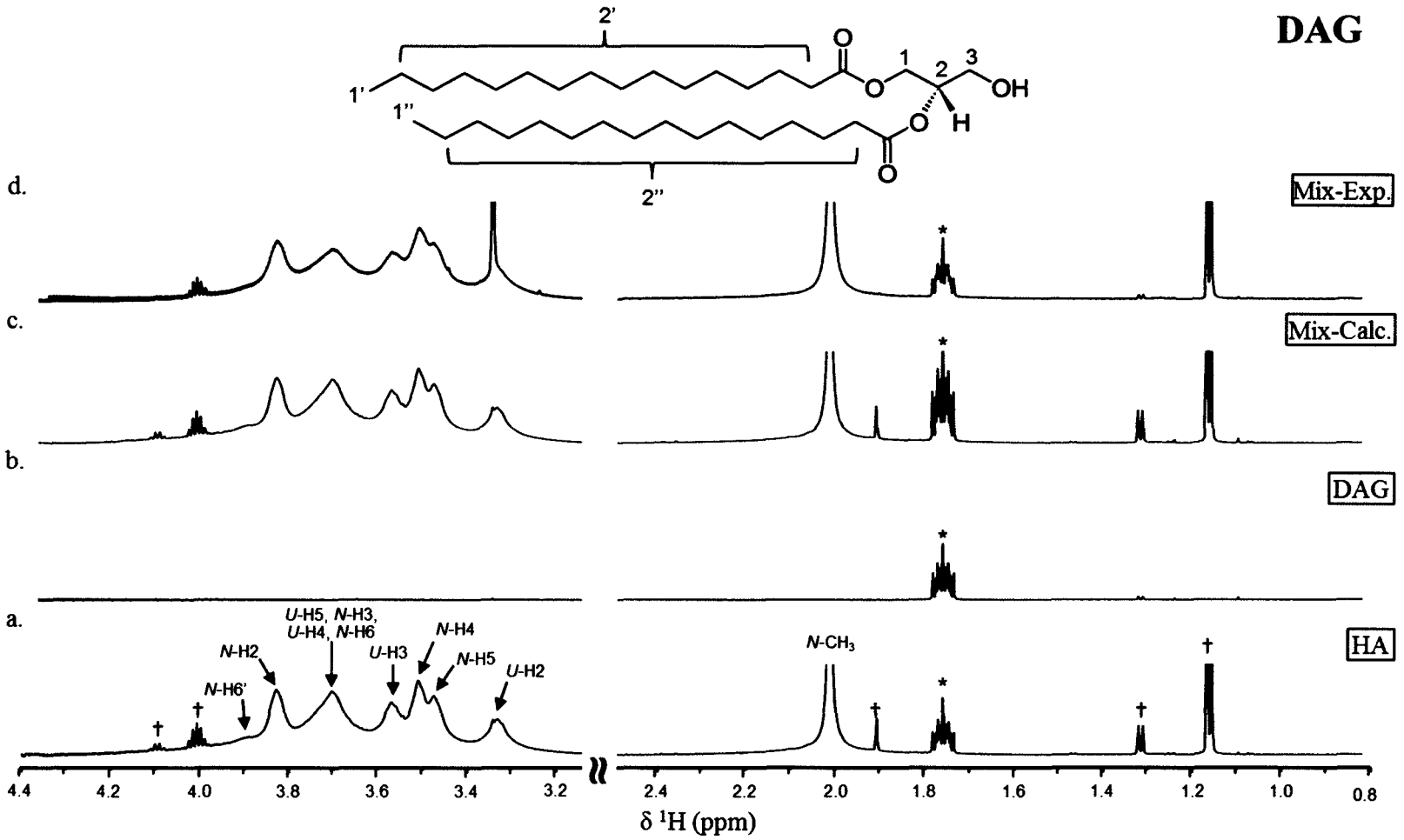

Figure 3-5. ^{1}H NMR spectra of a) HA, b) DAG, c) calculated addition of HA and DAG spectra, and d) experimental mixture of 1:1 (v/v) HA:DAG. * DSS (reference). † Contaminant.

DAG micelles interact with the hydroxyl group's along the HA chain. It is possible that the C=O and OH moieties of DAG interact with the hydroxyl groups at C2 and C4 of GlcU through H-bonding, thus leaving the *U*-H2 proton more exposed to the solvent. Narrowing of resonances, such as what is observed for *U*-H2, is caused by slower relaxation times (large T_2) and reveals enhanced flexibility and motion in the local environment of *U*-H2.

The NMR spectral traces for HA alone, SA alone, calculated mixture, and the experimental mixture are provided in Figure 3-6. In SA, the lack of unsaturation, and thus unbent acyl tail, allows for tighter packing than in micelles of OA, which has a site of unsaturation at the center of the 18-carbon tail. This difference is reflected by their large difference in melting points (mp = 13-14 °C for OA and for mp = 67-72 °C for SA) and demonstrates the very strong hydrophobic forces at play in SA micelles. Like DAG, both broadening of the HA ring protons and narrowing of the *U*-H2 resonance were observed. DAG has a mp of 66-69 °C, similar to that of SA, which may explain their similar behaviors alone and in the presence of HA.

The broadening of the HA ring proton resonances is slightly greater for the HA/SA mixture than for the HA/DAG sample. This indicates a tighter arrangement for HA in presence of SA compared to DAG. This may be the result of stronger H-bonding interactions of HA with SA compared to DAG. SA is capable of accepting a H-bond through its negatively-charged carboxylate group. The interaction between HA and the glycerol backbone of DAG appears weaker than the interaction of HA with carboxylate group of SA as indicated by a lesser degree of broadening for the HA ring protons. Indeed, the negative charge on SA would have a stronger drive to attract a nearby hydrogen for H-bonding.

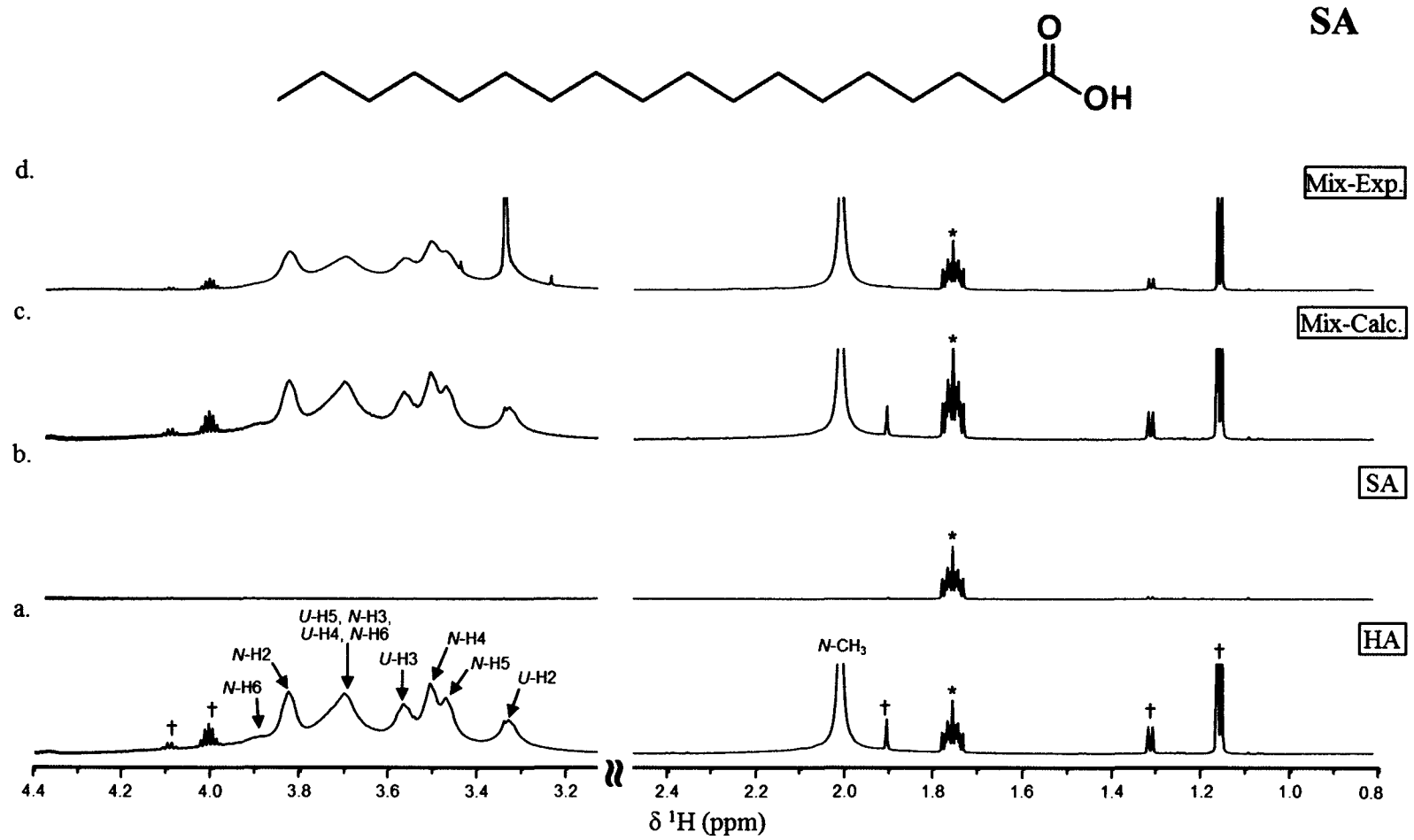

Figure 3-6. ^{1}H NMR spectra of a) HA, b) SA, c) calculated addition of HA and SA spectra, and d) experimental mixture of 1:1 (v/v) HA:SA. * DSS (reference). † Contaminant.

OA

The ^{1}H NMR spectral traces for HA alone, OA alone, calculated mixture, and the experimental mixture are provided in Figure 3-7. The hydrophobic forces in OA are not as strong as those in SA micelles due to the presence of a single site of unsaturation in acyl tail. The *cis* double bond creates a bend in the acyl tail and makes the packing in micelles less tight. Indeed, the midpoint phase transition temperature (T_m), where the packed acyl tails go from an ordered to a disordered phase, is 12 °C for OA, compared to almost 70 °C for SA. As a result, the spectrum of OA (Fig. 3-7b) reveals the signals for methylene, terminal methyl, and olefenic protons (not shown). The observed spectral changes between the mathematical addition (Fig. 3-7c) and the actual experimental mixture (Fig. 3-7d) reveal significant broadening of OA resonances in the experimental mixture. This is the result of a competition for hydrophobic forces between lipids and between lipids and the hydrophobic patches of HA. HA is proposed to be able to disrupt the hydrophobic interactions between OA molecules.

After mixing, significant broadening is observed in the acyl tails of OA and moderate broadening of the HA ring protons. Broadening of the acyl tail indicates that there are greater interactions in the mixture with HA than the micelles alone. It is reasonable to assume that interactions occur between OA acyl tails and hydrophobic patches along the HA chain. Broadening of the olefenic protons at 5.32 ppm (not shown) was also observed in the mixture and provides further evidence of hydrophobic interactions. Due to the bent nature of the acyl chain, the tail should be able to wrap around the HA chain.

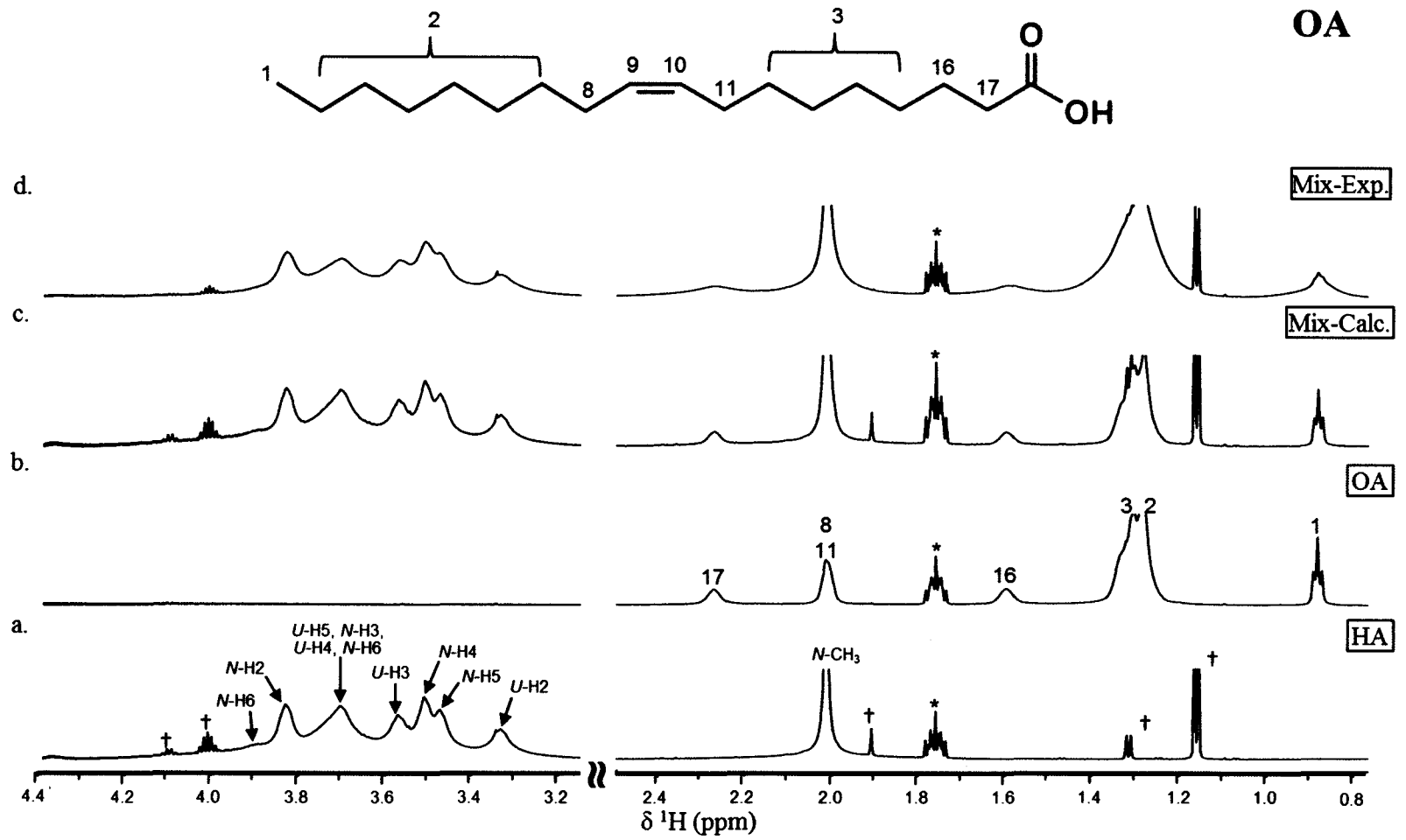

Figure 3-7. ^{1}H NMR spectra of a) HA, b) OA, c) calculated addition of HA and OA spectra, and d) experimental mixture of 1:1 (v/v) HA:OA. * DSS (reference). † Contaminant.

Interestingly, the narrowing of *U*-H2 was not observed. This could be attributed to the wrapping of an OA molecule with a single carboxylate head around the HA. A single carboxylate group may not be able to interact through H-bonds with the hydroxyl groups of C2 and C4 of GlcU thus leaving *U*-H2 unaffected. This differs from the proposed interaction of HA with SA micelles that have multiple carboxylate groups on the micelle's exterior.

LPC-OA

The ^{1}H NMR spectral traces for HA alone, LPC-OA alone, calculated mixture, and the experimental mixture are provided in Figure 3-8. Like OA, LPC-OA also features only one tail which may lead to tighter interaction with HA chain compared to two tails, such as was the case in DAG. In the spectrum of LPC-OA alone, resonances related to the acyl tails, similar to OA, were observed. In addition, resonances corresponding to the glycerol backbone and phosphocholine HG were also seen. Relative to the other lipids, LPC-OA caused the most dramatic effect in HA ring broadening and in the narrowing of the *U*-H2 resonance. The *U*-H2 resonance narrowing in the mixture of HA and LPC-OA was not observed when OA was present in the mixture. This suggests that the size of the phosphocholine moiety may be a factor in interactions that lead to the narrowing *U*-H2. In the case of OA, a single carboxylate group did not change the dynamics around the *U*-H2 proton. However, the larger phosphocholine with its positive charge is proposed to interact with the hydroxyl groups of HA and disturb the interactions that lead to the broad resonance of *U*-H2 in HA only.

Like OA, the hydrophobic forces between acyl tails of molecules packed in a micelle could be overcome by HA allowing the lipid-related resonances to be observed. It is expected that LPC-OA will have even weaker hydrophobic forces than OA due to the

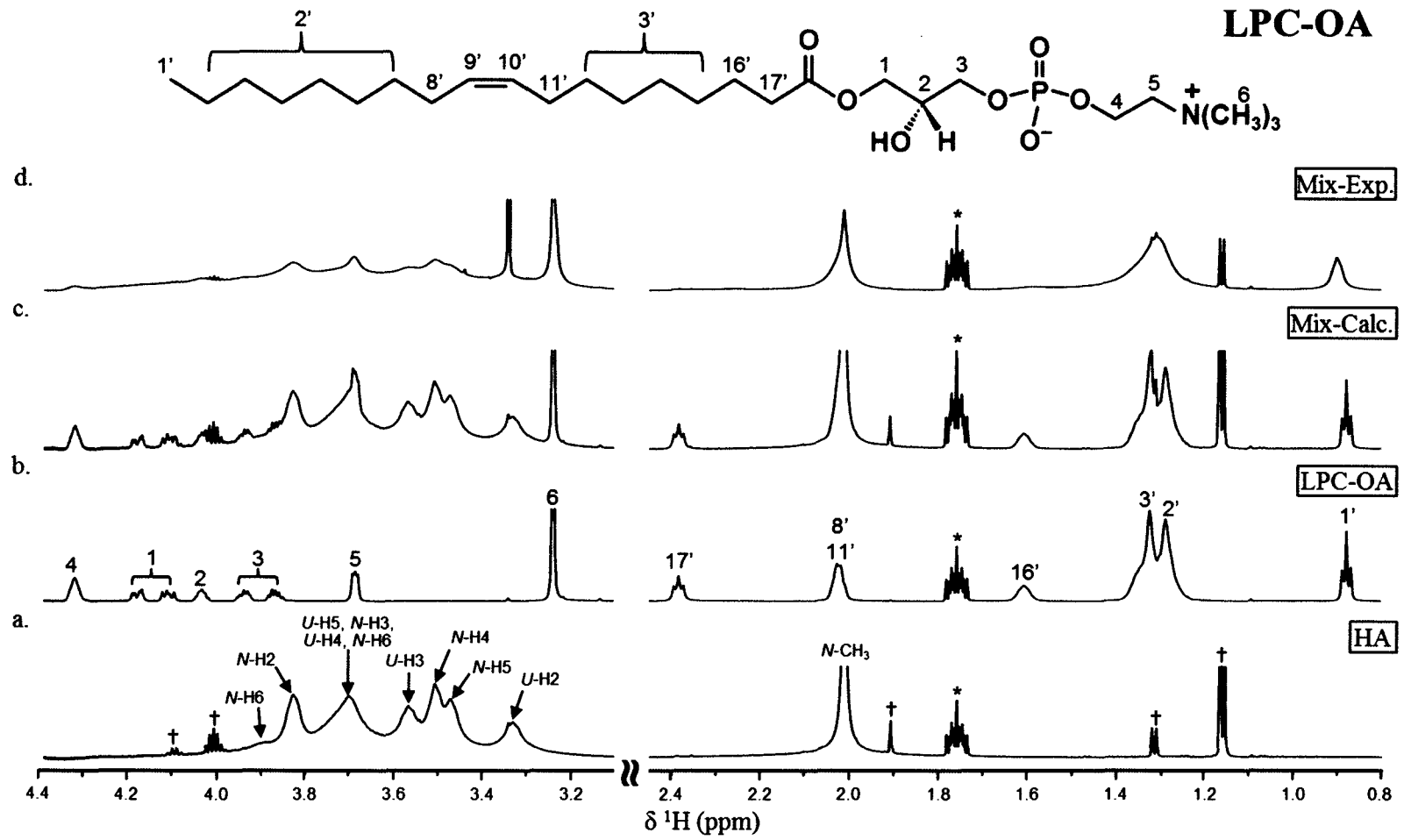

Figure 3-8. ^{1}H NMR spectra of a) HA, b) LPC-OA, c) calculated addition of HA and LPC-OA spectra, and d) experimental mixture of 1:1 (v/v) HA:LPC-OA. * DSS (reference). † Contaminant.

presence of bulky phosphocholine HG. The large HG of LPC-OA is proposed to keep the acyl tail of neighboring lipids further apart thus weakening the hydrophobic forces.[168]

Hydrophobic interactions between HA and LPC-OA are evidenced through broadening of the acyl tails. Like OA, the acyl tails are expected to wrap about the HA chain. LPC-OA showed significant broadening of the olefenic protons and acyl chains after mixing, but slightly less broadening than that observed for OA after mixing. This suggests that the presence of the HG reduces how close the acyl tails of LPC-OA can get to the hydrophobic patches of the HA chain. Additionally, a downfield shift was observed for the terminal methyl protons of the acyl tail indicating they are in a more polar environment after mixing. The terminal methyl groups are in a significantly hydrophobic environment in the center of the micelle, but experience a more polar environment upon interaction with the HA chain.

The glycerol backbone and choline protons were also broadened after mixing suggesting a more compact arrangement with HA than in the micelles. It seems logical that a positively-charged HG would be drawn to GlcU due to the negatively-charged carboxylate group. ^{31}P NMR showed a small downfield shift from -0.176 to -0.180 ppm of the phosphorus resonance after mixing. However, changes in chemical shift for ^{31}P cannot easily be correlated to either a more or less polar environment. The reason for this slight shielding effect is not known, but suggests at least some interaction involving the choline HG is occurring.

LPC-SA

The ^{1}H NMR spectral traces for HA alone, LPC-SA alone, calculated mixture, and the experimental mixture are provided in Figure 3-9. Unlike SA, all lipid-related resonances could be observed. The presence of the bulky choline HG appears to prevent

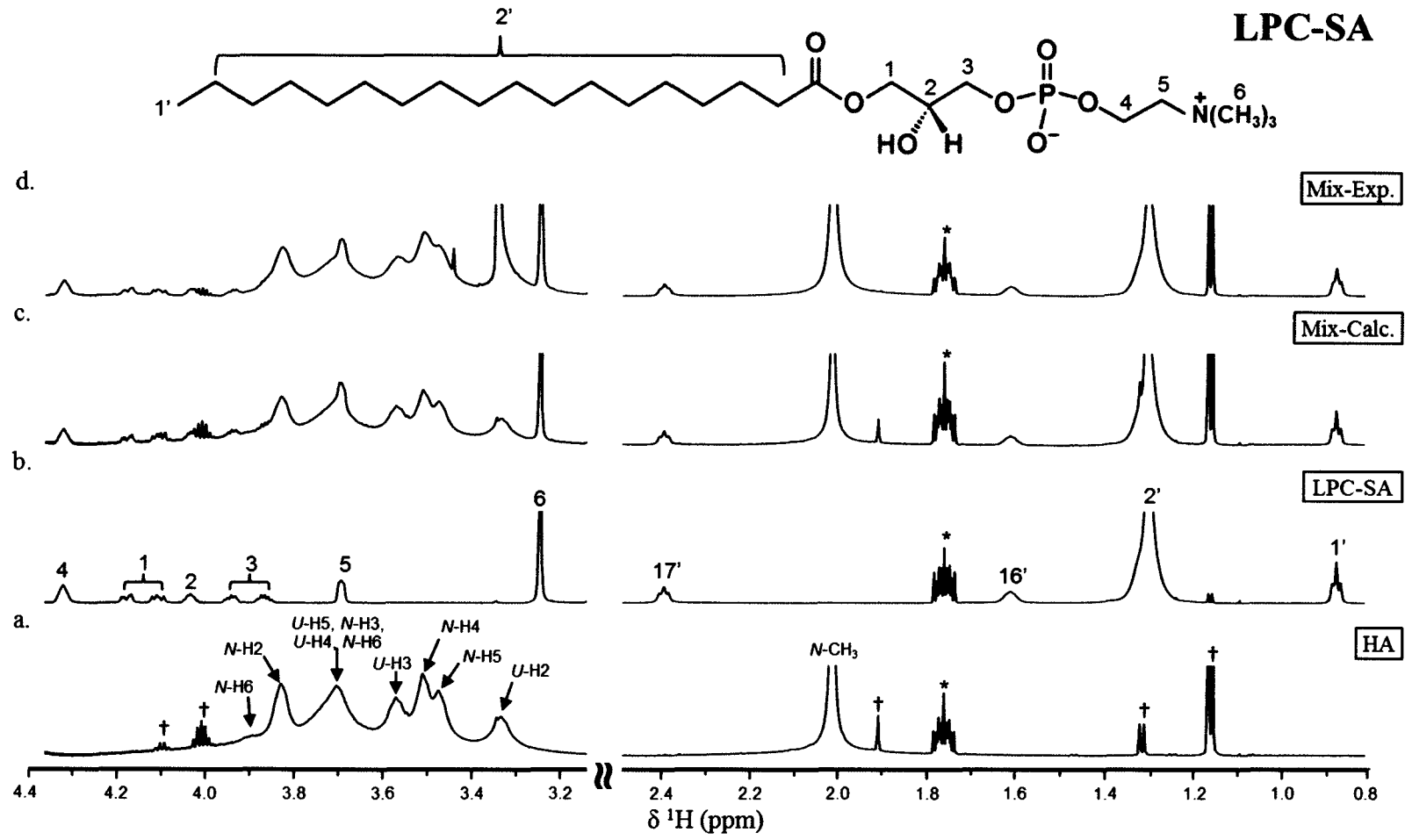

Figure 3-9. ^{1}H NMR spectra of a) HA, b) LPC-SA, c) calculated addition of HA and LPC-SA spectra, and d) experimental mixture of 1:1 (v/v) HA:LPC-SA. * DSS (reference). † Contaminant.

individual molecules from getting as close in the micelle, as compared to SA.[168] This results in weaker hydrophobic forces between molecules and allows HA to compete for hydrophobic tail of LPC-SA thus disrupting the micelle.

Broadening of HA ring protons and narrowing of the *U*-H2 resonance are both observed. However, both effects were less pronounced than those observed in the HA/LPC-OA mixture. This indicates that LPC-SA has weaker interactions with HA relative to LPC-OA. It is thought that the lack of double bond makes the acyl tail more rigid and unable to intertwine with the HA chain. Based on the lack of significant broadening for both HA and LPC-SA resonances, it appears that the interaction between the two is minimal.

The acyl tail protons are also only minimally broadened in LPC-SA and significantly less broadened than what was observed for OA and LPC-OA. These observation suggests that the flexibility of the acyl tail, either straight or bent, affects how tightly the tail can interact with the HA chain in solution. The lack of a double bond in LPC-SA prevents it from being able to wrap around the HA chain. For lipids containing unsaturated tails (i.e. LPC-OA), the bend in the tail allows for greater flexibility of the tail and enables its wrapping around the HA chain. It is possible that the tails of LPC-SA are near the HA chain but not intertwining and therefore we observe only slight broadening.

Only very minor broadening is observed in the glycerol backbone protons suggesting that they are not involved in the interaction with HA. However, slight broadening is observed for the choline protons suggesting that they may take part in the interaction with HA. Additionally, ^{31}P NMR showed a small change in the phosphate

resonance chemical shift from -0.182 to -0.179 ppm. As was the case in LPC-OA, the HG may be involved in the interactions that lead to the narrowing of *U*-H2.

PC

The ^{1}H NMR spectral traces for HA alone, PC alone, calculated mixture, and the experimental mixture are provided in Figure 3-10. In general, PC resonances are weaker in intensity than the observed resonances for the other lipid species, both before and after mixing with HA. This is the result of broadening caused by presence of lamellar (bilayer) vesicles instead of simple micelles which are formed by FAs and LPCs. The PC used in this study was from egg yolk and contained a mixture of acyl tails. According to the manufacturer, the predominant PC species contains a palmitoyl (16:0) and an oleoyl (18:1) tail. The T_m for this PC species is -2 °C. In comparison, the T_m for the dipalmitoyl PC species is 41 °C. This large difference shows the significance of a double bond, which creates a bend in the tail, on the packing of acyl tails within a micelle thus causing a reduction in the hydrophobic forces between tails. Unlike the LPCs, ^{31}P NMR revealed the phosphate resonance to be so broadened that it was undetectable in both the mixture and the control (PC alone). PC is known to form multi- or uni-lamellar vesicles in which the lipid bilayer(s) expose the charged HG to the aqueous phase and the acyl tails interact with other. In the bilayer, the phosphocholine HG is in a staggered arrangement such that the phosphate of one HG is near the choline of the neighboring HG.[168] These interactions are at least partially disrupted by HA as the resonances of PC can still be observed. This suggests more of an interaction that what was observed for DAG and SA. However, the mathematical and experimental spectra are quite similar suggesting much less of an interaction than what was observed for OA and the LPCs.

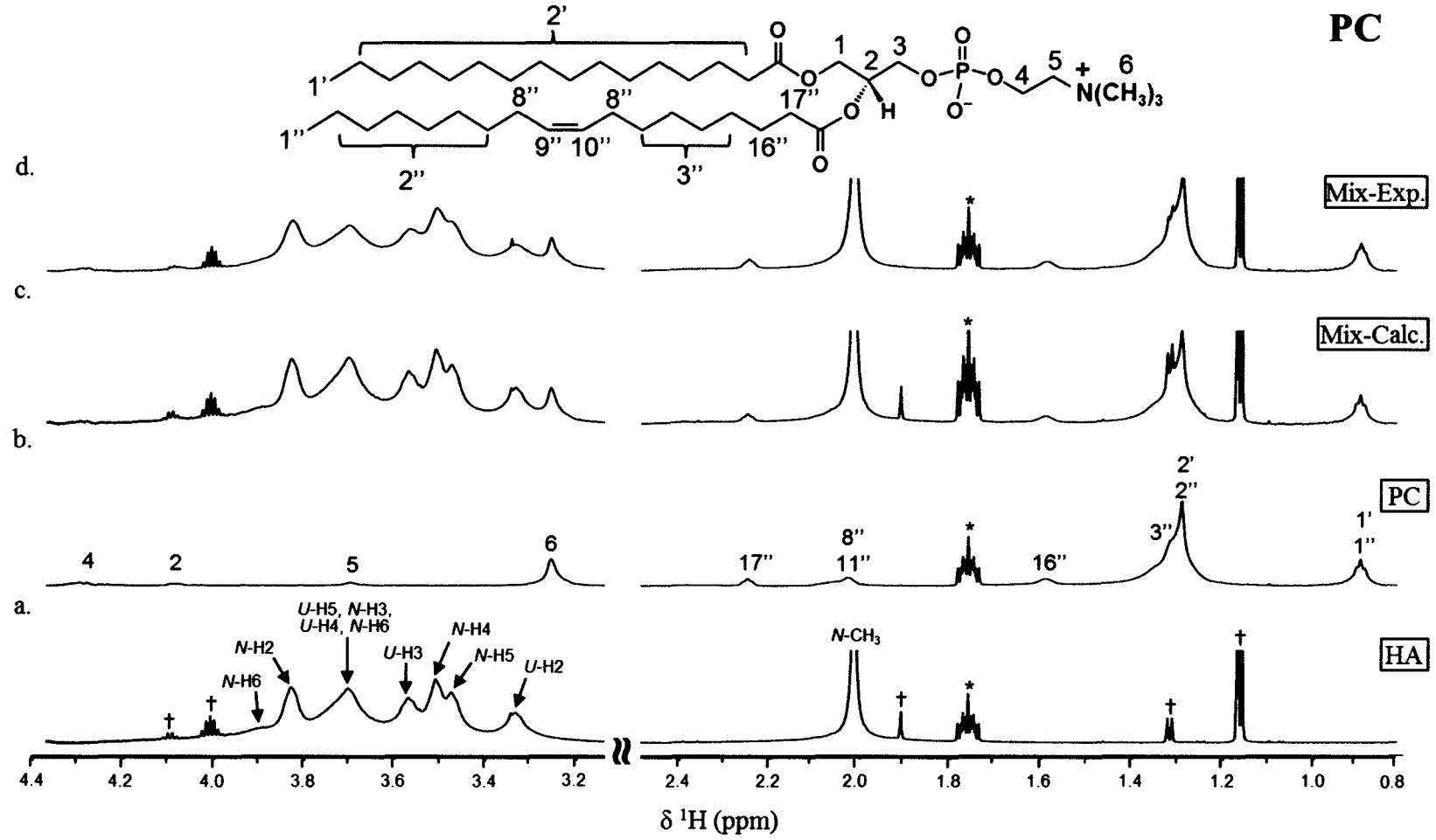

Figure 3-10. ^{1}H NMR spectra of a) HA, b) PC, c) calculated addition of HA and PC spectra, and d) experimental mixture of 1:1 (v/v) HA:PC. * DSS (reference). † Contaminant.

Moderate broadening of HA ring protons and minimal broadening of the acyl tail protons were observed after mixing. This indicates only minimal interactions with the HA chain as was the case with LPC-SA. The fact that PC has two tails instead of one may inhibit interactions with the HA chains due to the larger cross-sectional area of PC (as compared to LPCs). It is possible that the HA chain is able to accommodate a single acyl tail more easily than two acyl tails.

No broadening of either olefenic (not shown) or choline protons was observed which also suggests that PC may not be able to get close enough to the HA chain to be able to interact. HA is likely unable to disrupt the electrostatic interaction between neighboring phosphocholine HG in lipid bilayers. No narrowing of the *U*-H2 peak in HA also supports this postulate.

CONCLUSIONS

The biologically relevant, high-MW polymer was analyzed by NMR. Compared to the disaccharide analyzed in Chapter 2, differences in anomer chemical shifts were not observed and the polymer spectrum features considerable broadening due to slow correlation times and fast T_2 relaxation times. Past literature of polymeric HA has focused on the low-MW polymer due to the high viscosity and increased broadening associated with the high-MW polymer. Through the use of the 700 MHz NMR we were able to resolve most protons with the exception of one broad peak corresponding to the overlap of four ring proton resonances. Increases in temperature revealed slight narrowing and small downfield changes for most resonances. These rather small changes may result from the opening up of the polymer chain to allow for more interactions with the solvent.

^{1}H NMR was used to probe possible interactions occurring between HA and lipid-related species (FAs, LPCs, DAG, and PC). Spectral changes were monitored between control solutions and binary mixtures. OA was used as indication of hydrophobic interactions between acyl tails and hydrophobic patches along the HA chain. In comparison to SA, the lack of a double bond prevented HA from disrupting the strong hydrophobic forces in the SA micelles. LPCs were studied to examine the role of the HG in HA interactions. LPC-OA featured the greater changes in HA resonances compared to all lipid species analyzed. However, HA was shown to have tighter interaction with the oleoyl of OA due to the lack of a HG which allows it to get closer to the HA chain. The interactions of HA with LPC-OA were also compared to those with PC to evaluate the effect of one tail versus two tails. Due to size constraints, a single tail was able to interact closer with HA. SA, DAG, and PC were shown to have only minimal interactions with HA.

To our knowledge, no prior studies have analyzed the possible interaction between HA and lipids at the molecular level. Both hydrophobic and electrostatic interactions were found to play significant roles. Interactions were shown to favor an unsaturated, single acyl tail, attached to a positively-charged HG. These studies represent the first step in understanding the role lipids play in the two- and three-dimensional structure of HA.

CHAPTER 4

MALDI-MS STUDIES OF HA DISACCHARIDE & LIPIDS

INTRODUCTION

Mass spectrometers are equipped with a variety of ion sources and mass analyzers, each with inherent benefits and limitations, which can be targeted to specific applications. The review of all the possible combinations of ionization sources and mass analyzers is beyond the scope of this introduction. Instead, a brief background is provided on mass spectrometry (MS), followed by a more detailed description of matrix-assisted laser desorption ionization time-of-flight MS (MALDI-TOF-MS) which is of relevance to this dissertation. Results from previous MALDI-MS studies of hyaluronan, HA, and phospholipids, PLs, (and metabolites) are also presented.

Mass Spectrometry Background

Mass spectrometry (MS) is a widely used technique to analyze inorganic, organic, and biological molecules. From mass spectra, an analyte's elemental composition, isotopic ratio, and structure can be deduced.[169–171] In addition, MS can be used as a detection system following separation by a number of techniques, i.e. gas chromatography (GC), liquid chromatography (LC), and capillary electrophoresis (CE).[172] Prior separation for MS analysis may be necessary in the characterization of complex mixtures if the ionization method chosen results in a large number of fragments for each compound present.[170] MS is based upon the ionization of the analytes, separation

of ions on the basis of mass-to-charge ratio (*m/z*), and detection of ions by a mass analyzer. [172] Both positive and negative ions with one or more charges can be generated and detected. Dimers and trimers may also be observed if the concentration of the analyte is too high.

Depending on the ionization method used, 'soft' versus 'hard', varying degrees of fragmentation can occur.[172] Hard ionization methods form ions by breaking bonds leading to the formation of fragment ions. Soft ionization techniques do not break bonds and thus produce 'parent' ions that reveal the molecular weight (MW) of the native molecule. For these reasons, soft ionization techniques can be used for the analysis of complex mixtures. MALDI is a relatively soft form of ionization that has become popular over the past two decades for the detection and quantification of biomolecules, both large and small.[170,173,174]

Basic Principles in MALDI

In matrix-assisted laser desorption ionization (MALDI), laser radiation (often with ultraviolet, UV, frequencies) is impingent onto the sample/matrix spot.[175–177] The UV-absorbing matrix promotes the ionization along with desorption/ablation of the analyte into the gas phase.[178,179] MALDI-MS offers advantages of ease of use, quick analysis times, and high sensitivity extending to zeptomoles (10^{-21} mole) thus allowing the detection of biological compounds in single cells.[180] It is particularly ideal for biomolecules and large organic molecules and polymers because the limited fragmentation enables the detection of the parent ion in the singly charged state. MALDI has also been extended to the direct analysis of complex biological mixtures both *in situ* and *in vitro*.[96,181,182] In conjunction with a time-of-flight (TOF) mass analyzer, high mass resolution is commonly achievable up to several hundred kDa.[174]

MALDI requires only small volumes (0.5-1.0 μL) which are deposited ('spotted') into small wells on the surface of a metallic (i.e. stainless steel) 'MALDI plate'.[172] The sample and matrix, in appropriate molar ratios ($1:10^3$-10^4), are combined either directly on the plate (dried-droplet method) or prior to spotting (premix). Ideally, spotting should result in a thin, homogenous layer of matrix crystals in which the analyte is embedded (Fig. 4-1). Cocrystallization of the analyte with the matrix is critical in MALDI for ionization to take place.[183] Once the spots have dried, the MALDI plate can be introduced into the instrument, either under atmospheric pressure or vacuum (10^{-6} Torr) conditions. Although atmospheric MALDI provides softer ionization and less fragmentation, vacuum MALDI is often preferred due to its greater sensitivity compared to that of atmospheric MALDI.[172] Once inside the ionization chamber, a pulsing UV laser is rastered over a sample spot. The energy from the laser is transferred to the UV absorbing matrix causing the desorption/ablation of both matrix and analyte molecules into the gas phase creating a 'plume' containing various ions (Fig. 4-1).

In general, the ionization process can be divided into primary and secondary ionization steps which take place in the solid phase and the gaseous plume, respectively.[184–186] The primary step involves the conversion of neutral compounds into charged products, by influence of the laser pulse on the sample. This step takes place primarily in the solid phase and the ions are most often matrix-derived species.[185] Ionization mechanisms involved in the primary ionization step are not fully understood at this time and are likely to involve several different mechanisms operating simultaneously.[186] These may include multi-photon ionization, energy pooling, disproportionation, excited-state proton transfer, thermal ionization, desorption of preformed ions, and breakup of the sample into charged chunks and clusters.[186–190]

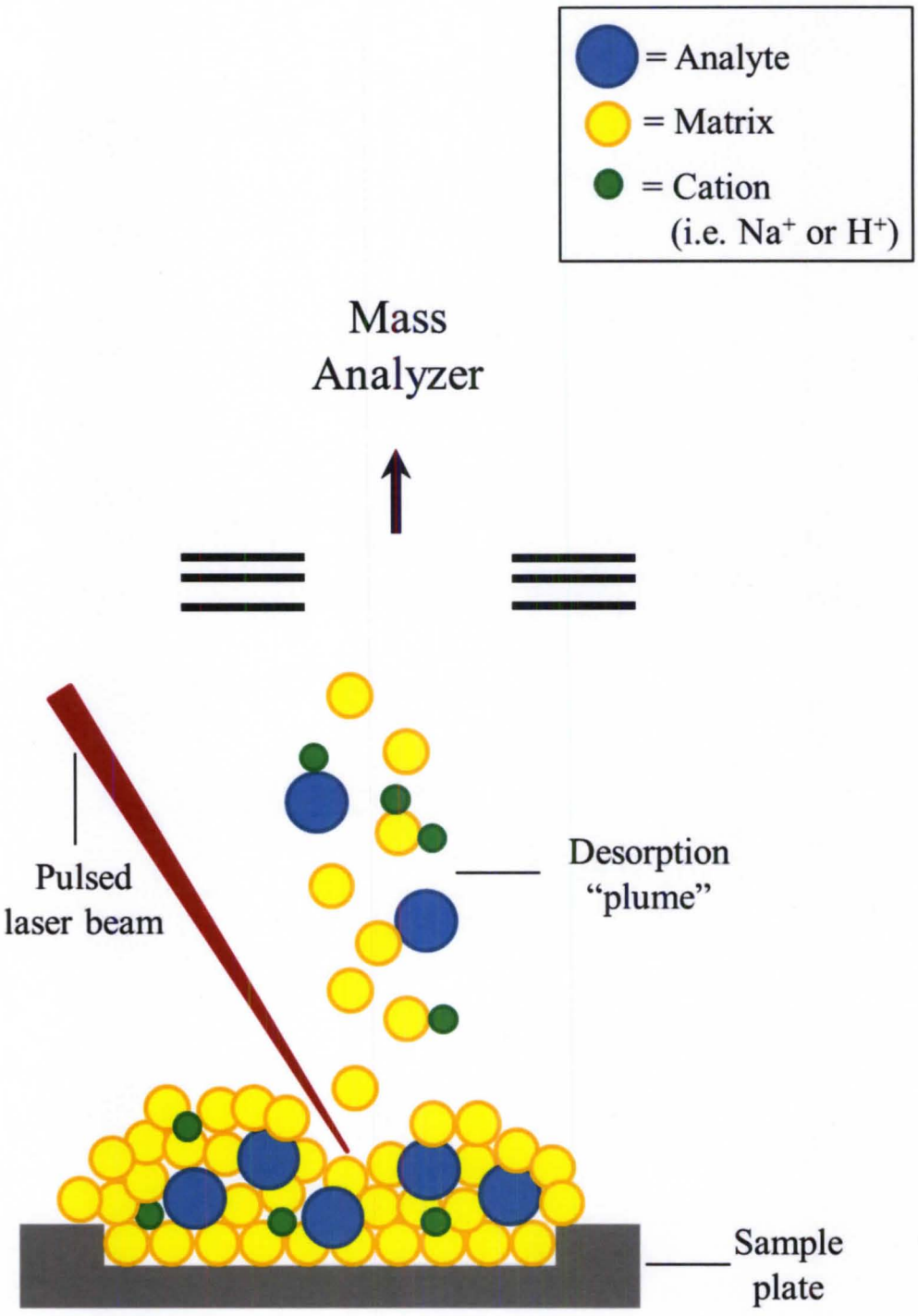

Figure 4-1. Ionization process in MALDI-MS. A pulsed laser beam is irradiated on the sample spot. Upon desorption/ablation, a gas phase plume is formed containing the matrix and analyte ions.

Secondary steps occur after desorption/ablation and in the gaseous plume that results. Collisions between the analyte (A) and the excess matrix (m) contribute to the ionization of A by various processes including electron transfer, proton transfer, and cation attachment or transfer.[191]

1. Proton transfer: $mH^+ + A \leftrightarrow m + AH^+$ and $(m\text{-}H)^- + A \leftrightarrow m + (A\text{-}H)^-$
2. Electron transfer: $m^+ + A \leftrightarrow m + A^+$ and $m^- + A \leftrightarrow m + A^-$
3. Cation transfer: $Na^+ + A \leftrightarrow m + ANa^+$

Ionization depends critically on the choice of matrix as well as the matrix to analyte ratio.[186] The matrix serves as either a proton donor or acceptor to the analyte and will thus ionize the analyte with either positive and negative charges, respectively. The deprotonation/protonation of the analyte is related to some extent to the acid-base characteristics of the matrix.[184] The presence of metal cations, such as Na^+ and K^+, also leads to formation of charged adducts. The formation of dimers and trimers is also possible particularly when the analytes are present in high concentrations. Singly charged ions are most common, but multiply charged ions can sometimes be formed.[188] The matrix also acts to separate analyte molecules from each other, to absorb energy from a UV laser, and to promote the vaporization of the analyte, as mentioned above. Requirements for a suitable matrix include high absorptivity at the laser wavelength, stability under low pressures (if vacuum MALDI is used), low extent of fragmentation, and good mixing properties with the analyte so as to produce homogenous cocrystallization.

A large number of matrices have been explored over the years mostly on a trial and error basis.[183] The pH of the matrix plays a role in the ionization, either positive or negative, of the analyte.[192] Acidic organic matrices favor protonation of the analyte and

formation of positively-charged ions.[193] Common acidic matrices, used in the analysis of both carbohydrate and PLs, are 2,5-dihydroxybenzoic acid (DHB) and cyano-4-hydroxy-cinnamic acid (CHCA).[194–197] On the other hand, nearly neutral or basic matrices favor deprotonation of the analyte and produce negatively-charged ions. Para-nitroaniline (PNA),[198,199] 9-aminoacridine (9AA),[200–202] and 2-(2-aminoethylamino)-5-nitropyridine (AAN)[203] have been used successfully in the past for the negative ionization of lipids.

In addition, various micro- and nano-sized inorganic compounds (metal oxides, metal salts, and single element nanoparticles[204]) can also be employed as MALDI matrices.[204–206] Inorganic matrices are characterized by low or no matrix background interferences, chemical inertness and better spot-to-spot reproducibility compared to the more traditional organic matrices.[182] Metal oxides are particularly attractive matrix candidates because their isoelectric points (IEPs) vary over a wide range of pH from acidic to basic. As with organic matrices, acidic oxides such as titania (IEP = 4-5) form predominantly cations, while basic oxides such as Fe_2O_3 (IEP = 8-9) are expected to promote the formation of anions.[182,207]

Basic Principles in TOF Mass Analyzer

MALDI is often coupled with a time-of-flight (TOF) mass analyzer which performs the separation of ions based on the time difference between the ionization pulse and the arrival of each ion at the detector.[169] In a TOF analyzer, the ions are accelerated by an electric field, with typical accelerating voltages (V_s) of 1 to 20 kV. The ions pass a charged grid and drift over a field-free space of length D, commonly between 0.50 and 3 m (Fig. 4-2).[170] Ideally, all ions leaving the source have the same kinetic energy (KE):

$$KE = \frac{1}{2}mv^2 = zeV_s$$

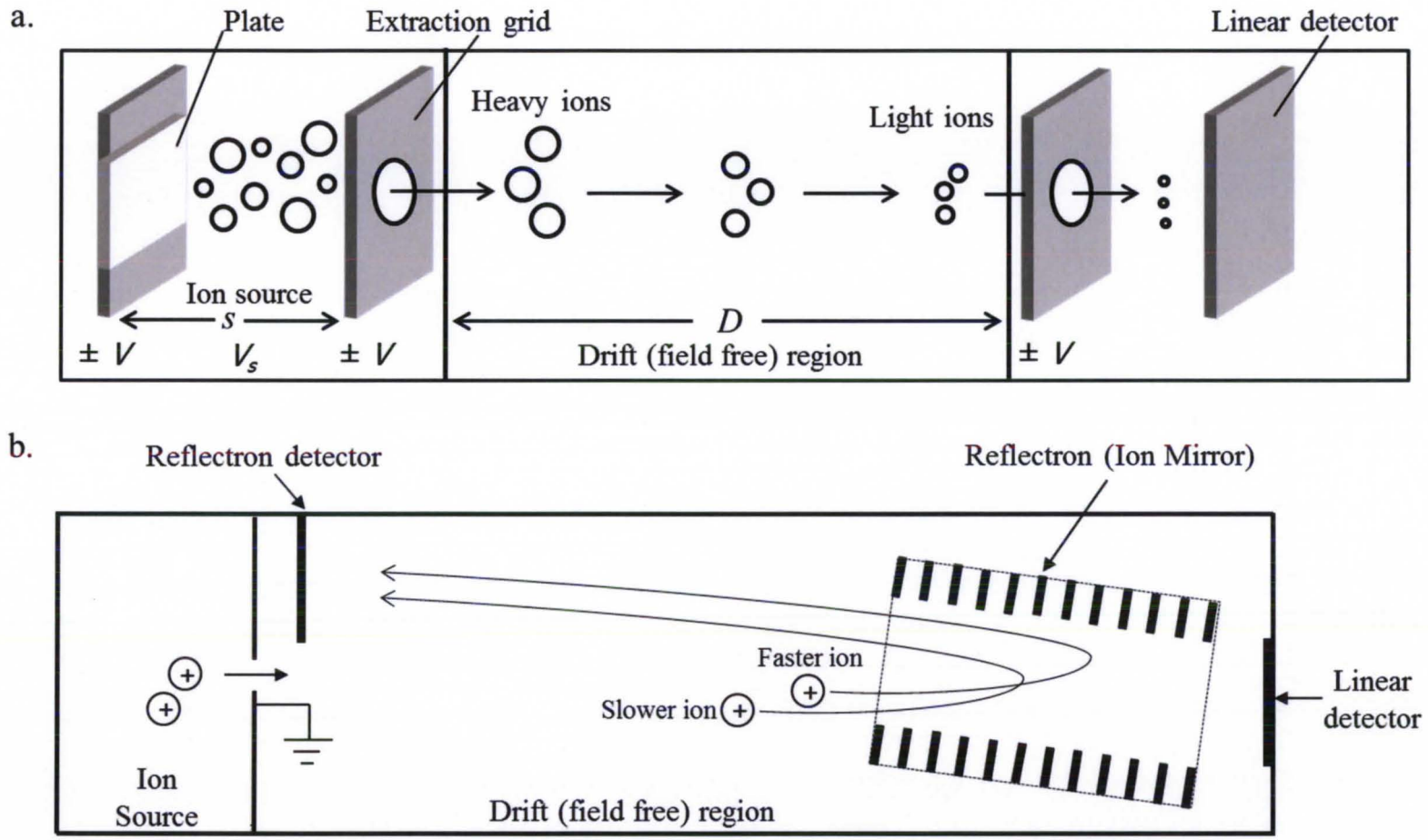

Figure 4-2. Time-of-flight (TOF) mass analyzers. a) Linear detection showing separation based on *m/z*. Lighter ions travel faster than heavy ions and reach the detector sooner. b) Reflection detection showing focusing of ions that vary in kinetic energy (KE). Fasters ions (higher KE) travel deeper into the reflectron and have longer path lengths compared to slower moving ions with less KE.

where m is the mass of the ion, v is the initial velocity, e is the charge of an electron and z is the number of charges on the ion. Their velocities in the drift region are inversely related to their masses:

$$v = \left(\frac{2zeV_s}{m}\right)^{1/2}$$

Ions with lower m and higher charge (z) arrive at the detector faster than those of higher m and lower z. The time of flight (t) can be expressed as follows:

$$t = \left(\frac{m}{2zeV_s}\right)^{1/2} D$$

Consequently the value of m/z can be inferred from the time of flight:

$$\frac{m}{z} = 2eV_s\left(\frac{t}{D}\right)^2$$

The TOF mass analyzer can operate in either positive or negative modes allowing the detection of positive and negative ions generated from the ionization processes.[169] Changing from one mode to another is performed simply by inverting the voltage at the source and reflectron. The resolution in TOF-MS is degraded if ions of the same mass do not arrive at the detector at the same time. Factors that can affect the resolution in TOF-MS include the initial conditions of the ions (temporal, spatial, and KE distributions), the formation of fragments, and the properties of the ion detector.[208]

Improvements to resolution lead to narrower peaks by decreasing differences in arrival time (t) to the detector for ions with the same m/z.[169] Temporal variations are the result of ions of equal m/z being formed at different times. An ion formed at time t_1 will reach the detector before an ion formed at $t_1 + \Delta t$. If Δt is constant, resolution can be improved by employing longer tubes that allow for longer drift times and decreases the impact of Δt relative to the total flight time.[169]

Loss of resolution due to KE distribution can be corrected through the use of a reflectron (also called reflector or electrostatic mirror) which reflects ions toward the detector.[178] More energetic ions penetrate deeper in the reflectron thus taking a slightly longer path to the detector (Fig. 4-2b). Ions with lower KE spend less time in the reflector and have a shorter flight trajectory but arrive at the reflector detector at about the same time as the ions with higher KE. Ions with the same *m/z* values, but different initial KE, are thus focused and differences in arrival time are decreased thus improving resolution.[209] Unfortunately, this comes at a cost of sensitivity loss because the ions are spread out once they turn around in the reflectron and only a fraction of the initial ion population can be collected by the detector. Furthermore, the reflectron reduces the accessible mass range to < 10,000 *m/z* due to metastable decay of large molecules in the flight tube.[178] This results in the intact molecular ions having a higher KE than their decay products and thus do not arrive at the detector at the same time. These fragment ions, which are often abundant, are observed by the reflectron but not in linear mode.

Another approach to improve resolution is through delayed extraction or time-lag energy focusing.[208,210] The mass resolution is enhanced by minimizing the initial velocity distribution of formed ions. This is achieved by allowing a short delay (~150 ns or less) between the laser pulse and the voltage pulse that extracts ions from the source.[169] In this time period the KE of the ions decreases and both the distribution of their initial velocity distribution and their temporal spread of entry times into the drift tube are reduced.

Post-Source Decay

Post-source decay (PSD) is a method of obtaining additional fragmentation from a selected precursor ion.[171] At higher laser intensities, some ions are decomposed into PSD fragments in the drift tube. These fragments are mainly formed by unimolecular

decomposition after the precursor ions are fully accelerated.[186] The fragment ions travel at the same velocity as the parent ions. However, the KE of the fragment ion (KE_{fr}) differs from that of the parent (KE_p) as given by:

$$KE_{fr} = KE_p(m_{fr}/m_p)$$

where m_{fr} and m_p are the masses for the fragment and parent ions, respectively. The fragment ions of lower KE are reflected more quickly than the precursor ion. As a result the fragment ions are not properly focused by the reflectron and appear at incorrect *m/z* values.[177] Fragments with lower KE can be focused by adjusting the voltage applied to the mirror. The PSD spectrum is collected at various mirror ratios, each ratio is chosen to focus correctly the fragment ions.[171] The focused spectral regions obtained at each mirror ratio are then 'stitched' together to produce the PSD spectrum. Analysis of the masses of fragmentation ions obtained by PSD can be used to aid structure determination but requires significant amounts of samples and is time-consuming.

Whereas PSD is specific to TOF mass analyzers, tandem MS (MS-MS) can be applied to a variety of other mass analyzers, such as orbitrap and quadrupole detectors, in addition to TOF.[171] MS-MS connects two mass analyzers in sequence. Similar to PSD, a precursor ion is selected to undergo additional fragmentation and the information obtained can be used for structural elucidation.[169]

Past MS Studies of HA

High-MW HA has not been detected by MS; however, HA oligomers up to ~10,000 Da have been characterized and differentiated in both the positive and negative ion modes.[211–213] Enzymatic degradation of HA polymer is required to produce fragments that lead to detectable ions. The choice of enzyme determines whether the GlcU residue at the nonreducing terminus is saturated or unsaturated.[36] Hyaluronidase (HAase)

enzymes lead to the fully saturated form of GlcU while HA lyase enzymes produce fragments containing a Δ^4-unsaturated, GlcU at the nonreducing end.[142,143] Digestion conditions and times determine the size of fragments obtained. Fragments containing an even-number of saccharides are most common; however, odd-number oligomers have been occasionally observed by MS, albeit at relatively low abundance compared to even-number oligomers.[214–216] Mass spectral analysis of HA fragments has been used in degradation monitoring applications and pharmaceutical formulation using HA fragments as drug delivery agents.[217–219]

Many of the previous studies have also employed separation techniques, such as high-performance liquid chromatography (HPLC), capillary electrophoresis (CE) and size-exclusion chromatography (SEC), to separate fractions containing different chain lengths and molecular weights.[59,213,220–223] Although much work has been performed on enzymatically digested HA, little is known about its fragmentation pathways.

Past ESI-MS Studies of HA

Like MALDI, electrospray ionization (ESI) is a soft ionization technique, but its method of ionization is quite different. In ESI, the sample solution is sprayed from the tip of an electrically charged capillary and nebulized to form small charged droplets of the sample solution at atmospheric pressure. These charged droplets are in turn desolvated to form gas phase ions. Solvent signals are typically not present in ESI spectra due to the practically complete removal of solvent from the charged droplets. In contrast to MALDI that involves a pulsed ionization method, the ionization in ESI is continuous, making it suitable for interfacing with a separation technique (i.e. LC or CE). Traditionally, ESI sources have been coupled to quadrupoles and quadrupole ion traps as mass analyzers. They are also more readily configured as tandem mass spectrometers for mass-selection

and subsequent fragmentation of a chosen ion. Unlike MALDI, samples need to be virtually free of salts otherwise they clog the capillary. Multiply charged ions (+2, +3, +4, etc.) are also much more common to ESI than MALDI, which adds complexity to mass spectra of mixtures.

ESI-MS of HA fragments obtained by digestions with HA lyase and HAase have revealed oligomers containing an odd-number of saccharides. Baker *et al.* observed odd-numbered oligomers in the negative mode for masses up to 8 kDa.[216] However, their presence was not observed by HPLC or MALDI analysis. Furthermore, relative intensities of the odd-numbered oligomers detected by ESI-MS showed a cone-voltage dependence that suggested that the odd-numbered oligomers resulted from collisional activation. It is therefore necessary to keep the cone voltage low and precisely controlled in ESI-MS. Under these conditions, ESI-MS results showing only even-numbered oligomers are in agreement with those obtained with other techniques.

ESI-MS has been coupled with HPLC to analyze HA oligosaccharides obtained from digests with HAase. Fragments were observed from the disaccharide-size up to n = 20 repeating units (~7,600 Da) and a series of negatively-charged species of different *m/z* ratios, were observed for each oligosaccharide.[224] Smaller HA species, di- and tetrasaccharide, exhibited mainly $[M-H]^-$ anions while hexa- to decasaccharide size fragments existed predominantly as a charge state of -2. Larger oligomers (from n = 6 up to n = 20 repeating disaccharide units) were characterized by even higher, -3 to -5, charge states. Furthermore, smaller HA species ($n \leq 20$) revealed anions containing an odd number of saccharide units, albeit in relatively low abundance. However, only even-numbered species were observed for HA species larger than n = 20.

Past MALDI-MS Studies of HA

One of the first studies showing the applicability of MALDI-MS to the MW characterization of enzymatically degraded HA was that of Yeung and Marecak in 1999.[212] Digests were separated using gel-filtration chromatography (GFC) and MALDI-MS was performed on fractions using DHB as matrix in the negative mode. Using the molecular mass obtained by MS, a calibration curve (up ~15,000 Da) was constructed for the GFC system to allow the MW characterization of other HA digests.

In 2006, Schiller and coworkers reported the detection of ng amounts of HA oligosaccharides obtained by enzymatic digestion (down to hexasaccharide size) by MALDI-MS in the positive and negative modes, using DHB as matrix.[225] They also evaluated the use of S/N ratio as a means of a quantitative measurement of concentration. A linear correlation between the S/N ratio and HA amount was observed between 0.8 pmol down to 40 fmol. The S/N and spectral resolution were found to depend largely on the size of the HA oligomer, with larger oligomers being detected with less sensitivity. Recently this group analyzed separated HA oligosaccharides (tetra-, hexa-, and octa-saccharide sizes) directly from thin-layer chromatography (TLC) plates, in the negative ion mode using 9AA as matrix.[226] However, they found that high content of formic acid used in the solvent system was responsible for the partial formylation of HA and minor loss of N-acetyl, but no other fragmentation was observed. In a short communication published in 2012, they reported the detection limits (DLs) of the HA tetrasaccharide using DHB and 9AA in both positive and negative ion modes.[227] Not surprisingly, 9AA provided the lowest DL in the negative ion mode (130 pg), while DHB provided the lowest DL in the positive ion mode (500 pg).

Toida *et al.* used trimethylsilyl diazomethane to derivatize HA to the methyl esterified form to facilitate the quantification of HA by MALDI-MS using α-cyano-4-hydroxycinnamic acid (CHCA) as matrix.[213] They analyzed HA oligosaccharides ranging from the tetrasaccharide size up to 34-mer (17 repeating disaccharide units). The major peaks in the positive ion spectra corresponded to $[M+Na]^+$ and in the negative ion mode was $[M-CH_3]^-$ ions. Methyl esterification of HA revealed higher sensitivity compared to the acidic (-COOH), sodium salt (-COONa), and ammonium salt ($-COONH_4$) forms of HA. Both the acidified and methyl esterified forms of HA afforded much simpler mass spectra compared to the salt forms, as they lacked peaks containing multiple metal/ammonium adducts. For example, the acidic form of HA showed only a single peak for each oligosaccharide while the sodium salt form contained multiple peaks for each oligosaccharide corresponding to multiple sodium adducts (i.e. $[M+Na]^+$ up to $[M-4H+5Na]^+$).

Past Tandem MS Studies of HA

Fast atom bombardment (FAB) collision-induced dissociation (CID) tandem MS (MS-MS) was shown to be able to differentiate between two disaccharide isomers: 1) ΔGlcU-GlcNAc (from HA) and 2) ΔGlcU-GalNac (disaccharide unit of chondroitin).[228] These disaccharides are epimers and thus differ in the position of the hydroxyl group at C4 of GlcNAc or GalNAc. Different fragmentation behavior was observed for the $[M+H]^+$ ion (m/z = 380) and a characteristic fragmentation ion was observed in ΔGlcU-GalNAc which allowed the two isomers to be distinguished. Interestingly, both ΔGlcU-GlcNAc and ΔGlcU-GalNAc showed fragments related to the GlcNAc/GalNAc monosaccharide (m/z = 222). However, these fragments were significantly more intense for ΔGlcU-GlcNAc. The authors propose that the C4 hydroxyl group of the GalNAc

residue in ΔGlcU-GalNAc may inhibit proton transfer and thus the formation of GalNAc related fragment ions.

Linhardt and coworker used reverse-phase HPLC-ESI-MS/MS to distinguish between HA and N-acetylheparosan (NaH) isomers.[229] NaH has the same chemical formula as HA, but the glycosidic linkage occurs between C1 of GlcU and C4 of GlcNAc (instead of C3 of GlcNAc in HA). Tandem MS of saccharides can result in fragmentation due to both glycosidic and cross-ring cleavages. Using the singly charged oligosaccharide precursor ions, MS-MS resulted in unique fragment ions in NaH compared to HA. These unique fragments correlated to the cross-ring cleavage of the GlcNAc residues in NaH oligosaccharides. They achieved detection limits better than 100 ng for each of the analyzed oligosaccharides.

Past MALDI Work on Lipids

MALDI-MS has become a useful, rapid, and sensitive tool for lipid analysis and characterization. They can be analyzed at the low nanomolar range and quantification is possible with the use of standards and calibration curves. Lipids can be extracted from the sample with methanol or chloroform/methanol and analyzed without further purification.

Lipid-related peaks can be detected in the either positive or negative ion mode although the intensity of peaks in the negative mode is generally weaker than in the positive mode. Lipids containing a choline headgroup (HG) (i.e. phosphatidylcholine , PC, phosphatidylethanolamine, PE, lyso-PCs, lyso-PEs, sphingomyelin, SM, dihydrosphingomyelin, DHSM) are ionized most efficiently in the positive ion mode because of the permanent positive charge on the choline moiety (Figure 1-11). For these zwitterionic compounds, only the protonation of the phosphate group is required to

produce a positively-charged ion. For other classes, such as phosphatidylinositols (PIs), phosphatidylglycerols (PGs) and phosphatidylserines (PSs), besides the protonation at the phosphate group, an extra proton (or metal cation) is required to produce a monovalent cation. Some classes of lipids such as diacylglycerols (DAGs) and triacylglycerols (TAGs) are detected only in the positive mode but do not form protonated ions and only metal cation adducts are observed instead. DHB is a matrix widely used for the detection of lipids in the positive ion mode. Peaks related to the protonated, group I metal adducts, and dimeric forms of lipids are commonly observed. This adds spectral complexity in the analysis of lipid species in a mixture.

Spectra in the negative mode appear much simpler than in the positive mode due to the presence of deprotonated species only and lack of metal adducts. Anions are formed by the loss of labile phosphate protons. Our group found PI to have the highest ionization efficiency in the negative ion mode using AAN as matrix, followed by PG and PS.[203] The high relative ionization efficiency (RIE) of PI may be attributed to the stabilization of the phosphate anion by formation of H-bonds with vicinal OH groups in the inositol HG.

Different matrices such as PNA, 9AA, and AAN have been evaluated by our group for the negative mode detection of PLs in lens tissue and soybean methanolic extracts.[203] AAN was shown to produce homogenous spots and exhibited enhanced sensitivity due to a greater amount of negative ions formed because of its high basicity (pH = 9.2 ± 0.1). Titanium micro- (TMs) and nanoparticles (TNs) were also explored as matrices by our group for the analysis of soybean extracts in the positive- and negative-ion modes.[182] TM ionized PLs *in vitro* but caused partial removal of HG moieties, leading to a higher than expected signal from phosphatidic acid (PAs).[182] TNs caused even

greater cleavage of the HGs and in some cases the parent ions could not be detected. Interestingly, *in situ* analysis of soybean slices with TNs produced only minor levels of HG cleavage.[182] It was proposed that the lower extent of cleavage may be the result of protection by tissue components and/or by their cellular organization that restricts direct contact with TN.[182] Ideally, one would like to suppress this cleavage so as to achieve accurate characterization and quantification.

Even though other groups have analyzed HA by MALDI-MS, in this work several matrices have been explored for their possible use in the detection of HA in the positive and negative ion modes and to understand the role of matrix pH on the ionization of the analyte. Neither the impact of HA on the ionization of lipids nor the possible influence of lipids on the ionization of HA has been explored. For this reason, the work discussed in this chapter focuses on model studies carried out in HA alone, lipids alone, and their mixtures. The information obtained in the project could aid in future *in situ* studies of the VH. Additionally, because HA has been used as an encapsulating agent for hydrophobic drugs,[43,44] studies were also conducted to evaluate interactions between HA and lipids that potentially protect them from cleavage that results in HG loss.

The following lipids were chosen for the MALDI-MS analysis of possible gas-phase interactions with ΔDiHA: fatty acids (FAs), LPCs, DAG, and PLs. FAs, stearic acid (SA, 18:0) and oleic (OA, 18:1), were selected to investigate if a single acyl tail containing a small negatively charged carboxylate group affects the RIE of ΔDiHA. LPCs containing either an oleoyl (LPC-OA) or a stearoyl (LPC-SA) acyl chain were chosen to evaluate the impact of a large positively charged headgroup on the RIE of ΔDiHA. Phospholipids were also analyzed to learn whether or not the presence of two acyl tails (rather than one) affects the gas-phase interactions with HA. The PLs were

selected on the basis of the type of charge on their headgroup. PA was selected due to the negative charge of the phosphate group, while PE and PC possess a positively-charged headgroup. Unlike in PE, the positive charge in PC is permanent and not pH dependent. Finally, DAG was chosen because while having two acyl chains it lacks a charged headgroup.

EXPERIMENTAL

Chemicals

Analytes. Hyaluronic acid disaccharide sodium salt or alpha-4-deoxy-L-*threo*-hex-4-enopyranosyluronic acid-[1→3] (α-ΔGlcU-(1→3)-GlcNAc or ΔDiHA), 1-oleoyl-2-hydroxy-*sn*-glycero-3-phosphocholine (LPC-OA), 1,2-dipalmitoyl-*sn*-glycerol (DAG), stearic acid (SA) and oleic acid (OA) were purchased from Sigma-Aldrich (St. Louis, MO). 1-Palmitoyl-2-oleoyl-*sn*-glycero-3-phosphoethanolamine (PE) and 1-stearoyl-2-hydroxy-*s*n-glycero-3-phosphocholine (LPC-SA) were obtained from Avanti Polar Lipids, Inc. (Alabaster, AL). 1,2-Dipalmitoyl-*sn*-glycero-3-phosphorylcholine (PC) and 1,2-dipalmitoyl-*sn*-glycero-3-phosphatidic acid (Na^+ salt) (PA) were acquired from Matreya (Pleasant Gap, PA). The chemical structures of all analytes and their molar masses are provided in Figure 4-3.

Matrices. 2,5-dihydroxybenzoic acid (DHB), 4-nitroaniline (or *para*-nitroaniline, PNA), 9-aminoacridine hydrochloride monohydrate (9AA), and 2-(2-aminoethylamino)-5-nitropyridine (AAN) were purchased from Aldrich Chemical Company, Inc. (Milwaukee, WI). The chemical structures of the organic matrices and their molar masses are provided in Figure 4-4. Titanium(IV) oxide 'nanopowders' was obtained from Sigma-Aldrich (St. Louis, MO). The manufacturer states a diameter of < 25 nm; however, strong

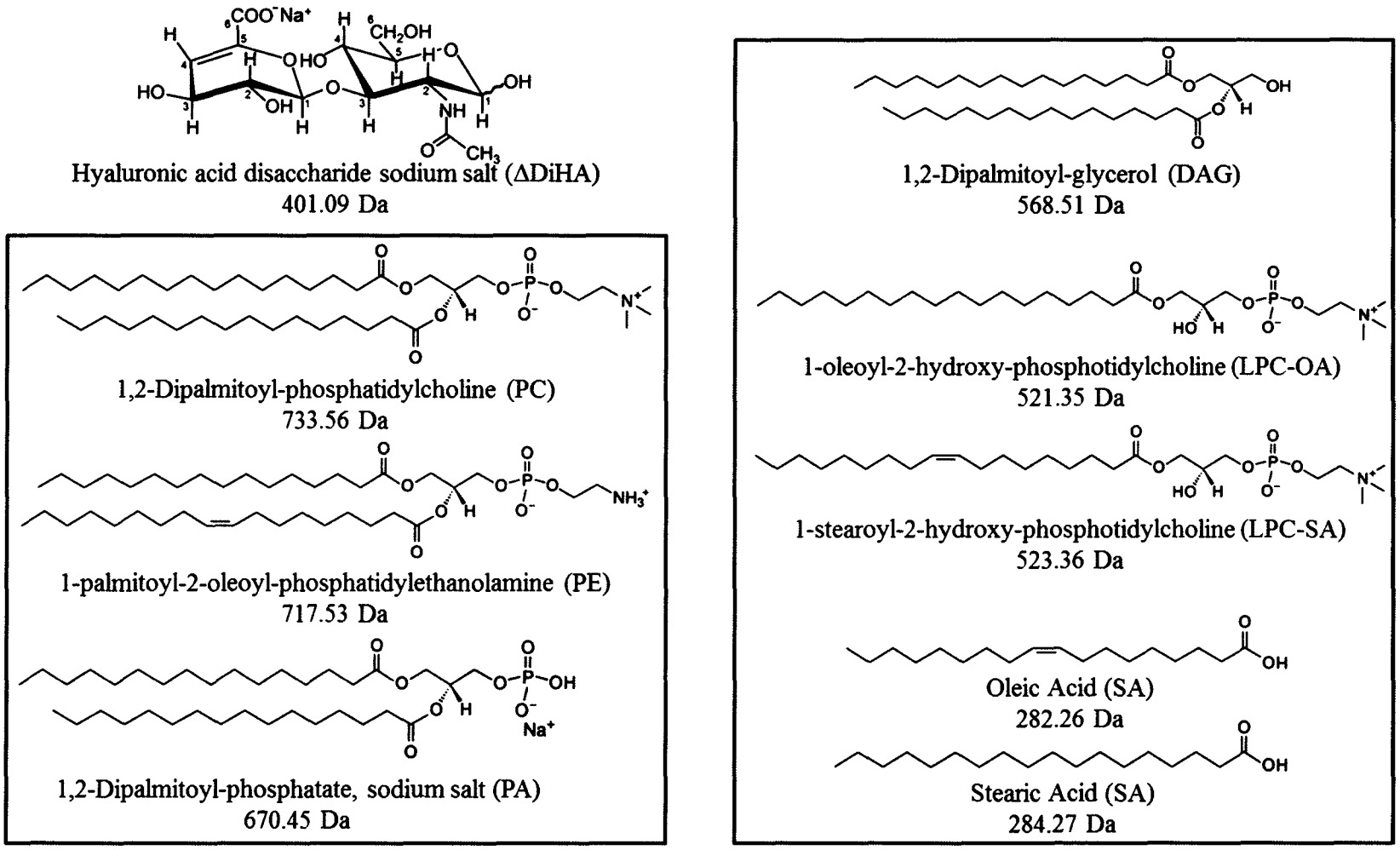

Figure 4-3. Structures and isotopic masses of HA disaccharide (ΔDiHA), phospholipids (PLs), and lipid metabolites used in ionization efficiency studies.

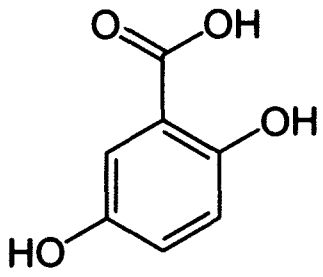

2,5-Dihydroxybenzoic acid
(DHB)
154.03 Da

p-Nitroaniline
(PNA)
138.04 Da

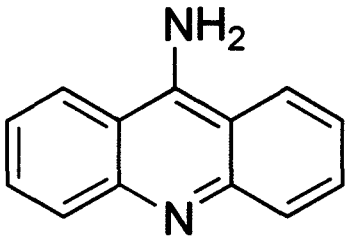

9-Aminoacridine
(9AA)
194.08 Da

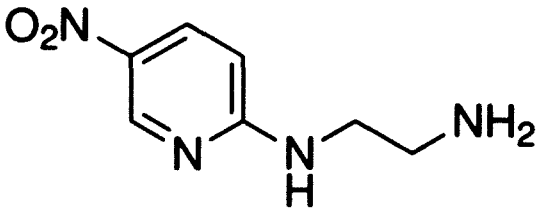

2-(2-Aminoethylamino)-5-nitropyridine
(AAN)
182.08 Da

Figure 4-4. Organic matrices used in MALDI-TOF-MS studies and their corresponding isotopic masses.

attractive forces among particles can lead to the formation of large aggregates in the μm range. Mandyz analyzed 'nanopowders' from different manufacturers and even after ultrasonication, the aggregate size remained in the micrometer range.[230] For this reason, the purchased nanopowder is referred to as titania microparticles (TMs) throughout this chapter. AgCl and CsCl were obtained from Sigma-Aldrich (St. Louis, MO).

Solvents. Methanol and chloroform were purchased from Sigma-Aldrich (St. Louis, MO). Barnstead Nanopure water (17.8 MΩ, • cm) was used in the preparation of solutions.

Sample Preparation

ΔDiHA was dissolved in H_2O at a concentration of 1 mg/mL (2.5 mM) in the matrix comparison studies. In the HG cleavage studies of PC by TM, 1.0 mg/mL PC (in MeOH) was prepared and combined with an equal volume of 1 mg/mL HA (in H_2O) in the ΔDiHA/PC mixture. In both of these studies, the premix spotting method was used: 1:1 volumes of HA and matrix was combined prior to spotting on the MALDI plate.

In the RIE comparison studies, PLs (PC, PE, and PA) and lipid metabolites (DAG, LPCs, and FAs) were analyzed alone and in combination with ΔDiHA. Individual solutions of each were prepared in MeOH at concentrations of 1.0 mM for lipids (and related metabolites) and 0.5 mM for ΔDiHA. PA, DAG, and SA required sonication for approximately 15 minutes to promote dissolving. Each lipid and lipid metabolite was combined, individually, with ΔDiHA so that seven mixtures were prepared: ΔDiHA/PC, ΔDiHA/PE, ΔDiHA/PA, ΔDiHA/DAG, ΔDiHA/LPC-SA, ΔDiHA/LPC-OA, ΔDiHA/SA, and ΔDiHA/OA. Mixtures were prepared by combining equal volumes of 2.0 mM lipid solutions with 1.0 mM ΔDiHA solutions so that the resulting concentrations of each were 1.0 and 0.5 mM, respectively, in the mixtures. Using the dried-droplet method, 0.5 μL of

analyte solution (or mixture) was spotted first, allowed to dry, and 0.5 μL matrix were spotted onto the MALDI plate.

Matrix Preparation

The acidic matrices (TM and DHB) were dissolved in the water and 1:1 MeOH:H_2O, respectively. Matrix concentrations were optimized to yield the highest S/N which was determined to be 10 mg/mL for both (0.125 M for TM and 0.065 M for DHB). The nearly neutral and basic matrices (PNA, 9AA and AAN) were dissolved in chloroform/methanol (2:1). These matrices were prepared at previously reported concentrations: 23.5 mg/mL (0.17 M) for PNA, 15 mg/mL (0.060 M) for 9AA, and 18.2 mg/mL (0.10 M) for AAN. All matrices were prepared fresh daily. The pH values measured (n = 5) for the resulting matrices were 2.5 ± 0.1 for DHB, 3.4 ± 0.2 for TM, 7.3 ± 0.3 for PNA, 6.6 ± 0.2 for 9AA and 9.2 ± 0.2 for AAN. In the analysis of FAs only, DHB was saturated with either cesium or silver chloride in an attempt to enable ionization.

MALDI-TOF-MS Analysis

All mass spectra were recorded using a Voyager Biospectrometry delayed extraction (DE) workstation (Applied Biosystems, Foster City, CA). All samples were spotted on a 100-well (10x10) stainless steel plate from Applied Biosystems. A 337-nm pulsed nitrogen laser is used for induction of sample ionization. The extraction voltage was 20 kV. Spectra were acquired in the reflector mode. Data Explorer, version 4.8 software (Foster City, CA) was used to analyze and process the mass spectra.

DHB and TM, due to their acidic nature, were the matrices of choice in the positive ion mode. The nearly neutral 9AA and the basic AAN matrices were used for negative ion mode. Both positive and negative modes were used for PNA. DHB matrix

was used solely in the RIE because it showed the greatest ionization and the highest reproducibility.

The laser power was adjusted to obtain high signal-to-noise ratio (S/N), while ensuring minimal fragmentation of the parent ions. The laser power was, however, necessarily held constant (at 1428) in the RIE comparison studies. Each spectrum was manually acquired and represents the average of at least 100 shots collected within a single MALDI spot.

Mass spectra were calibrated with a two-point mass calibration. This generally involved using a matrix peak as the low-mass calibration point and an analyte adduct or dimer for the high-mass calibration point. RIEs of analytes were calculated by summing analyte peak areas and setting them relative to the matrix peak areas. This was done on a minimum of five spectra for each sample and averages were calculated. Peak height and S/N were investigated for use in RIE calculations, but their relative standard deviations were greater than those using areas. Parent ion peaks, adduct peaks, fragmented peaks, and dimer peaks were necessarily included in RIE calculations to achieve reasonable standard deviations. Radical peaks were found to be significant in the DHB matrix. Radical peaks resulting from electron transfer reactions, appear in the spectra at *m/z* ratios equivalent to the mass of the corresponding neutral species and one *m/z* less than the corresponding charged ion. They appear in spectra along with the charged species and at almost equal intensities.

In order to compare averages from different populations, A and B, which have different individual standard deviations (s_A and s_B), it is necessary to calculate the pooled standard deviation (s_{AB}) to determine if the differences are real or only due to random error. In the case of the RIE studies presented in this chapter, the s_{AB} was calculated for

the alone and mixture averages. Based on the number of trials for each (n), s_{AB} was calculated as follows:

$$s_{AB} = \left[\frac{(n_A - 1)s_A^2 + (n_B - 1)s_B^2}{(n_A + n_B - 2)}\right]^{\frac{1}{2}}$$

Using the s_{AB}, the t value can be calculated:

$$t_{exp} = \frac{|\bar{x}_A - \bar{x}_B|}{s_{AB}\sqrt{\frac{1}{n_A} + \frac{1}{n_B}}}$$

If the calculated, experimental t value (t_{exp}) is less than the tabulated, theoretical t value (t_{theor}), then the two populations are not significantly different and the difference is due to random error. If, on the other hand, t_{exp} is greater than $t_{theor,}$ the two populations are significantly different and not due to random error.

Optimization. The effect of ΔDiHA solvent (H_2O vs. MeOH) on HA ionization was analyzed, in the DHB matrix. Increased ionization (~ two-fold) was observed in H_2O relative to MeOH. This likely due to a greater number of cations present in water compared to MeOH. In the RIE comparison studies, MeOH was necessarily used so that solvent was consistent among lipid and ΔDiHA solutions and mixtures. The dried-droplet method was also preferred in these studies as it produced spots of greater homogeneity providing for greater reproducibility among spots. RIEs were calculated using a variety of peak combinations before determining that inclusion of a greater number of peaks (i.e. isotopic and radical peaks) resulted in lower standard deviations.

RESULTS AND DISCUSSION

Comparison of Matrices of Different pHs for the Detection of ΔDiHA

Various matrices were tested to determine the one that provides greatest ionization for ΔDiHA and thus higher sensitivity. Acidic matrices were used to evaluate ionization in the positive ion mode while basic matrices were used to evaluate negative ion formation. Neutral, or nearly neutral, matrices were evaluated for detection in either positive or negative mode.

Positive Ion Detection

The acidic matrices, TM and DHB, and the nearly neutral matrix, PNA, were evaluated as matrices for the detection of ΔDiHA in the positive ion mode (Fig. 4-5). TN were also evaluated but ΔDiHA was not detected. Both DHB and TM matrices were successful at ionizing ΔDiHA (Fig. 4-5a and 4-5b); however, PNA ionized ΔDiHA only slightly thus leading to poor S/N (Fig. 4-5c). A calibration curve was constructed for TM and the lowest concentration that gave a reasonable signal (S/N $\geq$ 10) was 0.025 mg/ mL (62.5 pmoles per spot). This DL is not as good as that obtained with DHB and reported by Schiller and coworkers (DL = 40 fmols per spot) in 2006.[225] It is possible that the newer mass spectrometer used by Schiller's group provides greater sensitivity than our instrument (purchased in 1999). TM produced clean spectra void of any significant matrix-related peak. DHB had several matrix-related peaks in the lower mass range (100-300 *m/z*), but none that interfered with the detection of ΔDiHA (~350-450 *m/z*). The spectra using PNA, however, were plagued by a significant number of matrix-related peaks and clusters of peaks. PNA matrix-related peaks are spread over a larger mass range due the formation of dimers, trimers, etc. Additionally, PNA produces peaks that

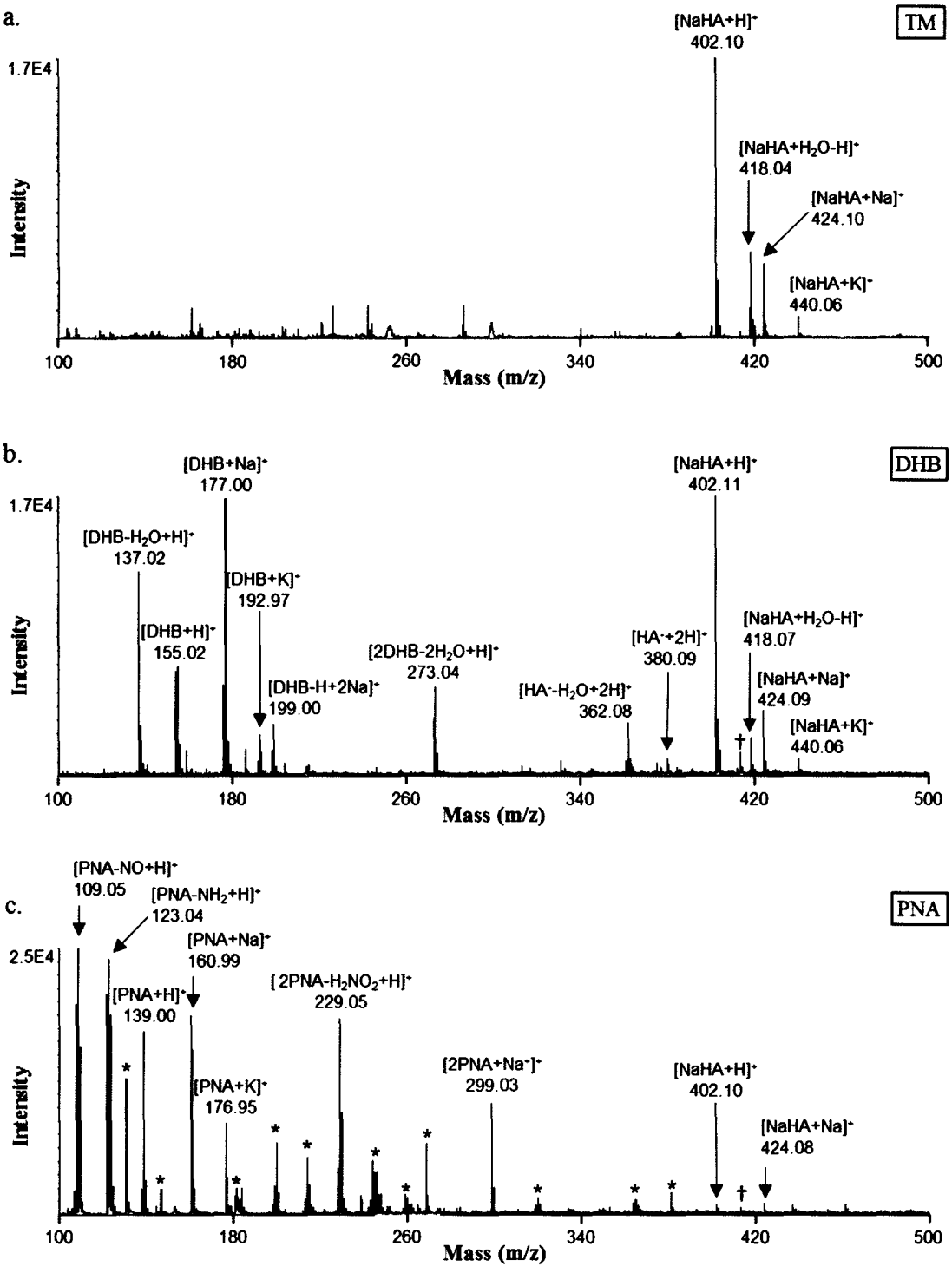

Figure 4-5. MALDI-MS spectra of 1.0 mg/mL ΔDiHA in a) TM b) DHB and c) PNA matrices in the positive ion mode. * Additional matrix-related peaks. † Plasticizer contaminant peak (m/z = 413).

overlap with the ΔDiHA peaks at 362 and 380 *m/z* units. For these reasons, PNA was ruled out as a suitable matrix for positive ion detection.

Observed ions for ΔDiHA and their calculated isotopic masses are provided in Table 4-1. Of these peaks, the protonated species, $[NaHA + H]^+$, was typically the most abundant. Other adducts of ΔDiHA with $m/z > 402$ have a slightly greater intensity relative to the parent ion, $[NaHA + H]^+$ ($m/z = 402$) in TM compared to DHB. This may be attributed to DHB competing for cations for ionization whereas TM matrix peaks were not detected. Interestingly, fragmented ΔDiHA ions (i.e. those with $m/z < 402$), which are present in the DHB spectra, are completely absent in TM. These lower mass peaks lack a sodium atom relative to the parent ion at $m/z = 402$. This may indicate a competition for Na^+ ions between ΔDiHA and the DHB matrix which results in fewer Na^+ ions available for the ionization of ΔDiHA. It is possible that since TM does not appear to adduct with cations, that sodium is present in sufficient amount such that all ΔDiHA ions contain at least one Na^+ ion.

Negative Ion Detection

The basic matric 9AA, and the nearly neutral matrix PNA, were evaluated as matrices the detection of ΔDiHA in the negative ion mode (Fig. 4-6). In the negative mode, only one ΔDiHA peak is detected ($m/z = 378$) corresponding to $[HA-H]^-$. PNA produces slightly fewer matrix-related peaks in the negative mode compared with positive mode. Unfortunately, a cluster of matrix peaks at 378 *m/z* interferes with the detection of ΔDiHA (Fig. 4-6a). 9AA also produces several matrix-related peaks but none interferes with the detection of ΔDiHA (Fig. 4-6b). AAN was also evaluated, but was unsuccessful at ionizing ΔDiHA. This was not expected as it was thought that the

ΔDiHA $C_{14}H_{20}NO_{11}Na$ ($mass_{iso}$ = 401.09)	
Ion	m/z_{iso}
$[HA^{-}-H_2O-+2H]^{+}$	362.11
$[HA^{-}-Na+2H]^{+}$	380.12
$[NaHA+H]^{+}$	402.10
$[NaHA+H_2O-H]^{+}$	418.10
$[NaHA+Na]^{+}$	424.08
$[NaHA+K]^{+}$	440.06

Table 4-1. Positive ions of ΔDiHA, and their corresponding isotopic masses, observed by MALDI-MS.

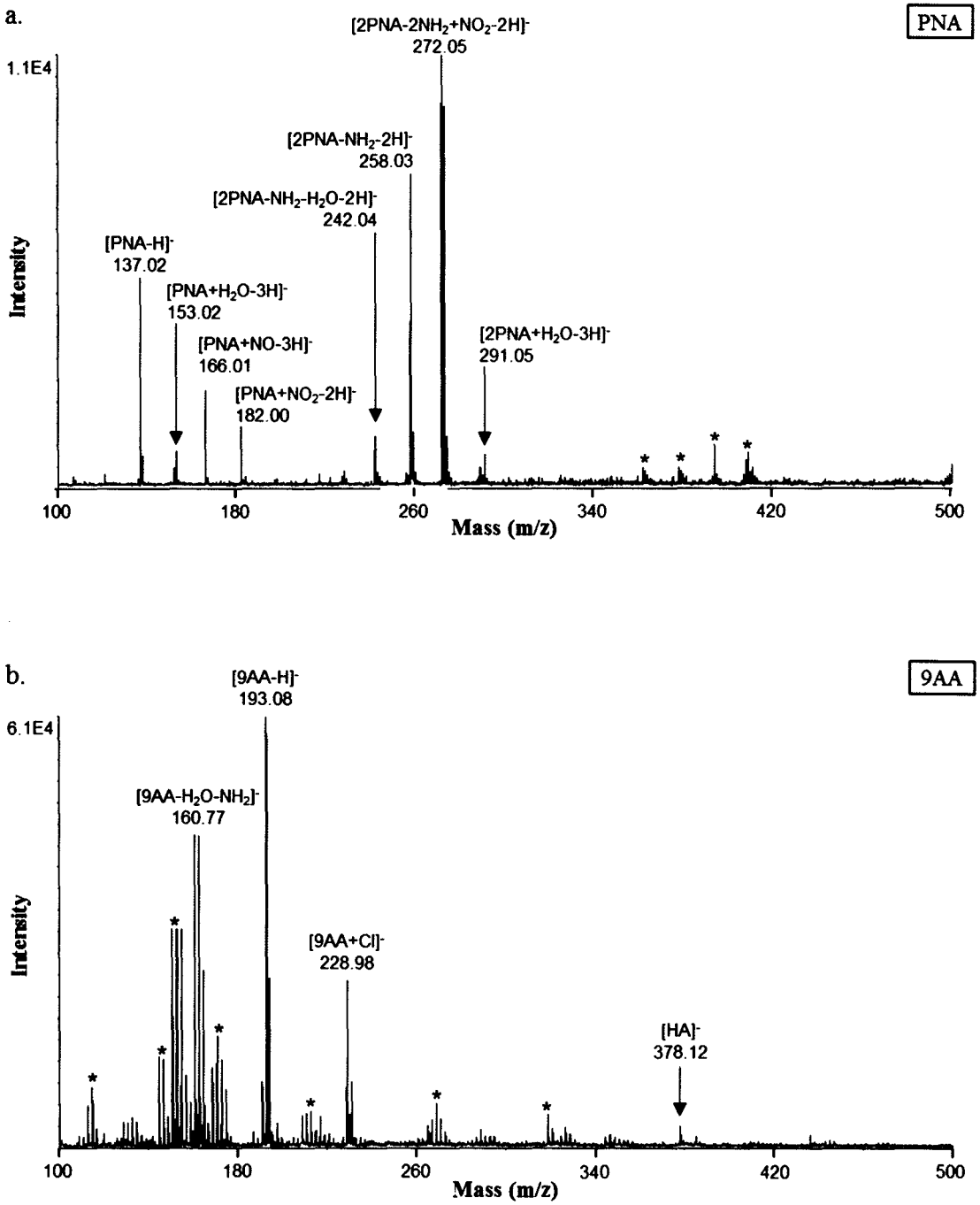

Figure 4-6. MALDI-MS spectra of 1.0 mg/mL ΔDiHA in a) PNA and b) 9AA matrices in the negative ion mode. * Additional matrix-related peaks.

high basicity of AAN could easily remove a proton from ΔDiHA. However, it is unclear at this time why negative ions were not observed when AAN was used as matrix.

Assignment and PSD of Select ΔDiHA Peaks

PSD was performed on select ions to confirm the assignments made in the positive ion mode. The PSD spectrum of $[NaHA+Na]^+$ (*m/z* = 424) is shown Fig. 4-7 and the other PSD spectra, $[NaHA+H_2O-H]^+$ (*m/z* = 418) and $[NaHA+H]^+$ (*m/z* = 402), are provided in Appendix B (Figs. B-3 and B-4). Of particular interest was to verify the peak at 418 *m/z* units as a true ΔDiHA-related peak. This was confirmed in the PSD spectra of the $[NaHA+Na]^+$ ion which revealed a mass fragment at *m/z* = 418 (Fig. 4-7a). Interestingly, fragmentation related to the GlcNAc monosaccharide was observed in all three PSD spectra, but no peaks related to the ΔGlcU monosaccharide were observed (Fig. 4-7b). This is in agreement with previous tandem MS studies of HA which also did not observe ΔGlcU fragments.[228] Although no reason has been given previously, it is plausible that the number of ions required to create a charge on the saccharide determines which saccharide is ionized. In the case of ΔDiHA, the GlcNAc residue only requires one cation to create a positive charge while ΔGlcU requires two cations (one to neutralize the COO^- and one to form the positive charge).

Effect of ΔDiHA on Headgroup Loss of PCs by TM

Cleavage of the PC HG occurs significantly when TM are used as matrix (Fig. 4-8a). This can be monitored by comparing the relative intensity of the peak at *m/z* = 184 corresponding to the cleaved and protonated HG, to the intensity of the parent ion at *m/z* = 734 *m/z*. DHB, in contrast, produces only minor degradation compared to TM (Fig. 4-8b). It also leads to small amounts of the corresponding lyso-PC ion (*m/z* = 496). It was hypothesized that in the presence of ΔDiHA, PC may experience protection from HG

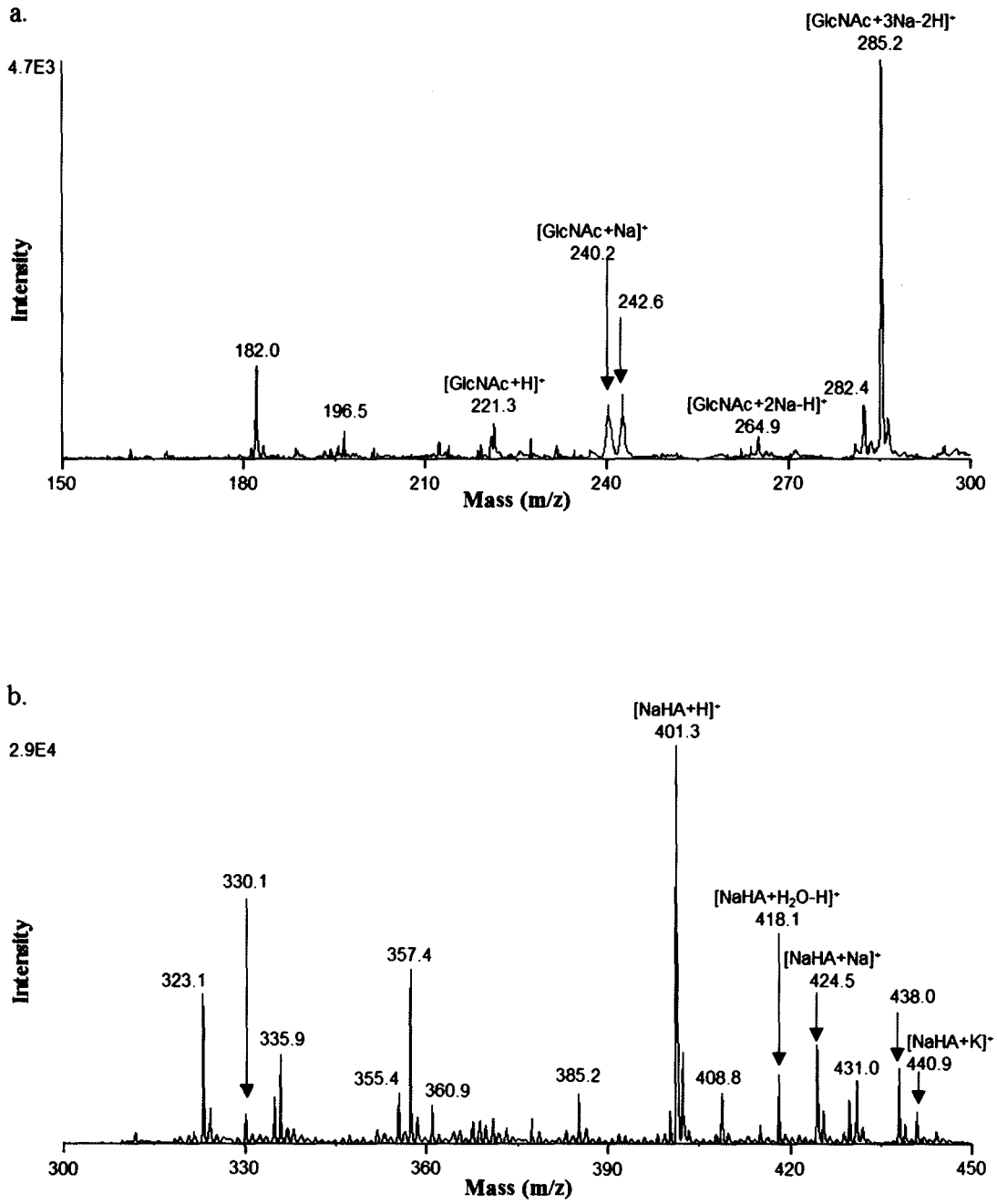

Figure 4-7. Post source decay (PSD) spectra of the ΔDiHA peak at *m/z* = 424.4 in the range of a) 150 - 300 b) 300 - 450 *m/z* units. Spectra were obtained in the positive ion mode using DHB as matrix.

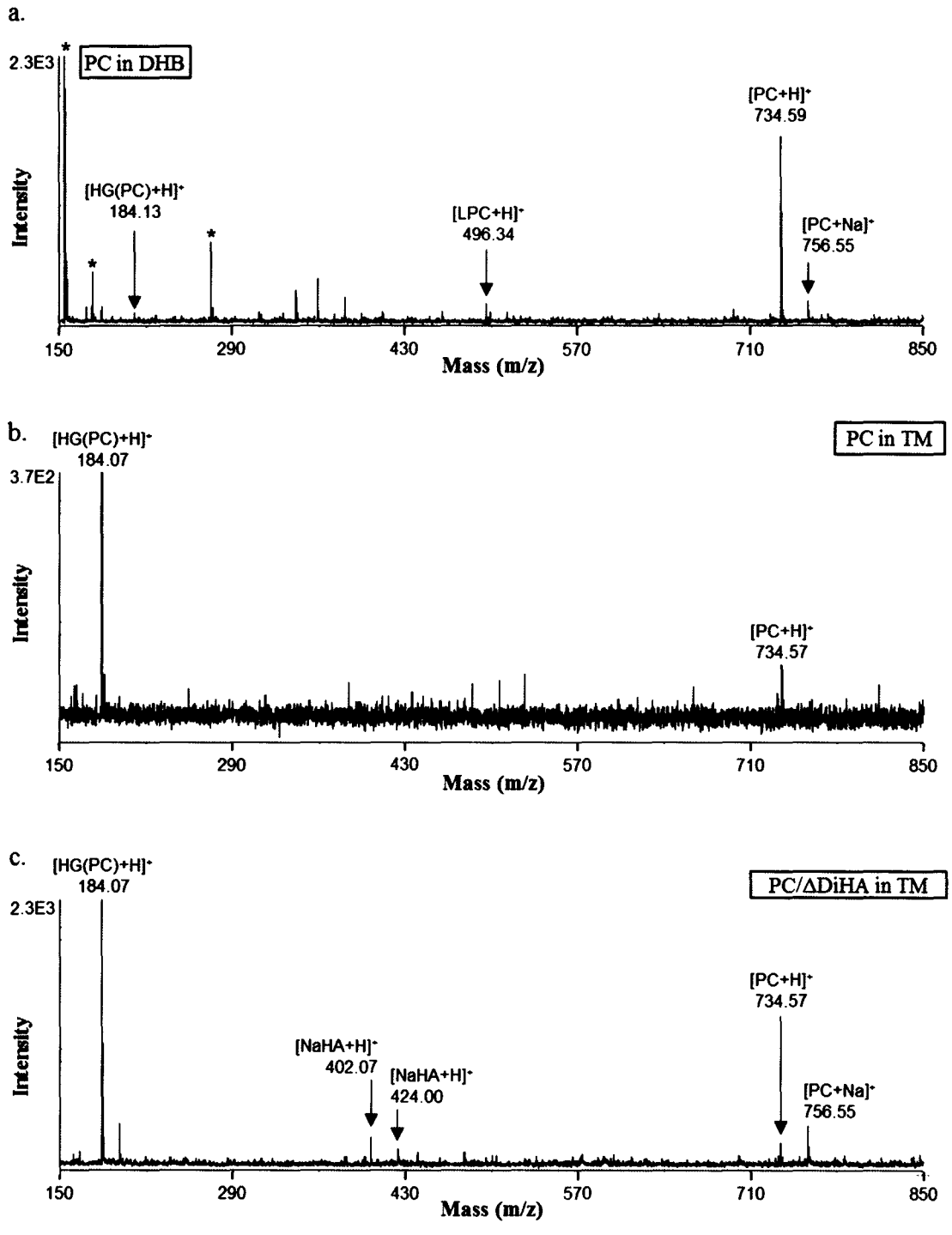

Figure 4-8. MALDI-MS spectra of PC in a) DHB, b) TM, and c) TM in the presence of ΔDiHA (1:1 v/v PC:ΔDiHA) in the positive ion mode. * Matrix-related peaks.

cleavage. However, through the analysis of ΔDiHA/PC mixtures using TM as matrix, no appreciable reduction in the intensity of the HG ion was observed in the presence of ΔDiHA (Fig. 4-8c). This suggests that ΔDiHA does not protect PC from HG cleavage. This does not rule out the possibility of ΔDiHA/PC interactions, but only that ΔDiHA does not interact with PC in a way that protects its HG from being cleaved.

Comparison of RIEs for ΔDiHA and PL Mixtures

Relative ionization efficiencies (RIEs) studies were performed in order to understand the ionization processes occurring and how the ionization of lipids and lipid metabolites may be affected by ΔDiHA. Each analyte was analyzed alone and in a 1:2 molar mixture of ΔDiHA and lipids. Concentrations were kept equal in the control solutions (single component) and in the mixtures so that equal molar amounts of each analyte would be present. RIEs were calculated as discussed in the Material and Methods section. DHB was chosen as the matrix for this analysis because of its suitability to the ionization of ΔDiHA and the minimal amount of HG group loss in PC. The PLs selected were PC, PE, and PA. These were chosen in order to investigate possible interaction between ΔDiHA and HGs of varying sizes. The lipid metabolites analyzed were DAG, LPCs-LPC(SA), LPC(OA), and FAs-SA, OA.

Spectra of the mixtures are shown in Figures 4-9 and 4-10 for the PLs and lipids metabolites, respectively. A bar graph (Fig. 4-11) summarizes the changes in ionization efficiencies for ΔDiHA and the lipids and gives error bars, for one standard deviation. Tables containing the experimental data (RIE averages, standard deviations, and number of trials) as well as results from statistical analysis (pooled standard deviations, t values, and confidence limits) are provided in Appendix B (Table B-2).

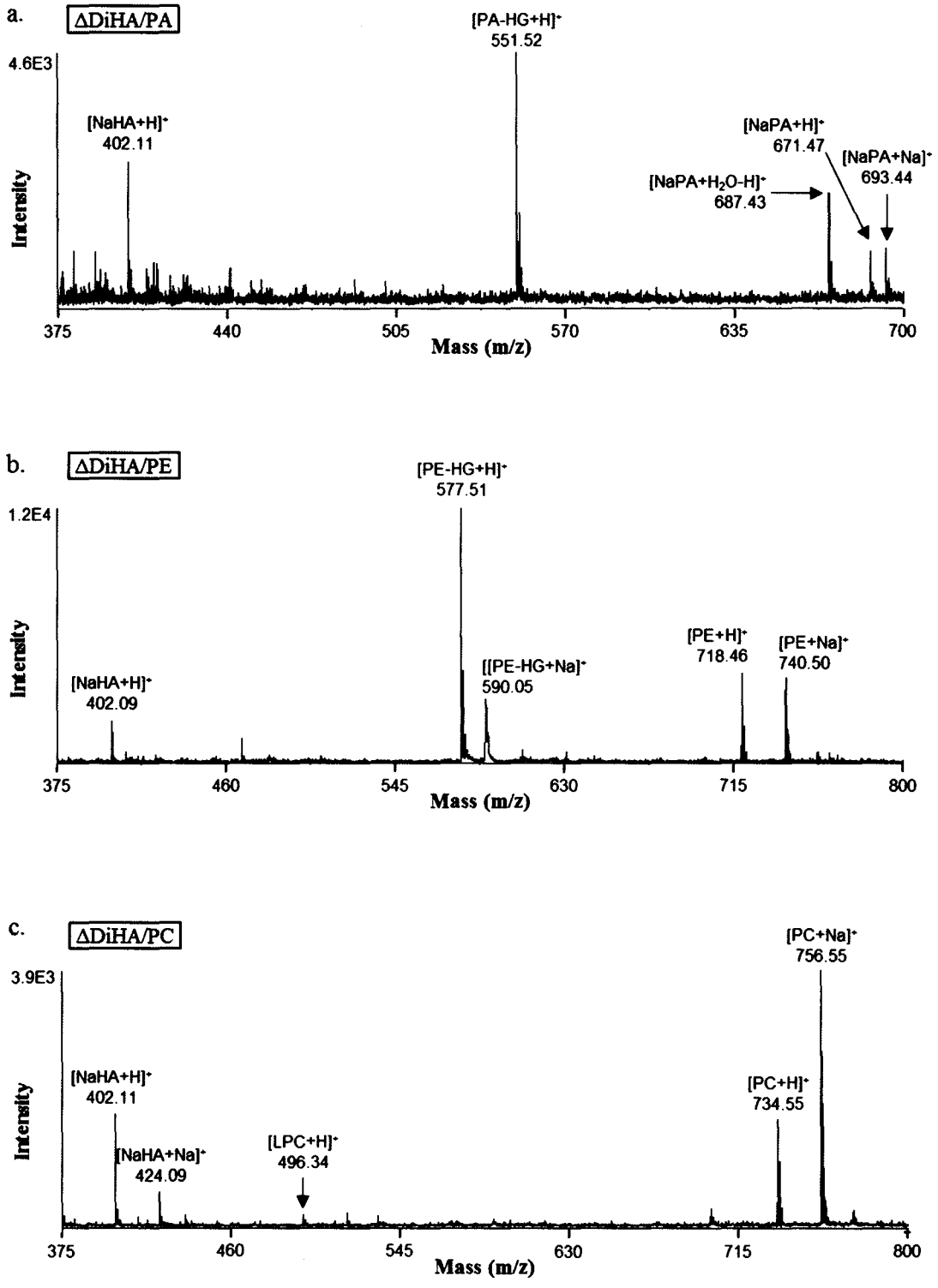

Figure 4-9. MALDI-MS spectra of 1:1 v/v ΔDiHA/lipid mixtures: a) ΔDiHA/PA b) ΔDiHA/PE c) ΔDiHA/PC mixtures. Spectra were obtained in the positive ion mode using DHB as matrix. HG = phosphocholine for PC and phosphoethanolamine for PE.

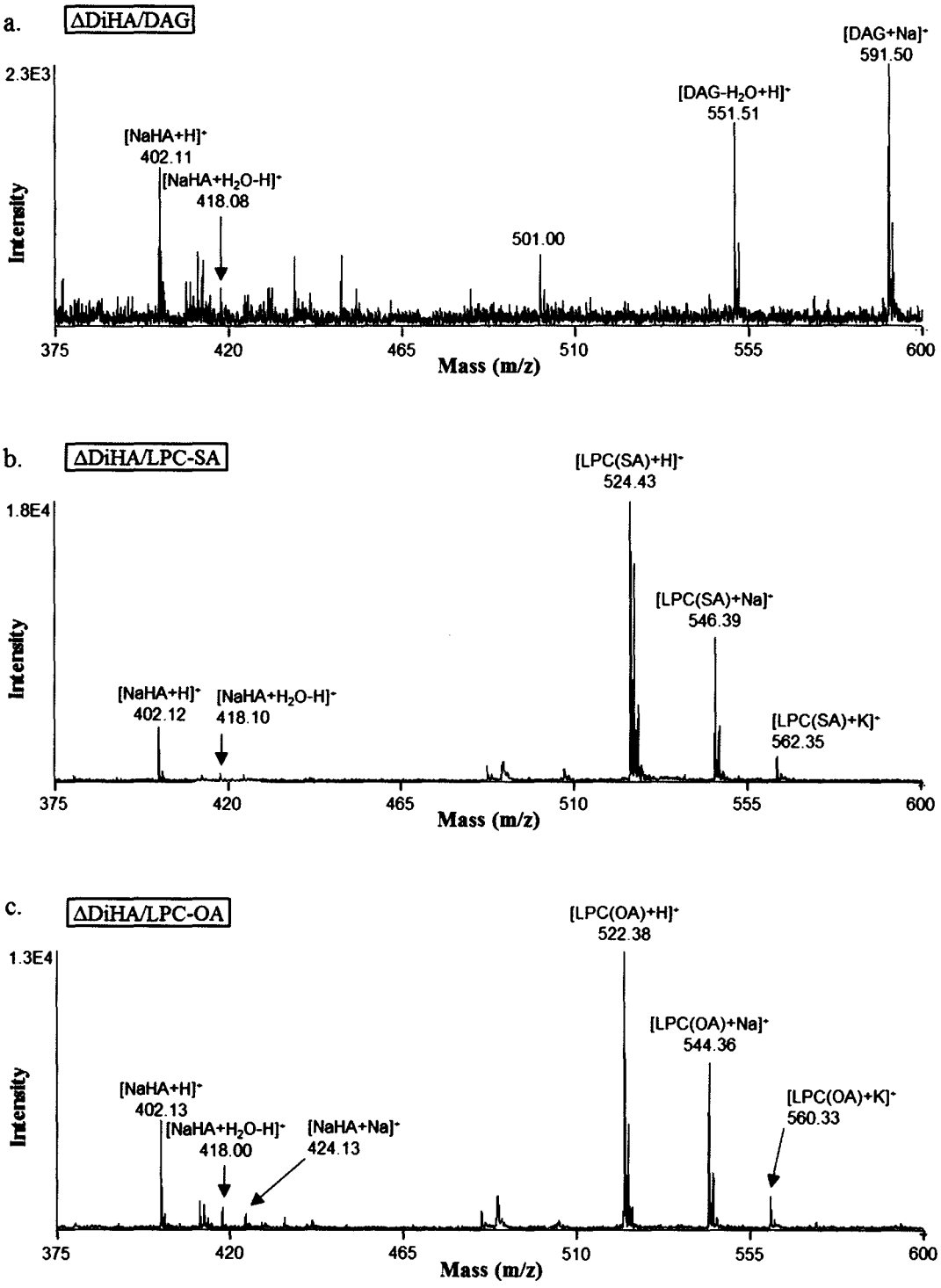

Figure 4-10. MALDI-MS spectra of 1:1 v/v ΔDiHA/lipid metabolite mixtures: a) ΔDiHA/DAG b) ΔDiHA/LPC-SA c) ΔDiHA/LPC-OA mixtures. Spectra were obtained in the positive ion ion mode using DHB as matrix.

a.

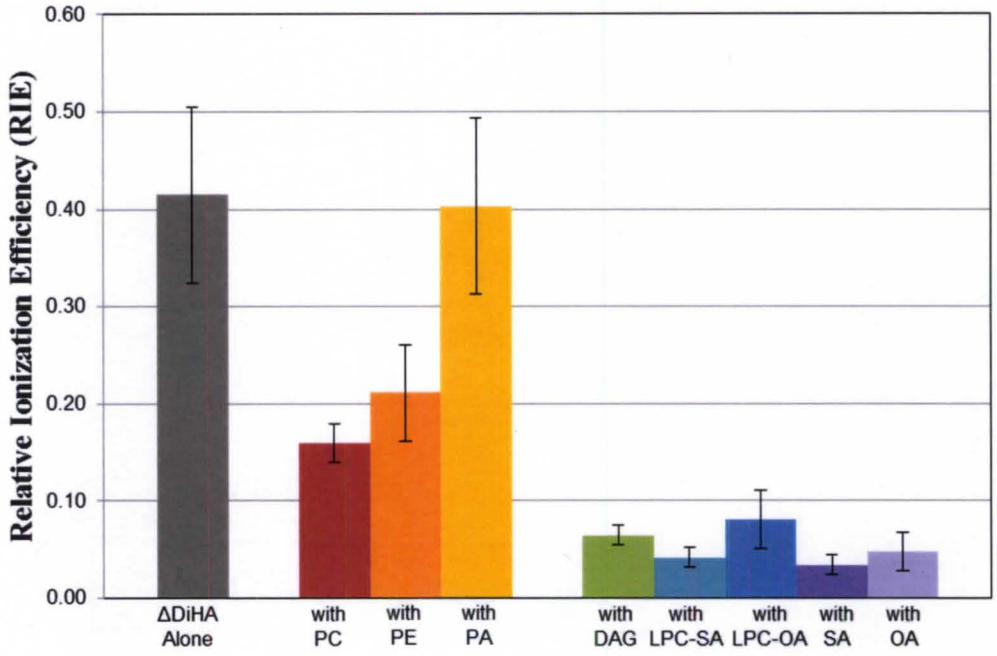

b.

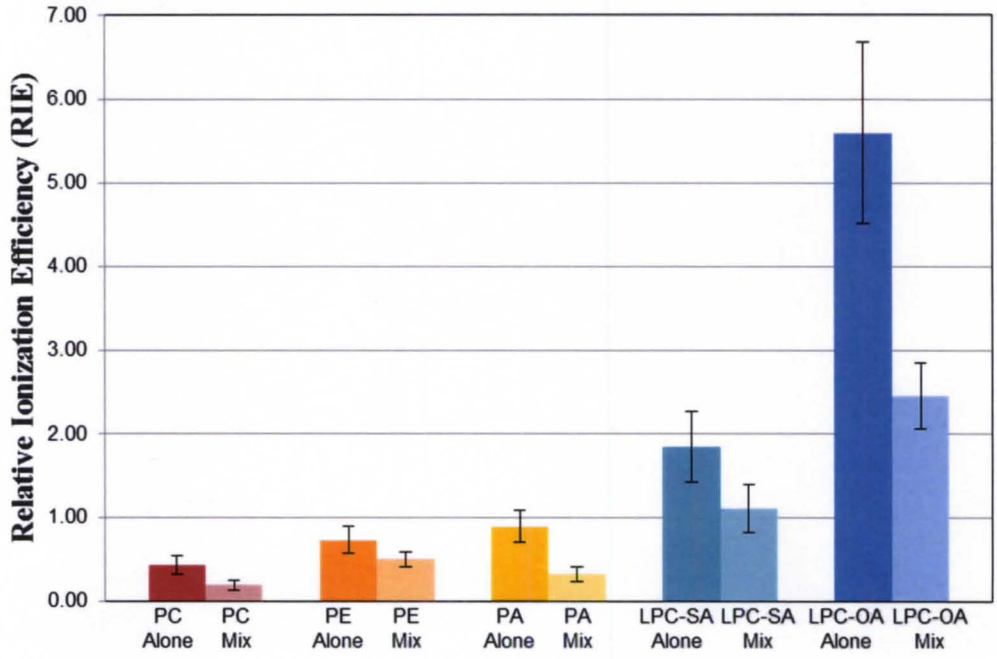

Figure 4-11. Changes in RIEs in HA/lipid mixtures. a) Effects on ΔDiHA's RIEs by lipids. b) Effects on lipids' RIEs by ΔDiHA. Error bars indicate a ± 1 standard deviation.

Spectra for the ΔDiHA/SA and ΔDiHA/OA mixtures are not shown as these analytes were undetectable even in the control solutions of SA or OA. This is not surprising due to their acidic nature. The deprotonated species would dominate the equilibrium and the formation of positively-charged ions is not favored. Cesium and silver chlorides were added in an attempt to promote ionization, however the FAs remained undetectable. This is in agreement with results from a previous study by Yu *et al.* who reported that the addition of Cs and Ag to FA solutions did not lead to observable ions in DHB.[231] They did find that using Cs and Ag with a polyporphin matrix was effective at ionizing FAs. Only ΔDiHA RIEs could be calculated in ΔDiHA/SA and ΔDiHA/OA mixtures and compared to the RIE of ΔDiHA alone. In the case of DAG, RIE calculations were not performed due to the poor S/N and the lack of reproducibility in peak areas.

Decreases in RIEs for both ΔDiHA and the lipid species are observed in the binary mixtures. Reductions in ionization efficiency are expected to occur if intermolecular interactions affect the polar regions of the analytes, as they are the sites that responsible for ionization. The following paragraphs discuss the possible reasons for the decrease in the RIE of ΔDiHA when the various lipids were included in the mixture and the impact of ΔDiHA on the RIE of the lipids. An approximately 50% decrease in RIE for all lipids was observed in the presence of ΔDiHA. In lipids containing a phosphocholine HG, interactions between ΔDiHA's COO^- and the positively-charged choline moiety may result in the blockage of the phosphate group from being ionized.

Effect of Lipids on the RIE of ΔDiHA

The ΔDiHA is negatively charged at neutral pH due to the presence of a carboxylate group on ΔGlcU. Therefore in order to be ionized with a positive charge of

+1, one proton or cation is required to neutralize the carboxylate and a second one is needed to provide the overall positive charge. Since a proton or cation will be preferentially drawn to the negatively-charged carboxylate, before any other position, this will be referred to as the first site of ionization. The location of the second site of ionization is unknown, but is believed to be on the GlcNAc ring due to the presence of more electronegative sites (hydroxyl groups) relative to ΔGlcU and thus a higher electron density. This possibility is supported by the presence of GlcNAc cationic fragments in the PSD spectra discussed previously. Interestingly no ΔGlcU-related fragments were detected in the positive mode.

As seen in Fig. 4-11a, the ionization of ΔDiHA was reduced in the presence of each of the various lipids tested except for PA. Unlike in Chapter 3, where the mixtures were prepared and analyzed in water, hydrophobic interactions are not expected to cause changes in ionization efficiency as the cation or proton transfer occurs at polar sites in the gas phase.

Impact of PLs on the RIE of ΔDiHA. PA had no effect on the ionization efficiency of ΔDiHA. This finding indicates that PA does not block either ionization site on ΔDiHA. Due to the negative charge of the phosphate group, PA is not expected to be attracted to the ΔGlcU containing the negatively carboxylate group. Although the location of second site of ionization is unknown, the lack of change in the ionization efficiency of ΔDiHA suggests that this site is not blocked by PA. An interaction between the two analytes cannot be ruled out (see next section) but such interaction does not block either ionization site on ΔDiHA.

PC and PE showed comparable effects on the reduction of ΔDiHA ionization efficiency. Both reduced the ionization efficiency by approximately one-half. Due to their

positively-charged HG, they are likely to be attracted to the negatively-charged carboxylate of ΔDiHA. However, interaction with the second ionization site cannot be conclusively ruled out.

Impact of Smaller Lipids on the RIE of ΔDiHA. Figure 4-11a reveals the significant reduction of the RIE of ΔDiHA when either LPCs, DAG or FAs were included in the sample. Indeed, they decrease the ionization efficiency by a factor of approximately eight, which is four times greater than the reduction caused by the PLs. Interestingly, the lack of significant difference in the reduction of ΔDiHA ionization efficiency caused by FAs and LPCs, suggests that the positively-charged choline HG does not play a significant role in blocking the ionization sites of ΔDiHA. DAG and LPCs affected ΔDiHA similarly; therefore, the phosphate group (absent in DAG) cannot be directly implicated in the interaction with ΔDiHA. The paragraphs below discuss possible interactions of ΔDiHA and each of individual lipids in the gaseous plume. All of these lipid metabolites contain only a single tail with the exception of DAG. Having a single tail reduces steric hindrance and could allow the lipids to be accommodated by ΔDiHA more easily. The conformation of DAG is generally considered to have to two acyl tails on the same side of the glycerol backbone. However, the gas phase is generally less understood than the solution phase and DAG may adopt a different conformation than it does in the solution phase. In the gas phase, the acyl tails of DAG may 'unravel' to form a single long chain with the glycerol backbone in the center of the molecule. In this way DAG resembles the other lipid metabolites which contain only a single tail. This may explain the similar effect of DAG and the other lipid metabolites on ΔDiHA's ionization efficiency.

In all cases, we cannot say with complete certainty which ionization site on ΔDiHA is being blocked. In fact either or both sites may be blocked. In the case of the FAs and PA which are negatively charged at neutral pH, they could not be attracted to ΔDiHA's carboxylate group. Therefore, for the FAs we propose that their interaction which ΔDiHA involves the blocking of the second ionization site.

Effect of ΔDiHA on the RIE of Lipids

The relative decreases of the ionization efficiency of all lipid species caused by the presence of ΔDiHA were similar in all species. This is indicative of gas phase interaction(s) between ΔDiHA and all the lipid species. For each lipid species, the ionization efficiency varies in the absence of ΔDiHA. For example, the LPCs started with higher ionization efficiency than the PLs. In the case of a positively-charged HG, the only requirement is the addition of a proton or cation to neutralize the negatively-charged phosphate group to obtain a positive charge on the molecule. Based on the data, having a single tail increases the ionization efficiency. The presence of two acyl tails increases the hydrophobic nature of the molecule and reduces the overall electron density. Therefore the drive is somewhat diminished to attract a proton or a cation.

Although the RIE of ΔDiHA was not affected by PA, the opposite was observed as ΔDiHA has a large effect on the ionization of PA. This indicates that interaction(s) do indeed occur between the two molecules; albeit one that does not block an ionization site on ΔDiHA. ΔDiHA, however, must partially block an ionization site on PA for the reduction in PA ionization efficiency to be observed. In proposing a model for this interaction, it is unlikely that PA will be near ΔGlcU due to its negative charge. If the second site of ionization for ΔDiHA is the electron-rich region of GlcNAc as proposed earlier, PA may interact with ΔDiHA through the acetamido group. In this way, H-

bonding between the phosphate group of PA and the amide proton of ΔDiHA may provide a stabilizing interaction that results in the blockage of the phosphate ionization site on PA.

If statistically different, ΔDiHA has the greatest effect on PA and the least effect on PE. This is surprising because PE has a positive charge and PA is negatively charged. This can be rationalized as the lack of a choline or ethanolamine HG inhibits the effects of ΔDiHA. To understand these differences, the ability of the HG to participate in H-bonding was evaluated. All the lipids are capable of accepting H-bonds through either the phosphate group or the nitrogen of choline or ethanolamine. PE is the only lipid whose HG is capable of donating a H-bond. Since PE was the least affected by ΔDiHA, it can be deduced that the H-bond donating from the lipid to ΔDiHA is not a critical interaction causing the reduction of lipid ionization efficiency in the presence of ΔDiHA. Therefore, it is proposed that the ability of the lipids to accept one or more H-bonds may play the biggest role in determining the extent of lipid interactions with ΔDiHA. In comparing abilities to accept a H-bond from ΔDiHA, it seems that having a positively-charged HG reduces the degree of H-bonds from ΔDiHA relative to PA which is negatively charged. With hydrogen being partially positive in terms of electronegativity, it will have the greatest desire to donate to a negatively-charged HG. Therefore, PA is proposed to experience the greatest reduction in ionization efficiency because of the formation of strong H-bonds with the OH groups of ΔDiHA. These bonds are expected to stabilize the negative charge of the phosphate and lead to the reduction of PA's ionization efficiency.

In the spectra of PA and PE mixture spectra (Figs. 4-9a and 4-9b), peaks corresponding to the loss of a HG are of high intensity, relative to the parent ion. This cleavage is not caused by ΔDiHA, as this cleavage is seen in the lipids alone. Lipids

containing a phosphocholine HG also show HG cleavage peaks (m/z = 184), but with much lower relative intensities. The exact causes of the HG cleavage in PA and PE are not known, but may be related to the laser fluence.

In Situ Detection of Lipids in the VH

Preliminary data have been obtained for porcine and human VH to optimize experimental conditions and to determine the presence of lipid and lipid metabolites. Through regional sampling of the VH, the source of lipids (lens or retina) may be determined. Lipids in the anterior portion are likely to originate from the lens, while lipids in the posterior portion would be more likely to come from the retina. PNA was found to be the most suitable matrix for *in situ* analysis, although detection with DHB was also possible.[95] PNA, however, gave mass spectra with higher S/N and more lipid-related peaks could be detected.

Spectra from the anterior portion of the VH did not reveal any lipid-related peaks and spectra from this region of the VH were of poor S/N. However, the posterior portion of both human and porcine revealed several lipid peaks, between m/z = 700-900, related to PCs and SMs (Fig. 4-12). Tentative assignments have been made for selected peaks which are given in Figure 4-12. Additionally, some lipid peaks were seen in both human and porcine species, such as those related to PCs. Some differences are expected due to the difference in the age between the porcine and human at the time of death. The porcine eye is much younger (< 5 years of age) than that of the human (54 years of age) and thus it is expected that the porcine eye will have undergone much less liquefaction than the human in its lifetime. However, mass spectra of the human eye were of much lower S/N due to liquefaction and subsequent dehydration of the eye that resulted during storage (~2 years at -20 °C). These preliminary studies represent the first time regional analysis of

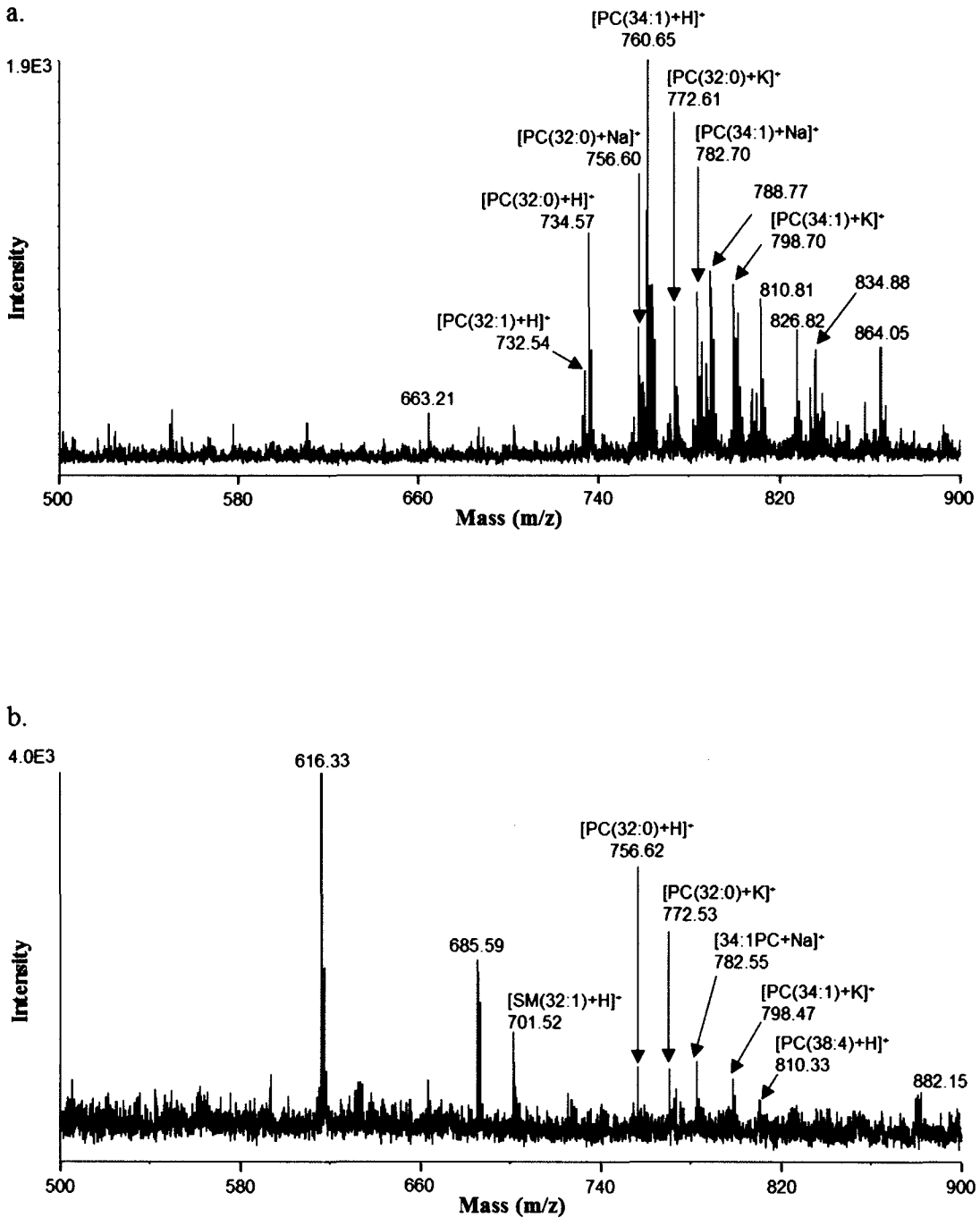

Figure 4-12. MALDI-MS spectra of posterior portions of the VH from: a) porcine and b) human eyes. Spectra were obtained in the positive ion mode using PNA as matrix. Tenative assignments are shown.

lipids has been carried out on the VH, but further optimization is needed. The data presented here suggest that more lipids exist in the posterior region of the VH, suggesting a retinal origin. Turnover of retinal cells may be a source of lipids and metabolites that contribute to age-related VH liquefaction.

CONCLUSIONS

Matrices with different pKa were compared for the detection of ΔDiHA by MALDI-MS. ΔDiHA was shown to favor positive ion detection using acidic matrices over negative ion detection with either neutral or basic matrices. DHB was found to be most suitable for ΔDiHA analysis due to its high S/N and lack of overlapping matrix peaks with the analyte.

Possible gas-phase interactions with lipids were inferred from changes in RIEs between the control solutions (one component alone) and binary mixtures. Reductions in RIEs are proposed to result from the partial blockage of an ionization site on the analyte. ΔDiHA was shown to decrease significantly the RIE of all lipid species. Indeed, even those lipids that were affected the least exhibited an approximately 50% decrease in RIE. LPC-OA and PA were found to be affected the most by ΔDiHA. It is possible that ΔDiHA interacts better with the HG of these two PLs because there is a single acyl chain in LPC-OA and, in the case of PA, the phosphate group is totally accessible. H-bonds between ΔDiHA and the phosphate group may stabilize the negative charge and prevent the protonation or cationization step needed to form the cation.

Changes in RIE for ΔDiHA were compared in the presence of different lipids. All lipids, except for PA, caused a reduction in the RIE of ΔDiHA. PC and PE showed the smallest changes in the loss of ΔDiHA RIE. Smaller lipids, such as FAs, LPCs, and OA

were found to cause the greatest reduction in the RIE of ΔDiHA. It was proposed that their smaller sizes favor interactions with ΔDiHA that block an ionization site(s) on ΔDiHA and prevent its ionization.

Although DHB was found to be the most suitable matrix in the *in vitro* studies, PNA gave better results for *in situ* analysis of biological samples. This trend was observed in previous studies by our group.[95] Therefore, exploratory studies were carried with PNA on the VH from porcine and human eyes. Regional differences emerge when comparing anterior and posterior portions of the VH. More lipids were found in the posterior region suggesting that they are of retinal origin. Tentative assignments were made corresponding to PC and SM species. However, further studies are needed to confirm these assignments. Nevertheless, these preliminary results do support the possibility that retinal lipids contribute to the liquefaction of the VH which, as presented in Chapter 1 of this dissertation, begins in the posterior region of the VH, closest to the retina.

CHAPTER 5

CONCLUSIONS AND FUTURE DIRECTIONS

The theme explored in this dissertation focused on the interactions between hyaluronan (HA) and lipids. Model studies on the disaccharide ΔDiHA and the polymeric form of HA have been performed in the absence and in the presence of lipids. Fatty acids (FAs), lyso-phosphatidylcholines (LPCs), diacylglycerol (DAG), and several phospholipids (PLs) were explored to understand their individual interactions and those with HA. Upon addition of lipids to aqueous solutions of polymeric HA, no physical changes could be visually detected. However, from nuclear magnetic resonance (NMR) spectral changes in line broadening, and to a less extent in chemical shifts of NMR resonances, the interactions between HA and the various lipids were inferred. Further model studies with the disaccharide ΔDiHA and lipids were carried out with the use of matrix-assisted laser desorption ionization mass spectrometry (MALDI-MS). Changes in the relative ionization efficiencies of ΔDiHA and lipids were used to evaluate the interaction of these compounds in the gas phase. The paragraphs below summarize the main conclusions and provide possible directions for future research.

Model Studies of ΔDiHA Anomers by NMR Spectroscopy

NMR studies revealed spectral complexity and required the use of powerful inverse 2D heteronuclear techniques to enable the assignment of all ^{1}H and ^{13}C

resonances of both anomeric forms of the disaccharide present in the sample.Temperature-dependent studies and determination of temperature coefficients for NH and OH groups have permitted the investigation of intra- and intermolecular H-bonding. Ring protons were found to be little affected by changes in temperature and only a small upfield shift (shielding) due to weakening of interactions with D_2O. The largest (least negative) temperature coefficient was found for the NH proton (-4.7×10^{-3} ppb/°C) of the α anomer indicating involvement in a relatively stronger intramolecular H-bond, compared to O**H** and N**H** of the β anomer. Based on previously reported torsional angles of the β-1,3 glycosidic linkage, H-bonds are found to be possible with either *U*-H2 or *U*-H3.

These studies were performed at rather low concentrations (4.18 μM) for the ΔDiHA. In the future, concentration-dependent studies may be carried out to understand the effect of concentration on H-bonding interactions among neighboring disaccharides. At higher concentrations, intermolecular H-bonding interactions between disaccharides are expected to compete with disaccharide-water H-bonds.

Model Studies of Polymeric HA and Interactions with Lipids in the Aqueous Phase

In comparison to the model disaccharide, the NMR spectra of polymer revealed considerable broadening and loss of anomeric differences. Temperature-dependent studies, in combination with theoretically calculated trends, suggested the opening up of the polymer and greater interactions with D_2O as the temperature increased. Hyaluronan and lipid mixtures were analyzed to probe possible interactions in solution. By monitoring changes in band broadening, and to a lesser extent changes in chemical shift, lyso-1-oleoyl-phosphatidylcholine (LPC-OA) was found to cause the greatest degree of

changes in HA. Through comparison of other lipid-related species, stronger interactions were found for lipids containing either a site of unsaturation and/or a large positively-charged HG such as choline. Hydrophobic interactions (between lipid acyl tails with hydrophobic patches along the HA chain) and hydrophilic interaction (involving polar groups of HA and the charged lipid HG) have been proposed.

Future studies should utilize through-space 2D NMR techniques such as Nuclear Overhauser Effect Spectroscopy (NOESY) and Rotating frame nuclear Overhauser Effect Spectroscopy (ROESY) so that through-space interactions (< 5 Å) can be detected between HA and the lipid molecules. These studies will help validate the models proposed in this work.

Model Studies of ΔDiHA and Interactions with Lipids in the Gas Phase

After optimization of the experimental conditions for the detection of ΔDiHA by MALDI-MS, DHB matrix was found to be the matrix of choice as it gave spectra with high S/N and no interfering matrix peaks in the positive-ion mode. ΔDiHA and lipid mixtures were then analyzed to establish whether or not their presence in the same sample had an effect on their respective RIEs. Indeed, significant reductions were observed in most cases. This suggests that gas phase interactions result in the partial blocking of ionization sites. Phosphatidic acid (PA) was the only lipid that did not affect the RIE of ΔDiHA. This has been attributed to repulsion between the negatively-charged PA and the negatively-charged carboxylate of ΔDiHA. This repulsion precludes the blocking of the most logical ionization sites of ΔDiHA. Smaller lipid metabolites were found to block the ionization site of ΔDiHA most effectively as inferred from the greatest reductions in the RIE of ΔDiHA.

Analysis of the vitreous humor (VH) directly to monitor for the presence of lipids, as well as age-related differences, is the long-term goal of these studies. However, the complexity of such analysis requires a thorough understanding of model studies for individual components. Due to the complex nature of the biological matrices, extraction and separation techniques will likely be required so that lipids can be detected with greater S/N. Optimization of VH studies will also require improvement of the protocol used for sectioning of the vitreous. Regional differences, as well as potential concentration gradients could be studied by MALDI-MS if sectioning can be done in a small enough manner.

Biological Aspects

The effects of lipid interaction within the VH are not currently known. Lipids, which are not native to the VH, may affect either major component of the VH biomatrix: collagen, HA, or both. It is therefore necessary to understand the effects of lipids on individual component of the VH first. In these studies, the interaction between lipids and HA have been probed through the analysis of binary mixtures which contain only HA and only one lipid species at a time. Ultimately, studies need to be performed on ternary mixtures of HA, collagen, and lipids. The studies presented herein have focused on HA and lipids exclusively and represent the first step in understanding the impact that lipids may have on the complex biomatrix of the VH.

Understanding molecular compositional and structural changes in the VH is relevant because of the significant liquefaction that occurs in the VH throughout the lifetime. Liquefaction results in the contraction of collagen fibrils with concurrent pooling of HA which compromises the structural integrity of the matrix. Because the

surrounding ocular tissues depend on the VH for mechanical support, liquefaction can lead to further complications such as posterior vitreous detachment. The roles of lipids in this degradative process are not completely known, but the results reported in Chapter 3 do show that HA interacts with lipids, particularly with those with sites of unsaturation.

Preliminary Studies

As preliminary studies for future work, the VH of both porcine (Fig. 5-1) and human species (Fig. 5-2) have been analyzed. The previous chapter presented preliminary studies performed on the VH by MALDI-MS. NMR analysis was also applied to the VH of both species. Additionally, a preliminary oxidation study was carried out on the porcine VH. In this study, a fresh, frozen eye was examined quickly (< 24 hours) after death and compared to an eye that was exposed to air and sunlight, at room temperatures, for more than 24 hours. These studies reveal significant differences between the NMR spectra collected for the two eyes. Specifically, the loss of some resonances was observed particularly of lower chemical shifts, and this was accompanied by an increase of resonances at high chemical shifts (5-8 ppm). This higher chemical shift region corresponds to proton resonances related to oxygen-containing moieties which are proposed to result from the oxidation caused by exposure to air and sunlight. The ^{1}H NMR spectrum of VH from the human eye is provided in Figure 5-2 and reveals the spectral complexity of this biological matrix.

It is clear from these preliminary data that the complexity of the VH will require a systematic approach to separate its components and evaluate their roles. Future studies, both NMR and MALDI-MS, must also examine the effects of lipids on collagen, the other major macromolecule of the VH. It is likely that the cooperative nature of HA and collagen together contributes to the overall stability of the VH. Model studies similar to

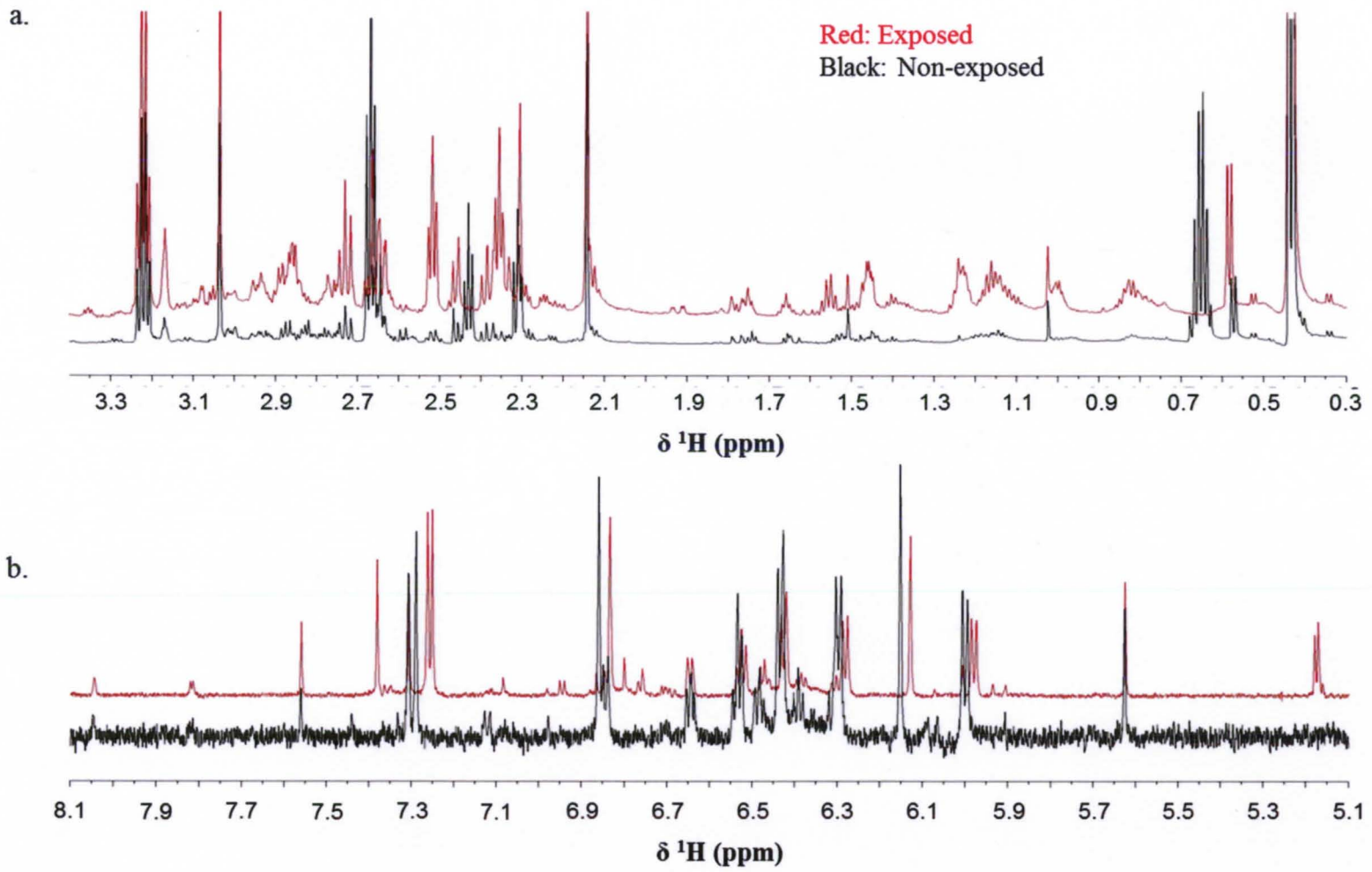

Figure 5-1. ^{1}H NMR spectra of non-exposed (black) and exposed (red) porcine VH. Comparison of the a) upfield (0.3 - 3.3 ppm) and b) downfield (5.1 - 8.1 ppm) regions.

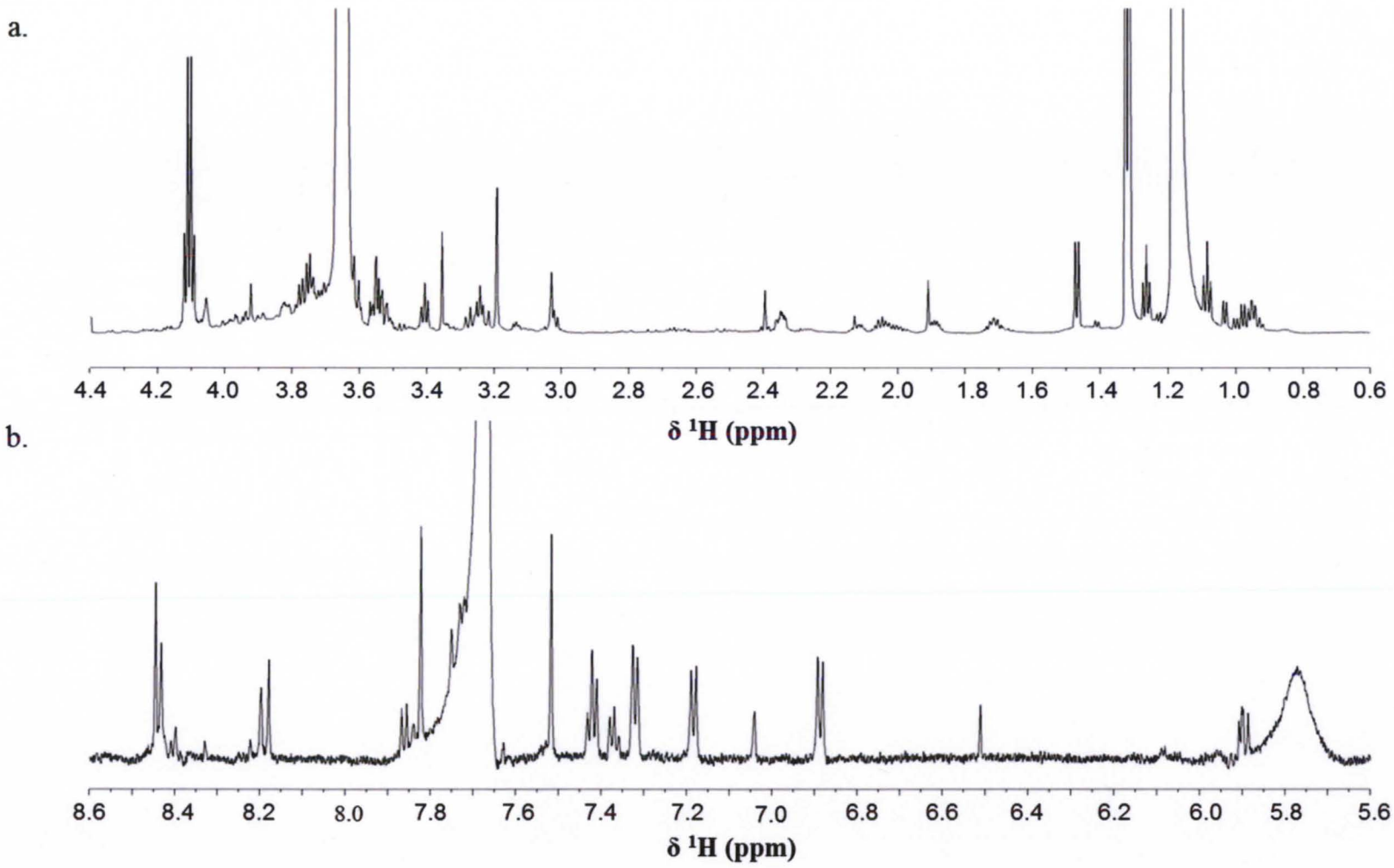

Figure 5-2. ^{1}H NMR spectra of VH from human eyes. Comparison of the a) upfield (0.6 - 4.4 ppm) and b) downfield (5.6 - 8.6 ppm) regions.

those presented here will be beneficial to understanding their potential. Once the interactions of lipids are understood for both HA and collagen separately, the ternary (HA/collagen/lipid) mixture can then be investigated. This will provide a more accurate and realistic model for the VH.

REFERENCES

1. *The biology of the eye*; Fischbarg, J., Ed.; Elsevier, 2006; Vol. 10.

2. *Duane's Foundations of Clincal Ophthalmology*; Tasman, W.; Jaeger, E. A., Eds.; Lippincott Williams & Wilkins, 2007.

3. Forrester, J. V. *The eye: basic sciences in practice*; 2nd ed.; Elsevier Health Sciences, 2002.

4. Bishop, P. N. Structural macromolecules and supramolecular organisation of the vitreous gel. *Progress in Retinal and Eye Research* **2000**, *19*, 323–344.

5. Nickerson, C. S.; Park, J.; Kornfield, J. A.; Karageozian, H. Rheological properties of the vitreous and the role of hyaluronic acid. *Journal of Biomechanics* **2008**, *41*, 1840–1846.

6. Fatt, I.; Weissman, B. A. *Physiology of the eye: an introduction to the vegetative functions*; 2nd ed.; Butterworth-Heinemann, 1992.

7. Sebag, J. *Vitreous: Structure, Function, and Pathobiology*; Springer, 1989.

8. Walker, F.; Patrick, R. S. Constituent monosaccharides and hexosamine concentration of normal human vitreous humour. *Experimental Eye Research* **1967**, *6*, 227–232.

9. Luyckx-Bacus, J.; Weekers, J. Etude Biometrique de l'Oeil Humain par Ultrasonographie (Biometric Study of the Human Eye by Ultrasonography). *Bull Soc Belge Ophtalmol* **1966**, *143*, 552–567.

10. Balazs, E. A. Fine structure of the developing vitreous. *Int Ophthalmol Clin* **1975**, *15*, 53–63.

11. Khurana, A. K. *Ophthalmology*; 3rd ed.; New Age International, 2005.

12. Kaufman, Paul L.; Alm, Albert *Adler's physiology of the eye*; 10th ed.; Mosby, 2002.

13. Streeten, B. A. Ch. 49-Disorders of the Vitreous. In *Pathobiology of ocular disease: a dynamic approach*; Garner, A.; Klintworth, G. K., Eds.; N. Dekker: New York, 1982; Vol. 2, pp. 1381–1419.

14. Hogan, M. J. The Vitreous, Its Structure, and Relation to the Ciliary Body and Retina. Proctor Award Lecture. *Invest Ophthalmol* **1963**, *2*, 418–445.

15. Fine, B. S.; Tousimis, A. J. The Structure of the Vitreous Body and the Suspensory Ligaments of the Lens. *Arch Ophthalmol* **1961**, *65*, 95–110.

16. Gartner, J. Vitreous electron microscopic studies on the fine structure of the normal and pathologically changed vitreoretinal limiting membrane. *Survey of Ophthalmology,* **1964**, *9*, 291–294.

17. Riordan-Eva, P.; Vaughan, D.; Asbury, T. *Vaughan & Asbury's general ophthalmology*; McGraw-Hill Professional, 2004.

18. Balazs, E. A.; Toth, L. Z. J.; Eckl, E. A.; Mitchell, A. P. Studies on the structure of the vitreous body: XII. Cytological and histochemical studies on the cortical tissue layer. *Experimental Eye Research* **1964**, *3*, 57–71.

19. Sakamoto, T.; Ishibashi, T. Hyalocytes. *Retina* **2011**, *31*, 222–228.

20. Sakamoto, T.; Ishibashi, T. Hyalocytes: essential cells of the vitreous cavity in vitreoretinal pathophysiology? *Retina (Philadelphia, Pa.)* **2011**, *31*, 222–228.

21. Sakamoto, T. Cell Biology of Hyalocytes. *Nippon Ganka Gakkai Zasshi* **2003**, *107*, 866–882; discussion 883.

22. Worst, J. G. F.; Los, L. I. *Cisternal anatomy of the vitreous*; Kugler Publications, 1995.

23. Berman, E. R. *Biochemistry of the eye*; Springer, 1991.

24. Balazs, E. A.; Laurent, T. C.; Laurent, U. B. G.; DeRoche, M. H.; Bunney, D. M. Studies on the Structure of the Vitreous Body: VIII. Comparative Biochemistry. *Archives of Biochemistry and Biophysics* **1959**, *81*, 464–479.

25. Balazs, E.A.; Denlinger, J.L. Aging changes in the vitreous. In *Aging and human visual function*; Sekuler, R.; Kline, D.; Dismukes, K.; Vision, N. R. C. (U. S.). C. on, Eds.; A.R. Liss, 1982.

26. Ali, S.; Bettelheim, F. A. Distribution of freezable and non-freezable water in bovine vitreous. *Curr. Eye Res.* **1984**, *3*, 1233–1239.

27. Castoro, J. A.; Bettelheim, F. A. Topographic Distribution of Water in Rhesus Monkey Vitreus. *Ophthalmic Research* **1986**, *18*, 87–89.

28. Cavallotti, C.; Cerulli, L. *Age-related changes of the human eye*; Springer, 2008.

29. Sebag, J. Age-related changes in human vitreous structure. *Graefe's Archive for Clinical and Experimental Ophthalmology* **1987**, *225*, 89–93.

30. Sebag, J. Ageing of the Vitreous. *Eye (Lond)* **1987**, *1*, 254–262.

31. Deguine, V.; Menasche, M.; Ferrari, P.; Fraisse, L.; Pouliquen, Y.; Robert, L. Free radical depolymerization of hyaluronan by maillard reaction products: Role in liquefaction of aging vitreous. *International Journal of Biological Macromolecules* **1998**, *22*, 17–22.

32. Akiba, J.; Ueno, N.; Chakrabarti, B. Age-related changes in the molecular properties of vitreous collagen. *Current Eye Research* **1993**, *12*, 951.

33. Bishop, P. N.; Holmes, D. F.; Kadler, K. E.; McLeod, D.; Bos, K. J. Age-Related Changes on the Surface of Vitreous Collagen Fibrils. *Invest. Ophthalmol. Vis. Sci.* **2004**, *45*, 1041–1046.

34. Los, L. I.; van der Worp, R. J.; van Luyn, M. J. A.; Hooymans, J. M. M. Age-Related Liquefaction of the Human Vitreous Body: LM and TEM Evaluation of the Role of Proteoglycans and Collagen. *Invest. Ophthalmol. Vis. Sci.* **2003**, *44*, 2828–2833.

35. Reháková, M.; Bakos, D.; Soldán, M.; Vizárová, K. Depolymerization reactions of hyaluronic acid in solution. *International Journal of Biological Macromolecules* **1994**, *16*, 121–124.

36. Pigman, W.; Rizvi, S.; Holley, H. L. Depolymerization of hyaluronic acid by the ORD reaction. *Arthritis & Rheumatism* **1961**, *4*, 240–252.

37. Uchiyama, H.; Dobashi, Y.; Ohkouchi, K.; Nagasawa, K. Chemical change involved in the oxidative reductive depolymerization of hyaluronic acid. *Journal of Biological Chemistry* **1990**, *265*, 7753 –7759.

38. Armand, G.; Chakrabarti, B. Conformational differences between hyaluronates of gel and liquid human vitreous: fractionation and circular dichroism studies. *Curr. Eye Res* **1987**, *6*, 445–450.

39. Ueno, N.; Sebag, J.; Hirokawa, H.; Chakrabarti, B. Effects of Visible-Light Irradiation on Vitreous Structure in the Presence of a Photosensitizer. *Exp. Eye Res* **1987**, *44*, 863–870.

40. Deeble, D. J.; Phillips, G. O.; Bothe, E.; Schuchmann, H.-P.; von Sonntag, C. The radiation-induced degradation of hyaluronic acid. *International Journal of Radiation Applications and Instrumentation. Part C. Radiation Physics and Chemistry* **1991**, *37*, 115–118.

41. Sebag, J. Anomalous posterior vitreous detachment: a unifying concept in vitreo-retinal disease. *Graefe's Archive for Clinical and Experimental Ophthalmology* **2004**, *242*, 690–698.

42. Akiba, J.; Ueno, N.; Chakrabarti, B. Molecular mechanisms of posterior vitreous detachment. *Graefe's Archive for Clinical and Experimental Ophthalmology* **1993**, *231*, 408–412.

43. Wang, J.; McLeod, D.; Henson, D. B.; Bishop, P. N. Age-dependent changes in the basal retinovitreous adhesion. *Invest. Ophthalmol. Vis. Sci.* **2003**, *44*, 1793–1800.

44. Sebag, J. Age-Related Differences in the Human Vitreoretinal Interface. *Arch Ophthalmol* **1991**, *109*, 966–971.

45. Steidl, S. M.; Steidl, S.; Hartnett, M. E. *Clinical Pathways In Vitreoretinal Disease*; Thieme, 2003.

46. Comper, W. D.; Laurent, T. C. Physiological function of connective tissue polysaccharides. *Physiol. Rev.* **1978**, *58*, 255–315.

47. Lehninger, A. L.; Nelson, D. L.; Cox, M. M. *Lehninger principles of biochemistry*; Macmillan, 2005.

48. Fraser, J. R. E.; Laurent, T. C.; Laurent, U. B. G. Hyaluronan: Its Nature, Distribution, Functions and Turnover. *J Intern Med* **1997**, *242*, 27–33.

49. Toole, B. P. Hyaluronan: From Extracellular Glue to Pericellular Cue. *Nat. Rev. Cancer* **2004**, *4*, 528–539.

50. Weigel, P. H.; Hascall, V. C.; Tammi, M. Hyaluronan Synthases. *Journal of Biological Chemistry* **1997**, *272*, 13997 –14000.

51. Prehm, P. Hyaluronate is synthesized at plasma membranes. *Biochem J* **1984**, *220*, 597–600.

52. Necas, J.; Bartosikova, L.; Brauner, P.; Kolar, J. Hyaluronic Acid (Hyaluronan): A Review. *Vet Med-Czech* **2008**, *53*, 397–411.

53. Mitra, A. K.; Arnott, S.; Sheehan, J. K. Hyaluronic acid: Molecular conformation and interactions in the tetragonal form of the potassium salt containing extended chains. *Journal of Molecular Biology* **1983**, *169*, 813–827.

54. Almond, A.; Brass, A.; Sheehan, J. K. Deducing polymeric structure from aqueous molecular dynamics simulations of oligosaccharides: predictions from simulations of hyaluronan tetrasaccharides compared with hydrodynamic and X-ray fibre diffraction data. *Journal of Molecular Biology* **1998**, *284*, 1425–1437.

55. Cleland, R. L.; Wang, J. L.; Detweiler, D. M. Polyelectrolyte properties of sodium hyaluronate. 2. Potentiometric titration of hyaluronic acid. *Macromolecules* **1982**, *15*, 386–395.

56. Garg, H. G.; Hales, C. A. *Chemistry and biology of hyaluronan*; Elsevier, 2004.

57. Balazs, E. A.; Laurent, T. C.; Jeanloz, R. W. Nomenclature of Hyaluronic Acid. *Biochem. J* **1986**, *235*, 903.

58) Laurent, T. C.; Ryan, M.; Pietruszkiewicz, A. Fractionation of hyaluronic acid the polydispersity of hyaluronic acid from the bovine vitreous body. *Biochimica et Biophysica Acta* **1960**, *42*, 476–485.

59. Baggenstoss, B. A.; Weigel, P. H. Size exclusion chromatography-multiangle laser light scattering analysis of hyaluronan size distributions made by membrane-bound hyaluronan synthase. *Analytical Biochemistry* **2006**, *352*, 243–251.

60. Balazs, E. A. The Vitreous. In *The Eye: a-b. Vegetative physiology and biochemistry*; Davson, H., Ed.; Academic Press: London, 1984; Vol. Ia, pp. 533–589.

61. Fessler, J. H.; Fessler, L. I. Electron microscopic visualization of the polysaccharide hyaluronic acid. *Proceedings of the National Academy of Sciences of the United States of America* **1966**, *56*, 141 –147.

62. Atkins, E. D.; Phelps, C. F.; Sheehan, J. K. The conformation of the mucopolysaccharides. Hyaluronates. *Biochem. J.* **1972**, *128*, 1255–1263.

63. Atkins, E. D.; Sheehan, J. K. Structure for hyaluronic acid. *Nature New Biol.* **1972**, *235*, 253–254.

64. Sheehan, J. K.; Gardner, K. H.; Atkins, E. D. T. Hyaluronic acid: a double-helical structure in the presence of potassium at low pH and found also with the cations ammonium, rubidium and caesium. *Journal of Molecular Biology* **1977**, *117*, 113–135.

65. Laurent, T. C. Studies on hyaluronic acid in the vitreous body. *J. Biol. Chem* **1955**, *216*, 263–271.

66. Ogston, A. G.; Stanier, J. E. The dimensions of the particle of hyaluronic acid complex in synovial fluid. *Biochem J* **1951**, *49*, 585–590.

67. Laurent, T. C. Biochemistry of Hyaluronan. *Acta Otolaryngol* **1987**, *Suppl. 442*, 7–24.

68. Scott, J. E.; Tigwell, M. J. Periodate oxidation and the shapes of glycosaminoglycuronans in solution. *Biochem J* **1978**, *173*, 103–114.

69. Atkins, E. D. T.; Meader, D.; Scott, J. E. Model for hyaluronic acid incorporating four intramolecular hydrogen bonds. *International Journal of Biological Macromolecules* **1980**, *2*, 318–319.

70. Scott, J. E.; Heatley, F.; Hull, W. E. Secondary structure of hyaluronate in solution. A 1H-n.m.r. investigation at 300 and 500 MHz in [2H6]dimethyl sulphoxide solution. *Biochem J* **1984**, *220*, 197–205.

71. Heatley, F.; Scott, J. E. A water molecule participates in the secondary structure of hyaluronan. *Biochem. J* **1988**, *254*, 489–493.

72. Scott, J. E.; Cummings, C.; Brass, A.; Chen, Y. Secondary and tertiary structures of hyaluronan in aqueous solution, investigated by rotary shadowing-electron microscopy and computer simulation. Hyaluronan is a very efficient network-forming polymer. *Biochemical Journal* **1991**, *274*, 699–705.

73. Laurent, T. C.; Ogston, A. G. The interaction between polysaccharides and other macromolecules. 4. The osmotic pressure of mixtures of serum albumin and hyaluronic acid. *Biochem J* **1963**, *89*, 249–253.

74. Laurent, T. C.; Laurent, U. B. G.; Fraser, J. R. E. Functions of Hyaluronan. *Ann Rheum Dis* **1995**, *54*, 429–432.

75. Laurent, T. C. Hyaluronan Research in Uppsala. *Ups. J. Med. Sci.* **2007**, *112*, 123–142.

76. Chakrabarti, B.; Park, J. W. Glycosaminoglycans: structure and interaction. *CRC Crit. Rev. Biochem.* **1980**, *8*, 225–313.

77. Sebag, J. Imaging vitreous. *Eye (Lond)* **2002**, *16*, 429–439.

78. Bos, K. .; Holmes, D. .; Meadows, R. .; Kadler, K. .; McLeod, D.; Bishop, P. . Collagen fibril organisation in mammalian vitreous by freeze etch/rotary shadowing electron microscopy. *Micron* **2001**, *32*, 301–306.

79. Ihanamäki, T.; Pelliniemi, L. J.; Vuorio, E. Collagens and collagen-related matrix components in the human and mouse eye. *Prog Retin Eye Res* **2004**, *23*, 403–434.

80. Scott, J. E. The chemical morphology of the vitreous. *Eye* **1992**, *6*, 553–555.

81. Bishop, P.; Ayad, S.; Reardon, A.; McLeod, D.; Sheehan, J.; Kielty, C. Type VI collagen is present in human and bovine vitreous. *Graefes Arch. Clin. Exp. Ophthalmol.* **1996**, *234*, 710–713.

82. Newsome, D. A.; Linsenmayer, T. F.; Trelstad, R. L. Vitreous body collagen. Evidence for a dual origin from the neural retina and hyalocytes. *The Journal of Cell Biology* **1976**, *71*, 59 –67.

83. Bishop, P. N.; Reardon, A. J.; McLeod, D.; Ayad, S. Identification of alternatively spliced variants of type II procollagen in vitreous. *Biochem. Biophys. Res. Commun.* **1994**, *203*, 289–295.

84. Snowden, J. M.; Eyre, D. R.; Swann, D. A. Vitreous structure. VI. Age-related changes in the thermal stability and crosslinks of vitreous, articular cartilage and tendon collagens. *Biochim. Biophys. Acta* **1982**, *706*, 153–157.

85. Le Goff, M. M.; Bishop, P. N. Adult vitreous structure and postnatal changes. *Eye* **2008**, *22*, 1214–1222.

86. Reddy, D. V. N.; Rosenberg, C.; Kinsey, V. E. Steady state distribution of free amino acids in the aqueous humours, vitreous body and plasma of the rabbit. *Experimental Eye Research* **1961**, *1*, 175–181.

87. Reddy, V. N. Dynamics of Transport Systems in the Eye. Friedenwald Lecture. *IOVS* **1979**, *18*, 1000–1018.

88. McGahan, M. C. Ascorbic acid levels in aqueous and vitreous humors of the rabbit: effects of inflammation and ceruloplasmin. *Exp. Eye Res.* **1985**, *41*, 291–298.

89. Friedenwald, J. S.; Buschke, W.; Michel, H. O. Role of Ascorbic Acid (vitamin C) in Secretion of Intraocular Fluid. *Archives of Ophthalmology* **1943**, *29*, 535–574.

90. KINSEY, V. E. Transfer of ascorbic acid and related compounds across the blood-aqueous barrier. *Am. J. Ophthalmol.* **1947**, *30*, 1262–1266.

91. Ringvold, A. Aqueous humour and ultraviolet radiation. *Acta Ophthalmol (Copenh)* **1980**, *58*, 69–82.

92. BALAZS, E. A. Studies on the structure of the vitreous body. I. The absorption of ultraviolet light. *Am. J. Ophthalmol.* **1954**, *38*, 21–28.

93. Rujoi, M.; Jin, J.; Borchman, D.; Tang, D.; Yappert, M. C. Isolation and Lipid Characterization of Cholesterol-Enriched Fractions in Cortical and Nuclear Human Lens Fibers. *Invest. Ophthalmol. Vis. Sci.* **2003**, *44*, 1634–1642.

94. Yappert, M. C.; Rujoi, M.; Borchman, D.; Vorobyov, I.; Estrada, R. Glycero- versus sphingo-phospholipids: correlations with human and non-human mammalian lens growth. *Experimental Eye Research* **2003**, *76*, 725–734.

95. Estrada, R.; Yappert, M. C. Regional phospholipid analysis of porcine lens membranes by matrix-assisted laser desorption/ionization time-of-flight mass spectrometry. *Journal of Mass Spectrometry* **2004**, *39*, 1531–1540.

96. Rujoi, M.; Estrada, R.; Yappert, M. C. In Situ MALDI-TOF MS Regional Analysis of Neutral Phospholipids in Lens Tissue. *Analytical Chemistry* **2004**, *76*, 1657–1663.

97. Estrada, R.; Puppato, A.; Borchman, D.; Yappert, M. C. Reevaluation of the phospholipid composition in membranes of adult human lenses by 31P NMR and MALDI MS. *Biochimica et Biophysica Acta (BBA) - Biomembranes* **2010**, *1798*, 303–311.

98. Bartley, W.; Van Heyningen, R.; Notton, B. M.; Renshaw, A. Fatty acid composition of lipids present in different parts of the ox eye. *Biochem J* **1962**, *85*, 332–335.

99. Broekhuyse, R. M. Phospholipids in tissues of the eye I. Isolation, characterization and quantitative analysis by two-dimensional thin-layer chromatography of diacyl and vinyl-ether phospholipids. *Biochimica et Biophysica Acta (BBA) - Lipids and Lipid Metabolism* **1968**, *152*, 307–315.

100. Swann, D.; Constable, I.; Caulfield, J. Vitreous structure, IV. Chemical composition of the insoluble residual protein fraction from the rabbit vitreous. *Invest. Ophthalmol. Vis. Sci.* **1975**, *14*, 613–616.

101. Kim, J. O.; Cotlier, E. Phospholipid distributions and fatty acid composition of lysophosphatidylcholine and phosphatidylcholine in rabbit aqueous humor, lens and vitreous. *Exp. Eye Res* **1976**, *22*, 569–576.

102. Reddy, T. S.; Birkle, D. L.; Packer, A. J.; Dobard, P.; Bazan, N. G. Fatty acid composition and arachidonic acid metabolism in vitreous lipids from canine and human eyes. *Curr. Eye Res* **1986**, *5*, 441–447.

103. Sebag, J.; Yee, K. M. P. Ch. 16-Vitreous: From Biochemistry to Clinical Relivance. In *Duane's Foundations of Clincal Ophthalmology*; Tasman, W.; Jaeger, E. A., Eds.; Lippincott Williams & Wilkins, 2005; Vol. 1.

104. Brady, R. O.; Kanfer, J. N.; Bradley, R. M.; Shapiro, D. Demonstration of a deficiency of glucocerebroside-cleaving enzyme in Gaucher's disease. *J. Clin. Invest.* **1966**, *45*, 1112–1115.

105. Peters, S. P.; Lee, R. E.; Glew, R. H. Gaucher's Disease, a Review. *Medicine (Baltimore)* **1977**, *56*, 425–442.

106. Jmoudiak, M.; Futerman, A. H. Gaucher Disease: Pathological Mechanisms and Modern Management. *British Journal of Haematology* **2005**, *129*, 178–188.

107. Kaiser, E.; Heinrich, E. Biochemistry of Gaucher's disease. *Wien. Klin. Wochenschr* **1968**, *80*, 257–260.

108. Shrier, E. M.; Barr, C. C.; Grabowski, G. A. Vitreous Opacities and Retinal Vascular Abnormalities in Gaucher Disease. *Arch Ophthalmol* **2004**, *122*, 1395–1398.

109. Fujiwaki, T.; Yamaguchi, S.; Tasaka, M.; Takayanagi, M.; Isobe, M.; Taketomi, T. Evaluation of sphingolipids in vitreous bodies from a patient with Gaucher disease, using delayed extraction matrix-assisted laser desorption ionization time-of-flight mass spectrometry. *Journal of Chromatography B* **2004**, *806*, 47–51.

110. Pasquali-Ronchetti, I.; Quaglino, D.; Mori, G.; Bacchelli, B.; Ghosh, P. Hyaluronan-Phospholipid Interactions. *Journal of Structural Biology* **1997**, *120*, 1–10.

111. Spagnoli, C.; Korniakov, A.; Ulman, A.; Balazs, E. A.; Lyubchenko, Y. L.; Cowman, M. K. Hyaluronan conformations on surfaces: effect of surface charge and hydrophobicity. *Carbohydrate Research* **2005**, *340*, 929–941.

112. Srinivasan, S. R.; Yost, K.; Radhakrishnamurthy, B.; Dalferes, E. R.; Berenson, G. S. Lipoprotein-hyaluronate associations in human aorta fibrous plaque lesions. *Atherosclerosis* **1980**, *36*, 25–37.

113. Ionov, R.; El-Abed, A.; Goldmann, M.; Peretti, P. Interactions of lipid monolayers with the natural biopolymer hyaluronic acid. *Biochimica et Biophysica Acta (BBA) - Biomembranes* **2004**, *1667*, 200–207.

114. Schnitzer, E.; Dagan, A.; Krimsky, M.; Lichtenberg, D.; Pinchuk, I.; Shinar, H.; Yedgar, S. Interaction of hyaluronic acid-linked phosphatidylethanolamine (HyPE) with LDL and its effect on the susceptibility of LDL lipids to oxidation. *Chemistry and Physics of Lipids* **2000**, *104*, 149–160.

115. Trommer, H.; Wartewig, S.; Böttcher, R.; Pöppl, A.; Hoentsch, J.; Ozegowski, J. H.; Neubert, R. H. H. The effects of hyaluronan and its fragments on lipid models exposed to UV irradiation. *International Journal of Pharmaceutics* **2003**, *254*, 223–234.

116. Peer, D.; Florentin, A.; Margalit, R. Hyaluronan is a key component in cryoprotection and formulation of targeted unilamellar liposomes. *Biochimica et Biophysica Acta (BBA) - Biomembranes* **2003**, *1612*, 76–82.

117. Gómez-Gaete, C.; Tsapis, N.; Silva, L.; Bourgaux, C.; Besnard, M.; Bochot, A.; Fattal, E. Supramolecular organization and release properties of phospholipid-hyaluronan microparticles encapsulating dexamethasone. *European Journal of Pharmaceutics and Biopharmaceutics* **2008**, *70*, 116–126.

118. Rouse, J. J.; Whateley, T. L.; Thomas, M.; Eccleston, G. M. Controlled drug delivery to the lung: Influence of hyaluronic acid solution conformation on its adsorption to hydrophobic drug particles. *International Journal of Pharmaceutics* **2007**, *330*, 175–182.

119. Crescenzi, V.; Taglienti, A.; Pasquali-Ronchetti, I. Supramolecular structures prevailing in aqueous hyaluronic acid and phospholipid vesicles mixtures: an electron microscopy and rheometric study. *Colloids and Surfaces A: Physicochemical and Engineering Aspects* **2004**, *245*, 133–135.

120. Darke, A.; Finer, E. G.; Moorhouse, R.; Rees, D. A. Studies of hyaluronate solutions by nuclear magnetic relaxation measurements. Detection of covalently-defmed, stiff segments within the flexible chains. *Journal of Molecular Biology* **1975**, *99*, 477–486.

121. Ghosh, P.; Hutadilok, N.; Adam, N.; Lentini, A. Interactions of hyaluronan (hyaluronic acid) with phospholipids as determined by gel permeation chromatography, multi-angle laser-light-scattering photometry and 1H-NMR spectroscopy. *International Journal of Biological Macromolecules* **1994**, *16*, 237–244.

122. Ghosh, J.; Hutadilok, N.; Lentini, A. NMR Studies of Hyaluronan(HA): Evidence of Competitive-Inhibition of Interchain Associations by Phospholipids Which May Result in Decreased Anti-inflammatory and Cartilage Protecting Properties of HA. *Heterocycles* **1994**, *38*, 1757–1774.

123. Becker, E. D. *High Resolution Nmr: Theory and Chemical Applications*; Academic Press, 2000.

124. Bruch, M. D. *Nmr Spectroscopy Techniques*; CRC Press, 1996.

125. Macomber, R. S. *A Complete Introduction to Modern NMR Spectroscopy*; 1st ed.; Wiley-Interscience, 1997.

126. Jacobsen, N. E. *NMR Spectroscopy Explained: Simplified Theory, Applications and Examples for Organic Chemistry and Structural Biology*; 1st ed.; Wiley-Interscience, 2007.

127. Crews, P.; Rodríguez, J.; Jaspars, M. *Organic structure analysis*; Oxford University Press, 2010.

128. Cierpicki, T.; Otlewski, J. Amide proton temperature coefficients as hydrogen bond indicators in proteins. *J. Biomol. NMR* **2001**, *21*, 249–261.

129. Dado, G. P.; Gellman, S. H. Intramolecular Hydrogen Bonding in Derivatives of .beta.-Alanine and .gamma.-Amino Butyric Acid; Model Studies for the Folding of Unnatural Polypeptide Backbones. *Journal of the American Chemical Society* **1994**, *116*, 1054–1062.

130. Dado, G. P.; Gellman, S. H. Structural and thermodynamic characterization of temperature-dependent changes in the folding pattern of a synthetic triamide. *Journal of the American Chemical Society* **1993**, *115*, 4228–4245.

131. Gellman, S. H.; Dado, G. P.; Liang, G. B.; Adams, B. R. Conformation-directing effects of a single intramolecular amide-amide hydrogen bond: variable-temperature NMR and IR studies on a homologous diamide series. *Journal of the American Chemical Society* **1991**, *113*, 1164–1173.

132. Rothemund, S.; Weisshoff, H.; Beyermann, M.; Krause, E.; Bienert, M.; Mügge, C.; Sykes, B. D.; Sönnichsen, F. D. Temperature coefficients of amide proton NMR resonance frequencies in trifluoroethanol: a monitor of intramolecular hydrogen bonds in helical peptides. *J. Biomol. NMR* **1996**, *8*, 93–97.

133. Kroon, J.; Kroon-Batenburg, L. M. J.; Leeflang, B. R.; Vliegenthart, J. F. G. Intramolecular versus intermolecular hydrogen bonding in solution. *Journal of Molecular Structure* **1994**, *322*, 27–31.

134. Anderson, C. E.; Pickrell, A. J.; Sperry, S. L.; Vasquez, T. E.; Custer, T. G.; Fierman, M. B.; Lazar, D. C.; Brown, Z. W.; Iskenderian, W. S.; Hickstein, D. D.; O'leary, D. J. NMR Detection of Intramolecular OH/OH Hydrogen Bond Networks: An Approach Using Isotopic Perturbation and Hydrogen Bond Mediated OH···OH J-Coupling. *Heterocycles* **2007**, *72*, 469–495.

135. Blundell, C. D.; Reed, M. A. C.; Almond, A. Complete assignment of hyaluronan oligosaccharides up to hexasaccharides. *Carbohydrate Research* **2006**, *341*, 2803–2815.

136. Scott, J. E.; Heatley, F.; Moorcroft, D.; Olavesen, A. H. Secondary structures of hyaluronate and chondroitin sulphates. A 1H n.m.r. study of NH signals in dimethyl sulphoxide solution. *Biochem J* **1981**, *199*, 829–832.

137. Cowman, M. K.; Cozart, D.; Nakanishi, K.; Balazs, E. A. 1H NMR of glycosaminoglycans and hyaluronic acid oligosaccharides in aqueous solution: The amide proton environment. *Archives of Biochemistry and Biophysics* **1984**, *230*, 203–212.

138. Kvam, B. J.; Atzori, M.; Toffanin, R.; Paoletti, S.; Biviano, F. 1H- and 13C-NMR studies of solutions of hyaluronic acid esters and salts in methyl sulfoxide: comparison of hydrogen-bond patterns and conformational behaviour. *Carbohydr. Res* **1992**, *230*, 1–13.

139. Heatley, F.; Scott, J. E.; Jeanloz, R. W.; Walker-Nasir, E. Secondary structure in glycosaminoglycuronans: N.m.r. spectra in dimethyl sulphoxide of disaccharides related to hyaluronic acid and chondroitin sulphate. *Carbohydrate Research* **1982**, *99*, 1–11.

140. Heatley, F.; Scott, J. E.; Casu, B. 1H-N.M.R. spectra of glycosaminoglycan monomers and dimers in solution in methyl sulphoxide and water. *Carbohydrate Research* **1979**, *72*, 13–23.

141. Cowman, M. K.; Hittner, D. M.; Feder-Davis, J. 13C-NMR Studies of Hyaluronan: Conformational Sensitivity to Varied Environments†. *Macromolecules* **1996**, *29*, 2894–2902.

142. Girish, K. S.; Kemparaju, K. The Magic Glue Hyaluronan and Its Eraser Hyaluronidase: A Biological Overview. *Life Sci* **2007**, *80*, 1921–1943.

143. Stern, R.; Kogan, G.; Jedrzejas, M. J.; Soltés, L. The Many Ways to Cleave Hyaluronan. *Biotechnol. Adv.* **2007**, *25*, 537–557.

144. Stern, R.; Jedrzejas, M. J. The Hyaluronidases: Their Genomics, Structures, and Mechanisms of Action. *Chemical Reviews* **2006**, *106*, 818–839.

145. Frost, G. I.; Csóka, T.; Stern, R. The Hyaluronidases: A Chemical, Biological and Clinical Overview. *Trends in Glycoscience and Glycotechnology* **1996**, *8*, 419–434.

146. Livant, P.; Rodén, L.; Rama Krishna, N. NMR studies of a tetrasaccharide from hyaluronic acid. *Carbohydrate Research* **1992**, *237*, 271–281.

147. Toffanin, R.; Kvam, B. J.; Flaibani, A.; Atzori, M.; Biviano, F.; Paoletti, S. NMR Studies of Oligosaccharides Derived from Hyaluronate: Complete Assignment of 1H and 13C NMR Spectra of Aqueous Di- and Tetra-Saccharides, and Comparison of Chemical Shifts for Oligosaccharides of Increasing Degree of Polymerisation. *Carbohydrate Research* **1993**, *245*, 113–120.

148. Nestor, G.; Kenne, L.; Sandström, C. Experimental evidence of chemical exchange over the β(1→3) glycosidic linkage and hydrogen bonding involving hydroxy protons in hyaluronan oligosaccharides by NMR spectroscopy. *Org. Biomol. Chem.* **2010**, *8*, 2795–2802.

149. Blundell, C. D.; DeAngelis, P. L.; Day, A. J.; Almond, A. Use of 15N-NMR to resolve molecular details in isotopically-enriched carbohydrates: sequence-specific observations in hyaluronan oligomers up to decasaccharides. *Glycobiology* **2004**, *14*, 999–1009.

150. Almond, A.; DeAngelis, P. L.; Blundell, C. D. Dynamics of Hyaluronan Oligosaccharides Revealed by 15N Relaxation. *J. Am. Chem. Soc.* **2005**, *127*, 1086–1087.

151. Blundell, C. D.; Almond, A. Temperature dependencies of amide 1H- and 15N-chemical shifts in hyaluronan oligosaccharides. *Magnetic Resonance in Chemistry* **2007**, *45*, 430–433.

152. Colebrooke, S. A.; Blundell, C. D.; DeAngelis, P. L.; Campbell, I. D.; Almond, A. Exploiting the carboxylate chemical shift to resolve degenerate resonances in spectra of 13C-labelled glycosaminoglycans. *Magnetic Resonance in Chemistry* **2005**, *43*, 805–815.

153. Scott, J. E. Secondary Structures in Hyaluronan Solutions: Chemical and Biological Implications. *Ciba Foundation Symposium* **1989**, *143*, 6–20.

154. Blundell, C. D.; Deangelis, P. L.; Almond, A. Hyaluronan: the absence of amide–carboxylate hydrogen bonds and the chain conformation in aqueous solution are incompatible with stable secondary and tertiary structure models. *Biochem. J.* **2006**, *396*, 487.

155. Cowman, M. K.; Feder-Davis, J.; Hittner, D. M. 13C NMR Studies of Hyaluronan. 2. Dependence of Conformational Dynamics on Chain Length and Solvent†. *Macromolecules* **2001**, *34*, 110–115.

156. Poppe, L.; Stuike-Prill, R.; Meyer, B.; van Halbeek, H. The solution conformation of sialyl-alpha (2----6)-lactose studied by modern NMR techniques and Monte Carlo simulations. *J. Biomol. NMR* **1992**, *2*, 109–136.

157. Sicinska, W.; Adams, B.; Lerner, L. A detailed 1H and 13C NMR study of a repeating disaccharide of hyaluronan: the effects of temperature and counterion type. *Carbohydrate Research* **1993**, *242*, 29–51.

158. Bociek, S. M.; Darke, A. H.; Welti, D.; Rees, D. A. The 13C-NMR spectra of hyaluronate and chondroitin sulphates. Further evidence on an alkali-induced conformation change. *Eur. J. Biochem* **1980**, *109*, 447–456.

159. Welti, D.; Rees, D. A.; Welsh, E. J. Solution Conformation of Glycosaminoglycans: Assignment of the 300-MHz 1H-Magnetic Resonance Spectra of Chondroitin 4-Sulphate, Chondroitin 6-Sulphate and Hyaluronate, and Investigation of an Alkali-Induced Conformation Change. *European Journal of Biochemistry* **1979**, *94*, 505–514.

160. Hofmann, H.; Schmut, O.; Sterk, H.; Pölzler, H. Relaxation time measurements of hyaluronic acid. *International Journal of Biological Macromolecules* **1983**, *5*, 229–232.

161. Scott, J. E.; Heatley, F. Hyaluronan forms specific stable tertiary structures in aqueous solution: A 13C NMR study. *Proceedings of the National Academy of Sciences of the United States of America* **1999**, *96*, 4850–4855.

162. Mikelsaar, R.-H.; Scott, J. E. Molecular modelling of secondary and tertiary structures of hyaluronan, compared with electron microscopy and NMR data. Possible sheets and tubular structures in aqueous solution. *Glycoconjugate Journal* **1994**, *11*, 65–71.

163. Napier, M. A.; Hadler, N. M. Effect of calcium on structure and function of a hyaluronic acid matrix: Carbon-13 nuclear magnetic resonance analysis and the diffusional behavior of small solutes. *Proc Natl Acad Sci U S A* **1978**, *75*, 2261–2265.

164. Finer, E. G.; Henry, R.; Leslie, R. B.; Robertson, R. N. NMR studies of pig low- and high-density serum lipoproteins. Molecular motions and morphology. *Biochim. Biophys. Acta* **1975**, *380*, 320–327.

165. Miertuš, S.; Scrocco, E.; Tomasi, J. Electrostatic interaction of a solute with a continuum. A direct utilizaion of AB initio molecular potentials for the prevision of solvent effects. *Chemical Physics* **1981**, *55*, 117–129.

166. Ditchfield, R. Self-consistent perturbation theory of diamagnetism -- I. A gauge-invariant LCAO - method for N.M.R. chemical shifts. *Molecular Physics: An International Journal at the Interface Between Chemistry and Physics* **1974**, *27*, 789.

167. Wolinski, K.; Hinton, J. F.; Pulay, P. Efficient implementation of the gauge-independent atomic orbital method for NMR chemical shift calculations. *Journal of the American Chemical Society* **1990**, *112*, 8251–8260.

168. Gennis, R. B. *Biomembranes: Molecular Structure and Function*; Springer, 2006.

169. Gross, J. H. *Mass Spectrometry: A Textbook*; 2nd ed.; Springer, 2011.

170. Baldwin, M. A. Mass Spectrometers for the Analysis of Biomolecules. In *Biological Mass Spectrometry*; Academic Press, 2005; Vol. Volume 402, pp. 3–48.

171. Smith, R. M. *Understanding Mass Spectra: A Basic Approach*; John Wiley & Sons, 2004.

172. Harris, D. C. *Quantitative Chemical Analysis*; Eighth ed.; W. H. Freeman, 2010.

173. Bahr, U.; Karas, M.; Hillenkamp, F. Analysis of biopolymers by matrix-assisted laser desorption/ionization (MALDI) mass spectrometry. *Fresenius' Journal of Analytical Chemistry* **1994**, *348*, 783–791.

174. Danis, P. O.; Karr, D. E.; Mayer, F.; Holle, A.; Watson, C. H. The analysis of water-soluble polymers by matrix-assisted laser desorption time-of-flight mass spectrometry. *Organic Mass Spectrometry* **1992**, *27*, 843–846.

175. Hillenkamp, F.; Tsarbopoulos, A.; Gross, M. L. Focus on desorption ionization and macromolecular mass spectrometry. *J. Am. Soc. Mass Spectrom* **2008**, *19*, 1041–1044.

176. Jagtap, R.; Ambre, A. Overview literature on matrix assisted laser desorption ionization mass spectroscopy (MALDI MS): Basics and its applications in characterizing polymeric materials. *Bulletin of Materials Science* **2005**, *28*, 515–528.

177. Karas, M.; Bahr, U.; Gie□mann, U. Matrix-assisted laser desorption ionization mass spectrometry. *Mass Spectrometry Reviews* **1991**, *10*, 335–357.

178. Hillenkamp, F.; Peter-Katalinić, J. *MALDI MS: a practical guide to instrumentation, methods and applications*; Wiley-VCH, 2007.

179. Cole, R. B. *Electrospray and Maldi Mass Spectrometry: Fundamentals, Instrumentation, Practicalities, and Biological Applications*; John Wiley & Sons, 2011.

180. Nilsson, C. L.; Karlsson, G.; Bergquist, J.; Westman, A.; Ekman, R. Mass Spectrometry of Peptides in Neuroscience. *Peptides* **1998**, *19*, 781–789.

181. Estrada, R.; Borchman, D.; Reddan, J.; Hitt, A.; Yappert, M. C. In Vitro and In Situ Tracking of Choline-Phospholipid Biogenesis by MALDI TOF-MS. *Analytical Chemistry* **2006**, *78*, 1174–1180.

182. Lorkiewicz, P.; Yappert, M. C. Titania Microparticles and Nanoparticles as Matrixes for in Vitro and in Situ Analysis of Small Molecules by MALDI-MS. *Analytical Chemistry* **2009**, *81*, 6596–6603.

183. Batoy, S. M. A. B.; Akhmetova, E.; Miladinovic, S.; Smeal, J.; Wilkins, C. L. Developments in MALDI - Mass Spectrometry: The Quest for the Perfect Matrix. *Applied Spectroscopy Reviews* **2008**, *43*, 485.

184. Dashtiev, M.; Wäfler, E.; Röhling, U.; Gorshkov, M.; Hillenkamp, F.; Zenobi, R. Positive and negative analyte ion yield in matrix-assisted laser desorption/ionization. *International Journal of Mass Spectrometry* **2007**, *268*, 122–130.

185. Fountain, S. T.; Lee, H.; Lubman, D. M.; Brodbelt, J. Ion fragmentation activated by matrix-assisted laser desorption/ionization in an ion-trap/reflectron time-of-flight device. *Rapid Commun. Mass Spectrom.* **1994**, *8*, 407–416.

186. Knochenmuss, R. Ion formation mechanisms in UV-MALDI. *The Analyst* **2006**, *131*, 966.

187. Liu, B.-H.; Lee, Y. T.; Wang, Y.-S. Incoherent Production Reactions of Positive and Negative Ions in Matrix-Assisted Laser Desorption/Ionization. *Journal of the American Society for Mass Spectrometry* **2009**, *20*, 1078–1086.

188. Karas, M.; Gluckmann, M.; Schafer, J. Ionization in matrix-assisted laser desorption/ionization: singly charged molecular ions are the lucky survivors. *J. Mass Spectrom.* **2000**, *35*, 1–12.

189. Lehmann, E.; Knochenmuss, R.; Zenobi, R. Ionization mechanisms in matrix-assisted laser desorption/ionization mass spectrometry: contribution of pre-formed ions. *Rapid Commun. Mass Spectrom.* **1997**, *11*, 1483–1492.

190. Ehring, H.; Karas, M.; Hillenkamp, F. Role of photoionization and photochemistry in ionization processes of organic molecules and relevance for matrix-assisted laser desorption lonization mass spectrometry. *Org. Mass Spectrom.* **1992**, *27*, 472–480.

191. Breuker, K.; Knochenmuss, R.; Zhang, J.; Stortelder, A.; Zenobi, R. Thermodynamic control of final ion distributions in MALDI: in-plume proton transfer reactions. *International Journal of Mass Spectrometry* **2003**, *226*, 211–222.

192. Breuker, K.; Knochenmuss, R.; Zenobi, R. Gas-phase basicities of deprotonated matrix-assisted laser desorption/ionization matrix molecules. *International Journal of Mass Spectrometry* **1999**, *184*, 25–38.

193. Wang, B. H.; Dreisewerd, K.; Bahr, U.; Karas, M.; Hillenkamp, F. Gas-phase cationization and protonation of neutrals generated by matrix-assisted laser desorption. *Journal of the American Society for Mass Spectrometry* **1993**, *4*, 393–398.

194. Harvey, D. J. Analysis of carbohydrates and glycoconjugates by matrix-assisted laser desorption/ionization mass spectrometry: An update for 2007–2008. *Mass Spectrometry Reviews* **2011**, *31*, 183–311.

195. Harvey, D. J. Matrix-assisted laser desorption/ionization mass spectrometry of carbohydrates. *Mass Spectrometry Reviews* **1999**, *18*, 349–450.

196. Fuchs, B.; Schiller, J. Application of MALDI-TOF mass spectrometry in lipidomics. *European Journal of Lipid Science and Technology* **2009**, *111*, 83–98.

197. Fuchs, B.; Süß, R.; Schiller, J. An update of MALDI-TOF mass spectrometry in lipid research. *Progress in Lipid Research* **2010**, *49*, 450–475.

198. Radhakrishnan, S.; Saujanya, C. Matrix mediated control of morphology in para-nitroaniline dispersed polymeric composites. *Materials Letters* **1996**, *28*, 341–346.

199. Estrada, R.; Yappert, M. C. Alternative approaches for the detection of various phospholipid classes by matrix-assisted laser desorption/ionization time-of-flight mass spectrometry. *Journal of Mass Spectrometry* **2004**, *39*, 412–422.

200. Vermillion-Salsbury, R. L.; Hercules, D. M. 9-Aminoacridine as a Matrix for Negative Mode Matrix-Assisted Laser Desorption/Ionization. *Rapid Communications in Mass Spectrometry* **2002**, *16*, 1575–1581.

201. Vaidyanathan, S.; Goodacre, R. Quantitative detection of metabolites using matrix-assisted laser desorption/ionization mass spectrometry with 9-aminoacridine as the matrix. *Rapid Commun. Mass Spectrom.* **2007**, *21*, 2072–2078.

202. Cerruti, C. D.; Benabdellah, F.; Laprévote, O.; Touboul, D.; Brunelle, A. MALDI Imaging and Structural Analysis of Rat Brain Lipid Negative Ions with 9-Aminoacridine Matrix. *Anal. Chem.* **2012**, *84*, 2164–2171.

203. Lorkiewicz, P.; Yappert, M. C. 2-(2-Aminoethylamino)-5-nitropyridine as a basic matrix for negative-mode matrix-assisted laser desorption/ionization analysis of phospholipids. *Journal of Mass Spectrometry* **2009**, *44*, 137–143.

204. Tanaka, K.; Waki, H.; Ido, Y.; Akita, S.; Yoshida, Y.; Yoshida, T.; Matsuo, T. Protein and polymer analyses up to m/z 100 000 by laser ionization time-of-flight mass spectrometry. *Rapid Communications in Mass Spectrometry* **1988**, *2*, 151–153.

205. Kinumi; Saisu; Takayama; Niwa Matrix-assisted laser desorption/ionization time-of-flight mass spectrometry using an inorganic particle matrix for small molecule analysis. *J Mass Spectrom* **2000**, *35*, 417–422.

206. Schürenberg, M.; Dreisewerd, K.; Hillenkamp, F. Laser Desorption/Ionization Mass Spectrometry of Peptides and Proteins with Particle Suspension Matrixes. *Anal. Chem.* **1998**, *71*, 221–229.

207. Gholipour, Y.; Giudicessi, S. L.; Nonami, H.; Erra-Balsells, R. Diamond, Titanium Dioxide, Titanium Silicon Oxide, and Barium Strontium Titanium Oxide Nanoparticles as Matrixes for Direct Matrix-Assisted Laser Desorption/Ionization Mass Spectrometry Analysis of Carbohydrates in Plant Tissues. *Analytical Chemistry* **2010**, *82*, 5518–5526.

208. Cotter, R. J. Peer Reviewed: The New Time-of-Flight Mass Spectrometry. *Anal. Chem.* **1999**, *71*, 445A–451A.

209. Stults, J. T. Matrix-assisted laser desorption/ionization mass spectrometry (MALDI-MS). *Current Opinion in Structural Biology* **1995**, *5*, 691–698.

210. Whittal, R. M.; Li, L. Time-lag focusing MALDI-TOF mass spectrometry. *American Laboratory 29*, 30–36.

211. Schiller, J.; Arnhold, J.; Benard, S.; Reichl, S.; Arnold, K. Cartilage degradation by hyaluronate lyase and chondroitin ABC lyase: a MALDI-TOF mass spectrometric study. *Carbohydrate Research* **1999**, *318*, 116–122.

212. Yeung, B.; Marecak, D. Molecular weight determination of hyaluronic acid by gel filtration chromatography coupled to matrix-assisted laser desorption ionization mass spectrometry. *Journal of Chromatography A* **1999**, *852*, 573–581.

213. Sakai, S.; Hirano, K.; Toyoda, H.; Linhardt, R. J.; Toida, T. Matrix assisted laser desorption ionization-time of flight mass spectrometry analysis of hyaluronan oligosaccharides. *Analytica Chimica Acta* **2007**, *593*, 207–213.

214. Blundell, C. D.; Almond, A. Enzymatic and chemical methods for the generation of pure hyaluronan oligosaccharides with both odd and even numbers of monosaccharide units. *Anal. Biochem.* **2006**, *353*, 236–247.

215. Tranchepain, F.; Deschrevel, B.; Courel, M.-N.; Levasseur, N.; Le Cerf, D.; Loutelier-Bourhis, C.; Vincent, J.-C. A complete set of hyaluronan fragments obtained from hydrolysis catalyzed by hyaluronidase: Application to studies of hyaluronan mass distribution by simple HPLC devices. *Analytical Biochemistry* **2006**, *348*, 232–242.

216. Price, K. N.; Tuinman, A.; Baker, D. C.; Chisena, C.; Cysyk, R. L. Isolation and characterization by electrospray-ionization mass spectrometry and high-performance anion-exchange chromatography of oligosaccharides derived from hyaluronic acid by hyaluronate lyase digestion: Observation of some heretofore unobserved oligosaccharides that contain an odd number of units. *Carbohydrate Research* **1997**, *303*, 303–311.

217. Soltés, L.; Kogan, G.; Stankovska, M.; Mendichi, R.; Rychlý, J.; Schiller, J.; Gemeiner, P. Degradation of high-molar-mass hyaluronan and characterization of fragments. *Biomacromolecules* **2007**, *8*, 2697–2705.

218. Soltés, L.; Stankovská, M.; Brezová, V.; Schiller, J.; Arnhold, J.; Kogan, G.; Gemeiner, P. Hyaluronan degradation by copper(II) chloride and ascorbate: rotational viscometric, EPR spin-trapping, and MALDI-TOF mass spectrometric investigations. *Carbohydrate Research* **2006**, *341*, 2826–2834.

219. Kühn, A. V.; Raith, K.; Sauerland, V.; Neubert, R. H. H. Quantification of hyaluronic acid fragments in pharmaceutical formulations using LC-ESI-MS. *Journal of Pharmaceutical and Biomedical Analysis* **2003**, *30*, 1531–1537.

220. Hayase, S.; Oda, Y.; Honda, S.; Kakehi, K. High-performance capillary electrophoresis of hyaluronic acid: determination of its amount and molecular mass. *Journal of Chromatography A* **1997**, *768*, 295–305.

221. Maccari, F.; Tripodi, F.; Volpi, N. High-performance capillary electrophoresis separation of hyaluronan oligosaccharides produced by Streptomyces hyalurolyticus hyaluronate lyase. *Carbohydrate Polymers* **2004**, *56*, 55–63.

222. Nagata, H.; Kojima, R.; Sakurai, K.; Sakai, S.; Kodera, Y.; Nishimura, H.; Inada, Y.; Matsushima, A. Molecular-weight-based hyaluronidase assay using fluorescent hyaluronic acid as a substrate. *Analytical Biochemistry* **2004**, *330*, 356–358.

223. Hokputsa, S.; Jumel, K.; Alexander, C.; Harding, S. E. Hydrodynamic characterisation of chemically degraded hyaluronic acid. *Carbohydrate Polymers* **2003**, *52*, 111–117.

224. Volpi, N. On-line HPLC/ESI-MS separation and characterization of hyaluronan oligosaccharides from 2-mers to 40-mers. *Anal Chem* **2007**, *79*, 6390–7.

225. Busse, K.; Averbeck, M.; Anderegg, U.; Arnold, K.; Simon, J. C.; Schiller, J. The signal-to-noise ratio as a measure of HA oligomer concentration: a MALDI-TOF MS study. *Carbohydrate Research* **2006**, *341*, 1065–1070.

226. Nimptsch, K.; Süß, R.; Riemer, T.; Nimptsch, A.; Schnabelrauch, M.; Schiller, J. Differently complex oligosaccharides can be easily identified by matrix-assisted laser desorption and ionization time-of-flight mass spectrometry directly from a standard thin-layer chromatography plate. *Journal of Chromatography A* **2010**, *1217*, 3711–3715.

227. Nimptsch, K.; Süß, R.; Schnabelrauch, M.; Nimptsch, A.; Schiller, J. Positive ion MALDI-TOF mass spectra are more suitable than negative ion spectra to characterize sulphated glycosaminoglycan oligosaccharides. *International Journal of Mass Spectrometry* **2012**, *310*, 72–76.

228. Ii, T.; Okuda, S.; Hirano, T.; Ohashi, M. Tandem mass spectrometry for characterization of unsaturated disaccharides from chondroitin sulfate, dermatan sulfate and hyaluronan. *Glycoconj J* **1994**, *11*, 123–32.

229. Zhang, Z.; Xie, J.; Liu, J.; Linhardt, R. J. Tandem MS Can Distinguish Hyaluronic Acid from N-Acetylheparosan. *Journal of the American Society for Mass Spectrometry* **2008**, *19*, 82–90.

230. Mandzy, N.; Grulke, E.; Druffel, T. Breakage of TiO2 agglomerates in electrostatically stabilized aqueous dispersions. *Powder Technology* **2005**, *160*, 121–126.

231. Yu, H.; Lopez, E.; Young, S. W.; Luo, J.; Tian, H.; Cao, P. Quantitative analysis of free fatty acids in rat plasma using matrix-assisted laser desorption/ionization time-of-flight mass spectrometry with meso-tetrakis porphyrin as matrix. *Analytical Biochemistry* **2006**, *354*, 182–191.

APPENDIX A

LIST OF ACRONYMS

9AA	9-aminoacridine
Å	angstrom
AAN	2-(2-aminoethylamino)-5-nitropyridine
Avg (x□)	average
B_0	applied magnetic field
B_{local}	local magnetic field
C=O	carbonyl
CD	circular dichroism
CE	capillary electrophoresis
Cer	ceramide
Cer1P	ceramide-1-phosphate
CHCA	α-cyano-4-hydroxycinnamic acid
CID	collision-induced dissociation
CMH	ceramide monohexoside
COMP	cartilage oligomeric matrix protein
conf lim	confidence limit
COO^-	carboxylate
COSY	correlation spectroscopy
CS	chondroitin sulfate
D	distance
Da	dalton
DAG	diacylglycerol
DE	delayed extraction
DEPT	distortionless enhancement by polarization transfer
DHB	2,5-dihydroxybenzoic acid
DHSM	dihydrosphingomyelin
DL	detection limit
DMSO	dimethyl sulfoxide
DPPC	di-palmitoyl-phosphatidylcholine
DSS	4,4-dimethyl-4-silapentane-1-sulfonic acid
e	charge of an electron
ECM	extracellular matrix
EPR	electron paramagnetic resonance
ESI	electrospray ionization
FA	fatty acid
FAB	fast atom bombardment

FID	free induction decay
FT	Fourier transform
GAG	glycosaminoglycan
GalNAc	N-acetylgalactosamine
GC	gas chromatography
GFC	gel-filtration chromatography
gHMBC	gradient heteronuclear multiple bond correlation spectroscopy
gHSQC	gradient heteronuclear single quantum correlation spectroscopy
GIAO	gauge including atomic orbital
GL	glycolipid
GlcNAc	N-acetylglucosamine
GlcU	glucuronic-acid
HA	hyaluronan
HA_6	hyaluronan hexasaccharide
HAase	hyaluronanidase
HA_p	polymeric HA
H-bond	hydrogen bond
HETCOR	HETeronuclear CORrelation spectroscopy
HG	headgroup
HMBC	heteronuclear multiple bond correlation spectroscopy
HMQC	heteronuclear multiple quantum correlation spectroscopy
HPLC	high-performance liquid chromatography
HS	heparin sulfate
HSQC	heteronuclear single quantum correlation spectroscopy
HyPE	HA covalently linked to PE
Hz	hertz
I	spin quantum number
IE	ionization efficiency
IEP	isoelectric points
IUPAC	International Union of Pure and Applied Chemistry
KE	kinetic energy
LC	liquid chromatography
LDL	low-density lipoproteins
LPC	lyso-phosphatidylcholine
LPC-OA	lyso-1-oleoyl-phosphatidylcholine
LPC-SA	lyso-1-stearoyl-phosphatidylcholine
m	mass
M	molar
m/z	mass-to-charge ratio
MALDI	matrix-assisted laser desorption ionization
MALDI-TOF-MS	matrix-assisted laser desorption ionization time-of-flight mass spectrometry
MALLS	multi-angle laser light scattering
MeOH	methanol
mp	melting point

MS	mass spectrometry
MS-MS	tandem MS
MW	molecular weight
n	number
NaH	N-acetylheparosan
NaHA	sodium hyaluronate
NH	Amide
NMR	nuclear magnetic resonance
NOESY	Nuclear Overhauser Effect SpectroscopY
ns	nanosecond
OA	oleic acid
OH	hydroxyl
PA	phosphatidic acid
PC	phosphatidylcholine (phosphocholine or phosphorylcholine)
PCM	polarizable continuum model
PDB	protein data bank
PE	phosphatidylethanolamine (phosphoethanolamine)
PFG	pulsed field gradient
PG	phosphatidylglycerol
PI	phosphatidylinositol
PL	phospholipid
PNA	para-nitroaniline
ppb	parts-per-billion
ppm	parts-per-million
PS	phosphatidylserine
PSD	post-source decay
PVD	posterior vitreous detachment
rf	radiofrequency
RIE	relative ionization efficiency
ROESY	Rotating frame Overhauser Effect SpectroscopY
RSD	relative standard deviation
S/N	signal-to-noise ratio
SA	steric acid
SD (s)	standard deviation
SD_{pooled} (s_{AB})	pooled standard deviation
SEC	size-exclusion chromatography
SL	sphingolipid
SM	sphingomyelin
t	time
T_1	spin-lattice (longitudinal) relaxation time
T_2	spin-spin (transverse) relaxation time
TAG	triacylglycerol
t_{exp}	experimental (calculated) t value
TLC	thin layer chromatography
T_m	midpoint phase transition temperature
TM	titanium microparticles

TMS	tetramethylsilane
TN	titanium nanoparticles
TOCSY	Total COrrelation SpectroscopY
TOF	time-of-flight
t_{theor}	theoretical (tabulated) t value
UV	ultraviolet
V	voltage
v	velocity
v/v	volume by volume
VH	vitreous humor
V_s	accelerating voltage
z	charge
γ	magnetogyric ratio
δ	chemical shift
ΔDiHA	unsaturated hyaluronan disaccharide
ΔGlcU	unsaturated glucuronic acid
ΔHA_4	unsaturated HA tetrasaccharide
$\Delta\delta/\Delta T$	temperature coefficient
$\Delta\nu$	peak width
$\Delta\nu_{1/2}$	peak width at half-height
□	dielectric constant
ν	frequency
σ	shielding tensor
σ_{diamag}	diamagnetic shielding tensor
σ_{iso}	isotropic shielding tensor
$\sigma_{paramag}$	paramagnetic shielding tensor
τ_c	correlation (tumbling) time

APPENDIX B

SUPPLEMENTAL INFORMATION

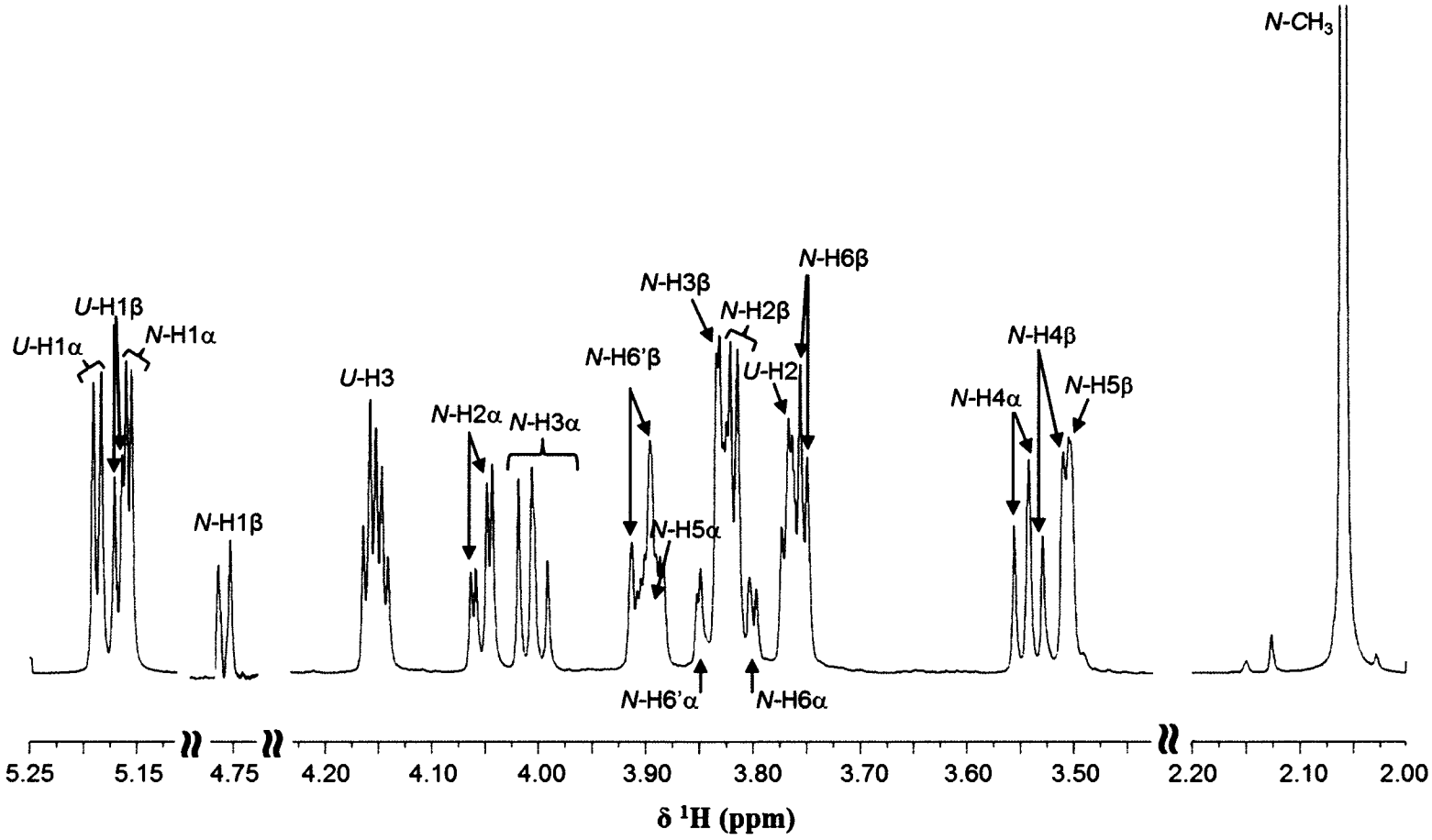

Figure B-1. ^{1}H NMR spectrum of ΔDiHA displaying all non-exchangeable proton resonances corresponding to both anomers (α and β) in solution. Sample was prepared at 1.67 mg/mL in D_2O and the spectra was obtained at 25 °C.

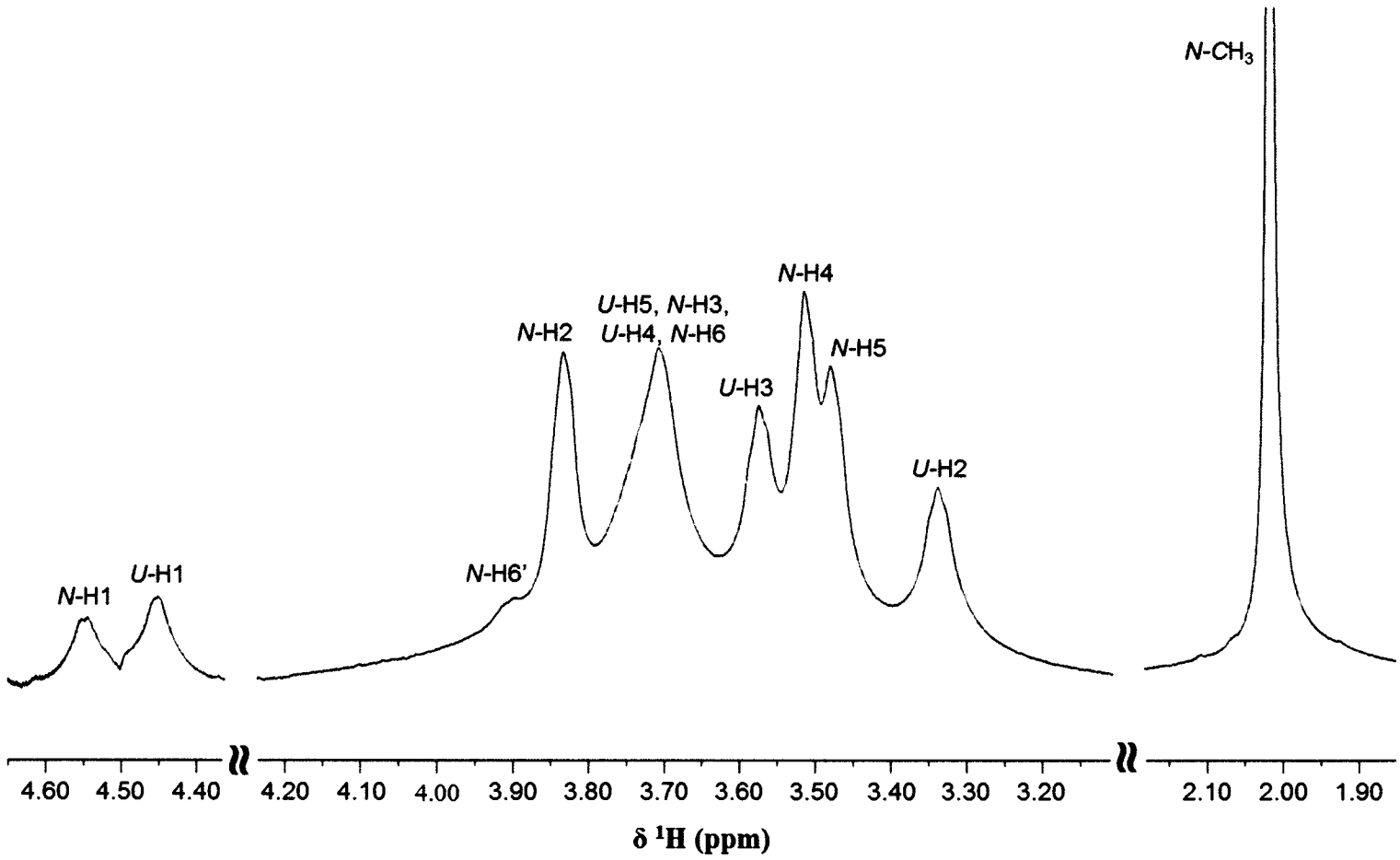

Figure B-2. ^{1}H NMR spectra of polymeric HA displaying all non-exchangeable proton resonances. Sample was prepared at 5 mg/mL in D_2O and the spectra was obtained at 25 °C.

.

	Chemical Shift δ (ppm)				ΔChemical Shift (ppm)		
					$\Delta\delta = \delta_{solv} - \delta_{no\ solvent}$		
Atom of Interest	**No solvent**	**$CHCl_3$ ε = 4.9**	**CH_3OH ε = 32.63**	**H_2O ε = 78.39**	**$\Delta CHCl_3$**	**ΔCH_3OH**	**ΔH_2O**
N-H1	4.1287	4.5025	4.7548	4.7965	0.3738	0.6261	0.6678
N-AcNH	1.5276	2.8766	3.5290	3.6554	1.3490	2.0014	2.1278
*N*H	2.7140	3.6804	4.2660	4.3692	0.9664	1.5520	1.6552
***N*-H2**	4.5352	4.4356	4.2452	4.2088	**-0.0996**	**-0.2900**	**-0.3264**
N-H2	2.7930	3.0122	3.3350	3.4126	0.2192	0.5420	0.6196
***N*-H4**	4.3549	4.3786	4.2565	4.2212	**0.0237**	**-0.0984**	**-0.1337**
N-OH4	0.8771	0.6940	1.0659	1.2795	-0.1831	0.1888	0.4024
***N*-H6**	4.5391	4.4917	4.4768	4.4767	**-0.0474**	**-0.0623**	**-0.0624**
N-H6'	3.8963	4.0120	4.0428	4.0460	0.1157	0.1465	0.1497
N-OH6	-0.3482	1.1304	1.7086	1.7894	1.4786	2.0568	2.1376
N-H5	2.8406	3.1779	3.4233	3.4672	0.3373	0.5827	0.6266
N-CH3	1.7591	1.7708	1.6989	1.6818	0.0117	-0.0602	-0.0773
N-CH3'	1.8030	1.9688	2.1354	2.1762	0.1658	0.3324	0.3732
N-CH3"	1.8286	2.1675	2.3217	2.3398	0.3389	0.4931	0.5112
U-H1	3.5368	3.7799	4.0488	4.1434	0.2431	0.5120	0.6066
***U*-H2**	3.4411	3.4999	3.3687	3.3274	**0.0588**	**-0.0724**	**-0.1137**
U-OH2	-1.6219	-0.5868	0.0027	0.3052	1.0351	1.6246	1.9271
U-H3	2.4451	2.8360	3.1536	3.2223	0.3909	0.7085	0.7772
U-OH3	1.3047	2.5723	3.1199	3.1827	1.2676	1.8152	1.8780
***U*-H4**	4.0749	3.9748	3.8788	3.8543	**-0.1001**	**-0.1961**	**-0.2206**
U-H5	3.1313	3.2235	3.3890	3.4241	0.0922	0.2577	0.2928
U-COOH	1.3066	2.4302	2.8455	2.8965	1.1236	1.5389	1.5899

Table B-1. Theoretically calculated chemical shifts for the HA disaccharide in solvents of different polarities (dielectric constants, ε). Changes in chemical shift, relative to HA in no solvent, are also provided.

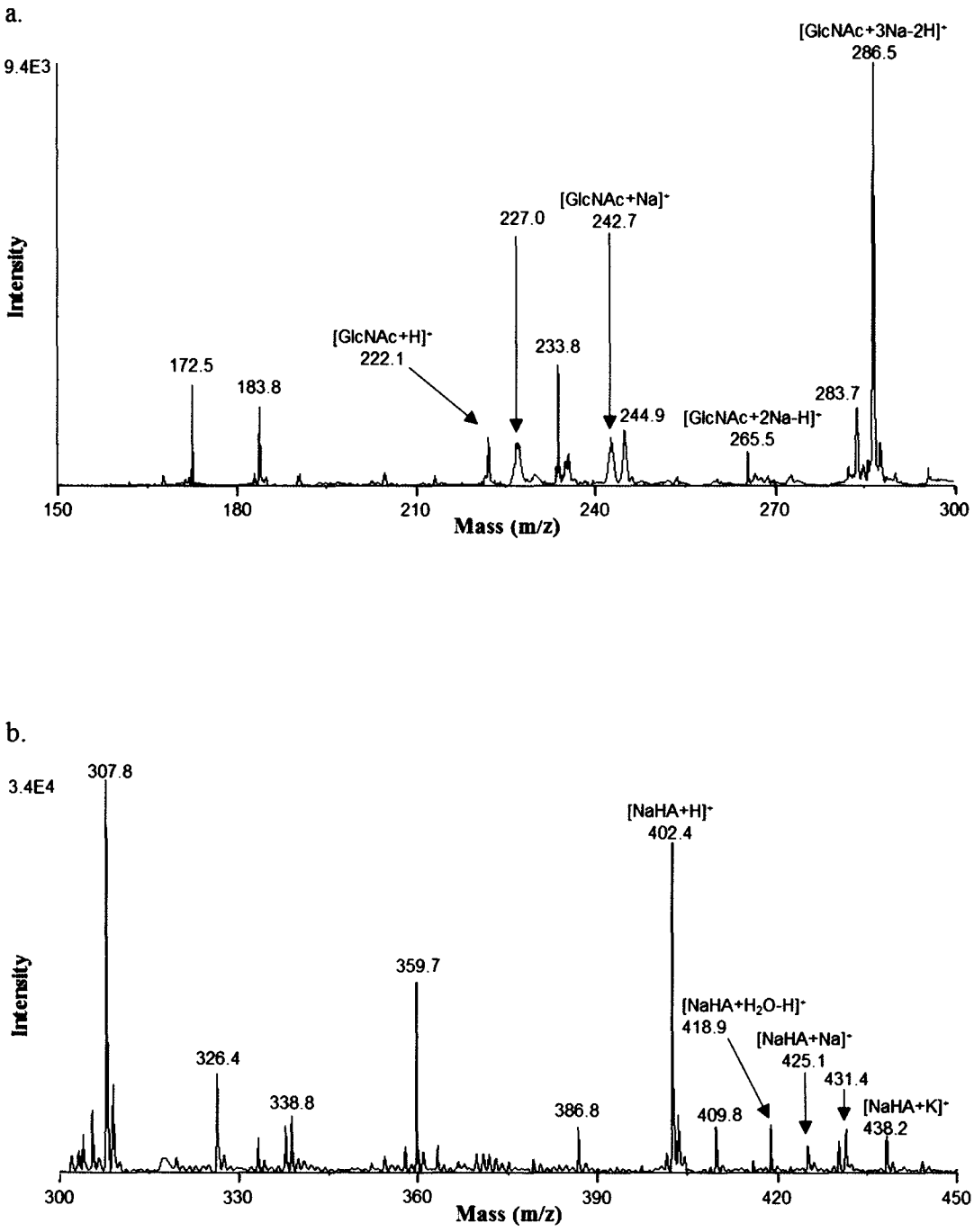

Figure B-3. Post source decay (PSD) spectra of the ΔDiHA peak at *m/z* = 402.4 in the range of a) 150 - 300 b) 300 - 450 *m/z* units. Spectra were obtained in the positive ion mode using DHB as matrix.

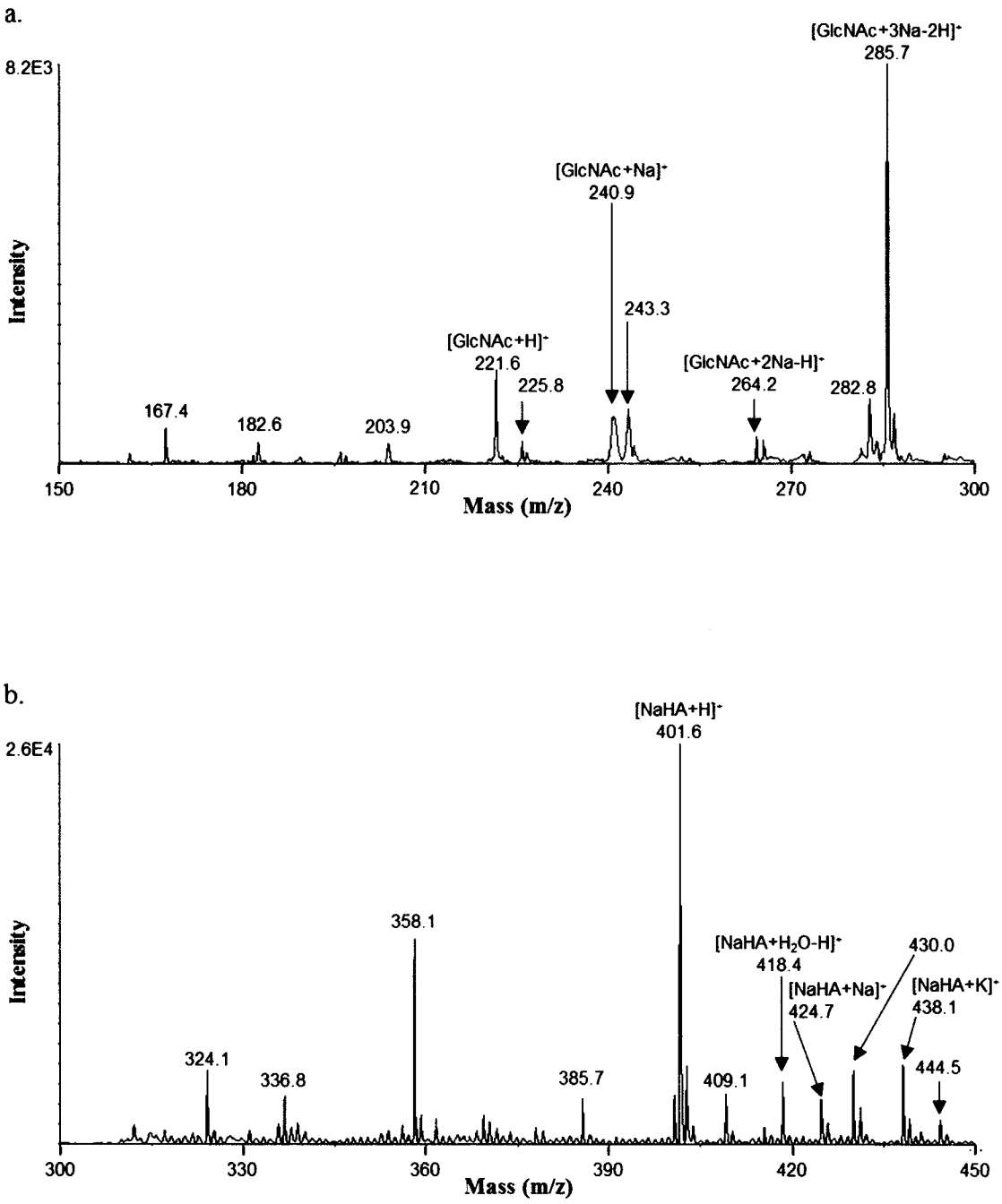

Figure B-4. Post source decay (PSD) spectra of the ΔDiHA peak at *m/z* = 418.0 in the range of a) 150 - 300 b) 300 - 450 *m/z* units. Spectra were obtained in the positive ion mode using DHB as matrix.

	HA Alone	HA Mix	PC Alone	PC Mix
RIE Avg	0.41	0.16	0.44	0.20
SD	0.09	0.02	0.11	0.06
n	5	7	7	7
Mix:Alone	0.38		0.45	
SD_{pooled}	0.06		0.09	
t_{calc}	7.27		5.20	
Conf Limit	> 99.95%		> 99.95%	

	HA Alone	HA Mix	PE Alone	PE Mix
RIE Avg	0.41	0.21	0.74	0.50
SD	0.08	0.05	0.16	0.09
n	5	5	6	5
Mix:Alone	0.51		0.68	
SD_{pooled}	0.07		0.13	
t_{calc}	4.88		2.94	
Conf Limit	> 99.95%		> 99.00%	

	HA Alone	HA Mix	PA Alone	PA Mix
RIE Avg	0.41	0.40	0.90	0.33
SD	0.08	0.09	0.19	0.08
n	5	5	5	5
Mix:Alone	0.97		0.36	
SD_{pooled}	0.08		0.14	
t_{calc}	0.23		6.23	
Conf Limit	no change		> 99.95%	

	HA Alone	HA Mix	DAG Alone	DAG Mix
RIE Avg	0.41	0.06	-----	-----
SD	0.13	0.03	-----	-----
n	5	5	-----	-----
Mix:Alone	0.16		-----	
SD_{pooled}	0.10		-----	
t_{calc}	5.70		-----	
Conf Limit	> 99.95%		-----	

	HA Alone	HA Mix	LPC-OA Alone	LPC-OA Mix
RIE Avg	0.41	0.08	5.60	2.45
SD	0.09	0.03	1.09	0.39
n	5	5	5	5
Mix:Alone	0.19		0.44	
SD_{pooled}	0.07		0.82	
t_{calc}	7.79		6.07	
Conf Limit	> 99.95%		> 99.95%	

	HA Alone	HA Mix	LPC-SA Alone	LPC-SA Mix
RIE Avg	0.41	0.04	1.85	1.11
SD	0.09	0.01	0.42	0.29
n	5	5	5	5
Mix:Alone	0.10		0.60	
SD_{pooled}	0.07		0.36	
t_{calc}	8.98		3.26	
Conf Limit	> 99.95%		> 99.00%	

	HA Alone	HA Mix	OA Alone	OA Mix
RIE Avg	0.41	0.05	-----	-----
SD	0.09	0.02	-----	-----
n	5	5	-----	-----
Mix:Alone	0.11		-----	
SD_{pooled}	0.07		-----	
t_{calc}	8.75		-----	
Conf Limit	> 99.95%		-----	

	HA Alone	HA Mix	SA Alone	SA Mix
RIE Avg	0.41	0.03	-----	-----
SD	0.09	0.01	-----	-----
n	5	5	-----	-----
Mix:Alone	0.08		-----	
SD_{pooled}	0.07		-----	
t_{calc}	9.19		-----	
Conf Limit	> 99.95%		-----	

Table B-2. Statistical analysis of relative ionization efficiencies (RIEs) for HA and lipids. Alone and mixture solutions: RIE averages (Avg), standard deviations (SD), and the number of spectra analyzed (n) are included. Alone/mixture comparisons: ratio of RIEs (mixture: alone), population standard deviation (SD_{pooled}), experimental t value (t_{calc}), and confidence limits (Conf Lim) are included.

CURRICULUM VITAE

NAME:	Kristen Ann Magness
ADDRESS:	Department of Chemistry University of Louisville 2320 South Brook Street Louisville, KY 40292
DOB:	Louisville, Kentucky - 10/20/81
EDUCATION & TRAINING:	B.A., Chemistry University of Louisville 2000-2006 M.S., Analytical Chemistry University of Louisville 2006-2010 Ph.D., Analytical Chemistry University of Louisville 2010-2012
AWARDS:	GEMS Fellowship 2006, 2007, 2008, 2010, 2011
PROFESSIONAL SOCIETIES:	American Chemical Society
NATIONAL MEETING PRESENTATIONS:	Science, Technology, Engineering Mathematics (STEM) Symposium National Meeting 2011 focusing on "Practical strategies for linking assessment, instruction, and learning" Participation in roundtable discussion at Partnership Institute for Math & Science Education Reform (PIMSER) Symposium 2011 focusing on "Generating new partnerships and collaboration across the STEM disciplines"

Poster Presentation at ACS 236th National Meeting 2008 focusing on "Identification of water-soluble and volatile compounds in Vernonia amygdalina using solid-phase micro extraction"

ACTIVITIES:

Chemistry Graduate Student Association
Public Relations 2008-2009

Graduate Student Council
Department Representative 2008-2009

Chemistry Graduate Student Association
Treasurer 2009-2010